Compressibility Approximations in Jovian Regimes: A Normal Mode Analysis

Submitted by Rebecca Holly Mitchell,

to the University of Exeter as a thesis for the degree of

Doctor of Philosophy in Mathematics,

February 2009.

I certify that all material in this thesis which is not my own work has been identified and that no material has previously been submitted and approved for the award of a degree by this or any other University.

..... (signature)

R H Mitchell

Abstract

The atmospheres and interiors of planetary and stellar systems has been studied in various forms, though the complexity of these systems currently makes full replication of their dynamics impossible. In order to make these complex systems tractable it is necessary to make significant simplifications. For many years models have concentrated on making use of the Boussinesq approximation, often with a constant density reference profile. More recently, anelastic approximations have been developed to allow for the analysis of some degree of reference state density variation. The validity of these approximations is well understood for modelling the adiabatic, inviscid, terrestrial atmosphere, however their use in modelling other regimes remains equivocal. We consider the fully compressible, Boussinesq, anelastic, quasi-hydrostatic and pseudo-incompressible equation sets governing fluid flow within a rotating, differentially heated system. We consider both tangent plane and spherical shell geometries and conduct a normal model analysis in order to examine the validity of these approximations outside of terrestrial parameters. We find the compressibility approximations can cause spurious distortion of the normal mode solutions including misrepresentation of the frequencies, growth/decay rates, and modal structure. This in turn can have knock on effects including energy redistribution. The level of distortion is found to be dependent on mode type, reference profile and geometry and varies according to approximated equation set. Selected eigenmodes and frequencies are presented and discussed.

We conclude that the most suitable approximated equation sets for use in modelling the various regions of the Jovian atmosphere depends primarily on the type of wave it is necessary to reflect most accurately; and that the scale analyses, upon which the approximated equation sets are based, provide a good indication of the regimes in which their use is appropriate.

Acknowledgements

I would like to gratefully acknowledge many people who have helped and supported me whilst I have undertaken this project. It is impossible to mention everyone who has helped me directly or indirectly; however, there are some that it would be remiss of me not to thank individually.

I would like to thank my supervisors; Professor Chris Jones who, prior to his move to Leeds, supervised me during my first year, and Professor John Thuburn who took me under his wing after Prof. Jones' departure. Prof. Jones' enthusiasm for the study of the Jovian regime is infectious, and was what led me to investigate further the various approximations that have been used in advancing our understanding of the complex dynamics of its atmosphere and interior. More recently, I would like to thank him for his role as lead author in writing up the work I aided with during my first year, and that he and Dr Kuzanyan have continued at Leeds. I cannot overstate my thanks to Prof. Thuburn for ensuring that I was able to continue my project, for his encouragement, advice, insightful comments and for pointing me in the right direction on so many occassions.

For financial aid I am indebted primarily to the Science and Technology Facilities Council who funded my full-time research. I would also like to thank Exeter University School of Engineering, Computer Science and Mathematics and the Royal Meteorological Society who have funded my attendance at conferences.

My thanks must also go to those whose support I could not have done without, foremostly my family but also my office mates and colleagues, both whilst studying and latterly whilst employed.

Finally my heartfelt thanks go to Karen, her support and encouragement have kept me sane through the tough times, without her I could not have completed this project and it is to her I dedicate this thesis.

Contents

Chapter 1

Motivation

The distinctive striped surface of Jupiter makes it one of the most easily recognisable planets in our solar system. For hundreds of years scientists have studied and endeavoured to understand the zonal bands and stripes, as well as the long lived storms such as the Great Red Spot. Early observations include those made by Hooke in 1664 and Cassini in 1665 while more recent technology has allowed closer inspection by the Galileo probe mission between 1989 and 2003.

The stripy appearance of the Jovian atmosphere can be attributed to zonal winds which transport cloud systems; the chemical composition of these clouds being responsible for the various different colours. Winds travelling in opposing directions form regions known as zones and belts; the zones are anticyclonic, therefore have an eastward jet on the poleward boundary and westward jet on the equatorward side and rotate clockwise in the northern hemisphere (Ingersoll et al., 2004 [37]). The belts are cyclonic, thus rotate in the opposite direction. Strong shears between the opposing winds give rise to the interesting structures that are often referred to as 'spots'; the most famous of these being a large anticyclonic vortex known as the Great Red Spot. Other complex 'weather' phenomena can be observed such as lightning and huge thunderstorms (see e.g. Boruki at al., 1982 [7]). These can be due to many different

contributors such as moist convection and the chemical make up of the atmosphere. Further to these visible phenomena are the strong magnetic field and magnetosphere; believed to be due in part to the deep convection of electrically conducting fluid within the Jovian interior (see e.g. Russell and Luhmann, 1997 [52]).

In order to accurately replicate the Jovian system it would be preferable to consider a model which closely resembles the system in both physical and dynamical senses. However, the complexity of planetary atmospheres and interiors means that this will remain beyond the realms of possibility for the foreseeable future. In considering the forementioned areas of interest the majority of groups choose to apply the continuum hypothesis, in which the physical properties of the fluid are taken to be well defined at all points, thus considering the fluid mechanics of the system rather than interactions between individual atoms and molecules. Solving the 3D, fully compressible fluid dynamic equations is also a problematic issue and it is necessary to make further simplifications in order to progress understanding of the dynamics of both the atmosphere and interior.

In attempting to model the large scale structures the source and depth of the zonal winds remains a topic of debate. Shallow and deep models compete for general acceptance. The source and depth of the winds are often treated as one problem, however Showman et al. (2006 [55]) point out that deep winds can arise from shallow forcing, and vice versa, therefore the problems should be treated as mutually distinct.

The shallow atmosphere model was first developed as early as 1951 by Hess and Panofsky [36]. They proposed that the winds in the deep atmosphere are weak, similar to those of the deep oceans; therefore, that the observed winds are shallow. The winds are in approximate geostrophic balance, therefore anticyclonic features are high pressure centres and cyclonic features low pressure centres. Since pressure decreases with altitude more slowly when the air is warm, warm-core features become more anticylconic with altitude. The negative temperature gradient across the Jovian

troposphere means that at depth the winds can be weakly cyclonic or anticyclonic, however at the 'surface' they are strongly anticyclonic. This implies that the zones are warm-core features. Within a convectively unstable atmosphere it is natural to assume that warm fluid rises, and cool fluid sinks; therefore that the fluid in the zones is gradually rising. Observations show that the cloud deck is higher in the zones than the belts, which is consistent with the view that the fluid in the zones is gradually rising as clouds tend to form on updrafts (Ingersoll et al., 2004 [37]).

Global shallow-water models, global circulation models and 2D barotropic models have achieved some success in replicating the zonal flow and have allowed considerable research into the long-lived storms also visible on the Jovian surface. Critics maintain that the most successful of these models prescribe latitudinal differential rotation at the lower boundary; therefore, implicitly assuming that differential rotation is maintained by deep thermal convection (see e.g. Evonuk and Glatzmaier, 2006 [29]) The extension of the winds into the deep interior motivates the competing theory with regard to the generation of zonal flow.

In a pioneering paper Busse (1976 [12]) utilised the Boussinesq approximation to investigate convection within a simplified model of the Jovian regime and proposed that the zonal winds are the surface manifestation of differentially rotating convective columns which are aligned with the axis of rotation and the result of thermal Rossby waves. In meteorological scenarios it is common to apply the Boussinesq approximation to a realistic reference state profile; in considering convection within the interior and interior atmosphere of Jupiter the Boussinesq approximations are usually utilised alongside the assumption that density perturbations are proportional to temperature perturbations with pressure perturbations being negligible, and the reference state density is uniform. This leads to a scenario which is almost incompressible, with the various assumptions being collectively referred to as Boussinesq, and the ensuing fluid motions referred to as incompressible convection. Within this regime it is

necessary to assume that the geostrophic approximation and Taylor-Proudman theorem are good approximations in order to maintain the columnar structure of the flow. This has provided the basis for many theoretical and experimental studies into the onset of convection within Boussinesq models and has ensured that this form of Boussinesq theory is now reasonably well understood. Similar models have also been used to model the Jovian dynamo. Taylor-Proudman theorem does not holod when utilising a stratified reference state that more closely resembles the Jovian regime, however it is often assumed by groups considering this theorem (see e.g. Dormy et al., 2004 [19]; Jones et al., submitted 2008 [38]) that the rapid rotation of Jupiter means that the Coriolis force is much greater than the destabilising component of the buoyancy force and the onset of convection will continue to be columnar. Recent research (Glatzmaier et al., 2009 [34]) suggests that, within a density stratified fluid, differential rotation can be maintained by turbulent convective motions without reliance on Taylor-Proudman theorem; however, the short columns that they consider continue to be aligned with the axis of rotation. Both turbulent and linearised convection continue to be studied by groups considering deep convection models. It is also worth noting however, that it is not certain that thermal Rossby waves will be dominant in the Jovian regime; Zhang et al. (2001 [67]) showed that at very low Prandtl number inertial modes will dominate over the thermal Rossby modes found at moderate Prandtl number.

Modelling of the smaller scale atmospheric phenomena is also complex, facing many of the problems that arise in modelling the terrestrial atmosphere with the added complexity that it is clearly far more difficult to obtain empirical data. For a more complete review of the atmospheric phenomena displayed within the Jovian regime see texts such as Vasavada and Showman (2005 [62]) or Ingersoll et al. (2004 [37]).

Essentially we see that modelling of global, large scale and small scale struc-

tures within a Jovian regime is extremely complex and that, similar to modelling terrestrial systems, it is not possible to consider them all within one model. The various simplifications made in order to model these systems must be appropriate to the structures the model is attempting to understand or replicate.

A primary simplification made in many models is to ignore the magnetic Lorentz forces generated by the fluid flow in the conducting regions of the Jovian interior. These forces are, of course, essential in considering the generation and maintenance of planetary dynamo problems. However, they add significant complexity and a thorough understanding of the dynamics of the non-magnetic case is often essential before progress can be made in understanding magnetoconvection. In this thesis we choose to concentrate on the non-magnetic case, though the techniques used could be extended to the magnetic case.

Geometric simplifications are also essential with spheres, spherical shells, annulus' and tangent planes all being investigated to good effect. The most appropriate type of geometric simplifiction made is dependent on the phenomenon being studied, and on the degree to which other complex areas are simplified. Experimental work has often concentrated on plane layer geometries though more recently experiments using the quasigeostrophic approximation and cyclindrical geometries have produced columnar convection and zonal flows similar to those predicted by Busse (see e.g. Aubert et al., 2001 [2]).

Historically the only viable theoretical models of deep interiors were those which considered reference state profiles in which the Boussinesq approximation applies, density perturbations are small relative to temperature perturbations and reference state density is uniform. This allows considerable simplification of the governing equations and the assumptions have generally been referred to collectively as the Boussinesq approximation. The use of these approximations has allowed huge progress to be made into the study of deep incompressible convection within the

interior as a possible source of the zonal flow observed on the surface. Studies by Chandrasekhar (1961 [13]), Roberts (1968 [50]) used these approximations and developed the asymptotic theory of the onset of convection in a rapidly rotating Boussinesq sphere. Since then many groups have developed these theories with varying degrees of success in reproducing fluid flow similar to the zonal winds on the Jovian surface (see e.g. Jones et al., 2003 [39]; Christensen, 2002 [14]; Heimpel et al., 2005 [35]). However, it is thought that the Jovian reference state has huge density variation, particularly in the outer regions of the planet. The density profile of the deep interior is also a topic of much research, however in general it is thought that the number of density scale heights across the deep convective region is likely to be approximately five (Evonuk and Glatzmaier, 2006 [29]). The assumption that reference state density is uniform is thought to be a severe approximation; therefore, whilst these Boussinesq models have provided enormous insight, the degree to which they resemble the Jovian system remains unclear.

Over the last 50 years there has been considerable effort in the meteorological field to consider the effects of compressibility in modelling the terrestrial atmosphere, yet ensure the governing equations remain feasible to solve. Technological advances in computing power have also aided progress. Some of these approximated systems have been adapted and used in astrophysical systems, seminally by Gilman & Glatzmaier (1981 [31]), who formed equation sets appropriate to the Solar regime. Most efforts have concentrated on solar and stellar convection zones, more recently planetary atmospheres have also been considered).

Evonuk & Glatzmaier (2004 [27]) concentrate primarily on the deep interior theories, and have shown that there are significant differences between the Boussinesq and anelastic systems. They expect that the anelastic system produces results closest to those of a fully compressible regime, however we note that the Boussinesq system they consider is effectively one in which the reference state density profile is

uniform. The size and complexity of their models mean we are unable to produce fully-compressible results for direct comparison. Jones et al. (submitted 2008 [38]) use the anelastic approximation to consider analytic and computational results for linearised systems with differing reference density profiles. Similarly to Evonuk and Glatzmaier they consider the Boussinesq equation set to be represented by the case in which there is almost no difference between the reference state density at the inner and outer surfaces of a spherical shell. They also show that the critical parameters for the onset of convection vary according to reference density profile.

In the most simplistic cases shallow models have also relied on the use of incompressible or Boussinesq models, using barotropic equation sets and considering tangent planes in which the Coriolis parameter $2\Omega\cos\phi$ is ignored (see e.g. Evonuk and Glatzmaier, 2006 [29]). More recent models allow some degree of compressibility, instead assuming isentropic states and often making use of the primitive hydrostatic equation sets. The Explicit Planetary Isentropic Coordinate Model (EPIC) (Dowling et al., 1998 [20]; Dowling et al., 2006 [21]) is the most well developed example of a global circulation model which utilises these simplifications in order to attempt to replicate the atmospheric dynamics of the Jovian regime.

It is clear that in modelling the dynamics of the Jovian system, and indeed other gas giants, there are a wide range of possible approaches. The most appropriate approach, and ensuing simplifications to the governing equation sets, are likely to rely heavily on the dynamic that is to be modelled. The goal of this thesis is to investigate, and examine the relative accuracy of, a number of approximations used in modeling the Jovian regime. As discussed earlier, the linearised Boussinesq equation set is reasonably well understood when utilised alongside a uniform density reference state, though is not well compared with a fully compressible equation set or one in which the reference state density profile is more realistic. The anelastic and pseudo-incompressible sets are less well used and their dynamics less well understood.

Normal mode analyses have long been used in order to gain insight into the dynamics of atmospheres (see e.g. Chandrasehkar, 1961 [13]), as they provide elementary solutions that isolate different aspects of the dynamics and allow identification of key features; they also provide useful test cases for numerical models. Within this thesis we will undertake a normal-mode analysis on various approximated, linearised equation sets; we will compare the results with those of a fully-compressible set. Davies et al. (2003 [18]) showed this method to be useful in comparing the relative accuracy of various dynamic approximations when applied to a terrestrial regime. We stress that in this instance we are endeavouring to differentiate between the behaviours of the differing equation sets within a non-terrestrial regime, rather than to attempt to accurately model the Jovian atmosphere or interior. Whilst both the atmosphere and interior of Jupiter are likely to be significantly affected by non-linear dynamics, a full and thorough understanding of the linear regime is a pre-requisite to advancing non-linear models; therefore, in this thesis we will compute solutions only for a linearised system.

Having motivated our study, the structure of this thesis is as follows. In chapter 2 we will formulate the governing equations for the fully-compressible set as well defining the reference state appropriate to our model. The parameters used in defining the reference state will be appropriate to the Jovian regime, though we note that this is also considerably simplified and a topic of research in its own right. In chapter 3 we will formulate the approximated equation sets. In chapter 4 we will undertake analytic analyses, ultimately considering a tangent plane to the sphere and an inviscid, isothermal reference state appropriate to the isothermal portion of the Jovian atmosphere. In chapter 5 we will undertake a computational analysis of an unstably stratified polytropic regime appropriate to the Jovian interior and interior atmosphere, considering an inviscid set on a tangent plane. In chapter 6 we will consider a similar computational analysis on a fully-spherical, unstably stratified, inviscid

regime. In chapter 7 we will extend studies of the onset of Boussinesq incompressible convection using the anelastic approximation to allow a stronger degree of compressibility and more realistic reference state, detailing work which has been included in Jones et al., (submitted 2008, [38]) and recently accepted for publication. Finally in chapter 8 we provide a summary of the results and recommendations for future work.

Chapter 2

Fully Compressible Model

2.1 Jupiter's structure

Jupiter differs from Earth in many ways; in considering atmospheric studies the key differences include the lack of a solid surface and existence of an internal heat source. Jupiter is sometimes referred to as a failed star as its chemical composition is largely hydrogen and helium and if it were slightly more massive it would reach the critical mass for thermonuclear fusion. Instead it formed a planet through collapse and compression, its core still retains heat from its formation and it is thought that it will continue cooling for billions of years. The lack of solid surface, and the considerably smaller amount of Solar energy that is absorbed, means that the internal heat source and fluid motions of the interior are almost certainly of crucial importance in understanding the motions of the outer atmosphere.

Unlike much of Earth's interior, the majority of the Jovian interior is sufficiently liquid that it is thought to obey the fundamental laws of fluid dynamics; consequently there has been significant emphasis on understanding the motions of the interior as an essential component of atmospheric studies. We will begin with an

overview of the Jovian structure, following with formulation of the governing equations appropriate to the regions of interest.

2.1.1 Internal structure

Rocky core

Jupiter is thought to have a dense, rocky core about which very little is known. It is thought that it contains a number of different elements and its size is equivocal; its existence has been inferred through gravitational measurements and planetary formation theories. Some groups suggest its mass accounts for somewhere between 3%-15% of Jupiters total mass (see e.g Elkins-Tanton, 2006 [26]), others suggest that high rates of core erosion by convective plumes in the interior may mean a solid core no longer exists, with gravitational measurements not yet sufficiently accurate to confirm or deny this (see e.g. Guillot et al., 2002 [33]). Evonuk and Glatzmaier (2004, [27]) have studied the effects of the size of a solid core on the equatorial flow in giant planets and found that surface zonal wind amplitudes, generated through a deep convection model, are strongly affected by the existence and size of the core. Many groups considering deep convection models choose only to consider the outer layers of the interior, however the boundary conditions applied to these models generally assume a core of some form. The temperature of the core is also equivocal, with early models predicting approximately 35,000 degrees Kelvin (Rogers, [51]) and later models suggesting a variety of different possible temperatures but in general agreeing it is likely to be close to 20,000 degrees Kelvin (Lewis, [45]).

Metallic hydrogen layer

It is sometimes postulated that the core is surrounded by a thin icy layer, however this is largely ignored in studies of the fluid motion within the interior and it is

assumed that the core is surrounded by a deep liquid region of metallic hydrogen. Hydrogen in this form has never been replicated on Earth but it is thought that the extreme pressure within this layer results in electrons being released from the hydrogen molecules , such that the region consists of hydrogen nucleii surrounded by a 'sea of electrons'. There is no defined surface to the region, however the temperatures are thought to vary between 10,000^{o}K and 20,000^{o}K (Lewis, [45]). The region is thought to extend from the core to approximately 80% of the Jovian radius, and to account for a significant portion of Jupiter's total mass. This region is likely to be convectively unstable and is the primary focus of studies into the source of the Jovian magnetosphere, which is the strongest magnetosphere within the solar system.

Molecular hydrogen layer

The final layer of the Jovian interior is a layer of hydrogen that undergoes a smooth transition from liquid to gas with increasing radius. The absence of a distinct boundary means that this layer is often known as an interior atmosphere, and is the layer of primary significance when considering deep convection models as a source of the surface jets.

It is generally accepted that Jupiters internal heat source is sufficiently strong that both the metallic and molecular hydrogen layers are unstably stratified, with considerable convective motion in both layers.

2.1.2 Atmospheric Structure

We have discussed that in Jovian regimes the outer layer of the interior and lower layers of the atmosphere are indistinguishable; altitude is therefore not defined in a systematic way across all groups. The various layers within the atmosphere are well defined according to temperature profile. Figure 2.1 displays a schematic of the

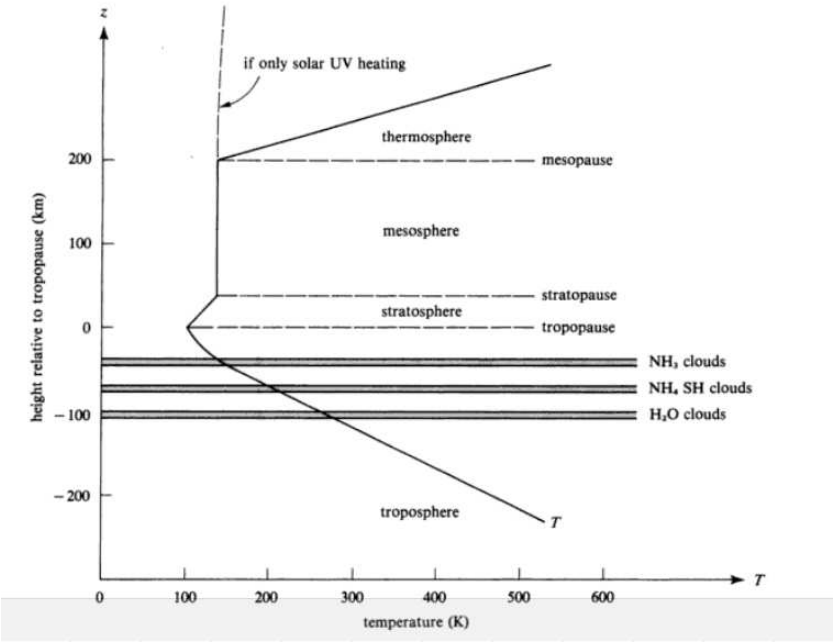

Figure 2.1: *Jovian atmospheric structure. Shu, 1982 [56]*

Jovian atmosphere with the 'surface' defined as the point at which the temperature profile first changes direction (close to the tropopause). It is also common for the 'surface' to be defined as the point at which the pressure is 1 bar. We see that the Jovian troposphere is unstably stratified and is the region in which the cloud layer is located; this region, and the molecular hydrogen layer of the interior, are the main areas of focus in modelling the zonal winds that transport the cloud systems and form the distinctive banded appearance.

Within this thesis we will concentrate on the molecular hydrogen layer within the interior, the unstably stratified troposphere and isothermal region of the stratosphere.

2.2 Governing Equations

In formulating a fully-compressible model appropriate to the Jovian atmosphere and interior we will first consider the equations governing the initial flow; from these deriving perturbation equations governing disturbances made to this reference state. The linearised versions of these perturbation equations will provide us with a model for which we can seek normal-mode solutions. Comparison of the solutions of this fully-compressible set with those of approximated equation sets will allow us to examine the accuracy and validity of these equation sets within regimes similar to those found on the gas giants. The equations are of a general nature and are appropriate for use in examining many planetary regimes; we specify the Jovian regime through use of an appropriate reference state, which is also defined within this chapter.

The axioms of most problems within fluid dynamics are the conservation laws for mass, momentum and energy which allow derivation of governing equations specific to the model in question. Alongside these we require an equation of state relating the various thermodynamic variables. We choose to consider a fluid governed by the ideal gas equation, bounded by a spherical shell with inner radius r_C and outer radius r_S. The equation of state for the fluid is

$$p = \rho R T, \tag{2.1}$$

where p , ρ and T represent pressure, density and temperature respectively, R is the specific gas constant. Equation (2.1) is not realistic at the very high pressures and densities thought to exist deep in the Jovian interior; at these pressures we see the break down of several of the assumptions on which the ideal gas equation is based. It is possible to consider more complicated equations of state, however it becomes significantly more difficult to manipulate and solve the governing equations and the ideal gas equation has been successfully used by many groups in order to provide a first approximation. The spherical shell rotates with constant angular velocity $\mathbf{\Omega}$.

It is convenient to use a terrestrial coordinate system in which λ, ϕ and r represent longitude, latitude and radius respectively. The unit vectors are then $\hat{\boldsymbol{\lambda}}$, $\hat{\boldsymbol{\phi}}$ and $\hat{\boldsymbol{r}}$,.

By specifying the velocity field as a function of space and time it is simple to demonstrate that the conservation of mass within the fluid can be expressed through the use of a mass continuity equation

$$\frac{D\rho}{Dt} + \rho\nabla.\,\boldsymbol{u} = 0, \tag{2.2}$$

where

$$\frac{D}{Dt} = \frac{\partial}{\partial t} + \boldsymbol{u}\,.\nabla,$$

is the material derivative and $\boldsymbol{u} = u\hat{\boldsymbol{\lambda}} + v\hat{\boldsymbol{\phi}} + w\hat{\boldsymbol{r}}$ represents the velocity field.

More complicated, though equally well accepted, are the Navier-Stokes equations which represent the conservation of momentum within the fluid. In a rotating frame of reference we then have

$$\frac{D\,\boldsymbol{u}}{Dt} + 2\boldsymbol{\Omega}\times\boldsymbol{u} + \boldsymbol{\Omega}\times(\boldsymbol{\Omega}\times\boldsymbol{r}) + \frac{1}{\rho}\nabla p - \boldsymbol{g} - \frac{1}{\rho}\boldsymbol{F} = 0, \tag{2.3}$$

where the Coriolis acceleration is represented by $2\boldsymbol{\Omega}\times\boldsymbol{u}$, the forces arising through viscous stresses are denoted by $\boldsymbol{F}$, $\boldsymbol{g}$ is the gravitational field and $\boldsymbol{\Omega}\times(\boldsymbol{\Omega}\times\boldsymbol{r})$ is the centrifugal component.

The thermodynamic equation is given by

$$\rho\frac{D\Upsilon}{Dt} = \nabla.\,\boldsymbol{D} - p\nabla.\,\boldsymbol{u} + \Phi, \tag{2.4}$$

where Υ is the specific internal energy, Φ represents the internal generation of heat and $\boldsymbol{D}$ is the diffusive energy flux.

The viscous components of the momentum and thermodynamic equations will be examined further in section 2.6.

Equations (2.2) - (2.4) are the non-approximated governing equations for our fully compressible model and are valid for many equations of state. In undertaking our

analysis we will use various manipulations of these equations alongside our equation of state (2.1). Using our ideal gas equation of state it is straightforward to show that for a perfect gas undergoing a constant volume process the thermodynamic equation can be simplified to

$$\rho \frac{D}{Dt}\left(C_V T\right) = \nabla . \boldsymbol{D} - p \nabla . \boldsymbol{u} + \Phi. \tag{2.5}$$

More detailed discussions on the components of these equations can be found in many classic texts such as Chandrasekhar (1961 [13]) and Batchelor (1967 [6]).

2.3 Gravitational Approximations

Since we have specified a spherical model, with centre of mass at the centre of the sphere, the true gravitational field can be defined as

$$\boldsymbol{g} = -\nabla \Phi_g,$$

and the centrifugal component of the momentum equation is given by

$$\boldsymbol{\Omega} \times \left(\boldsymbol{\Omega} \times \boldsymbol{r}\right) = \nabla \left[\frac{1}{2}\left(\boldsymbol{\Omega} \times \boldsymbol{r}\right)^2\right].$$

We choose to combine these to form an effective gravitational field such that

$$\boldsymbol{g_e} = -\nabla \Phi_e = -\nabla \left[\Phi_g - \frac{1}{2}\left(\boldsymbol{\Omega} \times \boldsymbol{r}\right)^2\right].$$

The momentum equation then becomes

$$\frac{D\,\boldsymbol{u}}{Dt} + 2\boldsymbol{\Omega} \times \boldsymbol{u} + \frac{1}{\rho}\nabla p - \boldsymbol{g_e} - \frac{1}{\rho}\boldsymbol{F} = 0. \tag{2.6}$$

Assuming that mass is distributed in a spherically symmetric manner the true gravitational field acts radially. However the centrifugal acceleration acts perpendicular to the axis of rotation, as a consequence the surfaces of constant Φ_e are not spherical but oblate spheroids. The ellipticity of these oblate spheroids varies across

the fluid zone and is largest at the outer surface. Within a terrestrial regime it is usual for meteorologists to approximate the effective gravitational potential as a function only of radius such that $\Phi_e = \Phi_e(r)$. Braginsky and Roberts (1994 [9]) also take this approach when considering the equations governing convection in the Earth's core. Saumon and Guillot (2004 [53]) note that the rapid rotation of Jovian planets produces a significant deformation of the planet and a non-spherical gravitational field. In considering the terrestrial atmosphere White et al., (2008 [64]) propose an orthogonal curvilinear coordinate system based on oblate spheroids which they find to be a good approximation for the near-Earth geopotentials in so far as Newton's uniform-density model adequately describes the real Earth. We have not found any evidence of the use of this system when modelling the Jovian regime. The breakdown of spherical symmetry within the reference state gives rise to complications and most groups choose to consider the simplified approach of a spherical body with radial gravitational field, thus ignoring the effects of the non-spherical shape of the Jovian planets and the non-radial component of the centrifugal acceleration. Since we are primarily attempting to gain a better understanding of the effects of dynamic approximations, rather than creating a realistic simulation, we choose to consider a spherical body and assume that the effective gravitational field acts radially such that

$$\boldsymbol{g_e} = -g(r)\hat{\boldsymbol{r}}. \tag{2.7}$$

For the remainder of this thesis we will use the convention that when referring to the 'vertical' direction we are referring to a vector acting in the opposite direction to gravity. Horizontal refers to the plane for which 'vertical' is the normal vector.

2.4 Instability

A major source of unstable modes within the Jovian regime is the adverse temperature gradients which, due to the internal heat source, exist within various regions of the

atmosphere and interior. These temperature gradients can lead to instability in the form of free convection. Forced convection can occur when the buoyancy term in the momentum equation can be neglected, for instance when it is small compared with the inertial force; however, as a form of heat transfer it is reliant on fluid motion which is due to some other driving force. It is thought that for large parts of the Jovian regime the predominant transferral of heat is via motion driven by the internal heat source, rather than by fluid motion that would exist in its absence. Forced convection is likely to be an important method of heat transferral in the upper atmosphere but it is thought not to be a predominant driving mechanism for the zonal circulations that are the focus of many studies, as a consequence we choose to focus on free convection in this thesis.

2.4.1 Free convection

If we consider a small fluid parcel in a non-rotating system in which gravity acts vertically, the motion of the parcel will be determined by its buoyancy relative to its surroundings. If the fluid parcel undergoes a vertical adiabatic displacement Δr, it will expand as it moves from a region of higher pressure to a region of lower pressure. The change in density of the fluid parcel is then given by

$$\Delta\rho_{ad} = \left.\frac{\partial\rho}{\partial r}\right|_{ad} \Delta r,$$

and the change in ambient density is given by

$$\Delta\rho = \frac{\partial\rho}{\partial r}\,\Delta r,$$

where subscript *ad* represents the adiabatic displacement and no subscript represents the surroundings. If the parcel is more buoyant than its surroundings it will rise, less buoyant and it will sink. Therefore we have a criterion for instability

$$\Delta\rho_{ad} < \Delta\rho \quad \Rightarrow \quad \frac{\partial\rho}{\partial r} > \left.\frac{\partial\rho}{\partial r}\right|_{ad}. \tag{2.8}$$

We now assume that the fluid expands as it is heated and that the fluid motion is slow, therefore that pressure perturbations equilibriate instantaneously through the production of sound waves. Recalling that we are considering the ideal gas equation as our equation of state, it is obvious that the temperature of the fluid is not conserved. We can then conclude that an equivalent condition for instability is given by

$$\left.\frac{\partial T}{\partial r}\right|_{ad} > \frac{\partial T}{\partial r}. \tag{2.9}$$

We now choose to consider the specific entropy s in order to specify the adiabatic temperature gradient. In meteorolgical applications it is common to refer to the adiabatic lapse rate, this refers to $-\partial T/\partial r|_{ad}$. Using the first and second laws of thermodynamics and our equation of state we find

$$s = C_P \ln T - R \ln p + \text{constant}, \tag{2.10}$$

where we can convert between variables using the equation of state, and the relationship between the specific gas constant R and specific heats at constant pressure C_P and constant volume C_V is

$$R = C_P - C_V.$$

Differentiating (2.10) we see that for an adiabatic displacement, i.e. constant s, we have

$$\left.\frac{C_P}{T}\frac{\partial T}{\partial r}\right|_{ad} = \left.\frac{R}{p}\frac{\partial p}{\partial r}\right|_{ad}.$$

Consideration of a motionless fluid in hydrostatic balance allows us to simplify equation (2.3)

$$\left.\frac{1}{\rho}\,\frac{\partial p}{\partial r}\right|_{ad} = -g,$$

therefore

$$\left.\frac{\partial T}{\partial r}\right|_{ad} = -\frac{g}{C_P}.$$

We are able to substitute this into equation (2.9) to show that instability arises if

$$\frac{\partial T}{\partial r} + \frac{g}{C_P} < 0. \tag{2.11}$$

We note that consideration of (2.10) shows that this criterion, known as the Schwarzchild criterion, can also be written in its familiar entropy form

$$\frac{\partial s}{\partial r} < 0. \tag{2.12}$$

Convective motion tends to stabilise the entropy gradients, thus we would expect that the more effective the convection the smaller the degree of superadiabaticity of the system. However, in order that convective instability is maintained it is necessary that the system remain superadiabatic. With this in mind we chose to follow Gilman and Glatzmaier (1981 [31]) and consider a system in which we define a small parameter ϵ which represents the relative departure of our system from adiabatic.

$$O(\epsilon) \lesssim 10^{-4}, \tag{2.13}$$

where the size of this parameter has been motivated by the size of a similar parameter for the top of the solar convection zone as given in Gilman and Glatzmaier (1981 [31]).

2.4.2 Effect of rotation

The Schwarzchild criterion may not be a sufficient condition for convective motion in a rotating system. Taylor Proudman theorem (see for example Chandrasehkar 1961 [13]) shows that if we consider the special case of a rapidly-rotating, inviscid, incompressible, constant density, steady flow in which the Coriolis force dominates over centrifugal forces and is balanced only by the pressure gradient, then there will be no variation in the motions parallel to the axis of motion. If we have applied a boundary condition stating that $w = 0$ at the boundaries then we would expect there to be no fluid motion parallel to the axis of rotation, and consequentially no convection. This applies to all adverse temperature gradients therefore rotation clearly has a significant effect on the onset of convection. Taylor-Proudman theorem applies

only in a very specific set of circumstances, breaking these conditions clearly allows convective motions to take place with instability criterion dependent on a number of factors. One such condition is the inclusion of a stratified reference state; Taylor-Proudman theorem does not hold in this case. However, many groups assume that, despite the stratified reference state, the rapid-rotation of Jupiter results in the Coriolis force dominating over the destabilising component of the buoyancy force such that convection onsets as tall-thin, helical columns that can be approximated through consideration of Taylor-Proudman theorem. It is believed that compressible, turbulent convection is less likely to demonstrate these properties (see e.g. Glatzmaier et al., (2009 [34]).

2.4.3 Potential temperature form

Since temperature is not conserved during adiabatic displacement of a fluid parcel many groups choose to consider a quantity known as the potential temperature. In defining the dry potential temperature we require that the effect of phase changes of constituents within the system are ignored, stating it to be the temperature that a parcel of dry fluid would have if brought adiabatically and reversibly from its initial state to a standard pressure, p_0

$$\theta = T\left(\frac{p_0}{p}\right)^{R/C_p}. \tag{2.14}$$

For neatness of notation and consistency with other groups we now use $\kappa = R/C_p$.

Using equation (2.10) we can see the potential temperature is related to specific entropy by

$$s = C_p \ln\theta + \text{constant}.$$

Thuburn et al. (2002 [60]) describe how the vertical structure functions of the various thermodynamic variables for free normal modes of a resting atmosphere suggest that the most economic and accurate way in which to compute normal mode solutions

is to use pressure and potential temperature as the thermodynamic prognostic variables rather than density and temperature. Therefore it can be convenient to write the thermodynamic equation (2.5) and mass continuity equation (2.2) in potential temperature and pressure form respectively.

$$C_P \frac{\rho T}{\theta} \frac{D\theta}{Dt} = \Phi + \nabla . \boldsymbol{D}, \tag{2.15}$$

$$\frac{(1-\kappa)}{p} \frac{Dp}{Dt} + \nabla . \boldsymbol{u} = \frac{1}{\theta} \frac{D\theta}{Dt}. \tag{2.16}$$

In this form the rate of change of internal energy due to compression and expansion is taken into account in the material derivative term in the thermodynamic equation.

We note that we only need two of equations (2.2), (2.5), (2.15) or (2.16) alongside the diagnostic equations and the Navier Stokes equation (2.6), to have a complete set. In deriving approximated equation sets, and the subsequent computational analysis, it is convenient to chose equations (2.15) and (2.16). This is also inkeeping with similar analysis undertaken by Davies et al. (2003 [18]), though they chose to use the Exner pressure form of equation (2.16).

2.5 Perturbation and Linearisation

As motivated in chapter 1 we will consider normal mode solutions for linearised equation sets, in doing so considering only infinitesimal perturbations to an initial reference system. The form this reference state takes in itself poses significant issues, but it is essential that it is itself a solution to the governing equations. Possible ways to proceed include considering a fixed initial state which remains unaffected by the perturbations or considering a mean atmosphere which is obtained by averaging the initial and perturbed states over a spherical surface for a given value of r and t. The most accurate method would be to consider a mean atmosphere as a reference state, however this adds significant complexity as it is then necessary to consider the

time-dependent modification of the mean atmosphere and its effect on the governing equations. In deriving an anelastic equation set to model solar convection Gilman and Glatzmaier (1981 [31]) justify their use of a time-independent reference state by stating that the difference between the mean state and the initial state will be no larger than the convective perturbations themselves. Assuming that eddy motion is $O(\epsilon)$, changes to the mean atmosphere will be $O(\epsilon^2)$, therefore consideration of a time independent reference state is justified if ϵ is small.

We choose to use a time-independent, motionless, hydrostatic reference state, denoting perturbations by a prime ' and the basic state by subscript s. We assume that the basic state variables are spatially functions only of radius and assume no approximation regarding the size of the perturbation terms at this stage. State variables f are then written

$$f(\lambda\,,\,\phi\,,\,r,\,t) = f_s(r) + f'(\lambda\,,\,\phi\,,\,r\,,\,t).$$

We have chosen to consider a reference state at rest; thus, non-zero velocity is a perturbation on the reference state and we have dropped the prime on velocity perturbations for consistency with other groups.

The diagnostic equations for this reference state are

$$p_s = \rho_s R T_s, \tag{2.17}$$

$$\theta_s = T_s \left(\frac{p_0}{p_s}\right)^{\kappa}, \tag{2.18}$$

and the hydrostatic condition gives

$$\frac{dp_s}{dr} = -\rho_s g. \tag{2.19}$$

Differentiating equation 2.18 with respect to radius shows that the reference state values are related such that

$$\frac{(1-\kappa)}{p_s}\frac{\partial p_s}{\partial r} = \frac{1}{\theta_s}\frac{\partial \theta_s}{\partial r} + \frac{1}{\rho_s}\frac{\partial \rho_s}{\partial r} \tag{2.20}$$

At this stage it is useful to define the buoyancy frequency N. This is the natural frequency at which a tall, thin parcel of fluid will oscillate when displaced vertically in statically stable surroundings.

$$N^2 = \frac{g}{\theta_s}\frac{\partial \theta_s}{\partial r}. \tag{2.21}$$

This is also known as the Brunt-Väisälä frequency. We also note that the speed of sound in the reference state C_s, is given by

$$C_s^2 = \frac{RT_s}{(1-\kappa)} \quad \Rightarrow \quad \frac{(1-\kappa)}{p_s}\frac{\partial p_s}{\partial r} = -\frac{g}{C_s^2}. \tag{2.22}$$

Therefore the density scale height $H_\rho = \left[-1/\rho_s \left(\partial \rho_s/\partial r\right)\right]^{-1}$ can be written as

$$\frac{1}{H_\rho} = -\frac{1}{\rho_s}\frac{\partial \rho_s}{\partial r} = \left(\frac{g}{C_s^2} + \frac{N^2}{g}\right). \tag{2.23}$$

The nonlinear fully compressible equations governing the perturbations are then as follows: the mass continuity equation in its pressure form

$$\frac{(1-\kappa)}{(p_s+p')}\left(\frac{Dp'}{Dt} + \boldsymbol{u}.\nabla p_s\right) + \nabla.\boldsymbol{u} = \frac{1}{(\theta_s+\theta')}\left(\frac{D\theta'}{Dt} + \boldsymbol{u}.\nabla\theta_s\right); \tag{2.24}$$

the momentum equations

$$(\rho_s+\rho')\left(\frac{Du}{Dt} + 2\Omega w\cos\phi - 2\Omega v\sin\phi + \frac{uw}{r} - \frac{uv\tan\phi}{r}\right) + \frac{1}{r\cos\phi}\frac{\partial p'}{\partial \lambda} - F_\lambda = 0, \tag{2.25}$$

$$(\rho_s+\rho')\left(\frac{Dv}{Dt} + 2\Omega u\sin\phi + \frac{vw}{r} + \frac{u^2\tan\phi}{r}\right) + \frac{1}{r}\frac{\partial p'}{\partial \phi} - F_\phi = 0, \tag{2.26}$$

$$(\rho_s+\rho')\left(\frac{Dw}{Dt} - 2\Omega u\cos\phi - \frac{(u^2+v^2)}{r}\right) + \rho' g + \frac{\partial p'}{\partial r} - F_r = 0; \tag{2.27}$$

the thermodynamic equation

$$C_P\left(\rho_s+\rho'\right)\left(T_s+T'\right)\left(\frac{D\theta'}{Dt} + \boldsymbol{u}.\nabla\theta_s\right) = \left(\theta_s+\theta'\right)\left(\Phi + \nabla.\boldsymbol{D}\right). \tag{2.28}$$

2.5.1 Linearisation

Modelling non-linear fluid motion introduces significant complexity. Whilst non-linear components of the governing equations are likely to have a considerable impact within the Jovian atmosphere and interior, it is essential to have a strong understanding of the linear regime before progress can be made in modelling the non-linear system. In this thesis we choose to concentrate solely on the linear regime.

The fully compressible equation set is linearised by considering perturbations to be small, therefore we neglect terms involving products of perturbations. Expansion of the equations of state into perturbed and reference state variables and the use of the equations of state governing the reference state, (2.17) and (2.18), allows the following relationships between perturbation variables

$$\frac{p'}{p_s} = \frac{\rho'}{\rho_s} + \frac{T'}{T_s} \quad \text{and} \quad \frac{\theta'}{\theta_s} + \frac{\rho'}{\rho_s} = (1-\kappa)\frac{p'}{p_s}. \tag{2.29}$$

The non-linear mass continuity equation, (2.24), is linearised to become

$$\frac{(1-\kappa)}{p_s}\frac{\partial p'}{\partial t} + \frac{w}{\theta_s}\frac{\partial \theta_s}{\partial r} + \frac{w}{\rho_s}\frac{\partial \rho_s}{\partial r} + \nabla.\,\boldsymbol{u} = \frac{1}{\theta_s}\left(\frac{\partial \theta'}{\partial t} + w.\nabla\theta_s\right). \tag{2.30}$$

The non-linear momentum equations, (2.25)-(2.27), become

$$\frac{\partial u}{\partial t} + 2\Omega w\cos\phi - 2\Omega v\sin\phi + \frac{1}{r\rho_s\cos\phi}\frac{\partial p'}{\partial \lambda} - \frac{F^\star_\lambda}{\rho_s} = 0, \tag{2.31}$$

$$\frac{\partial v}{\partial t} + 2\Omega u\sin\phi + \frac{1}{r\rho_s}\frac{\partial p'}{\partial \phi} - \frac{F^\star_\phi}{\rho_s} = 0, \tag{2.32}$$

$$\frac{\partial w}{\partial t} - 2\Omega u\cos\phi + (1-\kappa)\frac{p'}{p_s}g - \frac{\theta'}{\theta_s}g + \frac{1}{\rho_s}\frac{\partial p'}{\partial r} - \frac{F^\star_r}{\rho_s} = 0, \tag{2.33}$$

where $F^\star$ represents the linearised viscous terms. The non-linear thermodynamic equation, (2.28), becomes

$$\frac{\partial \theta'}{\partial t} + w\frac{\partial \theta_s}{\partial r} = \frac{\theta_s}{C_P\rho_s T_s}\left[\Phi^\star + (\nabla.\boldsymbol{D})^\star\right]. \tag{2.34}$$

where $\Phi^\star$ and $(\nabla.\boldsymbol{D})^\star$ represent linearised versions of the viscous and diffusive terms. We note that linearisation removes the metric terms in the momentum equation

and the advection of perturbed variables in each of the governing equations. It is important to remember that both the linear and non-linear equation sets would have further terms if we allowed our basic state to vary with time.

2.6 Viscous and Diffusive Terms

In determining the form of the viscous terms in both the momentum and thermodynamic equations we assume that the fluid is Newtonian. For a more complete derivation of the viscous terms see classic texts such as Batchelor (1967 [6]), the outcome of which shows that the viscous component of the momentum equation is given, in index notation, by

$$\boldsymbol{F} = \nu \frac{\partial}{\partial x_j} \rho \left(\frac{\partial u_i}{\partial x_j} + \frac{\partial u_j}{\partial x_i} \right) - \nu \frac{2}{3} \frac{\partial}{\partial x_i} \rho \frac{\partial u_j}{\partial x_j}. \tag{2.35}$$

This form of the viscous foce corresponds to a constant kinematic viscosity ν. An alternative, not explored in this thesis, would be to choose constant dynamic viscosity, $\mu = \rho\nu$. In many applications the viscosity will be a turbulent viscosity, whose precise form is uncertain, but the present form has the advantage of simplicity. Brito et al. (2004 [10]) suggest that the mean contribution of the Reynolds stress term which occurs in a turbulent system, can be represented by considering an effective viscosity in place of the molecular viscosity. The increase in significance of the viscous terms aims to compensate for neglecting the inertial terms. According to Frisch (1995 [30]) this analogy between effective and molecular momentum transport appears clearly in Lamb (1931 [44]) and is suggested in texts prior to this. For fully convective flows this effective viscosity is significantly larger than the molecular viscosity such that molecular viscosity is insignificant. Experimental work by Brito et al. (2004 [10]) has lent weight to this argument, as have computational geodynamo simulations at relatively high Ekman numbers (Jones 2000 [41], Olson et al. 1999 [49]).

The viscous regeneration of heat in the thermodynamic equation is given by

$$\Phi = 2\rho\nu_m \left(e_{ij}e_{ij} - \frac{1}{3}(\nabla . \boldsymbol{u})^2 \right), \tag{2.36}$$

where,

$$e_{ij} = \frac{1}{2}\left(\frac{\partial u_i}{\partial x_j} + \frac{\partial u_j}{\partial x_i} \right), \tag{2.37}$$

and again, a more detailed explanation can be found in various classic texts. The viscous regeneration of heat is inherently quadratic therefore is neglected when considering linearised equation sets.

It is widely accepted that the form of the diffusive energy flux in the thermodynamic equation is likely to be Fickian; a gradient of the prescribed variable multiplied by some coefficient of proportionality. When an electrically insulating fluid is in a steady state the main contibutors to this diffusive flux are radiation and conduction. In modelling the gas giants it is common to ignore the radiative terms, thus D can be modelled simply according to Fourier's law of conduction

$$D = k\rho C_P \nabla T, \tag{2.38}$$

where k is the coefficient of thermal diffusivity. The form this coefficient should take remains a subject of debate, it can be modelled as a constant or a function of position or velocity. The combined term $k\rho C_P$ is known as the thermal conductivity. Evonuk and Glatzmaier (2004 [27]) consider a similar term to model radiation, however they set the radiative diffusivity to be zero in the modelled convective zone.

Within astrophysical applications it is common to assume that molecular viscosity is sufficiently small that F and Φ will cause no discernible dissipation of energy or damping of normal modes. The Jovian thermosphere is an exception to this, however we do not choose to study this region of the atmosphere. It is also hypothesised that turbulence will give rise to a diffusion of entropy that is much larger than the molecular conductivity term in the thermodynamic equation. In comparing normal-mode solutions of approximated sets with solutions to a fully-compressible set we

concentrate on the inviscid sets. In chapter 7 we extend incompressible Boussinesq analysis to a compressible case, thus we discuss this turbulent diffusion in more detail in section 7.1.

2.7 Boundary Conditions

The application of boundary conditions can have a large impact on the actual motions which occur within a regime, particularly those closest to the boundaries. The exact boundary conditions appropriate to a Jovian regime are unknown, and are likely to remain so given the complexity of the planetary atmosphere and interior; we have seen in section 2.1 that there is no well defined boundary within the Jovian regime, however the application of boundary conditions is often essential in modelling the various regions of the interior and atmosphere. The most appropriate boundary conditions depend on the dynamical process that is being modelled or investigated. In this section we will discuss various possible boundary conditions, postponing a decision about which to use until a later stage.

We assume that no fluid leaves the model therefore considering impenetrable inner and outer boundaries, the kinematic boundary condition reduces to no normal flow at these surfaces, $w = 0$ at r_C and r_S. This is unlikely to be a realistic condition, particularly at the inner surface. However, the use of these conditions significantly simplies the analysis and numerical modelling and they are used by the majority of groups. Various groups have considered penetrative convection though we chose not to consider it in this thesis.

We choose to follow Jones et al. (submitted 2008 [38]) in considering the case in which s', and therefore θ', is equal to zero at the boundaries. We will see in chapter 7 that this allows proof that there will be no growing modes for negative Rayleigh number, thus allowing us to refer to the case in which $N^2 > 0$, as a stably

stratified regime. It is possible that with other entropy boundary conditions negative Rayleigh number instability can occur, thus fixing the entropy (and therefore potential temperature) at the boundaries allows us to limit growing mode solutions only to those which occur due to unstable stratification.

2.7.1 Rigid Surfaces

In the case in which a fluid is bounded by a rigid surface we apply no-slip conditions, specifically, that there is no tangential flow on the surface. Alongside the condition that there is no normal flow at the surfaces we then have

$$u = v = w = 0 \quad \text{at that surface.} \tag{2.39}$$

2.7.2 Free-Slip Surfaces

If we consider a viscous fluid at a horizontal free-slip boundary we require that the tangential viscous stresses, $\rho\nu\tau_{r\lambda}$ and $\rho\nu\tau_{r\phi}$, are zero at the boundary. The expressions for these tangential stresses are

$$\rho\nu\tau_{r\lambda} = \rho\nu\left(\frac{1}{r\cos\phi}\frac{\partial w}{\partial\lambda} + \frac{\partial u}{\partial r} - \frac{u}{r}\right), \tag{2.40}$$

$$\rho\nu\tau_{r\phi} = \rho\nu\left(\frac{1}{r}\frac{\partial w}{\partial\phi} + \frac{\partial v}{\partial r} - \frac{v}{r}\right). \tag{2.41}$$

Combining these expressions with the no normal flow condition and the no tangential stress condition we find that

$$r\frac{\partial}{\partial r}\left(\frac{u}{r}\right) = r\frac{\partial}{\partial r}\left(\frac{v}{r}\right) = 0 \quad \text{at that surface.} \tag{2.42}$$

The boundary conditions for a stress-free surface are then

$$\frac{\partial}{\partial r}\left(\frac{u}{r}\right) = \frac{\partial}{\partial r}\left(\frac{v}{r}\right) = w = 0 \quad \text{at that surface.} \tag{2.43}$$

It is also important that when we consider the equations in the terrestrial coordinate system we ensure that they remain non-singular at the poles.

2.8 Energetics

Since we will be comparing approximated equation sets to the linearised fully-compressible equation set it is necessary for us to consider the energetics of these sets in order to ensure that conservation properties are retained.

Taking scalar product of $\rho_s \boldsymbol{u}$ with the vector form the momentum equation (2.31)-(2.33) gives

$$\frac{\partial}{\partial t}\left[\rho_s \frac{(u^2+v^2+w^2)}{2}\right] + \boldsymbol{u}\,.\nabla p' - \boldsymbol{u}\,.\boldsymbol{F} + \left[(1-\kappa)\frac{p'}{p_s} - \frac{\theta'}{\theta_s}\right]\rho_s w g = 0. \tag{2.44}$$

The scalar product of $\rho_s g^2\theta'/(N^2\theta_s^2)$ with the thermodynamic equation (2.34) yields

$$\frac{\partial}{\partial t}\left(\frac{\rho_s}{2}\frac{g^2}{N^2}\left|\frac{\theta'}{\theta_s}\right|^2\right) + \rho_s w g \frac{\theta'}{\theta_s} = \rho_s \frac{g^2}{N^2\theta_s}\frac{\theta'}{\theta_s}Q. \tag{2.45}$$

Taking the scalar product of p' with the mass continuity equation (2.30) yields

$$\frac{\partial}{\partial t}\left(\frac{1}{2\rho_s}\frac{|p'|^2}{C_s^2}\right) + \frac{p' w N^2}{g} + \frac{p' w}{\rho_s}\frac{\partial \rho_s}{\partial r} + p'\nabla.\,\boldsymbol{u} = \frac{p'}{\theta_s}Q. \tag{2.46}$$

Summing equations (2.44) - (2.46) we find

$$\frac{\partial E}{\partial t} + \nabla.(p'\,\boldsymbol{u}) - \Lambda - \boldsymbol{u}\,.\boldsymbol{F} = 0, \tag{2.47}$$

where E represents the total perturbation energy density given by the sum of the kinetic, thermobaric and elastic perturbation energies

$$E = \frac{\rho_s}{2}\left(|u|^2 + |v|^2 + |w|^2 + \frac{g^2}{N^2}\left|\frac{\theta'}{\theta_s}\right|^2 + \frac{|p'|^2}{\rho_s^2 C_s^2}\right), \tag{2.48}$$

and

$$\Lambda = \left(\rho_s \frac{g^2}{N^2\theta_s}\frac{\theta'}{\theta_s} + \frac{p'}{\theta_s}\right)Q. \tag{2.49}$$

The transfer of energy between thermal and kinetic through the work done by bouyancy forces is sucessfully accounted for as the terms involved cancel where appropriate. We will see in chapter 7 that there can be no convective instability for negative Rayleigh number. Rayleigh number is a dimensionless quantity which can be veiwed as the

ratio of buoyancy forces to the product of thermal and momentum diffusivities and is negative only when $\partial s/\partial r > 0$. Changing variable from entropy to potential temperature does not affect the physics of the problem and the equation sets considered do not differ considerably; therefore, it is likely that the result given in chapter 7 will also apply to the equations in their potential temperature form and we would expect that there will also be no unstable modes for reference states in which $N^2 > 0$.

2.8.1 Rescaled Variables

Our equation for the total perturbation energy density (2.48) motivates a rescaling of our perturbed variables. Each term within this equation is multiplied by a factor of ρ_s, therefore following Daley (1988 [17]) it is useful to remove some of the effect of decreasing density with radius by defining new variables proportional to the square root of their contribution to the perturbation energy. This reduces the range of values used in computational analysis, which in turn is beneficial when numerically calculating eigenfunctions. Our rescaled variables are then

$$\boldsymbol{U} = (U,\, V,\, W) = \rho_s^{1/2}(u,\, v,\, w) = \rho_s^{1/2}\,\boldsymbol{u}\,, \quad \Theta = \rho_s^{1/2}\frac{\theta'}{\theta_s} \quad \text{and} \quad P = \rho_s^{-1/2}p' \tag{2.50}$$

Multiplying all equations by $\rho_s^{1/2}$ and considering the forementioned rescaling of variables we produce the following rescaled inviscid equation sets.

$$\frac{1}{C_s^2}\frac{\partial P}{\partial t} + \frac{W}{\theta_s}\frac{\partial \theta_s}{\partial r} + \frac{W}{2\rho_s}\frac{\partial \rho_s}{\partial r} + \nabla.\boldsymbol{U} = 0, \tag{2.51}$$

$$\frac{\partial U}{\partial t} + 2\Omega W\cos\phi - 2\Omega V\sin\phi + \frac{1}{r\cos\phi}\frac{\partial P}{\partial \lambda} = 0, \tag{2.52}$$

$$\frac{\partial V}{\partial t} + 2\Omega U\sin\phi + \frac{1}{r}\frac{\partial P}{\partial \phi} = 0, \tag{2.53}$$

$$\frac{\partial W}{\partial t} - 2\Omega U\cos\phi + \frac{\partial P}{\partial r} + \frac{P}{C_s^2}g + \frac{P}{2\rho_s}\frac{\partial \rho_s}{\partial r} - \Theta g = 0, \tag{2.54}$$

$$\frac{\partial \Theta}{\partial t} + \frac{W}{\theta_s}\frac{\partial \theta_s}{\partial r} = 0. \tag{2.55}$$

2.8.2 Rescaled Boundary Conditions

Since we have rescaled the governing equations we must also rescale the boundary conditions.

Rigid Surfaces

$$U = V = W = 0 \quad \text{at that surface.} \tag{2.56}$$

Free-Slip Surfaces

$$W = \frac{\partial}{\partial r}\left(\frac{U}{r\rho_s^{1/2}}\right) = \frac{\partial}{\partial r}\left(\frac{V}{r\rho_s^{1/2}}\right) = 0 \quad \text{at that surface.} \tag{2.57}$$

2.9 Reference Profiles

We have previously discussed that in considering linearised and perturbed equation sets we will expand about a reference state that is hydrostatic and independent of time. We then have several options available to define the reference profiles for the thermodynamic variables. We choose to consider an analytically tractable isothermal basic state and a more realistic polytropic basic state. The analytic tractability means that isothermal reference states are often considered in numerical modelling of the terrestrial atmosphere while polytropic models have been sucessfully used by several groups, including Jones et al. (submitted 2008 [38]) and Evonuk and Glatzmaier (2006 [29]), as a means of defining reference state profiles for modelling the convection zones of Gas Giants and stars.

2.9.1 Parameter Regime

We choose to concentrate specifically on a Jovian regime and thus use appropriate parameters. The specific gas constant $R = 3600\text{J kg}^{-1}\text{ K}^{-1}$ and the rate of angular rotation $\Omega = 1.74 \times 10^{-4} s^{-1}$ are taken from Vasavada and Showman (2005 [62]). The specific heat at constant pressure $C_p = 1.13 \times 10^4\text{ J kg}^{-1}\text{ K}^{-1}$ is taken from Baker and Schubert (1998 [3]). This suggests $\kappa \approx 0.32$.

Since Jupiter is a largely gaseous planet it is difficult to define an outer surface. If we define the surface to be at 1 bar pressure level then Jupiter is not a spherical planet; the polar radius of Jupiter is given by Vasavada and Showman (2005 [62]) to be $66,854$km whilst the equatorial radius is given to be $71,492$km. For convenience we consider an outer surface radius of $r_S = 70,000$km at 1 bar pressure level. We set the total mass of the model to be $M_s = 1.8 \times 10^{27}$kg similar to that given by various groups including Guillot (1999 [33]). When considering constant gravitational field we use a value similar to that used in Baker and Schubert (1998 [3]), $g_0 = 23\,\text{m s}^{-2}$; when considering variable gravitational field we use the standard calculations based on mass and radius.

2.9.2 Isothermal Reference State

An isothermal reference state is a physically unrealistic profile for the convective regions within the Jovian interior, however it will allow analytic analysis of the governing equations which will provide useful reference results for later computational analysis.

An isothermal reference state also holds particular relevance when considering the upper atmosphere of Jupiter. According to Seiff et al. (1997 [54]) the atmospheric region between 12 and 0.003 mb maintains a constant temperature of approx 160 K and lies between approx 80-300km altitude relative to a lower surface at 71350km.

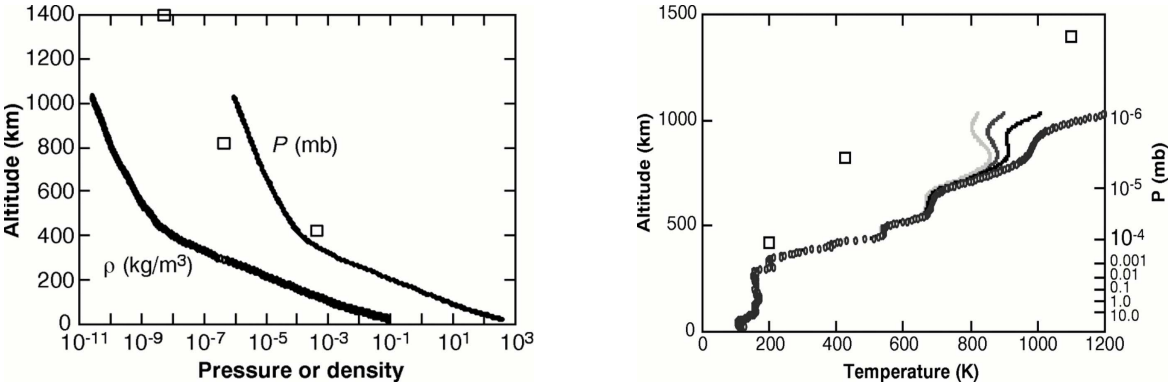

Figure 2.2: *Densities, pressures and temperatures for the atmosphere of Jupiter derived by Seiff et al. (1997 [54]) using data from the Galileo probe. This assumes a surface at radius of 71350 km.*

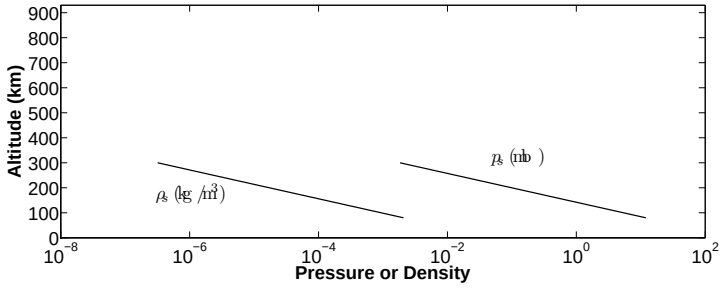

Figure 2.3: *Model isothermal reference profile for $g = g_0$. The isothermal model is only applicable between 80km and 300km altitude.*

Seiff et al. (1997 [54]) used measurements of the deceleration of the Galileo probe to produce density and pressure profiles up to 1000km altitude. Assuming an ideal gas equation of state and four possible upper boundary temperatures they produce temperature profiles which converge to within ±15K at 700km altitude as shown in Fig. 2.2. Examination of the profile shows clearly the isothermal region of interest. These figures are supported by similar analysis by Yelle et al. (1996 [65]).

Setting reference state temperature to be constant allows manipulation of the equation of state to yield the following relationships

$$\frac{1}{\rho_s}\frac{\partial \rho_s}{\partial r} = \frac{1}{p_s}\frac{\partial p_s}{\partial r}, \quad \frac{1}{\theta_s}\frac{\partial \theta_s}{\partial r} = -\frac{\kappa}{p_s}\frac{\partial p_s}{\partial r}. \tag{2.58}$$

Our assumption of a hydrostatic reference state then yields

$$\frac{\partial p_s}{\partial r} = -\rho_s g \;\Rightarrow\; \frac{1}{p_s}\frac{\partial p_s}{\partial r} = -\frac{g}{RT_s}. \tag{2.59}$$

This allows us to define the scale height H of the reference state to be

$$H \equiv \frac{RT_s}{g}. \tag{2.60}$$

If g = constant we set $z = 0$ to be at $z = r_C$, thus the outer surface of the spherical shell will now be at $z = r_S - r_C$. We are then able to write our reference state values in exponential form

$$\theta_s(z) = \theta_C \exp(\kappa z/H), \quad \rho_s(z) = \rho_C \exp(-z/H), \quad p_s(z) = p_C \exp(-z/H), \tag{2.61}$$

where subscript C denotes the value of the variable at the inner surface of the spherical shell. It is not possible to find analytic solutions to the governing equations using non-constant gravitational field, these will be considered during numerical analysis.

In order to create a reference profile for the isothermal portion of the upper atmosphere of Jupiter we set $r_C = 71430\,\mathrm{km}$, $r_S - r_C = 220\,\mathrm{km}$, $T_s = 160\,\mathrm{K}$ and using parameters described previously we calculate $H \sim 2.5 \times 10^4\,\mathrm{m} \sim 25\,\mathrm{km}$. The resulting profile is displayed in figure 2.3, it shows reasonable agreement with the isothermal section of the profile produced by Seiff et al. (1997 [54]). It is also worth noting that over this region the maximum expected variation in gravitational field is less than 1%, therefore we expect this to have little effect on the normal mode solutions.

2.9.3 Polytropic Reference State

The concept of polytropes and polytropic fluids was developed early in the study of stellar structure (see e.g. Collins, 1989 [16]). The polytropic equations of state are motivated by the fact that fully convective systems are efficient at transporting entropy through eddy diffusion processes, which we have seen can be accounted for

even in a linearised equation set. It is then reasonable to assume that these systems are close to adiabatic, the behaviour of a perfect gas can then be generalised such that a relationship between pressure and density can be produced. The specific entropy can be defined as

$$s = C_p \left(\frac{1}{\gamma} \ln p - \ln \rho \right) + \text{constant}, \tag{2.62}$$

where γ is the ratio of specific heats C_p/C_v. If we consider isentropic flow we then have

$$\frac{1}{\gamma p} \frac{dp}{dr} = \frac{1}{\rho} \frac{d\rho}{dr}, \tag{2.63}$$

leading to the relationship

$$p \propto \rho^{\gamma}. \tag{2.64}$$

This relationship was extended by various groups to allow modelling of superadiabatic and subadiabatic systems by introducing a polytropic index, n such that equation (2.64) becomes

$$p = A\rho^{1+1/n}, \tag{2.65}$$

where A is a constant. This assumption is best suited to systems that are close to adiabatic. For isentropic systems $(n+1)/n = \gamma$. We will be investigating a regime which is only marginally superadiabatic, therefore the polytropic assumption is reasonable.

2.9.4 Constant mass model

In modelling the outer regions of the interior or atmosphere of the Jovian regime it is common to use a spherical shell model in which the effective mass of the planet is contained within the inner sphere; hence assuming the mass of the fluid within the spherical shell is neglected. This corresponds to a gravity profile within the shell such that $g \propto 1/r^2$. This model has been used by various groups seeking to gain insight into the dynamics of convection within spherical shells (see e.g. Jones et al.,

submitted 2008 [38]). In finding a solution to equation (2.65) it is convenient to set $A = p_0/(\rho_0^{(1+1/n)})$. We can then show that

$$\rho_s = \rho_0 \left(\frac{GM_0\rho_0}{r(n+1)p_0} + c_0 \right)^n, \tag{2.66}$$

where c_0 is a constant, $G = 6.67 \times 10^{-11} m^3 kg^{-1} s^{-2}$ is the constant of gravitation and we have assumed that the gravity field is governed by Newtons law of universal gravitation.

Then

$$T_s = \frac{p_0}{R\rho_0} \left[\frac{GM_0\rho_0}{r(n+1)p_0} + c_0 \right] = T_0 \left[\frac{GM_0\rho_0}{r(n+1)p_0} + c_0 \right], \tag{2.67}$$

so density, pressure and potential temperature can all be written in terms of temperature as follows

$$\rho_s = \rho_0 \left(\frac{T_s}{T_0} \right)^n, \quad p_s = p_0 \left(\frac{T_s}{T_0} \right)^{n+1} \quad \text{and} \quad \theta_s = T_s \left(\frac{T_0}{T_s} \right)^{\kappa(n+1)}. \tag{2.68}$$

We then follow Jones et al. (submitted 2008 [38]) in supposing that N_ρ is the number of density scale heights within the polytrope such that $\rho_C/\rho_S = \exp(N_\rho)$. We are then able to show that

$$c_0 = -\frac{GM_0\rho_0}{(n+1)p_0 r_S} \left[\frac{\exp(N_\rho/n) - r_S/r_C}{\exp(N_\rho/n) - 1} \right]. \tag{2.69}$$

Therefore specifying the density scale factor N_ρ means that T_s is completely defined. Calculations show that the effect of increasing density scale factor on reference state temperature decreases rapidly with increasing density scale factor. For consistency with Jones et al. (submitted 2008 [38]) we choose to consider $N_\rho = 2$ and $N_\rho = 5$; it is not known whether these are realistic values for the Jovian regime, however they will offer the opportunity to assess the impact of small and large density variation on the various approximated equation sets. For $N_\rho = 2$ the reference density at the inner surface is approximately 7 times larger than the reference density at the outer surface, for $N_\rho = 5$ the reference density at the inner surface is approximately 150

times larger than the reference desity at the outer surface. It is clear that N_ρ measures the departure from a uniform density reference state, thus the limit $N_\rho \to 0$ represent the Boussinesq models that have historically been used to investigate the onset of convection within the Jovian regime.

Since we will be dealing with derivatives we do not need to assign values to ρ_0 and T_0 as the vertical derivatives are given by

$$\begin{aligned} \frac{1}{\rho_s}\frac{\partial \rho_s}{\partial r} = \frac{n}{T_s}\frac{\partial T_s}{\partial r}, \quad \frac{1}{p_s}\frac{\partial p_s}{\partial r} = \frac{(n+1)}{T_s}\frac{\partial T_s}{\partial r} \\ \text{and} \quad \frac{1}{\theta_s}\frac{\partial \theta_s}{\partial r} = \frac{[1-\kappa(n+1)]}{T_s}\frac{\partial T_s}{\partial r}. \end{aligned} \tag{2.70}$$

The unstably stratified regime is intended to be representative of the interior and interior atmosphere; thus, in line with Jones et al. (submitted 2008 [38]), we set $n = 2$. They explain that this value is motivated by the fact that according to models of Jupiter's atmosphere n varies from approximately 1 near the region in which there is a transition from metallic to molecular hydrogen, to 3 nearer the outer surface.

Lane-Emden Equation

The other popular method of defining a polytropic profile is to solve a coupled system involving a hydrostatic reference state, the polytropic equation of state and the Newtonian equation for gravitational field. This form of profile is not commonly used in modelling the outer region of the Jovian regime as it is considerably more complex than the constant mass model described in the previous section. The Lane-Emden profile is used to great effect in modelling stellar convection.

In deriving the Lane-Emden equation we consider a fluid filled sphere rather than a spherical shell.

We have assumed a motionless, hydrostatic reference state, thus

$$\frac{dp_s}{dr} = -\rho_s g. \tag{2.71}$$

Combining this with the polytropic assumption yields

$$\left(\frac{n+1}{n}\right) A\rho_s^{1/n}\frac{\partial\rho_s}{\partial r} = -\rho_s g. \tag{2.72}$$

Assuming a general mass profile $M(r) = 4\pi\int_0^r \rho_r r^2 dr$ and Newtonian gravitational field (in our equation sets this would mean ignoring all centrifugal effects), this leads to

$$\frac{1}{r^2}\frac{d}{dr}\left[\frac{r^2}{\rho_s}\left(\frac{n+1}{n}\right) A\rho_s^{1/n}\frac{d\rho_s}{dr}\right] = -4\pi G\rho_s. \tag{2.73}$$

where $G = 6.67\times10^{-11}\mathrm{m}^3\ \mathrm{kg}^{-1}\mathrm{s}^{-2}$ is the gravitational constant. We then define two dimensionless variables ξ and χ

$$\xi = r\left(\frac{4\pi G\rho_c^2}{(n+1)p_c}\right)^{1/2} \quad \text{and} \quad \chi = \left(\frac{\rho_s}{\rho_c}\right)^{1/n}, \tag{2.74}$$

where subscript c refers to the value of the variable at the centre of the sphere. This allows us to write (2.73) in non-dimensional form as

$$\frac{1}{\xi^2}\frac{d}{d\xi}\left(\xi^2\frac{d\chi}{d\xi}\right) + \chi^n = 0. \tag{2.75}$$

Boundary conditions for this equation are

$$\rho_s = \rho_c \text{ at } r = \xi = 0 \quad \text{and} \quad \lim_{r\to0}\frac{M(r)}{r^2} = 0 \Rightarrow \frac{d\chi}{d\xi} = 0 \text{ at } \xi = 0 \tag{2.76}$$

The Lane-Emden equation can only be solved analytically for $n = 0$, $n = 1$ and $n = 5$.

$$\chi = 1 - \frac{\xi^2}{6} \quad \text{for} \quad n = 0, \tag{2.77}$$

$$\chi = \frac{\sin\xi}{\xi} \quad \text{for} \quad n = 1, \tag{2.78}$$

$$\chi = \left(1 + \frac{\xi^2}{3}\right)^{-1/2} \quad \text{for} \quad n = 5. \tag{2.79}$$

Figure 2.4 shows the analytic solutions for $n = 0$, $n = 1$ and $n = 5$ and the numerically deduced solutions for $n = 2$, $n = 3$ and $n = 4$. The value of ξ at which $\chi = 0$ represents the outer surface of the model and is therefore denoted by subscript

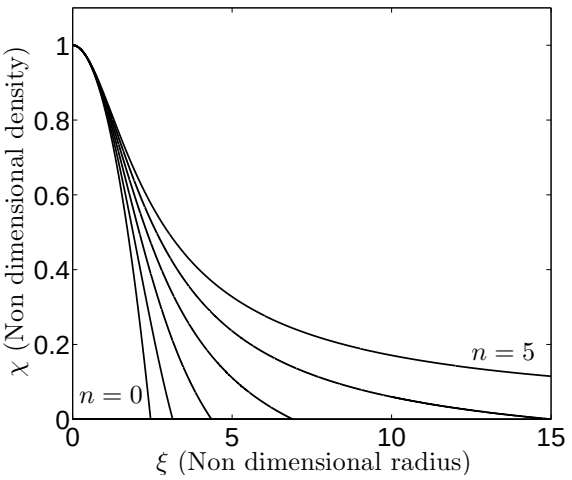

Figure 2.4: *Lane-Emden Solutions, from left to right* $n = 0$ *to* $n = 5$

S. We note that the $n = 5$ solution is asymptotic to $\chi = 0$, therefore this represents the case in which we never reach $\rho_s = 0$ thus no defined outer surface, this is also the case for all $n > 5$. Figure 2.4 also shows that the smaller the value of the polytropic index the more centrally condensed the model will be.

We chose a value for the radius of our model and are able to determine the value of ξ_S using linear interpolation, we are therefore able to convert our non-dimensional radius into actual radius

$$\frac{r_S}{\xi_S} = \left[\frac{(n+1)p_C}{4\pi G\rho_C^2}\right]^{1/2} = \left[\frac{A(n+1)}{4\pi G\rho_C^{(n-1)/n)}}\right]^{1/2} \qquad \Rightarrow \quad r = r_S\frac{\xi}{\xi_S}. \tag{2.80}$$

In order to calculate a value for ρ_C we consider the mean density ρ_m

$$\rho_m = \frac{3M_S}{4\pi r_S^3} = -3\rho_C\,\frac{1}{\xi}\frac{\partial\chi}{\partial\xi}\bigg|_S, \tag{2.81}$$

where we have calculated $\partial\chi/\partial\xi$ as a function of ξ whilst finding solutions to equation (2.73). This allows us to calculate the actual density profile of our model. We are also able to find the value of A since we now have values for all the other coefficients in (2.80). The basic state pressure is then

$$p_s = A\rho_s^{(n+1)/n} = A\rho_C^{(n+1)/n}\chi^{n+1}, \tag{2.82}$$

and assuming an ideal equation of state we have

$$T_s = \frac{p_s}{R\rho_s} = \frac{A}{R}\rho_c^{1/n}\chi. \tag{2.83}$$

We can calculate the mass profile and gravitational field using

$$M(r) = -4\pi\left(\frac{r_s}{\xi_s}\right)^3 \rho_c \xi^2 \frac{\partial\chi}{\partial\xi}, \qquad g = \frac{GM(r)}{r^2}. \tag{2.84}$$

2.10 Summary

In this chapter we have defined our fully compressible model, from which we will create approximated equations sets. The fully compressible model will provide the reference solutions which will allow us to compare the relative accuracy of the various approximated equation sets. We have also defined reference state profiles, which in contrast to other studies (Jones et al., submitted 2008 [38], Evonuk and Glatzmaier, 2006 [29]), are the same for all approximated equation sets.

Chapter 3

Approximated Equation Sets

In the previous chapter we have described the governing equations for a linearised, fully compressible equation set and defined the reference state profiles for our model. In deriving approximated equation sets we will consider the fully compressible equations and undertake scale analysis in order to determine terms which can be neglected, thus simplifying the equation sets. It is possible to use separate basic states for deriving approximated equation sets and perturbation equations, however it is common, and the method chosen in this thesis, to choose one state as the reference for undertaking both forms of simplification. We stress that any approximation made to an equation must be made consistently to all other equations within the set, failing to do this can lead to loss of conservation properties.

3.1 Boussinesq Equation Set

First published in 1903 the Boussinesq approximations [8] are the most commonly used approximations in fluid dynamics, however the full implications of the term 'Boussinesq' vary according to its implemention within a model. It is widely accepted that the primary simplification of the Boussinesq approximations is to reduce the mass

continuity equation to it's incompressible form

$$\nabla . \boldsymbol{u} = 0, \tag{3.1}$$

therefore limiting the velocity field to a solenoidal form and assuming that mass conservation can be replaced by volume conservation. It is also common that the Boussinesq approximation involves the neglect of density perturbations except where they are related to buoyancy; a further approximation, that is not used by all groups, allows simplification of the equation of state such that density perturbations are proportional to temperature perturbations. It is possible, and the technique used in some oceanagraphic studies, to then utilise the remaining terms from the non-linear mass continuity equation as the equation governing the evolution of density and to allow their application to a reference state which is realistic. We have found no evidence of this within studies of the Jovian interior and it is generally accepted by groups studying the onset of convection within the Jovian interior and interior atmosphere that the Boussinesq approximation also involves utilising a uniform density reference profile. It is commonplace to refer to these studies as 'incompressible convection'.

Within chapters 3-6 we choose not to assume constant density reference state, rather to apply the Boussinesq equations to a reference state which is appropriate to all equation sets and allows reference state density variation. In chapter 7 we apply the techniques used in traditional Boussinesq studies of the onset of convection to an anelastic equation set, comparing the anelastic results with those of a Boussinesq set with constant density reference state.

In addition to the use of the mass continuity equation governing an incompressible fluid the Boussinesq approximations prescribe that perturbations of thermodynamic variables are small compared to their reference state values. As with the fully-compressible equations we define the reference state to be hydrostatic, therefore when combined with the aforementioned limitation on the size of the perturbation

variables the momentum equation can be simplified to become

$$\frac{D\,\boldsymbol{u}}{Dt} + 2\boldsymbol{\Omega} \times \boldsymbol{u} + \frac{1}{\rho_s}\nabla p' + \frac{\rho'}{\rho_s} g\hat{\boldsymbol{r}} - \frac{1}{\rho_s}\boldsymbol{F} = 0, \tag{3.2}$$

and the perturbation equation of state is given by

$$\frac{\rho'}{\rho_s} = \frac{p'}{p_s} - \frac{T'}{T_s} = (1-\kappa)\frac{p'}{p_s} - \frac{\theta'}{\theta_s}. \tag{3.3}$$

Many groups then make the assumption that this equation of state can be further simplified by neglecting the pressure perturbation terms. This allows simplification of the buoyancy term such that

$$\frac{\rho'}{\rho_s} g \approx -\alpha T' g \approx -\frac{\theta'}{\theta_s} g,$$

where α is the coefficient of thermal expansion and the coefficient of expansion for most fluids is within the range $10^{-3} - 10^{-4} K^{-1}$.

Various groups including Speigel and Veronis (1960 [58]), Mahrt (1986 [47]) and Tritton (1989 [61]) have examined the Boussinesq approximation more formally. Tritton examines the specific case of steady flow and derives criteria for the 'Boussinesq' case in which pressure perturbations are ignored in the equation of state. Mahrt and Speigel and Veronis consider non-steady flow and conclude that there is a further restriction determining the time scale of the flow. Many other groups employ these approximations in their models without rigorously considering their validity.

The first Boussinesq assumption is that the perturbation variables are small compared to their basic state values

$$\frac{\rho'}{\rho_s} \ll 1, \;\; \frac{T'}{T_s} \ll 1, \;\; \frac{\theta'}{\theta_s} \ll 1, \;\; \text{etc.} \tag{3.4}$$

Applying this to the mass continuity equation yields

$$\frac{\boldsymbol{u}}{\rho_s}.\nabla\rho_s + \frac{1}{\rho_s}\frac{\partial \rho'}{\partial t} + \nabla.\,\boldsymbol{u} = 0.$$

Through scale analysis this becomes

$$-\frac{\rho_0 w^\star}{H_\rho} + \frac{\rho^\star}{\tau} + \frac{\rho_0 u^\star}{L} + \frac{\rho_0 w^\star}{d} = 0, \tag{3.5}$$

where ρ_0 is the reference state density scale, $\rho^\star$, $u^\star$ and $w^\star$ are the perturbation density, horizontal and vertical velocity scales, L is the horizontal length scale, d the vertical length scale, τ the Eulerian time scale and H_ρ the density scale height given by $H_\rho = (-\nabla\rho_s/\rho_s)^{-1}$.

Comparing the first and last terms of equation (3.5) we see that in order to neglect the first term we must have $d \ll H_\rho$. This effectively constrains the Boussinesq approximations to either fluids of constant basic state density or shallow motions within compressible fluids. In order to neglect the second term we require

$$\tau \gg \frac{\rho^\star}{\rho_0}\min\left[\frac{L}{u^\star}, \frac{d}{w^\star}\right].$$

Simplification of the momentum equation to the form of equation (3.2) simply requires that the perturbation variables are small compared to their basic state values. In order to further simplify this equation many groups choose to neglect the perturbation pressure component of the buoyancy term. If we assume that the buoyancy term in the momentum equation is at least comparable in size to the pressure gradient term, and assume the reference state to be hydrostatic, comparison of these terms then yields

$$\frac{p^\star}{p_0} \leq \frac{d}{H_i}\frac{\rho^\star}{\rho_0}$$

where p_0 and T_0 are the reference pressure and temperature scales, $H_i = RT_0/g$ is the pressure scale height for an isothermal atmosphere and we have utilised the fact that the reference state is hydrostatic. If $d \ll H_i$ we are able to further linearise the equation of state such that

$$\frac{\rho'}{\rho_s} \approx -\frac{T'}{T_s} \approx -\frac{\theta'}{\theta_s}. \tag{3.6}$$

This can then be substituted into the momentum equation to simplify the buoyancy term. However, if vertical motions are less strongly affected by bouyancy than they are by the perturbation pressure gradient then equation (3.6) does not hold and it may be necessary to include pressure perturbations in the buoyancy term. Since we

are considering the equations in their potential temperature form it is convenient to include the pressure perturbation terms in our momentum equation, if we were to neglect them the buoyancy term would be proportional to the temperature perturbation rather than the potential temperature perturbation. The inviscid Boussinesq momentum equation is then

$$\frac{D\,\boldsymbol{u}}{Dt} + 2\boldsymbol{\Omega} \times \boldsymbol{u} + \frac{1}{\rho_s}\nabla p' - \frac{\theta'}{\theta_s} g\hat{\boldsymbol{r}} = 0. \tag{3.7}$$

The Boussinesq thermodynamic equation is found by neglecting terms involving divergence of velocity or gradient of density thus in its inviscid form it becomes

$$\frac{D\theta'}{Dt} + \boldsymbol{u}\,.\nabla\theta_s = 0. \tag{3.8}$$

We note that if pressure perturbations are ignored then we are able to replace the potential temperature perturbation term with an equivalent temperature perturbation term. For comparison with other approximated forms we choose to leave the thermodynamic equation in its potential temperature form. As with the fully compressible set we linearise by treating velocity as a perturbation on the reference state and neglecting products of velocity and a perturbation variable.

In summary we have the following criteria

1. The perturbation variables are small compared to their reference state values

$$\frac{\rho'}{\rho_s} \ll 1 \text{ etc.}$$

2. The basic state density is limited such that either $\rho_s =$ constant or $d \ll H_\rho$.

3. The Eulerian timescale of the flow is limited such that

$$\tau \gg \frac{\rho^\star}{\rho_0} \min\left[\frac{L}{u^\star},\ \frac{d}{w^\star}\right].$$

4. Buoyancy is a significant component of the momentum equation and, if pressure perturbations are to be neglected, $d \ll H_i$.

3.1.1 Energetics

Undertaking a similar analysis to that of the fully compressible set we find that the linearised Boussinesq set is energy conserving, though the total perturbation energy is modified such that there is no contribution through elastic energy

$$E = \frac{\rho_s}{2}\left(|u|^2 + |v|^2 + |w|^2 + \frac{g^2}{N^2}\left|\frac{\theta'}{\theta_s}\right|^2\right). \tag{3.9}$$

3.1.2 Rescaled Boussinesq Set

In line with our manipulation of the fully compressible set we rescale the Boussinesq set using the variables

$$\boldsymbol{U} = (U, V, W) = \rho_s^{1/2}(u, v, w) = \rho_s^{1/2}\,\boldsymbol{u}\,, \quad \Theta = \rho_s^{1/2}\frac{\theta'}{\theta_s} \quad \text{and} \quad P = \rho_s^{-1/2}p'.$$

In the Boussinesq rescaling we are able to neglect terms involving derivatives of density thus our rescaled inviscid Boussinesq equation set is given by

$$\nabla.\boldsymbol{U} = 0 \tag{3.10}$$

$$\frac{\partial U}{\partial t} + 2\Omega W\cos\phi - 2\Omega V\sin\phi + \frac{1}{r\cos\phi}\frac{\partial P}{\partial \lambda} = 0 \tag{3.11}$$

$$\frac{\partial V}{\partial t} + 2\Omega U\sin\phi + \frac{1}{r}\frac{\partial P}{\partial \phi} = 0 \tag{3.12}$$

$$\frac{\partial W}{\partial t} - 2\Omega U\cos\phi + \frac{\partial P}{\partial r} - \Theta g = 0 \tag{3.13}$$

$$\frac{\partial \Theta}{\partial t} + \frac{W}{\theta_s}\frac{\partial \theta_s}{\partial r} = 0 \tag{3.14}$$

3.2 Anelastic Approximations

The anelastic approximations aim to allow investigation into the effects of density stratification without having to consider the computationally demanding fully compressible case. Initially developed by Batchelor (1953 [5]), then extended and dubbed

the 'anelastic equations' by Ogura and Phillips (1962 [48]), they have been modified numerous times in order to meet the criteria required for specific models.

Following Bannon (1996 [4]), there are three basic assumptions on which the derivations of anelastic sets rely:

1. The buoyancy force plays an important role in the momentum equation

2. The characteristic vertical displacement d of a fluid parcel is comparable to the density scale height H_ρ where

$$H_\rho = \left(-\frac{1}{\rho_s} \frac{d\rho_s}{dr} \right)^{-1}. \tag{3.15}$$

3. The perturbed values of the thermodynamic state variables at any height are small compared to their reference state value at that height.

$$\frac{|\,\theta'(\lambda,\ \phi,\ r)\,|}{\theta_s(r)} = O(\epsilon) \ll 1, \tag{3.16}$$

where ϵ is as defined in the previous chapter. At this stage some anelastic sets also require that the basic state is adiabatic such that $\theta_s = \theta_{ad}$, others such as Lipps and Hemler (1982 [46]) argue that the departure of the basic state from adiabatic must also be of the order ϵ

$$\frac{|\,\theta_s - \theta_{ad}\,|}{\theta_{ad}} = O(\epsilon) \ll 1. \tag{3.17}$$

Gilman and Glatzmaier (1980 [31]) take this approach employing values given by Gough and Weiss (1976 [32]) as appropriate to the solar convection zone in order to define their value of epsilon. In doing so they assume that global convection is driven by small departures of the reference state atmosphere from adiabatic such that $\epsilon \leq 10^{-4}$. Bannon (1996 [4]) suggests that equation (3.17) need not hold for diabatic flow in which the material derivative of the reference state potential temperature is balanced by the viscous regeneration of heat and diffusive terms in the thermodynamic equation.

Anelastic condition (3) allows us to linearise the mass continuity equation such that

$$\frac{\boldsymbol{u}}{\rho_s}.\nabla\rho_s + \frac{1}{\rho_s}\frac{\partial\rho'}{\partial t} + \nabla.\,\boldsymbol{u} = 0. \tag{3.18}$$

In deriving the Boussinesq equations we saw that in order to neglect the first term it is necessary that $d \ll H_\rho$, therefore anelastic condition (2) ensures that this term is retained in the anelastic set. Using the same scaling as for the Boussinesq derivations we find that in order to neglect the time derivative term we require

$$\tau \gg \frac{\rho^\star}{\rho_0}\min\left[\frac{H_\rho}{w^\star},\ \frac{L}{u^\star},\ \frac{d}{w^\star}\right]. \tag{3.19}$$

However, we find that for adiabatic flow this restriction is superceded by a further time-scale constraint imposed in deriving the anelastic thermodynamic equation. The anelastic mass continuity equation is then

$$\frac{\boldsymbol{u}\,.\nabla\rho_s}{\rho_s} + \nabla.\,\boldsymbol{u} = \frac{1}{\rho_s}\nabla.\,(\rho_s\,\boldsymbol{u}) = 0. \tag{3.20}$$

The thermodynamic equation, linearised through anelastic condition (3), can be written

$$\frac{D\theta_s}{Dt} + \frac{D\theta'}{Dt} = \frac{\theta_s}{C_P\rho_s T_s}\left(\nabla.\boldsymbol{D} + \Phi\right) \tag{3.21}$$

For adiabatic flow the right hand side of this equation is zero, thus the first and second terms on the left hand side must be of comparable order. If we consider a fluid parcel displaced adiabatically over our characteristic vertical displacement d then the ratio of perturbed to reference state potential temperature is given by

$$\frac{\theta'}{\theta_s} = O\left(\frac{d}{\theta_s}\frac{d\theta_s}{dr}\right) = \frac{d}{H_\theta} = O(\epsilon) \quad \text{where} \quad H_\theta = \left(\frac{1}{\theta_s}\frac{d\theta_s}{dr}\right)^{-1}. \tag{3.22}$$

Anelastic assumption (2) then enforces that the entropy scale height must be significantly larger than the density scale height such that

$$H_\theta \gg H_\rho. \tag{3.23}$$

Using equation (2.23) we see that this requires that $g/C_s^2 >> N^2/g$. Whilst it is not clear whether the convective motions within the interior and interior atmosphere are sufficiently efficient that the region is only marginally superadiabatic it is widely thought to be the case and thus N^2/g is likely to be small. However, the temperature and density profile is also an equivocal point, which in turn makes the speed of sound within the region unclear. Therefore, it is not obvious whether this condition is met within the Jovian interior and interior atmosphere. For the unstably stratified, constant mass polytropic model considered within chapters 5, 6 and 7 the reference state abides relatively well with (3.23). However, the polytropic model implicitly assumes that convection is efficient and the region close to adiabatic, therefore this is not a strong indication that the condition holds well in a realistic profile, rather that it should hold well for the polytropic profiles that are currently used to model it. For an isothermal regime the condition $g/C_s^2 >> N^2/g$ leads to $1 - \kappa >> \kappa$; in the isothermal portion of the Jovian atmosphere considered within chapter 4, $\kappa \approx 0.32$ therefore $H_\theta < H_\rho$ but not significantly so.

Bannon (1996) [4] points out that for diabatic flow this need not be the case. For diabatic flow the right hand side of equation (3.21) is non-zero and could balance the first term, as such imposing a different restriction on the reference state potential temperature profile.

Consideration of adiabatic flow imposes restrictions on the time scale of the motion. Undertaking scale analysis on the first and second terms of equation (3.21) yields

$$\frac{D\theta_s}{Dt} \Big/ \frac{D\theta'}{Dt} = O\left(\frac{w\tau}{\epsilon H_\theta}\right). \tag{3.24}$$

Undertaking a scale analysis on the vertical momentum equation we assume that the force arising from the vertical pressure gradient will tend to reduce the effect of the buoyancy force, thus we equate the buoyancy force with the vertical acceleration term

in order to provide a value for the terminal velocity of a falling fluid parcel

$$w \leq O\left(\epsilon g \tau\right). \tag{3.25}$$

We then have

$$\frac{D\theta_s}{Dt} \Big/ \frac{D\theta'}{Dt} \leq \frac{g\tau^2}{H_\theta}. \tag{3.26}$$

Recalling that for adiabatic flow the first and second terms of equation (3.21) are of comparable order and defining the buoyancy, or Brunt-Vaisala, frequency N

$$N^2 = \frac{g}{\theta_s}\frac{d\theta_s}{dr} = \frac{g}{H_\theta}. \tag{3.27}$$

we see that the only way to satisfy (3.26) is if the time scale of the fluid motion is of the same order as, or longer than, the inverse of the buoyancy frequency of the reference state

$$\tau \sim \frac{1}{N}. \tag{3.28}$$

Anelastic condition (3) allows the momentum equation to be linearised such that

$$\frac{D\,\boldsymbol{u}}{Dt} + 2\boldsymbol{\Omega} \times \boldsymbol{u} + \frac{1}{\rho_s}\nabla p' + \frac{\rho'}{\rho_s} g\hat{\boldsymbol{r}} - \frac{1}{\rho_s}\boldsymbol{F} = 0. \tag{3.29}$$

where the anelastic viscous terms are the same as for the fully compressible case with the exception that terms involving divergence of velocity are simplified such that

$$\nabla . \boldsymbol{u} = -\frac{w}{\rho_s}\frac{\partial \rho_s}{\partial r}. \tag{3.30}$$

3.2.1 Energetics

The linearised inviscid anelastic momentum equation can be written in the form

$$\frac{\partial\,\boldsymbol{u}}{\partial t} + 2\rho_s\boldsymbol{\Omega} \times \boldsymbol{u} + \nabla\left(\frac{p'}{\rho_s}\right) + \frac{p'}{\rho_s^2}\frac{\partial \rho_s}{\partial r} + \frac{\rho'}{\rho_s} g\hat{\boldsymbol{r}} = 0. \tag{3.31}$$

Using this equation and undertaking analysis of the energetics of the anelastic set we find

$$\frac{\partial E}{\partial t} + \nabla.(p'\,\boldsymbol{u}) + \left(\rho' + \frac{p'}{\rho_s g}\frac{\partial \rho_s}{\partial r}\right) wg + \rho_s \frac{\theta'}{\theta_s} wg = 0, \tag{3.32}$$

where

$$E = \frac{\rho_s}{2}\left(|u|^2 + |v|^2 + |w|^2 + \frac{g^2}{N^2}\left|\frac{\theta'}{\theta_s}\right|^2\right). \tag{3.33}$$

We note that similar to the Boussinesq set there is no contribution to the perturbation energy through elastic energy. Following Bannon (1996 [4]), the only way in which we can have an anelastic set which conserves energy is to modify the equation of state such that

$$\frac{\theta'}{\theta_s} = -\frac{p'}{g\rho_s^2}\frac{\partial \rho_s}{\partial r} - \frac{\rho'}{\rho_s}. \tag{3.34}$$

Therefore we have two possible forms of the anelastic momentum equation, energy conserving and non-energy conserving. The linearised, energy conserving, inviscid form is given by

$$\frac{\partial \boldsymbol{u}}{\partial t} + 2\rho_s \boldsymbol{\Omega} \times \boldsymbol{u} + \frac{1}{\rho_s}\nabla p' + \left(\frac{p'}{g\rho_s^2}\frac{\partial \rho_s}{\partial r} - \frac{\theta'}{\theta_s}\right) g\hat{\boldsymbol{r}} = 0. \tag{3.35}$$

The non-energy conserving form is found by linearising the equation of state using anelastic condition (3) resulting in the same equation of state as for the fully-compressible case

$$\frac{\rho'}{\rho_s} = (1-\kappa)\frac{p'}{p_s} - \frac{\theta'}{\theta_s}, \tag{3.36}$$

thus

$$\frac{\partial \boldsymbol{u}}{\partial t} + 2\rho_s \boldsymbol{\Omega} \times \boldsymbol{u} + \frac{1}{\rho_s}\nabla p' + \left[(1-\kappa)\frac{p'}{p_s} - \frac{\theta'}{\theta_s}\right] g\hat{\boldsymbol{r}} = 0. \tag{3.37}$$

We will consider both energy conserving and non-energy conserving sets in our later analysis.

3.2.2 Rescaled Anelastic Sets

The rescaled inviscid anelastic sets are given by

$$\nabla\left(\rho_s^{1/2}\boldsymbol{U}\right) = 0, \tag{3.38}$$

$$\frac{\partial U}{\partial t} + 2\Omega W\cos\phi - 2\Omega V\sin\phi + \frac{1}{r\cos\phi}\frac{\partial P}{\partial \lambda} = 0, \tag{3.39}$$

$$\frac{\partial V}{\partial t} + 2\Omega U \sin\phi + \frac{1}{r}\frac{\partial P}{\partial \phi} = 0, \tag{3.40}$$

The rescaled energy conserving (EC) vertical momentum equation is given by

$$\frac{\partial W}{\partial t} - 2\Omega U \cos\phi + \frac{\partial P}{\partial r} - \frac{P}{2\rho_s}\frac{\partial \rho_s}{\partial r} - \Theta g = 0. \tag{3.41}$$

Recalling that $C_s^2 = RT_s/(1-\kappa)$, the rescaled non-energy conserving (NEC) vertical momentum equation is given by

$$\frac{\partial W}{\partial t} - 2\Omega U \cos\phi + \frac{\partial P}{\partial r} + \frac{P}{C_s^2}g + \frac{P}{2\rho_s}\frac{\partial \rho_s}{\partial r} - \Theta g = 0. \tag{3.42}$$

The rescaled inviscid anelastic thermodynamic equation is given by

$$\frac{\partial \Theta}{\partial t} + \frac{W}{\theta_s}\frac{\partial \theta_s}{\partial r} = 0. \tag{3.43}$$

3.3 Pseudo-Incompressible Approximation

The Pseudo-Incompressible approximation was developed in the late 1980's by Durran (1989 [24]) in an attempt to overcome the perceived limitations of the anelastic systems. Recently it has been developed by a few groups considering supernovae (Zingale et al., 2006 [69]), though we have found no evidence of its use in modelling non-terrestrial planetary fluid flow. The Pseudo-Incompressible equation set aims to allow variation of both reference state density and potential temperature, simplifying the mass continuity equation but making no approximation to the momentum and thermodynamic equations. Durran (1989 [24]) proposed that under certain conditions the density term in the mass continuity equation can be replaced by a modified 'pseudo-density', that for a perfect gas is defined as $\rho^\star = \rho_s\theta_s/\theta$. This can then be combined with the unapproximated momentum and thermodynamic equations in order to yield an energy conserving equation set in which acoustic waves are not supported (Durran, 2008 [25]).

Using the pseudo-density the mass continuity equation is given by

$$\frac{1}{\rho^\star}\frac{D\rho^\star}{Dt} + \nabla.\,\boldsymbol{u} = 0. \tag{3.44}$$

Substituting into this with $\rho^\star = \rho_s\theta_s/(\theta_s + \theta')$, and recalling that our reference state is time independent, we find that

$$\frac{D}{Dt}\left(\frac{1}{\theta'}\right) + \frac{\boldsymbol{u}}{\theta_s}.\nabla(\theta_s) + \frac{\boldsymbol{u}}{\rho_s}.\nabla(\rho_s) + \nabla.\,\boldsymbol{u} = 0. \tag{3.45}$$

Combining this with the thermodynamic equation yields

$$\nabla.(\rho_s\theta_s\,\boldsymbol{u}) = \frac{Q}{\theta}. \tag{3.46}$$

It is then necessary to determine under what conditions it is acceptable to consider pseudo-density in place of density in the mass continuity equation.

The key assumption in deriving the Pseudo-Incompressible system is that pressure perturbations at any height are small compared to the reference state values at that height. i.e.

$$p' \ll p_s \quad \text{or} \quad \frac{|p'|}{|p_s|} = O(\epsilon) \ll 1. \tag{3.47}$$

The mass continuity equation in its unapproximated pressure form is given by equation (2.16). Using equation (3.47) we are able to linearise it such that

$$\frac{(1-\kappa)}{p_s}\left(\boldsymbol{u}\,.\nabla p_s + \frac{\partial p'}{\partial t} + \boldsymbol{u}\,.\nabla p'\right) + \nabla.\,\boldsymbol{u} = \frac{1}{\theta_s}\frac{D(\theta_s+\theta')}{Dt}. \tag{3.48}$$

Undertaking scale analysis using the same scaling as used in deriving the Boussinseq and anelastic approximations we follow Durran (1989 [24]) in assuming that $u/L \sim v/L \sim w/d$.

Undertaking scale analysis of the pressure terms, in a similar manner to that undertaken in deriving the anelastic approximation, we find

$$\frac{Dp'}{Dt}\Big/\frac{Dp_s}{Dt} = O\left(\frac{\epsilon H_p}{w\tau}\right), \tag{3.49}$$

where we use the hydrostatic reference state to show

$$H_p = \left(-\frac{1}{p_s}\frac{dp_s}{dr} \right)^{-1} = \frac{RT_s}{g}. \tag{3.50}$$

Since we are considering an ideal fluid we can define the speed of sound in the reference state C_s using

$$C_s^2 = \frac{RT_s(r)}{(1-\kappa)}. \tag{3.51}$$

Considering this and the maximum free-fall speed as given by equation (3.25) we can write

$$\frac{Dp'}{Dt} \Big/ \frac{Dp_s}{Dt} \leq O\left(\frac{(1-\kappa)C_s^2}{g^2\tau^2} \right). \tag{3.52}$$

Therefore in order to neglect Dp'/Dt it is necessary that

$$\frac{g^2\tau^2}{(1-\kappa)} \gg 1/C_s^2, \tag{3.53}$$

which is equivalent to small Mach number. The resulting equation set matches that derived through use of pseudo-density, thus establishes criterion for the application of the pseudo-incompressible approximation.

$$\nabla . \boldsymbol{u} + \frac{w}{\rho_s}\frac{d\rho_s}{dr} + \frac{w}{\theta_s}\frac{d\theta_s}{dr} = \frac{1}{\theta}\frac{D\theta}{Dt}. \tag{3.54}$$

3.3.1 Energetics

Undertaking an analysis similar to that of the fully-compressible set shows that the pseudo-incompressible set is energy conserving, though the total perturbation energy is modified such that there is no contribution through elastic energy

$$E = \frac{\rho_s}{2}\left(|u|^2 + |v|^2 + |w|^2 + \frac{g^2}{N^2}\left|\frac{\theta'}{\theta_s}\right|^2 \right). \tag{3.55}$$

3.3.2 Rescaled Pseudo-Incompressible set

The rescaled Pseudo-Incompressible momentum and thermodynamic equations are the same as for the fully compressible set, the inviscid continuity equation is given by

$$\frac{W}{\theta_s}\frac{\partial \theta_s}{\partial r} + \frac{W}{2\rho_s}\frac{\partial \rho_s}{\partial r} + \nabla.\boldsymbol{U} = 0 \tag{3.56}$$

3.4 Quasi-Hydrostatic Approximation

The equation of hydrostatic balance is a severe approximation that constrains the vertical accelerations to zero. Consideration of a quasi-hydrostatic equation set simplifies the equation set such that inspection of regimes in which the vertical accelerations are small, but non-zero, becomes much less computationally demanding than the fully compressible set without the severe constraints of the fully hydrostatic set. For this reason, the quasi-hydrostatic equation set is often used in modelling of large circulations in the terrestrial atmosphere. It is also used in the EPIC global circulation model (Dowling et al., 1998 [20]) which has been used to model the Jovian atmosphere.

In order to apply the fully hydrostatic approximation a simple scale analysis shows that for non-hydrostatic effects to be small the advective timescale L/U must be long compared with the buoyancy period $1/N$ such that

$$N \gg \frac{U}{L}. \tag{3.57}$$

Therefore for small horizontal scales or weak stratification we expect the quasi-hydrostatic approximation to break down. Similarly, scale analysis shows that the ratio of vertical to horizontal length scales must be much smaller than one, $d/L \ll 1$. These requirements allow the neglect of both $\partial w/\partial t$ and $2\Omega u \cos\phi$ in the vertical momentum equation. However, neglect of the coriolis term then means that for energetic

consistency it is necessary to also neglect the $2\Omega w \cos\phi$ term in the zonal momentum equation. The quasi-hydrostatic approximation, suggested by White and Bromley (1995, [63]), is based on the relaxation of the hydrostatic condition to systematically include $\cos\phi$ terms in the vertical and zonal momentum equations. This also ensures that angular momentum is conserved.

The governing equations for the quasi-hydrostatic approximation are then the same as those for the fully compressible case except that the acceleration term in the vertical momentum equation is neglected

$$2\Omega u \cos\phi + \frac{1}{\rho_s}\frac{\partial p'}{\partial r} + \frac{\rho'}{\rho_s}g = 0 \tag{3.58}$$

3.4.1 Energetics

Undertaking a similar analysis to that of the fully compressible set we find that the linearised quasi-hydrostatic set is energy conserving, though the total perturbation energy is modified such that there is no contribution through the vertical component of velocity

$$E = \frac{\rho_s}{2}\left(|u|^2 + |v|^2 + \frac{g^2}{N^2}\left|\frac{\theta'}{\theta_s}\right|^2 + \frac{|p'|^2}{\rho_s^2 C_s^2}\right). \tag{3.59}$$

3.4.2 Rescaled Quasi-Hydrostatic set

The rescaled quasi-hydrostatic continuity, thermodynamic and horizontal momentum equations are the same as for the fully compressible set. The inviscid vertical momentum equation is given by

$$-2\Omega U \cos\phi + \frac{\partial P}{\partial r} + \frac{P}{C_s^2}g + \frac{P}{2\rho_s}\frac{\partial \rho_s}{\partial r} - \Theta g = 0. \tag{3.60}$$

3.5 Switchable Equation Sets

In order to compare the various equation sets we follow Davies et al., (2003 [18]) and introduce a system of switches which can take the values zero or one. Setting all switches to be equal to one reproduces the fully compressible equation sets, other permutations produce the approximated sets as shown in table 3.1

Equation Set	δ_A	δ_B	δ_C	δ_D	δ_E	δ_H
Fully Compressible	1	1	1	1	1	1
Pseudo-Incompressible	0	1	1	1	1	1
Quasi-Hydrostatic	1	1	1	1	1	0
Anelastic EC	0	0	1	0	0	1
Anelastic NEC	0	1	1	0	1	1
Boussinesq	0	1	0	0	0	1

Table 3.1: Switch Settings

3.5.1 Nonlinear, unscaled equation sets

Implementation of these switches allows us to write the non-linear equation sets in their rescaled forms. The inviscid mass continuity equation in its pressure form is given by

$$\delta_A \frac{(1-\kappa)}{p}\frac{Dp'}{Dt} + \frac{p_s}{(p_s+\delta_A p')}\left(\delta_D \frac{w}{\theta_s}\frac{\partial \theta_s}{\partial r} + \delta_C \frac{w}{\rho_s}\frac{\partial \rho_s}{\partial r}\right) + \nabla.\,\boldsymbol{u} = 0. \tag{3.61}$$

The inviscid horizontal momentum equations are given by

$$(\rho_s + \delta_D \rho')\left(\frac{Du}{Dt} + Fw - fv + \frac{uw}{r} - \frac{uv\tan\phi}{r}\right) + \frac{1}{r\cos\phi}\frac{\partial p'}{\partial \lambda} = 0, \tag{3.62}$$

and

$$(\rho_s + \delta_D \rho')\left(\frac{Dv}{Dt} + fu + \frac{vw}{r} + \frac{u^2\tan\phi}{r}\right) + \frac{1}{r}\frac{\partial p'}{\partial \phi} = 0. \tag{3.63}$$

The inviscid vertical momentum equation is given by

$$\begin{aligned}(\rho_s + \delta_D\rho')\left(\delta_H\frac{Dw}{Dt} - Fu - \frac{(u^2+v^2)}{r}\right) + \delta_D\rho' g \\ + (1-\delta_D)\left[\delta_E(1-\kappa)\frac{p'}{p_s}g - \frac{\theta'}{\theta_s}g - (1-\delta_B)\frac{1}{\rho_s^2}\frac{\partial\rho_s}{\partial r}p'\right] + \frac{\partial p'}{\partial r} = 0,\end{aligned} \tag{3.64}$$

and the thermodynamic equation is given by

$$\left(1 + \delta_D\frac{\rho'}{\rho_s}\right)\frac{D\theta}{Dt} = 0. \tag{3.65}$$

The equation of state is given by

$$(p_s + p')^{(1-\kappa)}p_0^{\kappa} = (\rho_s + \rho')R(\theta_s + \theta') \tag{3.66}$$

3.5.2 Linearised, rescaled equation sets

The linearised, rescaled, inviscid equation sets display fewer differences as the linearised fully-compressible and pseudo-incompressible equation of state matches that of the non-energy-conserving anelastic set.

$$\frac{\delta_A}{C_s^2}\frac{\partial P}{\partial t} + \delta_D\frac{W}{\theta_s}\frac{\partial\theta_s}{\partial r} + \delta_C\frac{W}{2\rho_s}\frac{\partial\rho_s}{\partial r} + \nabla.\boldsymbol{U} = \delta_D\frac{\rho_s^{1/2}}{\theta_s}Q \tag{3.67}$$

$$\frac{\partial U}{\partial t} + FW - fV + \frac{1}{r\cos\phi}\frac{\partial P}{\partial\lambda} - \frac{F_\lambda}{\rho_s^{1/2}} = 0 \tag{3.68}$$

$$\frac{\partial V}{\partial t} + fU + \frac{1}{r}\frac{\partial P}{\partial\phi} - \frac{F_\phi}{\rho_s^{1/2}} = 0 \tag{3.69}$$

$$\delta_H\frac{\partial W}{\partial t} - FU + \frac{\partial P}{\partial r} + \delta_E\frac{P}{C_s^2}g + \delta_E\frac{P}{\rho_s}\frac{\partial\rho_s}{\partial r} - \Theta g - \delta_C\frac{P}{2\rho_s}\frac{\partial\rho_s}{\partial r} - \frac{F_r}{\rho_s^{1/2}} = 0 \tag{3.70}$$

$$\frac{\partial\Theta}{\partial t} + \frac{W}{\theta_s}\frac{\partial\theta_s}{\partial r} = 0. \tag{3.71}$$

For neatness of notation we have set $F = 2\Omega\cos\phi$ and $f = 2\Omega\sin\phi$.

3.6 Summary

Within this chapter we have defined the approximated equation sets, the normal mode solutions of which we will compare with the normal mode solutions of the fully compressible set. It is well known that each form of approximation considered will suppress the internal acoustic modes, therefore we expect that these will be filtered by all approximated sets. Whilst we acknowledge that the accuracy of the equation sets is likely to be significantly reduced when considering a non-linear regime, a thorough understanding of their relative accuracy within a linearised regime should provide an indication as to which set will be most appropriate for advancing non-linear models.

We have seen that traditionally the application of the Boussinesq approximation in modelling a Jovian regime has involved the consideration of a uniform density reference state and the neglect of pressure perturbations; within chapters 4, 5 and 6 we consider the less restrictive case in which we apply the Boussinesq approximation to a realistic density profile, and do not neglect pressure perturbations. We expect that this will result in a set of solutions which will be more realistic than those of a uniform density Boussinesq regime, however we expect that for reference states with larger density variation we will see larger differences between the Boussinesq and fully-compressible solutions. Since the Boussinesq approximation requires that a fluid parcel does not experience large variation in density we expect that shallow modes will be more accurately represented than deeper modes. The Boussinesq approximation also requires that the buoyancy force is a signifcant component of the momentum equation, therefore we expect the approximation to be weaker for modes with large horizontal scale than those of similar depth and shorter horizontal scale. The anelastic sets involve less stringent conditions on the density profile, but continue to assume that the buoyancy force plays an important role in the momentum equation. Therefore, similarly to the Boussinesq set, we expect that the approximations will break down on both large horizontal and vertical scales. As discussed in the scale analysis,

the condition $H_\theta >> H_\rho$ does not hold well within the isothermal regime considered within chapter 4, but is significantly better for the polytropic regime considered within chapters 5, 6 and 7. Therefore, we expect that the anelastic sets will be more accurate than the Boussinesq equation set, but will continue to display significant deviation from the fully-compressible set when considered alongside an isothermal atmosphere, or on large horizontal or vertical scales. The pseudo-incompressible set utilises a still less severe approximation to the mass continuity equation, allowing consideration of density perturbations but ignoring the effects of pressure perturbations. We therefore expect that the modes of this set will more accurately represent the fully-compressible solutions in both isothermal and polytropic regimes; since the pseudo-incompressible equation does not place such strict restrictions on the reference profiles we expect the stronger representation to be most obvious for the deepest modes. The quasi-hydrostatic set also imposes restrictions on the reference profile; we expect it to be poor in representing modes in a weakly stratified atmosphere and one in which the atmosphere is unstably stratified. The quasi-hydrostatic set is also likey to display significant misrepresentation of modes which have short horizontal scales. In the proceeding chapters we will consider analysis of the equation sets used alongside reference profiles appropriate to the Jovian regime.

Chapter 4

Analysis of Isothermal Regime

In this chapter we will undertake analytic analysis on the linearised, rescaled equation sets developed in the previous chapter. This will provide useful reference solutions for later computational analysis and provide insight into the differences in the solutions for the various equation sets.

When considering the Boussinesq approximation the continuity equation asserts that the velocity field is solenoidal. Some analytic progress can then be made by taking the curl and double curl of the momentum equation in its vector form and seeking solutions, in terms of spherical harmonics, for the radial components of the vorticity and velocity. Introducing a streamfunction formalisation, writing the solenoidal field in terms of poloidal and toroidal components, then allows the further components of velocity to be written in terms of the aforementioned radial components of velocity and vorticity. This method results in a set of ODE's which most often must be solved numerically. Significant simplification of the geometry can allow further analytical progress. It is also possible to use this method for anelastic sets since in this case we see that $\rho_s \boldsymbol{u}$ is solenoidal, though the introduction of terms involving derivatives of reference state density complicates the analysis. The mass continuity equation for the adiabatic pseudo-incompressible set also defines a

Equation Set	δ_A	δ_B	δ_C	δ_D	δ_E	δ_H
Fully Compressible	1	1	1	1	1	1
Pseudo-Incompressible	0	1	1	1	1	1
Quasi-Hydrostatic	1	1	1	1	1	0
Anelastic EC	0	0	1	0	0	1
Anelastic NEC	0	1	1	0	1	1
Boussinesq	0	1	0	0	0	1

Table 4.1: Switch Settings

solenoidal vector field such that $\nabla.(\rho_s\theta_s\,\boldsymbol{u}) = 0$, and thus can also be analysed in this manner. This adds the further complication through terms involving derivatives of potential temperature. Solenoidal analysis becomes less useful when considering the fully compressible, quasi-hydrostatic and non-adiabatic pseudo-incompressible sets as we are no longer able to relate the components of velocity using solenoidal decomposition. This method is used to extend the asymptotic theory of uniform density Boussinesq convection to the compressible case in chapter 7, and is included within Jones et al., (submitted 2008 [38]). Since we are unable to apply this method of analysis to all equation sets, we must consider alternative methods in order to compare solutions with those of a fully compressible equation set.

For all equation sets we note that the coefficients in the switchable linearised equations are independent of time and longitude; therefore we are able to consider separable solutions such that

$$\left.\begin{array}{lcl} U & & \hat{U}(\phi,r) \\ V & & \hat{V}(\phi,r) \\ W & = & \hat{W}(\phi,r) \\ P & & \hat{P}(\phi,r) \\ \Theta & & \hat{\Theta}(\phi,r) \end{array}\right\} \exp(im\lambda - i\sigma t). \tag{4.1}$$

Substitution into the governing equations, and boundary conditions, yields an eigenvalue problem for the frequency σ and non-longitudinal structure of the normal modes. When combining these equations it is immediately obvious that the viscous terms add significant complexity. Following Thuburn et al. (2002 I [60]), consideration of an inviscid set allows us to eliminate $\hat{U}$,$\hat{V}$ and $\hat{W}$ or $\hat{\Theta}/N^2$ to form two equations in $\hat{P}$ and $\hat{\Theta}/N^2$ or $\hat{W}$. However, these must still be solved numerically. In order to make further analytic progress it is necessary to make further simplifications. For the remainder of this chapter we will consider several possible simplifications that may aid our analysis. Initially we will consider an inviscid, non-rotating spherical system, extending the analysis of Thuburn et al. (2002 I [60]) to include our rescaled, switchable terms. We then extend analysis undertaken by groups such as Thuburn et al. (2002 II [59]), Kasahara and Qian (2000 [43]) and Davies et al. (2003 [18]) by considering normal mode solutions for an inviscid F-f plane under a Jovian parameter regime.

4.1 Analytic analysis of an inviscid, non-rotating system

Thuburn et al. (2002 I [60]) showed that considering a fully compressible, inviscid, non-rotating system allows further analytic analysis. In this system we note that there is no driving mechanism for Rossby waves, thus Rossby modes will degenerate to stationary vortical modes. We extend the analysis through use of the switchable terms, and after some manipulation we are able to produce an equation solely in $\hat{P}$

$$\frac{1}{r^2}\left(\frac{\partial}{\partial r}+\delta_D\frac{N^2}{g}+\frac{\delta_C}{2\rho_s}\frac{\partial\rho_s}{\partial r}\right)\left(\frac{r^2}{(N^2-\delta_H\sigma^2)}\left[\frac{\partial}{\partial r}+\delta_E\frac{g}{C_s^2}+\left(\delta_E-\frac{\delta_C}{2}\right)\frac{1}{\rho_s}\frac{\partial\rho_s}{\partial r}\right]\right)\hat{P} - \delta_A\frac{\hat{P}}{C_s^2}-\frac{\nabla_m^2\hat{P}}{r^2\sigma^2}=0, \tag{4.2}$$

where

$$\nabla_m^2 = -\left(\frac{m}{\cos\phi}\right)^2 + \frac{1}{\cos\phi}\left[\frac{\partial}{\partial\phi}\left(\cos\phi\frac{\partial}{\partial\phi}\right)\right]$$

Following Thuburn et al. (2002 I [60]) we write the pressure structure function as a product of a horizontal structure function and a radial structure function

$$\hat{P} = \hat{P}_\Phi(\phi)\hat{P}_R(r) \tag{4.3}$$

Substituting this into equation(4.2) we find

$$\frac{1}{\hat{P}_R}\left(\frac{\partial}{\partial r} + \delta_D\frac{N^2}{g} + \frac{\delta_C}{2\rho_s}\frac{\partial\rho_s}{\partial r}\right)\left(\frac{r^2}{(N^2-\delta_H\sigma^2)}\left[\frac{\partial}{\partial r} + \delta_E\frac{g}{C_s^2} + \left(\delta_E - \frac{\delta_C}{2}\right)\frac{1}{\rho_s}\frac{\partial\rho_s}{\partial r}\right]\right)\hat{P}_R - \delta_A\frac{r^2}{C_s^2} - \frac{1}{\sigma^2\hat{P}_\Phi}\nabla_m^2\hat{P}_\Phi = 0. \tag{4.4}$$

For all equation sets we see that the radial dependence is contained within the first two terms of (4.4), and the latitudinal dependence is contained within the final term. The term involving latitudinal dependence must then be constant such that the solutions for $\hat{P}_\Phi$ are associated Legendre functions and the complete horizontal structures are spherical harmonics. The final term then takes the form $l(l+1)/\sigma^2$ for non-negative integer l, which allows us to write (4.4) as a one-dimensional eigenvalue problem for σ and the vertical structure

$$\left(\frac{\partial}{\partial r} + \delta_D\frac{N^2}{g} + \frac{\delta_C}{2\rho_s}\frac{\partial\rho_s}{\partial r}\right)\left(\frac{r^2}{(N^2-\delta_H\sigma^2)}\left[\frac{\partial}{\partial r} + \delta_E\frac{g}{C_s^2} + \left(\delta_E - \frac{\delta_C}{2}\right)\frac{1}{\rho_s}\frac{\partial\rho_s}{\partial r}\right]\right)\hat{P}_R - \delta_A\frac{r^2}{C_s^2}\hat{P}_R + \frac{l(l+1)}{\sigma^2}\hat{P}_R = 0, \tag{4.5}$$

and the boundary condition $W = 0$ on the inner and outer boundaries becomes

$$\left[\frac{\partial}{\partial r} + \delta_E\frac{g}{C_s^2} + \left(\delta_E - \frac{\delta_C}{2}\right)\frac{1}{\rho_s}\frac{\partial\rho_s}{\partial r}\right]\hat{P}_R = 0 \tag{4.6}$$

at these boundaries.

Setting all switches equal to one yields the fully compressible set given by equation (3.8) of Thuburn et al. (2002 I [60]). We note that the switchable terms indicate

that none of the approximated equation sets fully replicate the fully-compressible system.

Thuburn et al. show that for the fully-compressible equation set there are only a few special cases in which further analytical progress can be made. Setting $\sigma = 0$ yields the steady solutions. This simplifies the initial equations such that $\hat{W} = 0$ and $m = 0$ for all equation sets, while $\hat{U}$ and $\hat{V}$ can be any horizontally non-divergent velocity field with arbitrary dependence on radius. $\hat{P}$ must be independent of latitude. We also see that

$$\hat{\Theta} g = \left[\frac{\partial}{\partial r} + \delta_E \frac{g}{C_s^2} + \left(\delta_E - \frac{\delta_C}{2} \right) \frac{1}{\rho_s} \frac{\partial \rho_s}{\partial r} \right] \hat{P}. \tag{4.7}$$

Setting all switches equal to one yields the rescaled version of equation (3.5) of Thurburn et al (2002 I [60]). The quasi-hydrostatic, pseudo-incompressible and non-energy conserving anelastic sets yield the same solution as for the fully compressible set. The switchable terms allow for the adjustments made to the equations of state for the Boussinesq and energy-conserving anelastic sets, ensuring that equation (4.7) shows that the perturbed state must be in hydrostatic balance for all approximated equation sets.

Thuburn et al. (2002 I [60]) also show that, in general, external acoustic modes must have non-zero $\hat{W}$. If we attempt to find solutions in which $\hat{W} = 0$ we find that in the fully-compressible case this can only be achieved for $\sigma = 0$, or for special reference state temperature profiles. This remains the case for approximated equation sets

Further analysis can be made by comparing a shallow atmosphere with a 'slightly-deep' atmosphere. In making the shallow atmosphere approximation we replace r with a constant a and replace $\partial/\partial r$ with $\partial/\partial z$. We denote the vertical structure function and eigenvalues in this case with a subscript s such that we have,

for example $\hat{P}_{R_s}$. The shallow atmosphere version of equation (4.2) is then

$$\left(\frac{\partial}{\partial z}+\delta_D\frac{N^2}{g}+\frac{\delta_C}{2\rho_s}\frac{\partial\rho_s}{\partial z}\right)\left(\frac{a^2}{(N^2-\delta_H\sigma_s^2)}\left[\frac{\partial}{\partial z}+\delta_E\frac{g}{C_s^2}+\left(\delta_E-\frac{\delta_C}{2}\right)\frac{1}{\rho_s}\frac{\partial\rho_s}{\partial z}\right]\right)\hat{P}_{R_s} - \delta_A\frac{a^2}{C_s^2}\hat{P}_{R_s}+\frac{l(l+1)}{\sigma^2}\hat{P}_{R_s}=0. \tag{4.8}$$

This is the switchable version of equation (B.1) in Thuburn et al. (2002 I [60]). If we then assume that the solutions to the 'slightly-deep' atmosphere case are given by

$$\begin{aligned} r &= a+z,\\ \hat{P}_R &= \hat{P}_{R_s}+\hat{P}_{R'},\\ \sigma^2 &= \sigma_s^2+\sigma_\epsilon, \end{aligned} \tag{4.9}$$

where z, $\hat{P}_R$ and σ_ϵ are small compared with a, $\hat{P}_R$ and σ_s^2, respectively. Following Thuburn et al. (2002 I [60]) we then substitute these quantities into equation (4.2), subtract equation (4.8) and drop terms that are products of small quantities to give

$$\begin{aligned} &\left(\frac{\partial}{\partial r}+\Gamma_{R1}\right)\left[\frac{a^2}{(N^2-\delta_H\sigma_s^2)}\left(\frac{\partial}{\partial r}+\Gamma_{R2}\right)\right]\hat{P}_{R'}-\left[\delta_A\frac{a^2}{C_s^2}+\frac{l(l+1)}{\sigma^2}\right]\hat{P}_{R'}\\ &+\delta_H\left(\frac{\partial}{\partial z}+\Gamma_{R1}\right)\left[\frac{a^2\sigma_\epsilon}{(N^2-\delta_H\sigma_s^2)^2}\left(\frac{\partial}{\partial z}+\Gamma_{R2}\right)\right]\hat{P}_{R_s}-\sigma_\epsilon\frac{l(l+1)}{\sigma_s^4}\hat{P}_{R_s}\\ &+\left(\frac{\partial}{\partial r}+\Gamma_{R1}\right)\left[\frac{2az}{(N^2-\delta_H\sigma_s^2)}\left(\frac{\partial}{\partial r}+\Gamma_{R2}\right)\right]\hat{P}_{R_s}-\delta_A\frac{2az}{C_s^2}\hat{P}_{R_s}=0, \end{aligned} \tag{4.10}$$

where

$$\begin{aligned} \Gamma_{R1} &= \delta_D\frac{N^2}{g}+\frac{\delta_C}{2\rho_s}\frac{\partial\rho_s}{\partial r}=\left(\delta_D-\frac{\delta_C}{2}\right)\frac{N^2}{g}-\frac{\delta_C}{2}\frac{g}{C_s^2},\\ \Gamma_{R2} &= \delta_E\frac{g}{C_s^2}+\left(\delta_E-\frac{\delta_C}{2}\right)\frac{1}{\rho_s}\frac{\partial\rho_s}{\partial r}=\left(\frac{\delta_C}{2}-\delta_E\right)\frac{N^2}{g}+\frac{\delta_C}{2}\frac{g}{C_s^2}. \end{aligned} \tag{4.11}$$

This is the switchable version of equation (B.5) in Thuburn et al. (2002 I [60]). We note that in the fully-compressible case $\Gamma_{R1}=-\Gamma_{R2}$, as given in Thuburn et al. (2002 I [60]). Consideration of the switchable terms shows that this is the case for all approximated sets except the non-energy conserving anelastic set, in which $\delta_D\neq\delta_E$.

In the pseudo-incompressible and quasi-hydrostatic sets Γ_{R1} and Γ_{R2} are the same as for the fully-compressible set. In the Boussinesq case $\Gamma_{R1} = -\Gamma_{R2} = 0$.

In the energy-conserving anelastic set we find that Γ_{R1} and Γ_{R2} are modified, but that the relationship $\Gamma_{R1} = -\Gamma_{R2}$ remains. However, we see that whilst the $\Gamma_{R1} = -\Gamma_{R2}$ relationship remains, the signs of Γ_{R1} and Γ_{R2} are not necessarily the same as for the fully-compressible set. There are four possible scenarios:

$$
\begin{aligned}
&1) \quad \left|\frac{N^2}{g}\right| > \left|\frac{g}{C_s^2}\right| \text{ and } \frac{N^2}{g} > 0 \\
&\qquad \Rightarrow \quad |\Gamma_{R1}|_{EC} > |\Gamma_{R1}|_{Full}\,,\; sgn\left(\Gamma_{R1}\right)_{EC} = -sgn\left(\Gamma_{R1}\right)_{Full} \\
&2) \quad \left|\frac{N^2}{g}\right| > \left|\frac{g}{C_s^2}\right| \text{ and } \frac{N^2}{g} < 0 \\
&\qquad \Rightarrow \quad |\Gamma_{R1}|_{EC} < |\Gamma_{R1}|_{Full}\,,\; sgn\left(\Gamma_{R1}\right)_{EC} = -sgn\left(\Gamma_{R1}\right)_{Full} \\
&3) \quad \left|\frac{N^2}{g}\right| < \left|\frac{g}{C_s^2}\right| \text{ and } \frac{N^2}{g} > 0 \\
&\qquad \Rightarrow \quad |\Gamma_{R1}|_{EC} < |\Gamma_{R1}|_{Full}\,,\; sgn\left(\Gamma_{R1}\right)_{EC} = sgn\left(\Gamma_{R1}\right)_{Full} \\
&4) \quad \left|\frac{N^2}{g}\right| < \left|\frac{g}{C_s^2}\right| \text{ and } \frac{N^2}{g} < 0 \\
&\qquad \Rightarrow \quad |\Gamma_{R1}|_{EC} < |\Gamma_{R1}|_{Full}\,,\; sgn\left(\Gamma_{R1}\right)_{EC} = sgn\left(\Gamma_{R1}\right)_{Full}
\end{aligned}
\tag{4.12}
$$

In the non-energy conserving anelastic case we find that Γ_{R1} is modified such that it matches that of the energy-conserving anelastic set, whilst Γ_{R2} is not modified and matches that of the fully-compressible set. For the non-energy conserving anelastic set the sign and magnitude of Γ_{R1} relative to the fully-compressible case follows the same rules as for the energy-conserving set, as shown in 4.12. Since $(\Gamma_{R2})_{NEC} = (\Gamma_{R2})_{Full}$ we can then see that in scenarios 1) and 2) $sgn(\Gamma_{R1})_{NEC} = sgn(\Gamma_{R2})_{NEC}$, which is not the case for any other set. Within an isothermal regime we note that $N^2/g = \kappa/H$ and $g/C_s^2 = (1-\kappa)/H$, thus if $\kappa < 0.5$ and $H > 0$, as is

the case in the isothermal portion of the Jovian atmosphere, scenario 3) will be true and $sgn(\Gamma_R 1)_{NEC} = -sgn(\Gamma_R 2)_{NEC}$. For all other reference states it is necessary to consider the scenarios as shown above.

In cases in which $\Gamma_{R1} = -\Gamma_{R2}$ we are able to multiply by $\hat{P}_{R_s}$ and integrate from inner boundary r_C to outer boundary r_S, by parts where necessary using the boundary conditions $(\partial/\partial r + \Gamma_{R2})\hat{P}_{R_s} = 0$ and $(\partial/\partial r + \Gamma_{R2})\hat{P}_{R'} = 0$ on the boundaries, leading to the switchable version of (B.6) in Thuburn et al. (2002 I [60]).

$$\sigma_\epsilon = -\frac{\int_{r_C}^{r_S} 2az\left[1/\left(N^2 - \delta_H\sigma_s^2\right)\left[\left\{(\partial/\partial r) + \Gamma_{R2}\right\}\hat{P}_{R_s}\right]^2 + (\delta_A/C_s^2)\hat{P}_{R_s}^2\right]dr}{\int_{r_C}^{r_S}\left[\delta_H a^2/(N^2 - \delta_H\sigma_s^2)^2\left[\left\{(\partial/\partial r) + \Gamma_{R2}\right\}\hat{P}_{R_s}\right]^2 + \left\{l(l+1)/\sigma_s^4\right\}\hat{P}_{R_s}^2\right]dr}. \tag{4.13}$$

Continuing to follow Thuburn et al. (2002 I [60]) we initially consider stable internal gravity modes; in this case $(N^2 - \delta_H\sigma_s^2) > 0$, therefore the denominator is always positive and the numerator is dependent on the value of z. If we set $a = r_C$ then $z > 0$, implying that the numerator is positive and in turn σ_ϵ is negative. Alternatively, if we set $a = r_S$ then $z < 0$, implying that the numerator is negative and σ_ϵ is positive. Thus for a 'slightly-deep' atmosphere extending from r_C to r_S the stable, internal gravity modes have frequencies which lie between those for a shallow atmosphere with $a = r_C$ and those for a shallow atmosphere with $a = r_S$ such that

$$\sigma^2_{a=r_S} < \sigma^2_{\text{slightly deep}} < \sigma^2_{a=r_C}. \tag{4.14}$$

We note that the switchable terms do not affect this relationship, though they are likely to alter the magnitude of σ_ϵ. Thuburn et al. (2002 I [60]) attribute this relationship to the modification of the horizontal pressure gradient terms through application of the shallow atmosphere approximation. For a given horizontal mode structure, and hence defined p'_λ and p'_ϕ, $|(1/r)p'_\lambda|$ will be smaller than $|(1/r_C)p'_\lambda|$ etc, leading to slower accelerations and smaller frequencies. For stable acoustic modes this relationship no longer necessarily follows, as $(N^2 - \delta_H\sigma_s^2) < 0$ and the numerator

is no longer of definite sign. This is not the case for the quasi-hydrostatic set, in which $\delta_H = 0$. In this case the relationship between shallow and slightly-deep modes holds for stable acoustic modes as well as internal gravity modes. This is in agreement with the physical explanation, and numerical calculations of terrestrial normal modes, given by Thuburn et al. (2002 I [60]). They suggest that when the vertical wavelength is much smaller than the horizontal wavelength the dominant factors in determining the frequency are no longer the horizontal pressure gradients. However, when the vertical wavelength is comparable to the horizontal wavelength they find that the frequencies of the acoustic modes of a terrestrial atmosphere follow a similar pattern to that of the stable gravity modes - they point out that in this instance the horizontal pressure gradients become comparable in significance to other aspects of the dynamics. In the quasi-hydrostatic set we have made the assumption that the ratio of vertical wavelength to horizontal wavelength is small, and that vertical accelerations are not significant compared with horizontal accelerations; therefore, our result lends weight to the argument made by Thuburn et al., (2002 I [60]).

We have seen in previous chapters that $N^2 < 0$ is a condition of instability, therefore if we are considering an unstable atmosphere we see that $(N^2 - \delta_H \sigma_s^2) < 0$; thus, like acoustic modes, we are no longer able to assign a definite sign to σ_ϵ. For a convectively unstable atmosphere we expect that there will be modes in which the vertical accelerations dominate over the horizontal accelerations. For these modes we expect that the differences between the eigenfrequencies calculated for shallow and 'slightly-deep' models will follow a similar pattern to that found by Thuburn et al. (2002 I [60]) for the acoustic modes.

4.2 Inviscid F-f Plane

We have seen that considering a non-rotating, inviscid system is not a sufficient simplification to allow analytic solutions. We chose to make a simplification used in many models of the terrestrial atmosphere and consider an F-f plane. This is a tangent plane to the sphere in which $F = 2\Omega\cos\phi$ and $f = 2\Omega\sin\phi$ are set to be constants appropriate to the latitude at which we consider our F-f plane. The F-f plane allows a cartesian coordinate system to be utilised, significantly simplifying the governing equations.

We extend work undertaken by Thuburn et al. (2002 II [59]), Davies et al. (2003 [18]) and Kasahara and Qian(2000 [43]) in which they find solutions to shallow terrestrial atmospheres. Thuburn et al. (2002 II [59]) consider an F-f plane and find normal mode solutions for the fully compressible, isothermal regime in an effort to explain the differences between shallow and deep atmospheres; in particular to consider the effects of the F terms, which are ignored in traditional shallow atmosphere models. Kasahara and Qian (2000 [43]) consider the shallow atmosphere in which F terms are ignored and, through use of a switchable term, highlight the difference between fully-compressible and quasi-hydrostatic equation sets for an isothermal, terrestrial atmosphere. Davies et al. (2003 [18]) endeavour to explain the differences between various approximated equation sets for a shallow, isothermal, terrestrial atmosphere.

In this section we extend their work by considering switchable equation sets on an F-f-plane, under an isothermal regime appropriate to the isothermal region of the Jovian atmosphere. This regime has considerably different parameters to the terrestrial regime not least of which being that it is almost three times as deep, yet a significantly smaller proportion of the relevant planetary radius. Unlike Davies et al. (2003 [18]) we consider the F-f-plane rather than an f-plane, as the effects of the F terms are less well known in a Jovian regime.

Setting f to be constant enforces that there will still be no driving mechanism for the Rossby modes; however, if we assume that the inclusion of non-constant f will not significantly alter the structure of these modes we are able to consider the structure of the degenerate modes to provide an indication towards the effects of the approximations on the Rossby modes.

The coefficients in the F-f plane governing equations are independent of x, y and t therefore we are able to consider separable solutions of the form

$$\left.\begin{array}{lcl} U & & \hat{U}(z) \\ V & & \hat{V}(z) \\ W & = & \hat{W}(z) \\ P & & \hat{P}(z) \\ \Theta & & \hat{\Theta}(z) \end{array}\right\} \exp(ik_x x + ik_y y - i\sigma t), \tag{4.15}$$

where k_x and k_y are the horizontal wavenumbers such that $2\pi/k_x$ and $2\pi/k_y$ are the horizontal wavelengths.

Little progress can be made using the viscous equation set, therefore we have chosen to consider the inviscid case. The equations governing the inviscid F-f plane are given by equations (3.67)-(3.71), inserting (4.15) as appropriate allows them to be written

$$-i\sigma\delta_A\frac{\hat{P}}{C_s^2} + \delta_D\frac{N^2}{g}\hat{W} + \delta_C\frac{\hat{W}}{2\rho_s}\frac{\partial\rho_s}{\partial z} + ik_x\hat{U} + ik_y\hat{V} + \frac{\partial\hat{W}}{\partial z} = 0, \tag{4.16}$$

$$-i\sigma\hat{U} + F\hat{W} - f\hat{V} + ik_x\hat{P} = 0, \tag{4.17}$$

$$-i\sigma\hat{V} + f\hat{U} + ik_y\hat{P} = 0, \tag{4.18}$$

$$-i\sigma\delta_H\hat{W} - F\hat{U} + \frac{\partial\hat{P}}{\partial z} + \delta_E\frac{\hat{P}}{\rho_s}\frac{\partial\rho_s}{\partial z} + \delta_E\frac{\hat{P}}{C_s^2}g - \hat{\Theta}g - \delta_C\frac{\hat{P}}{2\rho_s}\frac{\partial\rho_s}{\partial z} = 0, \tag{4.19}$$

$$-i\sigma\hat{\Theta} + \frac{N^2}{g}\hat{W} = 0. \tag{4.20}$$

Combining the horizontal momentum equations, (4.17) and (4.18), allows us to write

$$\hat{U} = \frac{1}{(\sigma^2 - f^2)}\left[(ik_y f + k_x\sigma)\hat{P} - i\sigma F\hat{W}\right], \tag{4.21}$$

$$\hat{V} = \frac{1}{(\sigma^2 - f^2)} \left[(k_y \sigma - i k_x f)\hat{P} - fF\hat{W} \right]. \tag{4.22}$$

Substitution of these and the thermodynamic equation, (4.20), into the mass continuity equation (4.16) and vertical momentum equation (4.19) yields

$$\begin{aligned} &\left[\frac{\partial}{\partial z} + \delta_D \frac{N^2}{g} + \frac{\delta_C}{2\rho_s}\frac{\partial \rho_s}{\partial z} + \frac{1}{(\sigma^2 - f^2)}(\sigma k_x - i k_y f)F \right] \hat{W} \\ &+ \left[\frac{i\sigma}{(\sigma^2 - f^2)}(k_x^2 + k_y^2) - \delta_A \frac{i\sigma}{C_s^2} \right] \hat{P} = 0, \end{aligned} \tag{4.23}$$

and

$$\begin{aligned} &i\sigma \left[\frac{\partial}{\partial z} - \frac{F}{(\sigma^2 - f^2)}(i k_y f + k_x \sigma) + \frac{\delta_E}{\rho_s}\frac{\partial \rho_s}{\partial z} + \delta_E \frac{g}{C_s^2} - \frac{\delta_C}{2\rho_s}\frac{\partial \rho_s}{\partial z} \right] \hat{P} \\ &- \left[N^2 + \frac{\sigma^2 F^2}{(\sigma^2 - f^2)} - \sigma^2 \delta_H \right] \hat{W} = 0, \end{aligned} \tag{4.24}$$

where we assume $f^2 \neq \sigma^2$.

It is possible to eliminate either $\hat{P}$ or $\hat{W}$, however for an arbitrary reference state the resulting equations must be solved numerically. In order to make further analytic progress we must consider a reference profile in which g, N^2 and C_s^2 are constant. Enforcing constant C_s^2 limits the analytical analysis to an isothermal reference state.

For the isothermal profile with constant gravitational field we then have

$$i\sigma \left[\frac{d}{dz} + A \right] \left[\frac{d}{dz} + C \right] \hat{P} - i\sigma B D \hat{P} = 0, \tag{4.25}$$

where

$$\begin{aligned} A &= \delta_D \frac{N^2}{g} + \frac{\delta_C}{2\rho_s}\frac{d\rho_s}{dz} + \frac{F}{(\sigma^2 - f^2)}(\sigma k_x - f i k_y), \\ B &= \frac{1}{(\sigma^2 - f^2)}(k_x^2 + k_y^2) - \frac{\delta_A}{C_s^2}, \\ C &= -\frac{F}{(\sigma^2 - f^2)}(f i k_y + \sigma k_x) + \frac{\delta_E}{\rho_s}\frac{\partial \rho_s}{\partial z} - \frac{\delta_C}{2\rho_s}\frac{\partial \rho_s}{\partial z} + \delta_E \frac{g}{C_s^2}, \\ D &= \sigma^2 \delta_H - \frac{\sigma^2 F^2}{(\sigma^2 - f^2)} - N^2. \end{aligned} \tag{4.26}$$

We note that using notation used in the previous section, in which we considered a

non-rotating inviscid set,

$$\begin{aligned} A &= \Gamma_{R1} - \frac{F}{(\sigma^2 - f^2)}(fik_y - \sigma k_x), \\ C &= \Gamma_{R2} - \frac{F}{(\sigma^2 - f^2)}(fik_y + \sigma k_x), \end{aligned} \tag{4.27}$$

thus A and C are the 'rotating' versions of Γ_{R1} and Γ_{R2}. It is interesting to note that in the case of an f-plane $A = \Gamma_{R1}$ and $C = \Gamma_{R2}$. Whilst the switchable components of A and C are held within the Γ_{R1} and Γ_{R2} terms we note that we do not yet know how σ is affected by the approximations made to the fully-compressible equation set. Therefore, unlike in the non-rotating case, we are unable to draw conclusions about the relative signs and magnitudes of A and C for the fully-compressible and approximated equation sets. The boundary condition $\hat{W} = 0$ on $z = 0$ and $z = z_T$ yields

$$\left[\frac{d}{dz} + C\right]\hat{P} = 0 \quad \text{on } z = 0 \text{ and } z = z_T. \tag{4.28}$$

Continuing to be guided by Thuburn et al. (2002 II [59]) we make a change of variable

$$\hat{P} = \tilde{P}(z) \exp\left[-\left(\frac{C + A}{2}\right) z\right], \tag{4.29}$$

where we note that

$$-\left(\frac{C + A}{2}\right) = -\frac{1}{2}\left[\Gamma_{R1} + \Gamma_{R2} + \frac{2Ffik_y}{(\sigma^2 - f^2))}\right]. \tag{4.30}$$

We have seen in section 4.1 that , with the exception of the non-energy conserving anelastic set, $\Gamma_{R1} = -\Gamma_{R2}$. Therefore we note that when considering the f-plane it is not necessary to make the change of variable, with the exception of the non-energy conserving anelastic set. Since we are dealing with an isothermal regime in which $\kappa < 0.5$ and $H > 1$ it is also unnecessary to make the change of variable for the non-energy conserving anelastic set on an f-plane. We also note that comparison of 4.29 with (3.12) of Thuburn et al. (2002 II [59]) shows that in rescaling our equation set we have removed a systematic variation with height equal to

$$\exp\left[-\frac{1}{2}\left(\frac{N^2}{g} + \frac{g}{C_s^2}\right) z\right] = \exp\left[\frac{1}{2\rho_s}\frac{\partial \rho_s}{\partial z} z\right]. \tag{4.31}$$

Having introduced the aforementioned change of variable equation (4.25) becomes

$$i\sigma \left[\frac{d^2}{dz^2} + k_z^2 \right] \tilde{P} = 0, \tag{4.32}$$

where

$$k_z^2 = -BD - \frac{(C-A)^2}{4} \tag{4.33}$$

subject to boundary condition

$$\left[\frac{d}{dz} + \frac{(C-A)}{2} \right] \tilde{P} = 0 \quad \text{on } z = 0 \text{ and } z = z_T. \tag{4.34}$$

It should be noted that both BD and $(C-A)$ are real, thus k_z^2 is real. We also note that the $\sigma = 0$ solution to equation (4.32) represents the degenerate Rossby mode.

We have seen in section 2.9.2 that for the isothermal case with constant gravitational field the reference state variables are defined as

$$\theta_s(z) = \theta_C \exp(\kappa z/H), \quad \rho_s(z) = \rho_C \exp(-\delta_C z/H), \tag{4.35}$$

where θ_C and ρ_C are constants defining the potential temperature and density at the lower boundary, and the atmospheric scale height is given by

$$H = \frac{RT_s}{g}. \tag{4.36}$$

We can then see that

$$\frac{1}{H} = -\frac{1}{\rho_s}\frac{d\rho_s}{dz}, \quad \frac{1}{H} = \frac{g}{C_s^2(1-\kappa)}, \quad \text{and} \quad \frac{1}{H} = \frac{N^2}{\kappa g}. \tag{4.37}$$

These can be substituted into A, B, C and D as appropriate.

4.3 External Modes

4.3.1 Vertical Structure

We consider the boundary conditions (4.34) and find that for $k_z^2 < 0$ they can only be satisfied when

$$k_z^2 = -\left(\frac{C-A}{2}\right)^2 \tag{4.38}$$

from equation (4.33) this implies that $BD = 0$. We then have

$$\tilde{P} = \hat{P}(0)\exp\left[-\left(\frac{C-A}{2}\right)z\right], \tag{4.39}$$

where $\hat{P}(0)$ is an arbitrary constant with dimensions of pressure that provides the amplitude of the pressure perturbation. The vertical structure functions of the rescaled variables for the external modes are then

$$\hat{P} = \hat{P}(0)\exp\left[\left(\frac{F(\sigma k_x + fik_y)}{(\sigma^2 - f^2)}\right)z\right]\exp\left[\left(\frac{\delta_E\kappa}{H}\right)z - \left(\frac{\delta_C}{2H}\right)z\right], \tag{4.40}$$

$$\hat{W} = 0, \tag{4.41}$$

$$\hat{\Theta} = 0, \tag{4.42}$$

$$\hat{U} = \frac{(\sigma k_x + fik_y)}{(\sigma^2 - f^2)}\hat{P}, \tag{4.43}$$

$$\hat{V} = \frac{(\sigma k_y - fik_x)}{(\sigma^2 - f^2)}\hat{P}. \tag{4.44}$$

Taking into account the rescaling of the variables we find

$$p' = \hat{P}(0)\rho_C^{1/2}\exp\left[\left(\frac{F(\sigma k_x + fik_y)}{(\sigma^2 - f^2)} - \frac{(\delta_C - \delta_E\kappa)}{H}\right)z\right]\exp\left[i(k_x x + k_y y - \sigma t)\right], \tag{4.45}$$

$$u = \frac{\hat{P}(0)}{\rho_C^{1/2}}\frac{(\sigma k_x + fik_y)}{(\sigma^2 - f^2)}\exp\left[\left(\frac{F(\sigma k_x + fik_y)}{(\sigma^2 - f^2)} + \frac{\delta_E\kappa}{H}\right)z\right]\exp\left[i(k_x x + k_y y - \sigma t)\right], \tag{4.46}$$

$$v = \frac{\hat{P}(0)}{\rho_C^{1/2}}\frac{(\sigma k_y + fik_x)}{(\sigma^2 - f^2)}\exp\left[\left(\frac{F(\sigma k_x + fik_y)}{(\sigma^2 - f^2)} + \frac{\delta_E\kappa}{H}\right)z\right]\exp\left[i(k_x x + k_y y - \sigma t)\right]. \tag{4.47}$$

Setting all switches equal to one yields the fully compressible solutions derived in Thuburn et al. (2002 II [59]). Setting F and k_y equal to zero yields the equivalent form of the solutions derived for a switchable f-plane by Davies et al. (2003 [18]).

Equations (4.45) - (4.47) indicate that the structure of the solutions can be altered through distortion of the frequency or through distortion by the switchable terms. Frequency distortion will be discussed in section 4.3.2. The switchable terms only distort the external modes in the Boussinesq and energy conserving anelastic cases, for all other cases $\delta_E = \delta_C = 1$ as for the fully compressible set. The height-dependence of the energy-conserving anelastic modes is spuriously reduced by a factor of $\exp(\kappa z/H)$, this equates to a factor of approximately 1.33 for $z = H$ and increases for larger values of z. The height-dependence of pressure for the Boussinesq set is amplified by a factor of $\exp((1-\kappa)z/H)$; setting $\kappa = 0.32$ as appropriate to a Jovian atmosphere (see section 2.9.2) this equates to a factor of approx 1.97 at $z = H$. We have previously discussed that the region of the Jovian atmosphere that isothermal analysis is most appropriate to lies between 80 and 300 km from the outer surface; therefore, H is calculated to be approximately 25 km thus the height-dependence distortion caused by the Boussinesq and energy conserving anelastic approximations will be significant in this region. Fig 4.1 displays this in graphical form for the degenerate Rossby mode, the variables plotted are $P/\hat{P}(0)$ and $U/\hat{P}(0)$ as we have seen in 4.31 that rescaling the perturbation variables to these convenient forms allows us to remove the effects of the systematic variation of amplitude with altitude caused by density variation. The horizontal length scale for the plotted variables is comparable to the Rossby radius of deformation; the length scale at which rotational effects become as important as buoyancy effects. For the isothermal region of the Jovian atmosphere this is approximately given by

$$\text{Rossby radius} = \frac{NH_0}{f} \approx 1785\text{km}. \tag{4.48}$$

The distortion of height dependency for the Boussinesq and non-energy-conserving

anelastic set can be seen clearly over the isothermal region of the Jovian upper atmosphere. We note that similar effects are seen for different horizontal length scales.

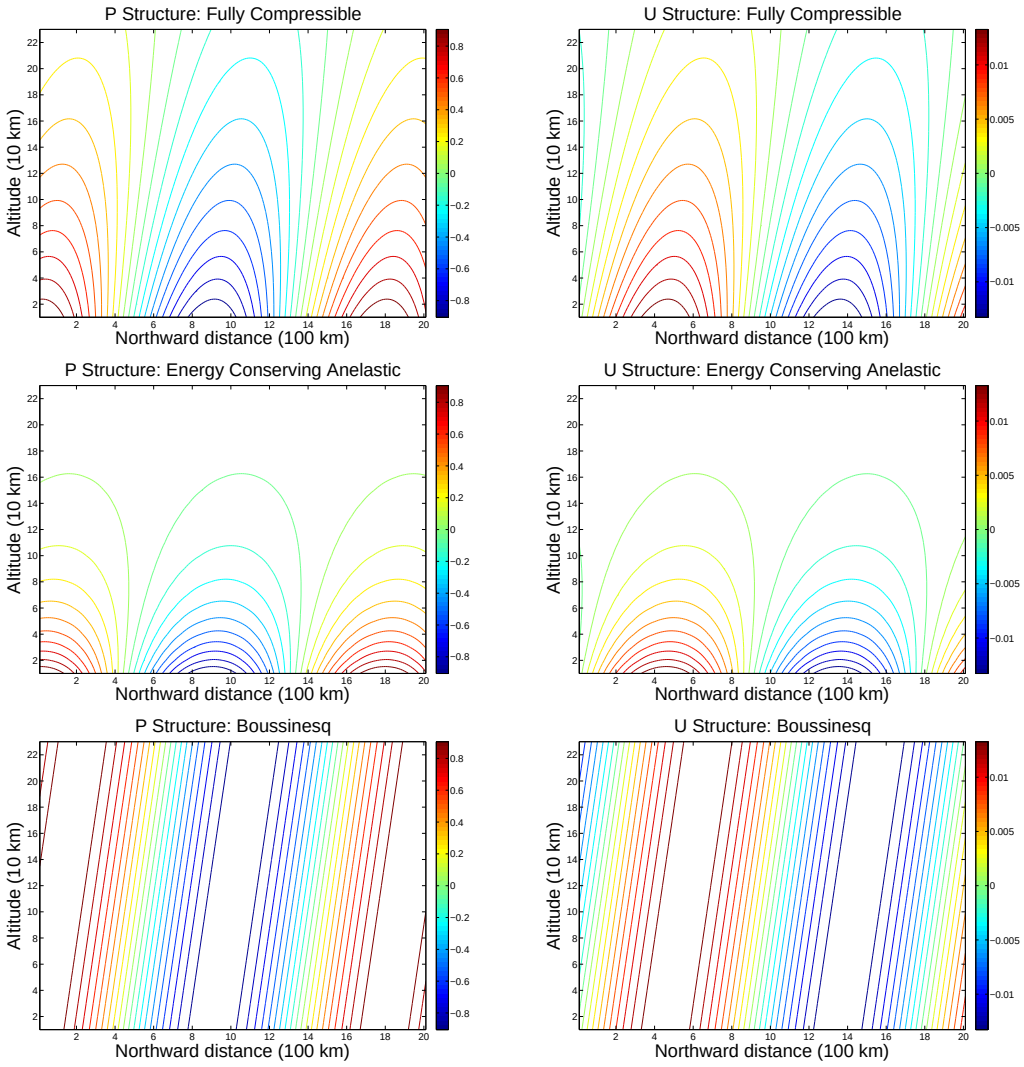

Figure 4.1: *Latitude-height P and U structure for degenerate external Rossby mode on an F-f plane at $45^o N$. Isothermal reference state as appropriate to isothermal region of Jovian upper atmosphere. Horizontal wavelength = O(Rossby radius), therefore $k_x = k_y = 3.5 \times 10^{-6} m^{-1}$. Origin of figures set to be at the inner surface, $r_C = 71,430 km$.*

4.3.2 Dispersion relation

Construction of a dispersion relation will allow us to ascertain the differences between the frequencies of the various approximated equation sets, this in turn will allow further examination of the effect of frequency discrepancies on the vertical structure.

We have shown that for the external modes $BD = 0$, therefore the dispersion relation is

$$\left[\delta_A\left(\sigma^2 - f^2\right) - C_s^2\left(k_x^2 + k_y^2\right)\right]\left[\left(N^2 - \sigma^2\delta_H\right)\left(\sigma^2 - f^2\right) + F^2\sigma^2\right] = 0. \tag{4.49}$$

For cases in which $\delta_A = \delta_H = 1$ there are six roots to equation (4.49), however the four roots given by

$$\left[\left(N^2 - \sigma^2\delta_H\right)\left(\sigma^2 - f^2\right) + F^2\sigma^2\right] = 0, \tag{4.50}$$

turn out to be spurious and do not satisfy the governing equations. These roots arise due to the fact that if we combine equations (4.23) and (4.24) to form an equation governing $\hat{P}$ we find there is a singular term $[(\delta_H\sigma^2 - N^2)(\sigma^2 - f^2) - F^2\sigma^2]^{-1}$. If $\delta_H = 0$ two of these spurious roots are filtered, such that they are not solutions to the approximated equation set in question.

The remaining roots are defined by

$$\delta_A\sigma^2 = \delta_A f^2 + C_s^2\left(k_x^2 + k_y^2\right). \tag{4.51}$$

These are the external acoustic modes. If $\delta_A = 0$ these roots are filtered from the solutions of the approximated equation set in question.

Through consideration of the switchable terms we can see that these modes are filtered from all approximated equation sets except the quasi-hydrostatic set. In the quasi-hydrostatic case we note that the external acoustic modes are the same as those of the fully compressible equation set. The external Rossby mode is given by $\sigma = 0$, this is not a solution to equation (4.51) as this solution is taken into consideration in

equation (4.32). The degenerate frequency of the Rossby modes is captured correctly by all approximated sets.

Effect of F terms

The dispersion relation given by equation (4.51) shows that the frequencies of the external acoustic modes are not affected by terms involving F, as such they are identical to the external acoustic modes on a shallow atmosphere f-plane.

The vertical structure functions for p', u and v each contain F solely in the term:

$$\exp\left[\left(\frac{F(\sigma k_x + f i k_y)}{(\sigma^2 - f^2)}\right) z + \frac{a}{H} z\right] \tag{4.52}$$

where $a = -(\delta_C - \delta_E \kappa)$ for p' and $a = \delta_E \kappa$ for u and v. If the F term in the exponent of (4.52) is significant compared with the $1/H$ term then the inclusion of the F term will have a significant effect on the vertical structure compared with that of the f-plane.

We again consider the isothermal region of the Jovian atmosphere together with the dispersion relation for the external acoustic modes. We find that the maximum value for the real part of the F term is found when considering the f-F plane at 45^o latitude and maximal values of the horizontal wavelength, naturally this is constrained by the circumference of the Jovian model. The maximum value of the real part of the F term is then of the order 10 times smaller than the terms involving $1/H$, indicating that the amplitude difference between the f-plane and F-f-plane will be small. However the inclusion of the F terms also introduces an imaginary component, this component gives rise to a vertical phase tilt. In practice the phase tilt and amplitude distortion created by the exclusion of F terms is often insignificant. However, figure 4.2 shows that in the case of the degenerate Rossby mode the tilt produced by the inclusion of F terms is noticeable for horizontal wavelength

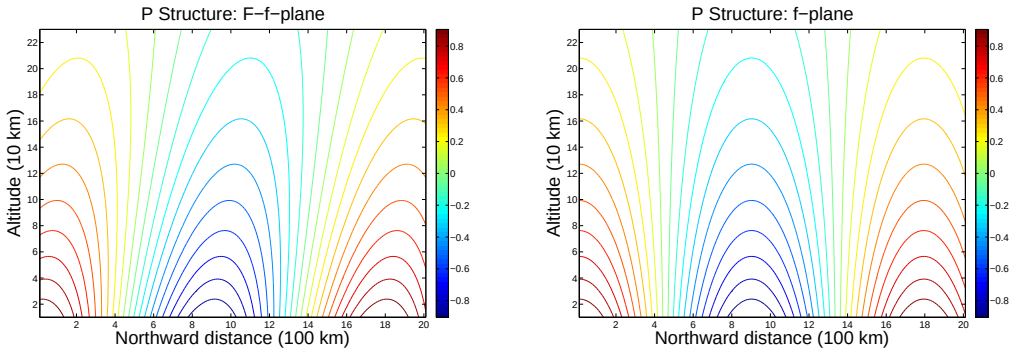

Figure 4.2: *Latitude-height P structure for degenerate external Rossby mode on a fully compressible F-f plane at $45^o N$, and a fully compressible f-plane at $45^o N$. Isothermal reference state as appropriate to isothermal region of Jovian upper atmosphere. Horizontal wavelength = O(Rossby radius), therefore $k_x = k_y = 3.5 \times 10^{-6} m^{-1}$. Origin of figures set to be at the inner surface, $r_C = 71,430 km$.*

comparable to the Rossby radius of deformation. We note that in the case of the degenerate Rossby modes, the tilting effect introduced by the F terms is obvious for modes with horizontal wavelengths smaller than approximately 2.5 times the Rossby radius of deformation.

4.3.3 External Modes: Summary

Within this section we have seen that there are several possible external mode solutions. The first of these, the degenerate external Rossby mode, has zero frequency which is accurately captured by all equation sets. The vertical structure of these degenerate modes is accurately captured by quasi-hydrostatic, pseudo-incompressible and non-energy-conserving anelastic sets. The height dependency of the Boussinesq and energy-conserving anelastic sets is distorted. Most equation sets produce four spurious roots which 'exist' due to a singular term in the equation governing $\hat{P}$, the quasi-hydrostatic set only produces two of these spurious roots. Finally, the quasi-

hydrostatic and fully-compressible sets produce eastward (prograde) and westward (retrograde) propogating external acoustic mode solutions. The vertical structure and eigenfrequencies of the external acoustic modes are accurately replicated by the quasi-hydrostatic set. The external acoustic modes are filtered by all other equation sets.

4.4 Internal Modes

4.4.1 Vertical Structure

The second set of solutions to our governing equations are given by the internal modes. There are infinitely many internal modes corresponding to the case when $k_z^2 > 0$. The solutions are of the form

$$\tilde{p} = \hat{P}(0)\left[k_z\cos(k_z z) - \left(\frac{C-A}{2}\right)\sin(k_z z)\right], \tag{4.53}$$

where $k_z = m\pi/z_T$ with m a positive integer, $z_T = r_S - r_C$ and $\hat{P}(0)$ is an arbitrary constant defining the amplitude of the pressure perturbation at the ground. The vertical structure functions are then

$$\hat{P} = \hat{P}(0)\left[k_z\cos(k_z z) - \left(\frac{C-A}{2}\right)\sin(k_z z)\right]\exp\left[-\left(\frac{C+A}{2}\right)z\right], \tag{4.54}$$

$$\hat{W} = \frac{i\sigma}{D}\left[k_z^2 + \left(\frac{C-A}{2}\right)^2\right]\hat{P}(0)\sin(k_z z)\exp\left[-\left(\frac{C+A}{2}\right)z\right], \tag{4.55}$$

$$\hat{\Theta} = \frac{-i}{\sigma}\frac{N^2}{g}\hat{W}, \tag{4.56}$$

$$\hat{U} = \frac{1}{(\sigma^2 - f^2)}\left[(\sigma k_x + fik_y)\hat{P} - Fi\sigma\hat{W}\right], \tag{4.57}$$

$$\hat{V} = \frac{1}{(\sigma^2 - f^2)}\left[(\sigma k_y - fik_x)\hat{P} - fF\hat{W}\right], \tag{4.58}$$

where

$$\frac{C-A}{2} = -\frac{F\sigma k_x}{(\sigma^2 - f^2)} + \Gamma, \tag{4.59}$$

$$\frac{C+A}{2} = -\frac{Ffik_y}{(\sigma^2 - f^2)} - \frac{(\delta_E - \delta_D)\kappa}{2H}, \tag{4.60}$$

$$D = \sigma^2\delta_H - \frac{\sigma^2 F^2}{(\sigma^2 - f^2)} - N^2, \tag{4.61}$$

$$\Gamma = \frac{\delta_C - (\delta_E + \delta_D)\kappa}{2H}. \tag{4.62}$$

We note that referring to the notation used in section 4.1 we have $\Gamma = \Gamma_{R2} - \Gamma_{R1}$, where we have now written it in a form which allows us to compare its value for all equation sets.

As with the external modes we are easily able to convert these to the full solutions for the perturbation variables. We note that the switches enabling us to swap between equation sets feature in several places in the internal mode vertical structure functions; setting all switches equal to one yields the solutions for the fully compressible set obtained by Thuburn et al. (2002 II [59]). Setting F and k_y equal to zero yields solutions equivalent to those found in Davies et al. (2003 [18]). The external modes suffer vertical structure distortion only through distortion of the height-scale, however the internal modes are able to be distorted in three ways: 1. distortion of height-dependency; 2. relocation of modal zeroes; 3. energy redistribution.

Distortion of Height-Dependency

Distortion of height-dependency is determined either via the switchable component $\exp[(\delta_E - \delta_D)\kappa z/2H]$, or by frequency distortions. The non-energy-conserving anelastic set is the only equation set for which $\delta_E - \delta_D$ is non-zero, it is therefore affected by a spurious growth with height through the term $\exp(\kappa z/2H)$ which for the isothermal region of the Jovian atmosphere is a factor of approximately 1.38 at $z = H$. Since we are discussing the re-scaled variables it is important to note that in the Boussi-

nesq case despite $\delta_E = \delta_D$ being zero there is still distortion of height dependency of the perturbation variables. When reverting to the original perturbation variables it is necessary to take into account the reference state density, in the Boussinesq case this is considered constant thus the perturbation variables will suffer a lack of growth with height equal to the factor $\exp(-z/2H)$, this equates to a factor of approximately 0.61 at $z = H$. Figure 4.3 shows these height-dependency distortion factors for the degenerate Rossby mode on an F-f-plane, and all internal modes on an f-plane. It is important to note that significant frequency distortion would also lead to height-dependency distortion, this will be discussed at a later stage.

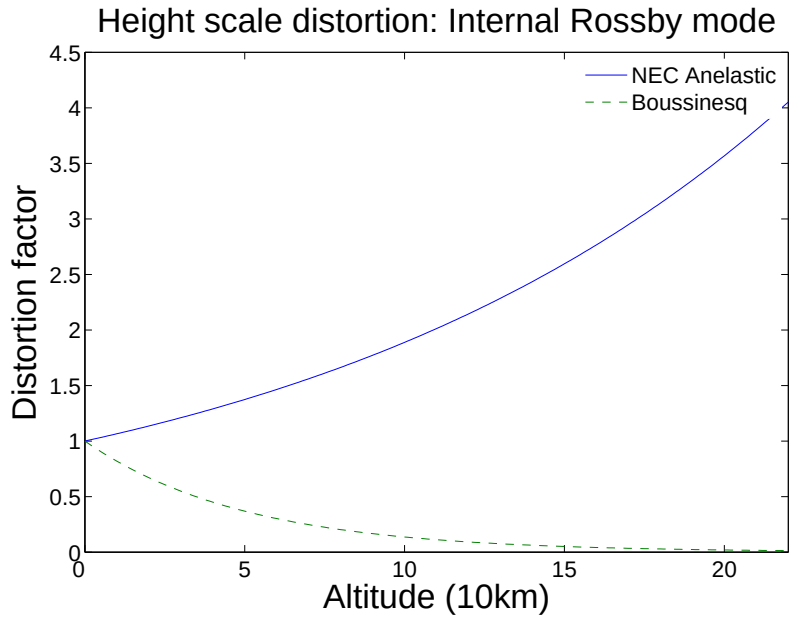

Figure 4.3: *Height-dependency distortion factor for internal Rossby modes on an F-f-plane, and all internal modes on an f-plane. Reference state as appropriate to isothermal region of Jovian atmosphere. Origin set to be at the inner surface,* $r_C = 71,430km$.

Relocation of Modal Zeros

Unlike the external modes the internal modes have modal zeros which are governed by

$$k_z \cos(k_z z) - \left(\frac{C-A}{2}\right) \sin(k_z z) = 0 \quad \Rightarrow \quad \tan(k_z z) = \left[\frac{2k_z}{C-A}\right], \tag{4.63}$$

where

$$\frac{2k_z}{(C-A)} = \frac{k_z(\sigma^2 - f^2)}{\Gamma(\sigma^2 - f^2) - F\sigma k_x}. \tag{4.64}$$

The relocation of modal zeros relative to the fully compressible case is then determined by the approximated forms of Γ and σ. Γ differs from the fully compressible value for both anelastic sets and the Boussinesq case. Therefore, these equation sets will certainly be affected by modal zero relocation. We note that for the degenerate Rossby mode $\tan(k_z z) = k_z/\Gamma$ and is independent of k_x and F. In the Boussinesq case $\Gamma = 0$ therefore $\tan(k_z z) = \infty$ which leads to $k_z z = (2n+1)\pi/2$ for integer n. To aid in the analysis of the redistribution of perturbation energy amongst the prognostic variables, it is convenient to write

$$k_z \cos(k_z z) - \left(\frac{C-A}{2}\right) \sin(k_z z) \equiv \left[k_z^2 + \left(\frac{C-A}{2}\right)^2\right]^{1/2} \cos\left[k_z z + \Delta\right], \tag{4.65}$$

where $\Delta = \tan^{-1}\left[(C-A)/2k_z\right]$ is a phase such that we always take the principal value of $\tan^{-1}$. We are then able to see that relocation of the modal zeroes will occur when there are changes to the roots of

$$\cos\left(k_z z + \Delta\right) = 0. \tag{4.66}$$

Figure 4.4 shows the phase shift Δ vs. internal mode number for zeros of the degenerate internal Rossby mode on an $F-f$-plane. The Boussinesq approximation yields a spurious phase shift of zero for all mode numbers. Both anelastic sets also show significant relocation of the modal zeroes particularly for the deepest modes. The quasi-hydrostatic and pseudo-incompressible sets are not featured on the figure as

the modal zeroes are accurately captured and match those of the fully compressible modes.

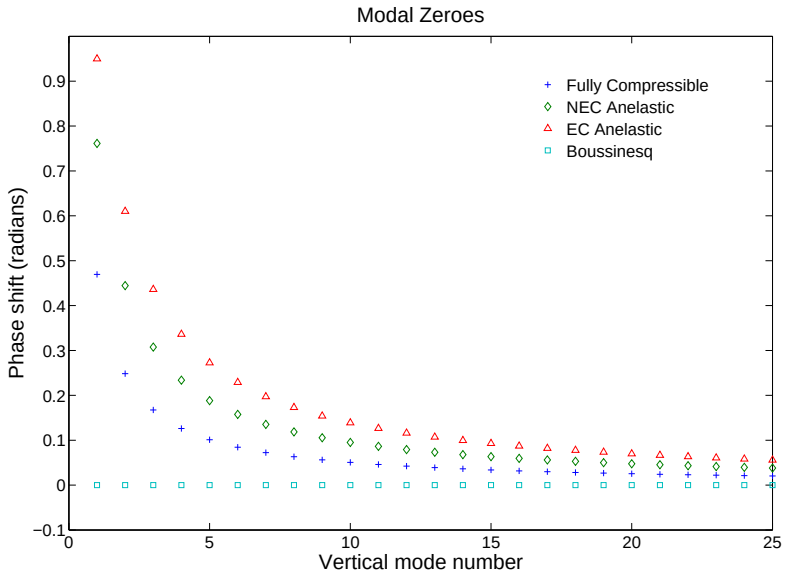

Figure 4.4: *Relocation of modal zeros, degenerate internal Rossby mode. Reference state appropriate to isothermal region of Jovian upper atmosphere.*

We will discuss the dispersion relation for σ at a later stage, this will allow us to further analyse the extent to which the switchable terms will have an effect on the zeros of the internal gravity and acoustic modes. We expect that distortion of the modal zeroes due to disortion of sigma will only be significant in cases where $k_x/k_z \ll 1$, $\sigma > f$ and $k_z > \Gamma$.

Energy Redistribution

Spurious distortion of the perturbation variables can lead to the redistribution of perturbation energy. We have seen that the perturbation energy is given by (2.48)

$$\begin{aligned} E &= \frac{\rho_s}{2}\left(|u|^2+|v|^2+\delta_H|w|^2+\frac{g^2}{N^2}\left|\frac{\theta'}{\theta_s}\right|^2+\frac{\delta_A}{\rho_s^2}\frac{|p'|^2}{C_s^2}\right) \\ &= \frac{1}{2}\left(|U|^2+|V|^2+\delta_H|W|^2+\frac{g^2}{N^2}|\Theta|^2+\frac{\delta_A}{C_s^2}|P|^2\right). \end{aligned} \tag{4.67}$$

Therefore, it is clear that if for example, the horizontal velocity was spuriously amplified and all other perturbation variables were accurately represented, there would be a repartitioning of energy amongst the perturbation variables with the horizontal velocity accounting for a greater portion of the perturbation energy than it otherwise would. The switchable components within 4.67 show that the perturbation energy is not defined accurately by any of the approximated sets, indeed in the non-energy-conserving anelastic set this quantity is no longer conserved. The differing definitions of perturbation energy make it difficult to quantify the energy redistribution between variables but consideration of the component variables gives qualitative insight.

In the case of the external modes the switchable term which causes distortion of normal modes of the energy-conserving anelastic and Boussinesq sets is common to all the perturbation variables, it therefore does not cause any change in the distribution between variables. Therefore, in all approximated equation sets the overall energy varies but the relative contribution made by each variable remains accurately represented.

The internal modes of the approximated sets suffer from more extensive energy redistribution. As with the external modes the $\exp[-(C+A)/2]$ factor distorting the height-scale is common to all variables and thus does not cause energy redistribution. However, the coefficients governing the amplitudes of the variables contributing to the normal mode perturbation energy contain Γ and σ and are not common to each variable. For each approximated set we note that if either of these factors differs

from that of the fully compressible set there will be some energy redistribution to a lesser or greater extent. Consideration of the degenerate Rossby mode shows that both anelastic sets, and the Boussinesq set will cause energy redistribution, the other approximated sets accurately capture Γ thus don't cause such spurious redistribution. Whilst it is difficult to quantify the level of energy redistribution caused, some indication can be gained by considering the factor $[k_z^2 + (C-A)^2/4]^{1/2}$. We saw in section 4.4.1 that we are able to write

$$k_z \cos(k_z z) - \left(\frac{C-A}{2}\right) \sin(k_z z) \equiv \left[k_z^2 + \left(\frac{C-A}{2}\right)^2\right]^{1/2} \cos\left[k_z z + \Delta\right].$$

This factor is seen in our definition of $\hat{P}$, however it is the square of this factor which is seen in the definition of $\hat{W}$. Consequently, if the value of $[k_z^2 + (C-A)^2/4]^{1/2}$ for the approximated equation sets differs from that of the fully-compressible set there will be repartitioning of energy between $\hat{P}$ and $\hat{W}$, thus also the other thermodynamic and velocity variables. Figure 4.5 shows the ratio of the approximated form of this factor to the fully compressible form for the degenerate Rossby mode. We then find that the distortion of this factor is significant for each of the sets in which $\Gamma \neq ((1-2\kappa)/(2H))$. For the deepest modes the energy-conserving anelastic set is distorted by as much as 50%. The energy redistribution occurring due to the quasi-hydrostatic and pseudo-incompressible approximations is dependent on σ, thus the degenerate internal Rossby mode doesn't suffer from energy redistribution in these cases. If σ is accurately represented the distribution of energy for the internal gravity modes will also be accurately represented, this will be discussed further when considering the approximated internal mode frequencies.

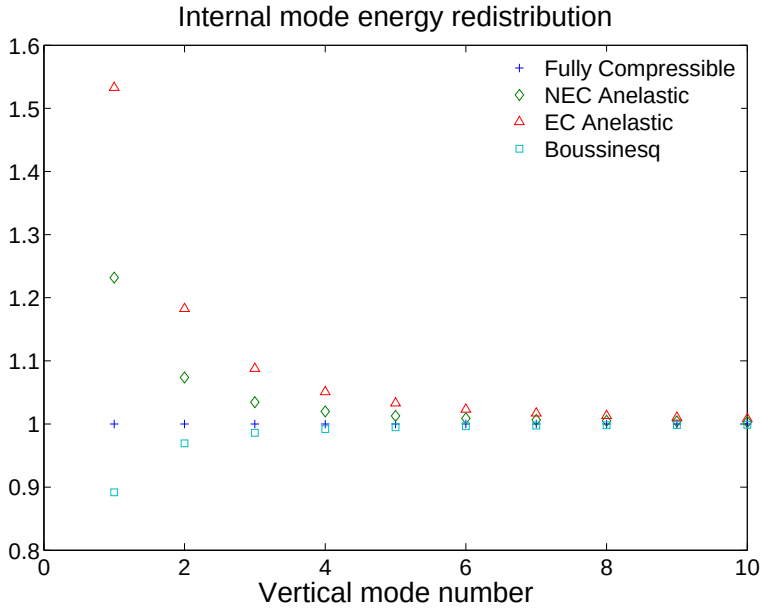

Figure 4.5: *Ratio of approximated set to fully compressible set for the amplitude term* $[k_z^2 + (C-A)^2/4]^{1/2}$ *for degenerate internal Rossby mode. Reference state appropriate to Isothermal region of Jovian atmosphere.*

4.4.2 Dispersion relation

Once again we consider equation (4.33) in order to derive a dispersion relation, this time for the internal modes

$$\begin{aligned}\left[\delta_A\left(\sigma^2-f^2\right)-C_s^2\left(k_x^2+k_y^2\right)\right]\left[\left(N^2-\sigma^2\delta_H\right)\left(\sigma^2-f^2\right)+F^2\sigma^2\right] \\ +C_s^2\left[k_z^2(\sigma^2-f^2)^2+\{\Gamma(\sigma^2-f^2)-Fk_x\sigma\}^2\right]=0\end{aligned} \tag{4.68}$$

where

$$\Gamma=\frac{\delta_C-(\delta_E+\delta_D)\kappa}{2H}. \tag{4.69}$$

This sixth degree polynomial is a switchable form of the dispersion relation for a compressible atmosphere given by Thuburn et al. (2002 II [59]). Four roots of equation (4.68) correspond to the eastward and westward propogating internal acoustic and gravity modes. Setting $\delta_A = 0$ or $\delta_H = 0$ eliminates two of these modes, which we expect to be the eastward and westward propogating internal acoustic modes. It is

not immediately obvious why the further two roots exist but Thuburn et al showed them to be dependent on both the inclusion of the F terms and the top and bottom boundary conditions. Kasahara (2003 [42]) examined these modes in more detail, referring to them as Boundary-Induced Inertial modes (BII) and detailing how they seem to be dependent on the inclusion of both F terms and upper and lower boundaries. Durran and Bretherton (2004 [23]) explain how these modes are not traditional boundary induced waves such as edge waves, which have a distinctly different spatial structure and cannot exist in the absence of a boundary; rather they are superpositions of 'inertio-gravity' waves which can exist in an unbounded domain. Crucially they show that whilst the frequencies and wavenumbers of inertio-gravity waves and BII modes can be very different, the dynamics which underlie them are very similar. This is in contrast to the differences between acoustic and inertio-gravity waves, or indeed edge waves. Finally, as with the external modes the degenerate Rossby mode does not appear in the dispersion relation as it is eliminated in forming equation (4.33).

In order to simplify the dispersion relation further we consider the f-plane, and discuss the effect of neglecting the F terms. The frequencies σ_f for the f-plane are defined by a quadratic in σ_f^2

$$\left[\delta_A\left(\sigma_f^2 - f^2\right) - C_s^2 k^2\right]\left(N^2 - \sigma_f^2\delta_H\right) + C_s^2(\sigma_f^2 - f^2)\left(k_z^2 + \Gamma^2\right) = 0. \tag{4.70}$$

Here we have set $k^2 = \left(k_x^2 + k_y^2\right)$. This is in order that we can consider both the scenario in which the f-plane refers to equation sets in which only the F terms have been neglected, as well as the case in which the f-plane refers to equation sets in which all y dependence has been neglected. Davies et al. (2003 [18]) consider the latter of these scenarios, they seek solutions proportional to $\exp(ik_x x - i\sigma t)$ and derive a dispersion relation identical to the one in which we set $k^2 = k_x^2$.

The solutions to (4.70) correspond to symmetrical eastward and westward propagating pairs of internal acoustic and gravity modes. If we consider the switchable

terms we find that if $\delta_A\delta_H = 0$ the dispersion relation is reduced to a quadratic in σ_f. This confirms that, as expected, the internal acoustic modes are filtered in all approximated sets and the frequencies produced by the resulting dispersion relation correspond to the internal gravity modes. As shown by Davies et al. (2003 [18]) the frequencies of the internal gravity modes are then found by the following:
for Anelastic and Pseudo-Incompressible sets, $\delta_A = 0$,$\delta_H = 1$

$$\sigma_f^2 = f^2 + \frac{k^2(N^2 - f^2)}{k_z^2 + \Gamma^2 + k^2}; \tag{4.71}$$

for Quasi-hydrostatic set $\delta_H = 0$,$\delta_A = 1$

$$\sigma_f^2 = f^2 + \frac{k^2 N^2}{\frac{N^2}{C_s^2} + \Gamma^2 + k_z^2}; \tag{4.72}$$

for Boussinesq set $\Gamma = 0$

$$\sigma_f^2 = f^2 + \frac{k^2(N^2 - f^2)}{k_z^2 + k^2} \tag{4.73}$$

Figures 4.6-4.13 show the approximated f-plane fequencies in which all y dependence has been neglected, alongside the numerically calculated F-f-plane frequencies for the same isothermal region of the Jovian atmosphere. As has previously been discussed this is a layer of depth approximately 220km with inner surface at radius $r = 71,430$km, $\kappa = 0.32$ and $T_s = 160K$. The figures also display the ratio of approximated frequency to fully compressible frequency for each equation set.

For short horizontal wavelength (60km) the ratio of quasi-hydrostatic to fully compressible sets is not displayed graphically. This is because the large distortion of this set means that it becomes difficult to identify differences between the other sets. We note from figure 4.6 that the distortion of the quasi-hydrostatic set on an f-plane is as much as 400% for the deepest modes, whilst on an F-f-plane this is increased to 550%. This level of misrepresentation will also cause significant energy redistribution, and relocation of modal zeroes. At this horizontal wavelength the other approximated equation sets misrepresent the f-plane frequencies by less than 1.5% for all vertical

mode numbers; and the F-f-plane frequencies are misrepresented by less than 0.75% for all vertical mode numbers. It is interesting to note that the inclusion of F terms increases the vertical mode number at which the approximated sets overestimate the freqency rather than underestimate it.

Figure 4.8 illustrates that at horizontal wavelength $k_x = 600$km, $k_y = 0$km on an f-plane, and $k_x = k_y = 600$km on an F-f-plane the approximated equation sets cause significant errors in the calculation of frequency. The Boussinesq set misrepresents the frequency by over 40% for the deepest modes on an f-plane with the Boussinesq F-f-plane misrepresentation reduced to approximately 23% for vertical mode number $m = 1$. In both the case of the f-plane and F-f-plane the quasi-hydrostatic set is now the most accurate of the approximated equation sets, overestimating the frequency by less than 10% for the f-plane frequencies and less than 5% for the F-f plane frequencies. All approximated sets are most severely misrepresented for the deepest modes; only the energy conserving anelastic set underestimates the frequency with the quasi-hydrostatic set underestimating the deepest mode on the F-f-plane and all other approximated sets overestimating all frequencies. We note that for all approximate sets and the fully compressible set the deepest F-f-plane frequencies are approximately 20% larger than the f-plane frequencies at the same vertical mode number.

Figure 4.10 shows the inaccuracies caused for modes with horizontal wavelength approximately equal to the the Rossby radius of deformation, which we have previously calculated to be approximately 1,785km for the isothermal region of the Jovian atmosphere. We see that, as for horizontal wavelength equal to 600km, the Boussinesq set has the most significant misrepresentation - almost 70% for the deepest modes on an f-plane and almost 50% on an F-f-plane. At this horizontal wavelength the misrepresentation of the frequencies of the pseudo-incompressible and non-energy-conserving sets is also significant for the deepest modes. On an F-f-plane the pseudo-

incompressible set displays errors of similar magnitude to the Boussinesq set while the non-energy-conserving anelastic set has maximum errors of just under 25% on both an f-plane and an F-f-plane. The energy-conserving anelastic and quasi-hydrostatic sets display maximum errors of less than 2%. For all approximated equation sets, though in particular the Boussinesq and pseudo-incompressible sets, this error reduces quickly with mode number. For $m = 2$ the misrepresentation of the Boussinesq set has reduced to just above and just below 20% for the f and F-f planes respectively, by $m = 10$ the mispresentation is less than 2% for all equation sets. Once again, the frequencies calculated for an F-f-plane are larger than those on an f-plane.

Figure 4.12 shows the inaccuracies caused for modes with horizontal wavelength equal to the circumfrence of Jupiter. At this wavelength the frequencies of the normal modes are close to $2\Omega \sin\phi$, and are misrepresented by less than 0.05% for all approximated equation sets. It is interesting to note that, unlike the other horizontal wavelengths we have considered, at this horizontal wavelength modal frequencies are more severely misrepresented by approximated sets on an F-f-plane than they are on an f-plane.

Consideration of the frequencies calculated for an f-plane in which some y dependence has been retained through inclusion of k_y terms shows that inclusion of some y dependence means the error in calculation of modal frequencies lies somewhere between the misrepresentation displayed by the approximated equation sets on an f-plane with no y dependence and those on an F-f-plane. This reduces the misrepresentation displayed by the approximated equation sets for all horizontal wavelengths considered with the exception of horizontal wavelength comparable to the Jovian circumference.

It is interesting to note that in all cases considered the inclusion of F-terms causes the frequency to be increased compared to the f-plane. For the deepest modes, with shortest horizontal wavelength, the difference between the f-plane and F-f-plane

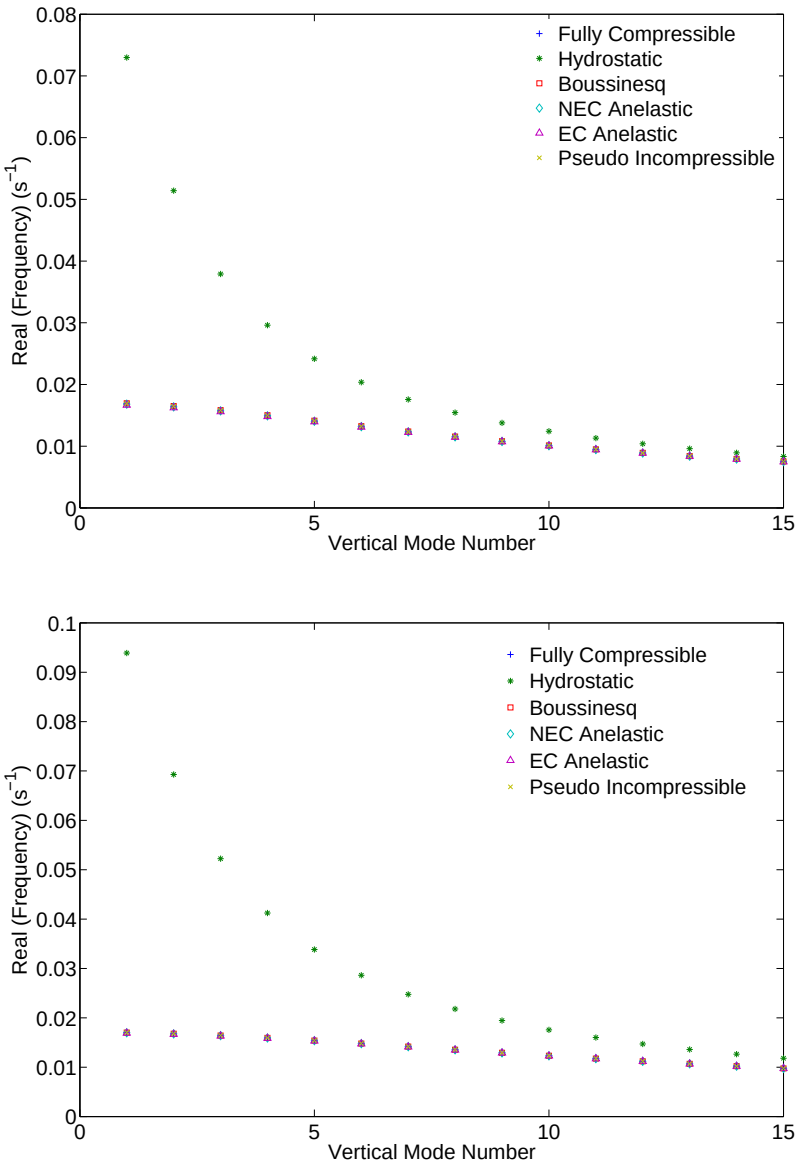

Figure 4.6: *Above: f-plane freqency σ_f and, Below: F-f-plane frequency σ. Both versus internal mode number m for horizontal wavelength $= 60km$. Parameter regime appropriate to isothermal region of Jovian atmosphere.*

frequencies is much larger than the differences found by Thuburn et al. (2002 II [59]) for the terrestrial atmosphere.

With the exception of the quasi-hydrostatic set the frequencies of modes on

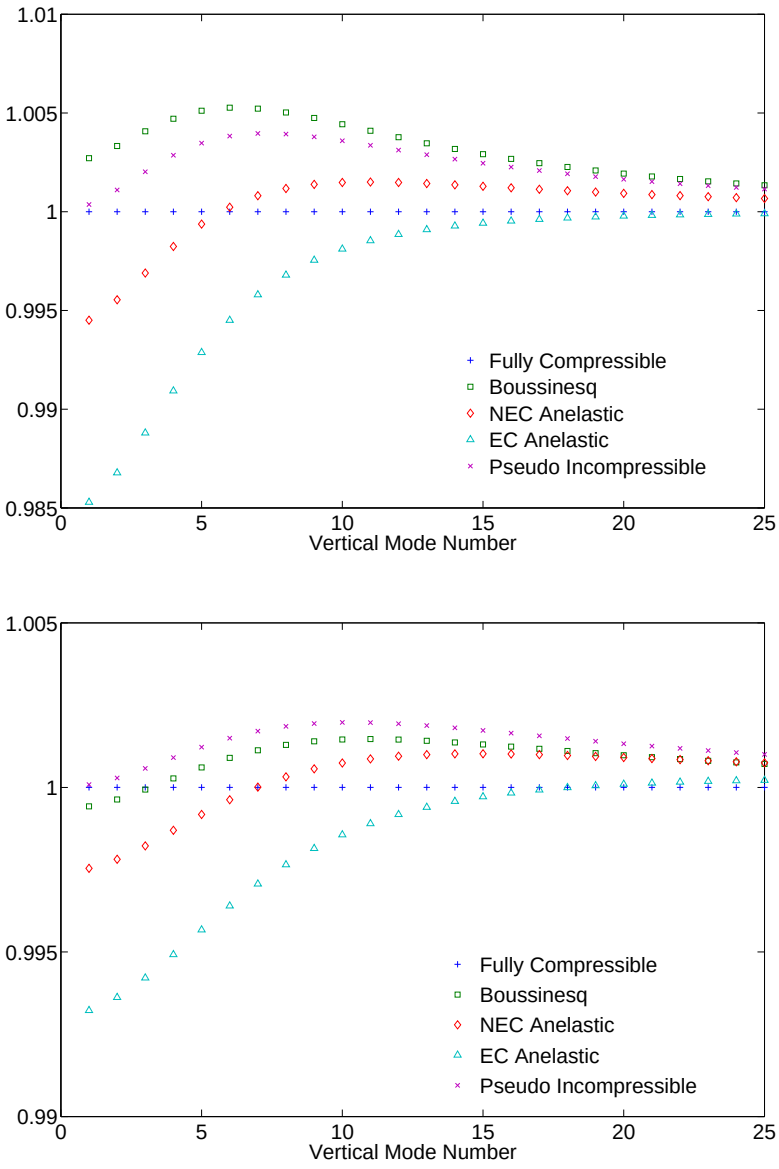

Figure 4.7: *Above: Ratio of approximated f-plane frequency σ_f to fully compressible f-plane frequency and, Below: Ratio of approximated F-f-plane frequency to fully compressible F-f-plane frequency σ. Both versus internal mode number m for horizontal wavelength $= 60km$. Parameter regime appropriate to isothermal region of Jovian atmosphere.*

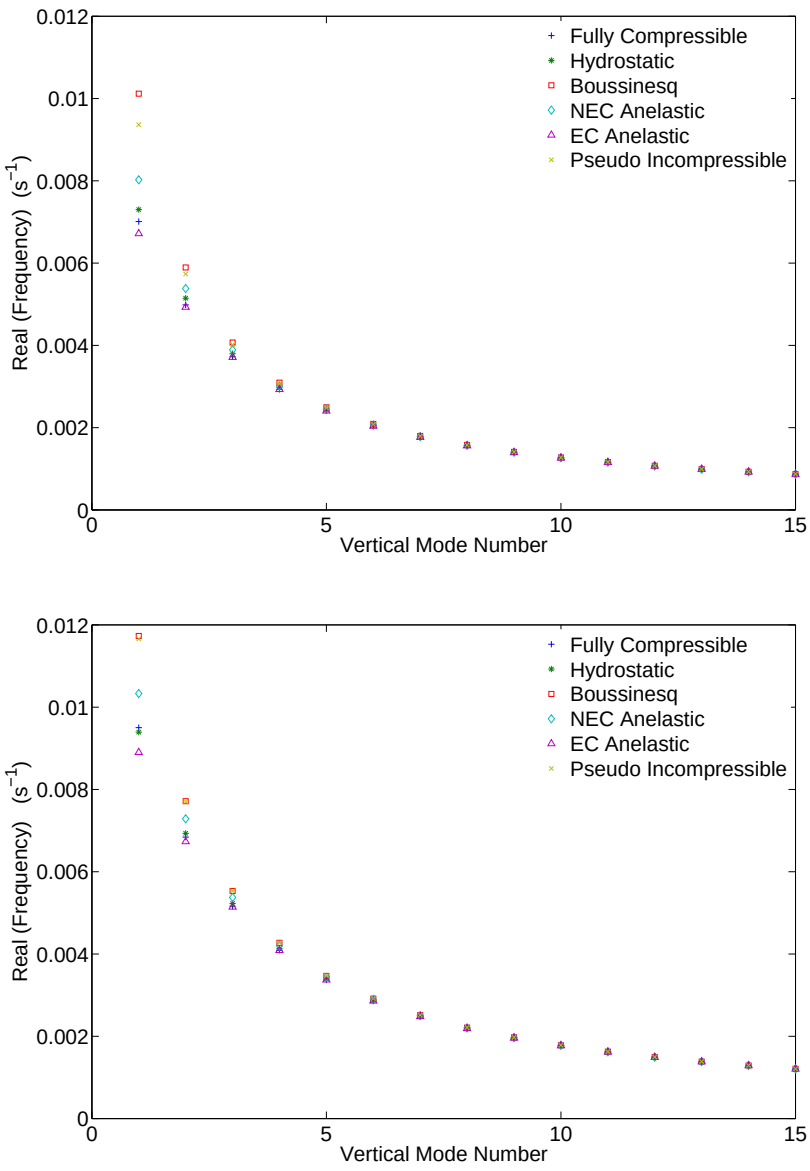

Figure 4.8: *Above: f-plane frequency σ_f and, Below: F-f-plane frequency σ, both versus internal mode number m for horizontal wavelength $= 600km$. Parameter regime appropriate to isothermal region of Jovian atmosphere.*

both an f-plane and an F-f-plane are least strongly affected by the approximated equation sets for very shallow gravity modes in which $k/k_z \ll 1$ or modes in which the horizontal wavelength is significantly smaller than the layer depth, though note

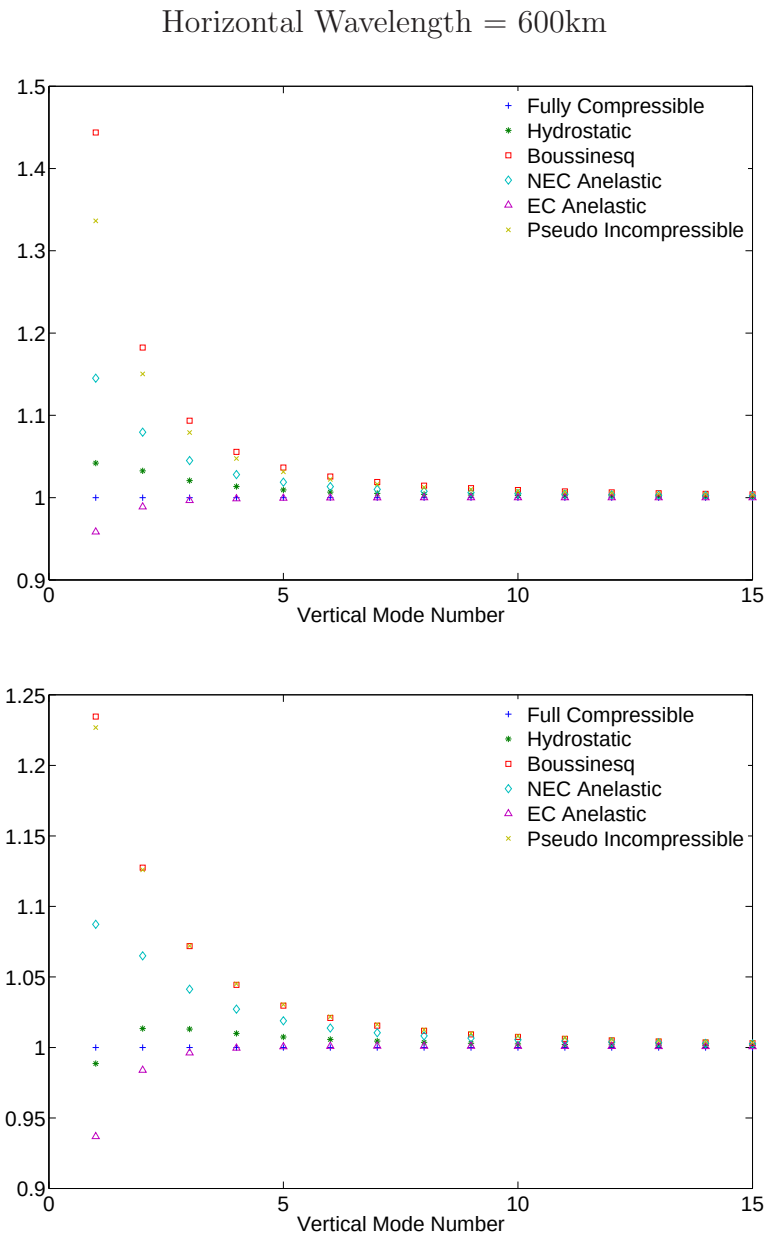

Figure 4.9: *Above: Ratio of approximated f-plane frequency σ_f to fully compressible f-plane frequency and, Below: Ratio of approximated F-f-plane frequency to fully compressible F-f-plane frequency σ, both versus internal mode number m for horizontal wavelength = 600km. Parameter regime appropriate to isothermal region of Jovian atmosphere.*

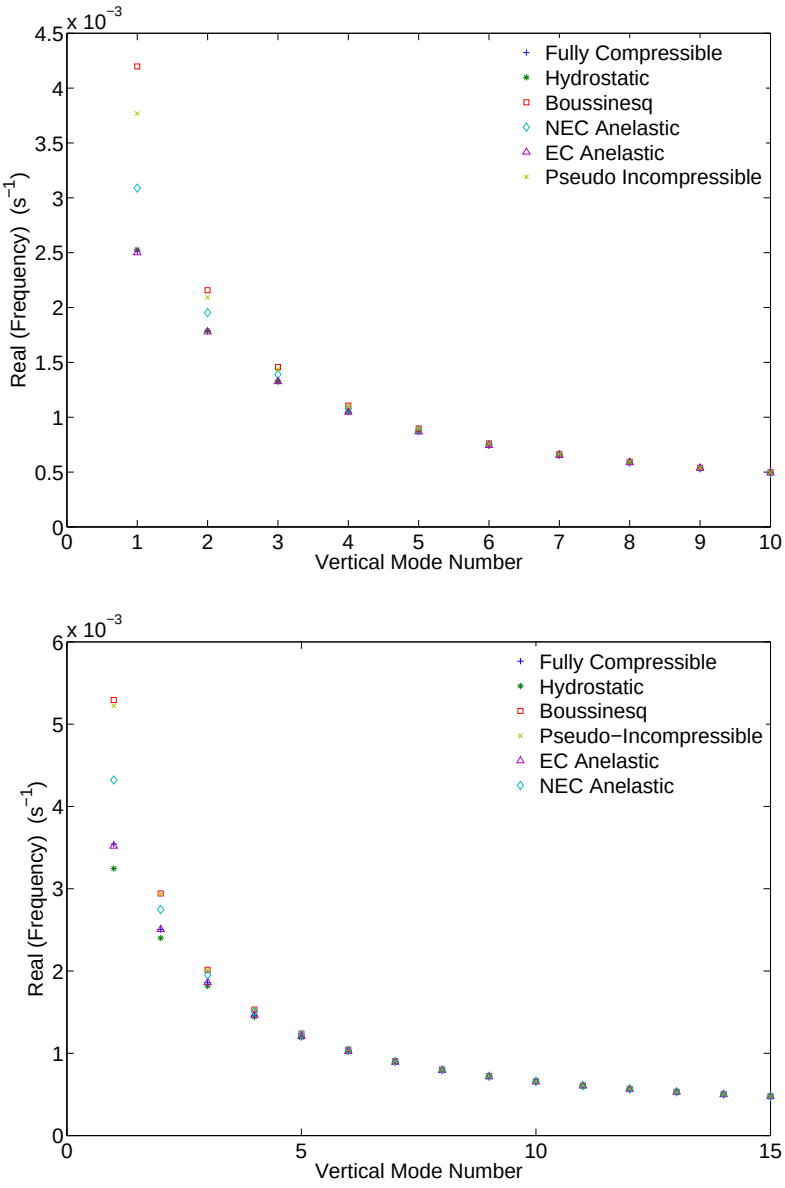

Figure 4.10: *Above: f-plane frequency σ_f and, Below: F-f-plane frequency σ, both versus internal mode number m for horizontal wavelength = Rossby radius. Parameter regime appropriate to isothermal region of Jovian atmosphere.*

that it is the deepest modes at any horizontal wavelength that are most strongly misrepresented.

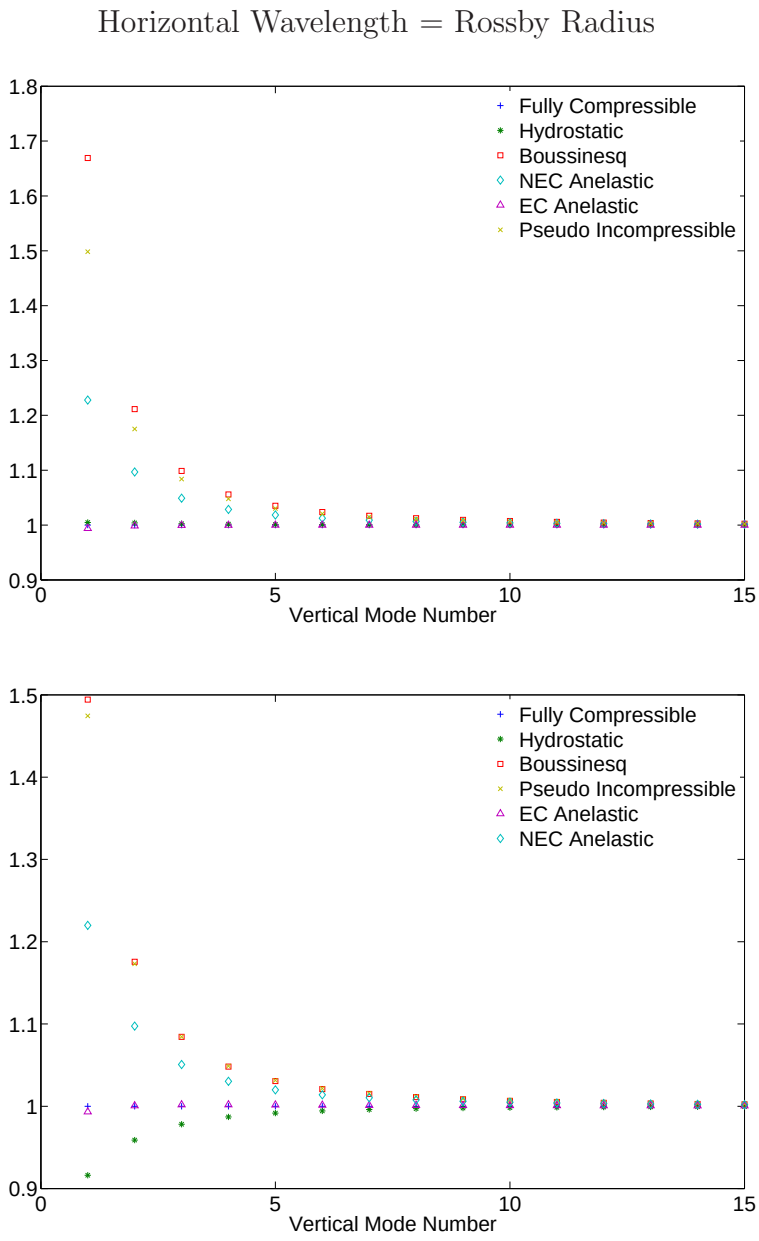

Figure 4.11: *Above: Ratio of approximated f-plane frequency σ_f to fully compressible f-plane frequency and, Below: Ratio of approximated F-f-plane frequency to fully compressible F-f-plane frequency σ, both versus internal mode number m for horizontal wavelength = Rossby Radius. Parameter regime appropriate to isothermal region of Jovian atmosphere.*

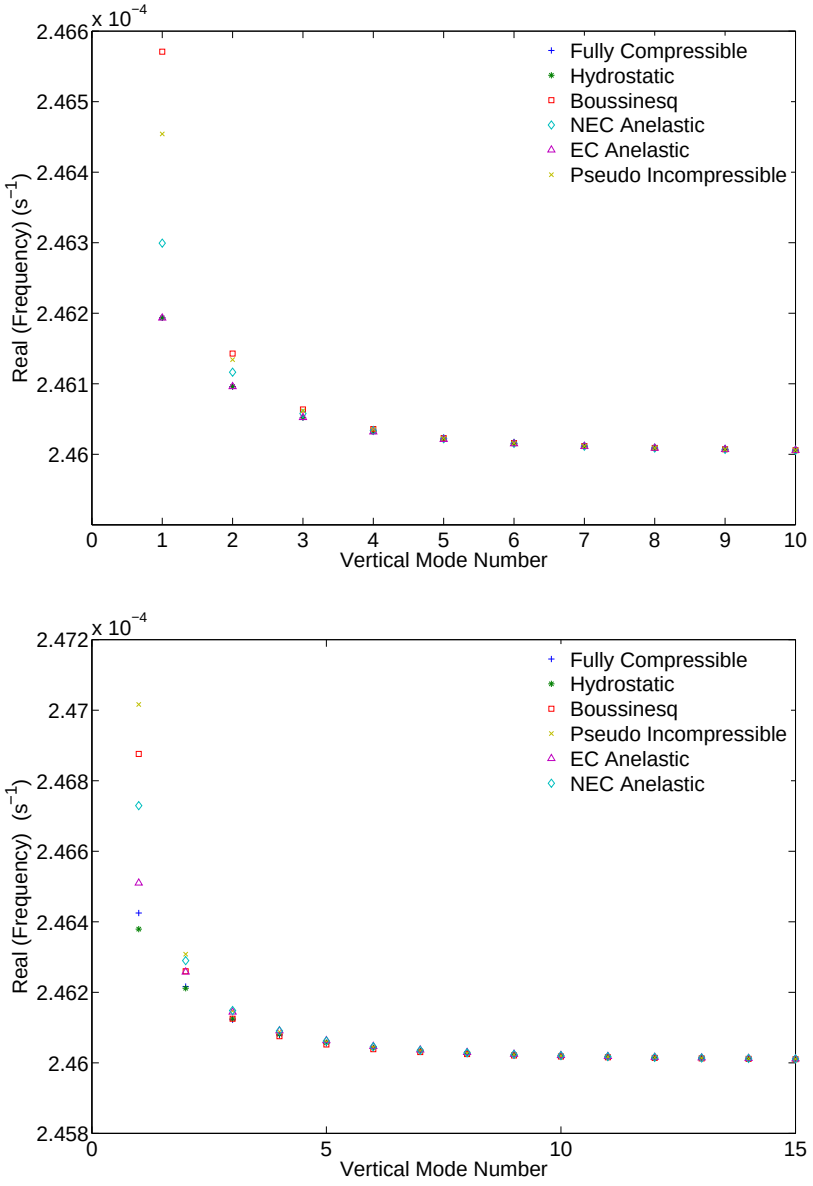

Figure 4.12: *Above: f-plane frequency σ_f and, Below: F-f-plane frequency σ, both versus internal mode number m for horizontal wavelength = Jovian Circumference. Parameter regime appropriate to isothermal region of Jovian atmosphere.*

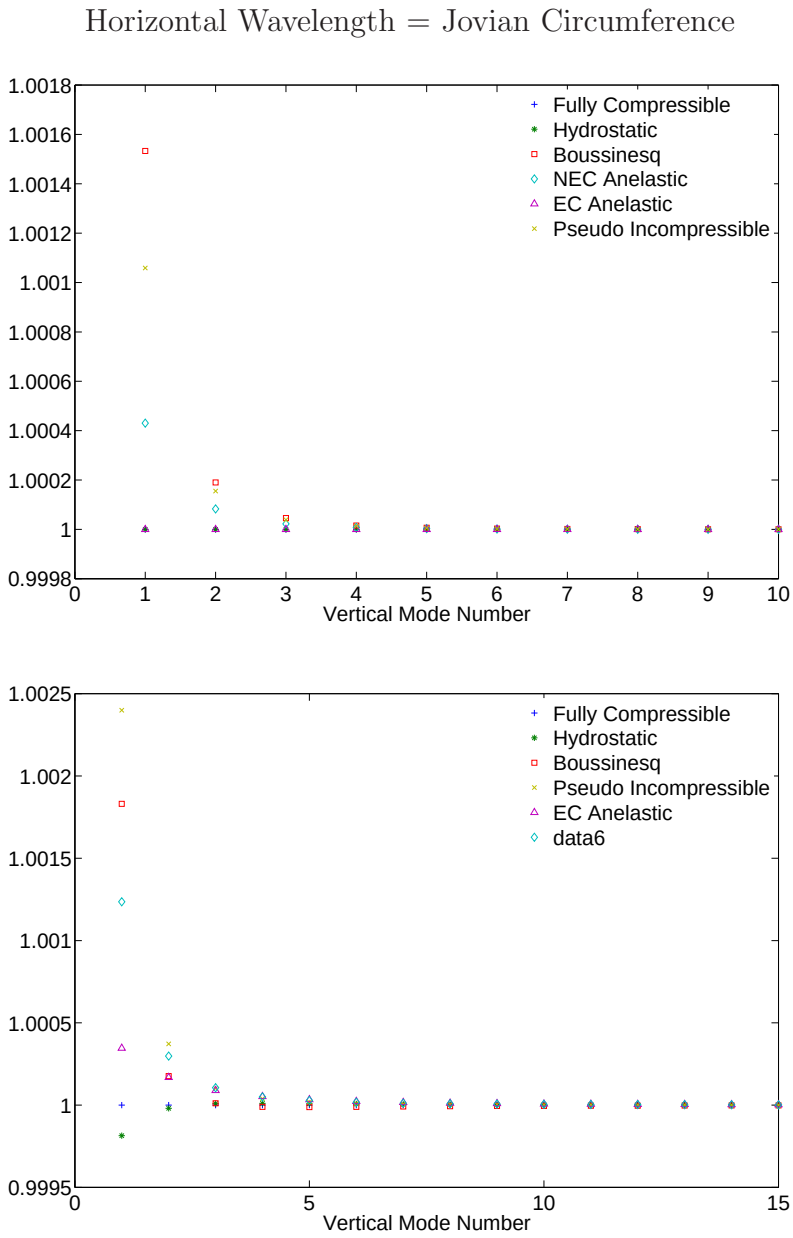

Figure 4.13: *Above: Ratio of approximated f-plane frequency σ_f to fully compressible f-plane frequency and, Below: Ratio of approximated F-f-plane frequency to fully compressible F-f-plane frequency σ, both versus internal mode number m for horizontal wavelength = Jovian Circumference. Parameter regime appropriate to isothermal region of Jovian atmosphere.*

4.5 Summary

As expected, all approximated sets filter the internal acoustic modes. The external acoustic modes of the fully compressible set are exactly replicated by the quasi-hydrostatic set, and filtered by all other approximated sets. The degenerate external Rossby mode is correctly identified by all equation sets. The structure of the modes of the non-energy-conserving anelastic and pseudo-incompressible sets are unaffected by switchable terms; however, the structure function contains terms involving frequency therefore, since the Rossby modes are degenerate, we are unable to ascertain how much the structure will be affected by any misrepresentation of the Rossby mode frequencies in a set in which f is allowed to vary with latitude. The energy-conserving anelastic and Boussinesq sets cause distortion of the height-dependency of the external Rossby mode, however only the Boussinesq set causes energy redistribution between the perturbation variables. The inclusion of F terms can add significant vertical tilt to the external modes of the isothermal region of the Jovian atmosphere, though amplitude distortion due to these terms appears to be small. The effect of inclusion of F terms on the eigenstructures of external modes for isothermal regions with different parameter regimes can be found through consideration of the relative sizes $F(\sigma k_x + f i k_y)/(\sigma^2 - f^2)$ and a/H where $a = -(\delta_C - \delta_E \kappa)$ for p' and $a = \delta_E \kappa$ for u and v.

The internal mode solutions of all approximated sets are distorted in some way. The height-dependency of the internal modes is accurately captured by all except the non-energy-conserving anelastic and Boussinesq sets; the height-dependency distortion suffered by these modes is significant over the isothermal region of the Jovian atmosphere. The Boussinesq set and both anelastic sets suffer from relocation

of the modal zeros; this relocation reduces in significance with increase in internal mode number. The other approximated sets suffer from relocation of modal zeros when the approximated frequency is significantly different to the fully compressible frequency. For the internal gravity modes all approximated equation sets suffer from energy redistribution. The degree to which this occurs is dependent on their representation of Γ and σ. Energy redistribution for the degenerate internal Rossby mode occurs for the Boussinesq set and both anelastic sets. With the exception of the quasi-hydrostatic set the internal mode frequencies are least significantly affected for very shallow gravity modes or modes in which the horizontal wavelength is significantly smaller than the layer depth. At any specified horizontal wavelength it is the deepest modes which are most strongly misrepresented. In the quasi-hydrostatic case the modal frequencies are well represented providing that the ratio of horizontal to vertical scales is large; there is very little difference between the representation of the deepest and shallowest of these modes.

The overall representation of the normal modes is in agreement with the expected accuracy determined via scale analysis. As predicted, the Boussinesq set displays the most significant overall misrepresentation with poor representation of frequency for the deepest modes and, until the limit $\sigma \to \pm f$ is approached, increasing inaccuracy with increasing horizontal wavelength. The Boussinesq set also displays misrepresentation of modal zeroes, and distortion of height dependency when returning to the unscaled perturbation form of the approximated equations. Figure 4.14 clearly shows the relocation of modal zeroes for the P structure of a Boussinesq internal gravity wave on an F-f plane. If we were to return the perturbation to its unscaled p' form we would also see significant distortion of the height dependency of the mode, thus we note that the re-scaling of the perturbation variables relieves some of the severity of the misrepresentation. As predicted by the scale-analysis misrepresentation of the overall structure is most severe for modes with large horizontal or

vertical scales.

The anelastic sets also display significant overall misrepresentation with distortion of both the frequency and the general structure; the energy-conserving set more accurately represents the frequencies and height dependency of the modes, while the non-energy-conserving set more accurately represents the location of the modal zeroes and modal amplitude. It is also worth noting that the anelastic sets misrepresent amplitude more severely than the Boussinesq set. Figure 4.14 shows the relocation of modal zeroes and misrepresentation of amplitude for the P structure of an anelastic internal gravity wave. If one is able to utilise re-scaled variables, retrospectively applying a function of reference state density to return the modes to their unscaled forms, there is little to recommend the anelastic sets over the Boussinesq set. If one is utilising unscaled equation sets the anelastic sets display considerably better overall representation of the structure than the Boussinesq set; the energy-conserving anelastic set imposes a greater restriction on the reference profile than that of the non-energy-conserving anelastic set, however it is energetically consistent thus likely to more useful in simulatory models. Once again, the scale analysis is accurate in predicting that the modes of the anelastic set are most severely misrepresented for the deepest modes and, until the limit $\sigma \rightarrow \pm f$ is approached, those with longest horizontal wavelength.

The structure of the pseudo-incompressible set is remarkably accurate, with deviation from the fully-compressible set being due only to misrepresentation of frequency. We expected this to be the case, as scale analysis suggested that the pseudo-incompressible approximation requires the least stringent conditions for applicability. It is interesting to note that the pseudo-incompressible set produces some of the most severe distortions to the frequency; this suggests that whilst the overall accuracy is strong, if the propagation of the mode is of primary interest it may be more appropriate to consider alternative approximations. Similarly to the Boussinesq and

anelastic sets, the misrepresentation of the frequency is most dramatic for modes with large vertical or horizontal scales. Figure 4.14 shows the strong performance of the pseudo-incompressible set in replicating the P structure of an internal gravity mode.

The reference state under consideration is reasonably strongly stratified, thus scale analysis suggests that the quasi-hydrostatic set should perform well for modes with large horizontal scales. The analytic solutions are in agreement with this expectation, with the representation of the overall mode being entirely governed by the representation of the frequency and the frequency of modes with short horizonal scale being significantly misrepresented. Figure 4.14 shows the strong representation, by the quasi-hydrostatic set, of an internal gravity mode with reasonably long horizontal scale. For modes with large horizontal scale the quasi-hydrostatic set is the most appropriate set within this region of the Jovian regime.

Finally we highlight the importance of including F terms in the analysis of the Jovian regime, figure 4.15 displays the shift of U structure relative to P structure induced by including the F terms.

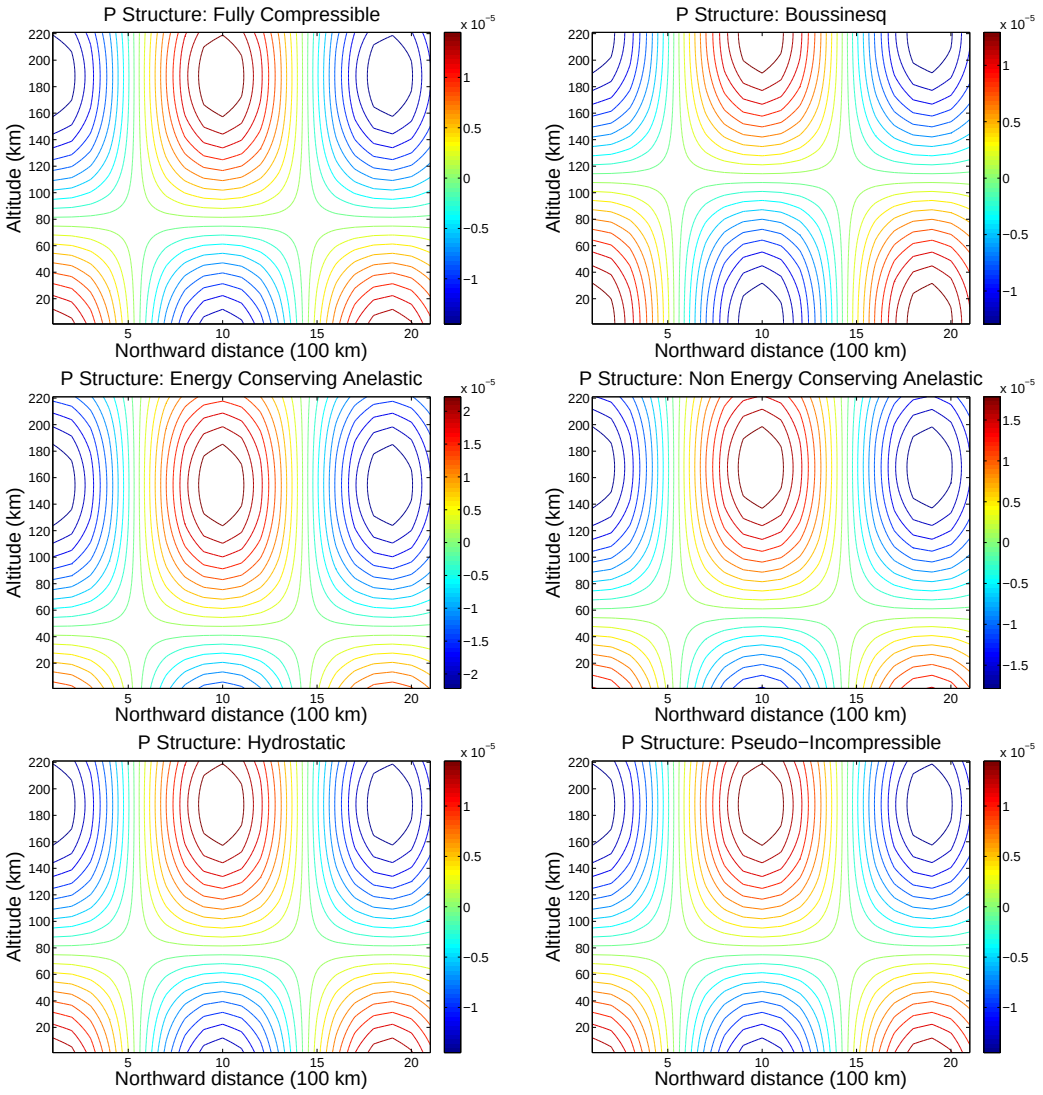

Figure 4.14: *P-structure of internal gravity modes on F-f-plane. Vertical mode number $m = 1$, horizontal wavelength = Rossby radius, $k_x = k_y = 3.52 \times 10^{-6} m^{-1}$. σ_f as calculated by f-plane dispersion relation, $\sigma_f = 0.00237 s^{-1}$ for fully compressible case. Note the changes in amplitude and shift of modal zeros for approximated sets.*

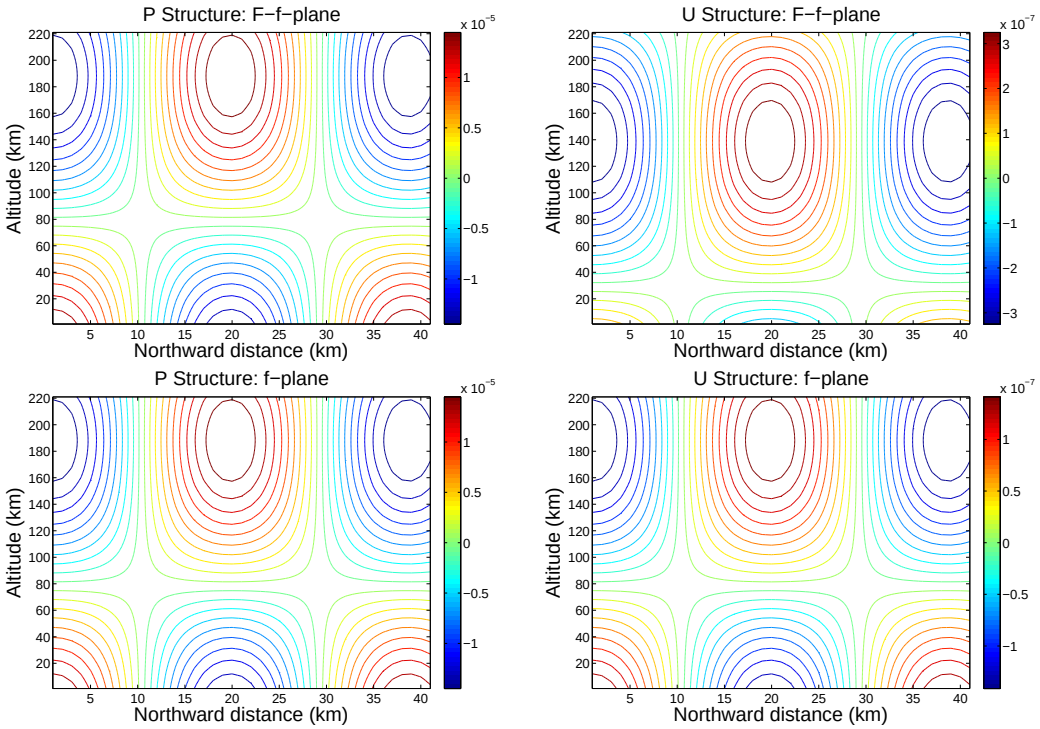

Figure 4.15: *P and U structure of a deep internal gravity modes on $F-f$-plane and on an f-plane. Vertical mode number $m = 1$, $k_x = 1.6 \times 10^{-4} m^{-1}$, $k_y = 3.52 \times 10^{-6} m^{-1}$. σ_f as calculated by f-plane dispersion relation, $\sigma_f = 0.0171 s^{-1}$ for fully compressible case. Note the vertical shift of the U structure relative to the P, and increase in amplitude of U introduced by the F terms.*

Chapter 5

F-f Plane: Polytropic Regime

We saw in Chapter 4 that we are only able to find analytic solutions for an inviscid, isothermal reference state. In order to ascertain the effects of the approximated equation sets under reference states relevant to convecting systems it is necessary to undertake computational analysis. In this chapter we will consider inviscid polytropic reference states on an F-f-plane.

Within an unstably stratified regime we expect that some of the inertio-gravity modes will become unstable and exhibit growing and decaying normal modes driven by bouyancy forces. Whilst Taylor-Proudman theorem applies strictly only to a rapidly rotating, inviscid, incompressible regime we expect that in the absence of viscosity and diffusion convective motions will onset as tall-thin columns parallel to the axis of rotation, as they have been shown to do in a convectively unstable uniform density Boussinesq plane layer (see for example Chandrashekhar, 1961 [13]). This is discussed in more detail in chapter 7 where we extend the asymptotic theory on the onset of Boussinesq convection to the compressible case. The convective columns expected at onset are made up of Rossby waves and our F-f-plane geometry does not allow for these modes. Therefore, within this chapter we expect to find that the fastest growing modes will be unstable inertial modes which take the form of vertical

columns with the smallest horizontal wavelength, thus largest horizontal values of k_x and k_y, and largest vertical wavelength.

The introduction of a non-isothermal reference state means that the problem is no longer analytically tractable, however consideration of the internal mode dispersion relations found for the analytically tractable isothermal case in Chapter 4 support this view. We remind ourselves that the dispersion relations for the approximated equation sets on an isothermal, inviscid f-plane are given by the following:
for Anelastic and Pseudo-Incompressible sets, $\delta_A = 0$,$\delta_H = 1$

$$\sigma_f^2 = f^2 + \frac{k^2(N^2 - f^2)}{k_z^2 + \Gamma^2 + k^2}; \tag{5.1}$$

for Quasi-Hydrostatic set $\delta_H = 0$,$\delta_A = 1$

$$\sigma_f^2 = f^2 + \frac{k^2 N^2}{\frac{N^2}{C_s^2} + \Gamma^2 + k_z^2}; \tag{5.2}$$

for Boussinesq set $\Gamma = 0$

$$\sigma_f^2 = f^2 + \frac{k^2(N^2 - f^2)}{k_z^2 + k^2}, \tag{5.3}$$

We then assume that these dispersion relations give an indication of the frequency of modes for other reference state profiles, we can set $N^2 < 0$ to suggest the likely profile of the most strongly growing and decaying modes.

On an f-plane we would expect all values of σ to be purely real or purely imaginary. Inclusion of F terms will allow growing and decaying modes with non-zero frequency. We note that whilst we do not investigate the critical values for the onset of convection in detail within this chapter the dispersion relations given above suggest that the various approximated equation sets will have differing criteria. If we set k^2 and k_z^2 to be constant the various equation sets will have differing values of Γ^2 and N^2 at which σ becomes imaginary, thus suggesting differing critical values for the onset of convection.

The modes with largest growth/decay rates will be found for maximum $k^2 = k_x^2 + k_y^2$ and minimum k_z^2, and those found for the Boussinesq set should have larger

growth/decay rates than those found for the pseudo-incompressible and anelastic sets. Based on the relative sizes of Γ for the approximated equation sets we would expect that the energy-conserving anelastic set will have larger growth/decay rates than the non-energy-conserving set, which will have larger growth/decay rates than the pseudo-incompressible set. The size of the growth/decay rates of the unstable modes for the quasi-hydrostatic set will be dependent on the relative size of N^2/C_s^2 and Γ^2. However, assuming that $|\Gamma^2| > |N^2/C_s^2|$ we would expect that the modes with maximum vertical wavelength and minimum horizontal wavelength will have significantly larger growth/decay rate than those of other approximated equation sets. We expect that the quasi-hydrostatic set will most significantly misrepresent the fully-compressible case as the condition for its application, that vertical accelerations are negligible compared with gravitational accelerations, is less likely to be relevant in a convectively unstable atmosphere and we have seen through scale analysis that the quasi-hydrostatic set is unlikely to perform well when $|N^2|$ is small or $N^2 < 0$. The inclusion of F terms will modify the dispersion relation such that we expect maximum instability to be partially dependent on minimising $2\boldsymbol{\Omega}.\boldsymbol{k}$; thus we would expect that for specified horizontal and vertical wavelengths on an F-f-plane the modes with largest growth/decay rates will be found at the pole.

Once again we consider solutions of the form

$$\left.\begin{array}{lcl} U & & \hat{U}(z) \\ V & & \hat{V}(z) \\ W & = & \hat{W}(z) \\ P & & \hat{P}(z) \\ \Theta & & \hat{\Theta}(z) \end{array}\right\} \exp(ik_x x + ik_y y - i\sigma t). \tag{5.4}$$

This allows us to convert the problem into a matrix eigenvalue problem of the form

$$\boldsymbol{A}\hat{\boldsymbol{s}} = i\sigma \boldsymbol{B}\hat{\boldsymbol{s}} \tag{5.5}$$

where $\hat{\boldsymbol{s}}$ is a state vector consisting of all the values of $\hat{U}$, $\hat{V}$, $\hat{W}$, $\hat{P}$ and $\hat{\Theta}$. The matrix

problem can then be solved numerically. We choose to follow Thuburn et al. (2002 II [59]) and represent the dynamical and thermodynamic variables on a staggered grid. We then use straightforward centred differences and centered averages to vertically discretize the equations.

Thuburn et al. (2002 I [60]) concluded that the vertical structure of normal modes in a terrestrial regime suggests that density and temperature should be analytically eliminated in favour of pressure and potential temperature as the prognostic thermodynamic variables, and that potential temperature and vertical velocity should be staggered in the vertical with respect to the other dynamic prognostic variables, the so-called Charney-Phillips grid. Similar grid structures have been used by other groups considering convection in non-terrestrial regimes (for example Evonuk and Glatzmaier (2006 [29]), therefore we choose to follow the recommendations of Thuburn et al (2002 I [60]).

5.0.1 Numerical Method

In order to compute the eigenvalues and eigenvectors of our matrix eigenvalue problem we choose to write fortran 90 code and make use of NAG routine F02GJF. This routine uses the QZ algorithm in order to solve matrix problems of the form given by 5.5. It is worth noting that the routine does not produce eigenvalues σ_j; it instead returns α_j and β_j such that $\sigma_j = \alpha_j/\beta_j$ where $j = 1, 2, 3....n_m$ and n_m is the order of the matrices $\boldsymbol{A}$ and $\boldsymbol{B}$. The division by β_j is the responsibility of the user's code as it is possible that $\beta_j = 0$. We are considering five prognostic variables on a staggered grid. Since we are considering an inpenetratable surface, thus $\hat{W} = 0$, and have chosen to set $\hat{\Theta} = 0$ at the surfaces we then formulate tendency equations for $\hat{U}$, $\hat{V}$ and $\hat{P}$ at each of n_z vertical levels, and $\hat{W}$ and $\hat{\Theta}$ at each of $nz-1$ vertical levels. The matrices $\boldsymbol{A}$ and $\boldsymbol{B}$ are then of the order $n_m = 5 * n_z - 2$.

The region appropriate to the deep convection model of the Jovian interior is thought to be $\sim 10^4$km, therefore the ratio of inner to outer radii is approximately 0.85. Evonuk and Glatzmaier (2006 [28]) showed that the ratio of inner to outer radii can have a significant impact when modelling 3D turbulent convection, however, the computational expense of the numerical methods used means that the models are restricted to approximated equation sets. It is also important to remember that it is difficult to justify use of a constant mass polytropic model for low radius ratios.

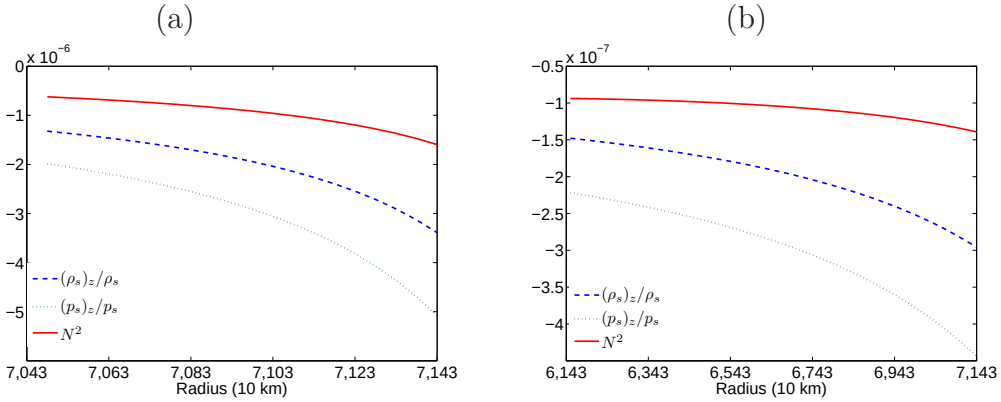

Figure 5.1: *Gradients for reference states with $N_\rho = 2, n = 2$, (a) Layer of depth 1,000km, (b) Layer of depth 10,000km. Note that N^2 has units s^{-1}, $(\rho_s)_z/\rho_s$ and $(p_s)_z/p_s$ have units m^{-1}.*

Figures 5.1 (a) and (b) show the Brunt Vaisala frequency, density gradient and pressure gradient for layers of depth 1,000km and 10,000km, based on the constant mass polytropic model. In this case vertical gradients are denoted with a subscript z. As expected for a layer 10 times as deep, with the same density scale factor and polytropic index, the gradients of the reference state variables are approximately 10 times smaller. However, the manner in which they relate to each other remains similar. Therefore we expect that similar structures and misrepresentations will be found for both layer depths. With this in mind we choose to consider a layer of depth 1,000km as the resulting solutions will have smaller resolution based errors for the same number of grid points. We use 100 vertical grid levels for each prognostic

variable. Therefore, the distance between data points for the same variable will be $10km$, and the distance between variables that are not located on the same grid points, such as $\hat{P}$ and $\hat{\Theta}$, will be $5km$. We have discussed in section 2.9.4 that we will consider $N_\rho = 2$ and $N_\rho = 5$, therefore models with 2 and 5 density scale heights across the layer respectively. The use of 100 vertical grid levels provides several grid points per density scale height, thus also per pressure scale height.

We also see that by setting the polytropic index $n = 2$ we have $N^2 < 0$. Whilst this is not a sufficient condition for instability we expect to find some unstable solutions as this is a similar parameter regime to that used in Jones et al. (submitted 2008 [38]) whilst studying the onset of convection in Boussinesq and anelastic models.

Testing of the numerical method on the analytically tractable isothermal regime shows that the method is robust and displays a good degree of accuracy. Comparison of results for various numbers of grid levels indicates that 100 grid levels is ample to provide sufficient accuracy to determine the differences between the approximated and fully-compressible equation sets.

Unless stated otherwise results discussed are for an F-f-plane at $\phi = 45^o$.

5.1 Solutions for the Inviscid, Polytropic F-f plane

5.1.1 Acoustic Modes

Eigenfrequencies

As expected we find that all approximated sets filter the internal acoustic modes, and that only the quasi-hydrostatic set succeeds in finding solutions for the external acoustic modes. Table 5.1 shows the percentage by which the quasi-hydrostatic set overestimates the frequency of the external acoustic modes for various horizontal

wavelengths and density scale factors, on an F-f-plane at $\phi = 45\%$. As with the isothermal case we find that the distortion of the frequencies of these modes is most dramatic for shortest horizontal wavelength. Increasing the number of density scale heights in the reference state also increases the amount by which the frequencies of these modes are misrepresented.

	+ve Mode	
Horizontal Wavelength	$N_\rho = 2$	$N_\rho = 5$
1/4 x Depth	31.20%	122.41%
Depth	17.29%	55.20%
2 x Depth	6.70%	20.21%
10 x Depth	0.10%	0.14%

Table 5.1: *Percentage by which the quasi-hydrostatic set overestimates the fully compressible external acoustic mode frequencies. Layer depth*=1,000km.

For horizontal wavelength comparable to, or larger than, the layer depth the horizontal wavelength has small effect on the frequency of the acoustic modes. For horizontal wavelength equal to one quarter of the layer depth the magnitude of frequencies of the deepest acoustic modes is increased compared to those of modes with similar depth but longer horizontal wavelengths. For all horizontal wavelengths the frequencies of the modes for density scale factor $N_\rho = 2$ are larger in magnitude than those with equivalent depth for a reference state with density scale factor $N_\rho = 5$.

Eigenfunctions

In contrast to the isothermal case, in the polytropic regime the quasi-hydrostatic set also completely misrepresents the vertical structure eigenfunction for the external acoustic mode. This is as we would expect as scale analysis suggests that the quasi-hydrostatic set will not perform well when N^2 is small or negative.

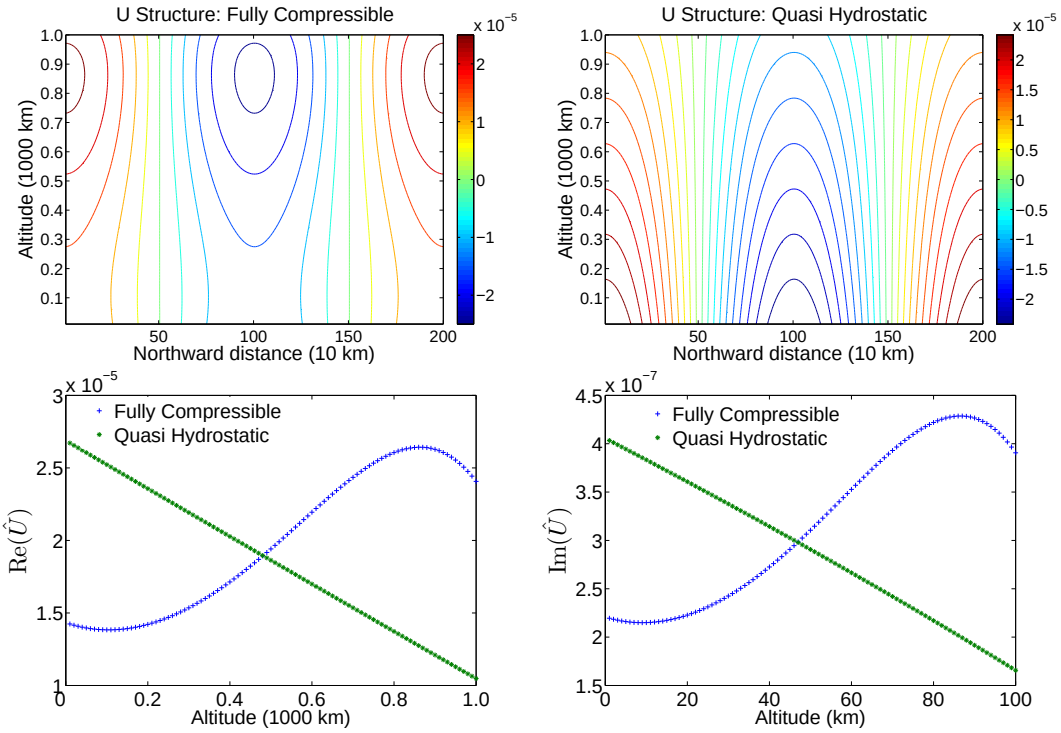

Figure 5.2: *Above: Real* (U) *structure and Below:* $\hat{U}$ *structure, for fully compressible and quasi hydrostatic sets for the external acoustic mode on an* F*-*f*-plane at* $\phi = 45\%$*. Horizontal wavelength* $= 2\times$ *layer depth* $= 2000km$*.*

As an example of this figure 5.2 shows the U structure of the external acoustic mode for horizontal wavelength equal to 2000km, or 2 times the depth of the layer, and density scale factor $N_\rho = 2$. The $\hat{U}$, $\hat{V}$ and $\hat{P}$ vertical structure of the quasi-hydrostatic external acoustic mode is linear rather than the sinusoidal variation shown by the fully compressible set. The maximum amplitude of the mode is also mislocated; the maximum amplitude of the quasi-hydrostatic external acoustic mode is located adjacent to the inner boundary whereas the maximum amplitude for the equivalent mode for the fully compressible set is located closer to the outer boundary. We will see that the density factor which is used to convert U to u etc, serves to disguise some of this distortion but there remains a significant spurious lack of growth with height for the quasi-hydrostatic external acoustic mode.

In further contrast with the isothermal case $\hat{W}$ and $\hat{\Theta}$, are non-zero for the polytropic regime. Thuburn et al. (2002 II [59]) showed that for the isothermal terrestrial regime w and θ are zero for the fully compressible F-f-plane, but non-zero for the fully compressible spherical regime. They attribute the zero vertical velocity of the isothermal F-f-plane primarily to the geometrical effects of the tangent plane and shallow-atmosphere approximation; our solutions demonstrate that this does not apply for all reference state profiles.

Figure 5.3 shows the real component of the W structure, and the real and imaginary components of the $\hat{W}$ structure, for the quasi-hydrostatic and fully compressible sets. We see that the modal zeroes are correctly located but that the amplitude, and location of the maximum amplitude, are spuriously misrepresented.

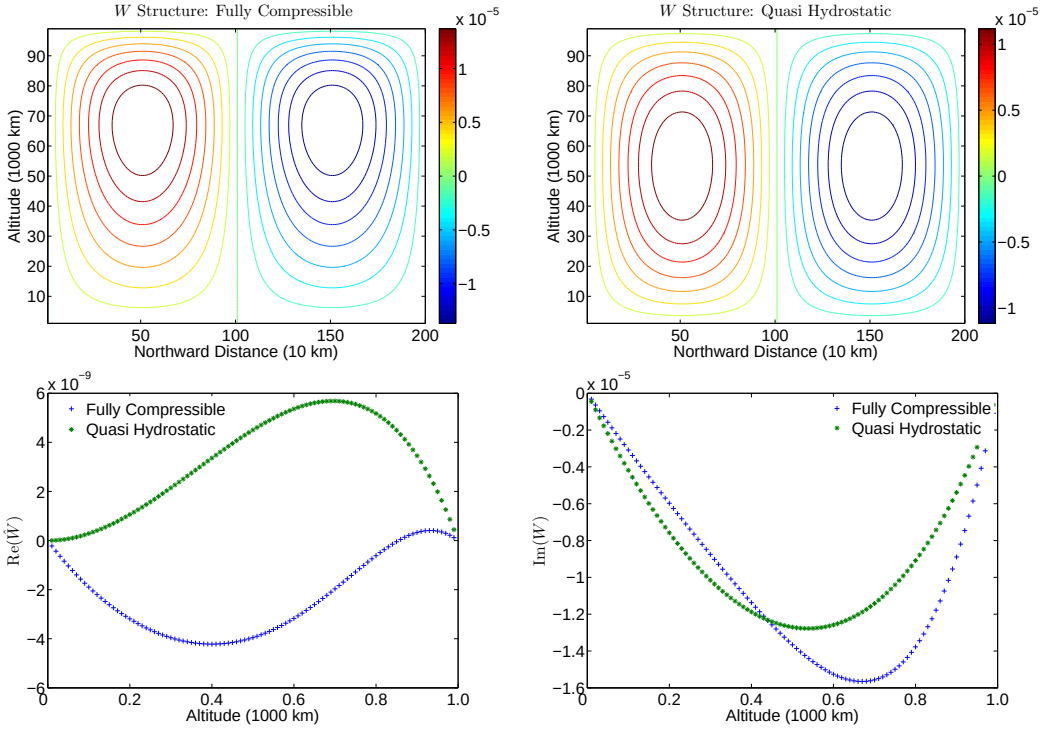

Figure 5.3: *Above: Real* (W) *structure and, below:* $\hat{W}$ *structure, for fully compressible and quasi hydrostatic sets for the external acoustic mode on an* F-f*-plane at* $\phi = 45\%$. *Horizontal wavelength* $= 2\times$ *layer depth* $= 2000km$.

Note that these structures are at arbitrary time $t = 0$; the evolution of the modes with time is dependent on the frequency of the mode which is itself misrepresented as discussed in the previous section.

We recall that we rescaled our variables to remove some of the systematic variation in vertical structure due to reference state density, therefore if we are to compare the structure of the perturbation quantities for reference states with different density scale factors we must consider the appropriate structures of ρ_s. We showed in Chapter 2 that

$$\rho_s = \rho_0 \left(\frac{GM_0\rho_0}{r(n+1)p_0} + c_0 \right)^n = \rho_0 \left(\frac{T_s}{T_0} \right)^n , \tag{5.6}$$

therefore

$$u = \rho_s^{-1/2} U = \rho_0^{-1/2} \left(\frac{T_0}{T_s} \right)^{n/2} U \quad \Rightarrow \quad u \propto \left(\frac{1}{T_s} \right)^{n/2} U \quad etc \tag{5.7}$$

Until this point it has not been necessary to prescribe a value for ρ_0, however for the layer depths in which we are interested the depth to radius ratio is sufficiently small that, within the layer, reference state temperature decreases almost linearly with increasing radius. This leads to the fact that density decreases rapidly as we approach the outer surface; the larger the density scale factor the more rapidly the density decreases with increasing radius. The location at which we define ρ_0 will have an impact on the amount by which modes for differing reference profiles are affected by their return to an unscaled form; this is of importance if one is considering a Boussinesq set to have a constant density reference profile, thus one in which we consider the limit as N_ρ tends to zero (see for example Jones et al. (submitted 2008 [38]). Assuming we define ρ_0 at the same point within the layer for each value of N_ρ, the position of ρ_0 will impact upon the reference state density profile for the varying values of N_ρ, which in turn affects the magnitude and profile of the rescaling factor. Figures 5.4 and 5.5 display this graphically

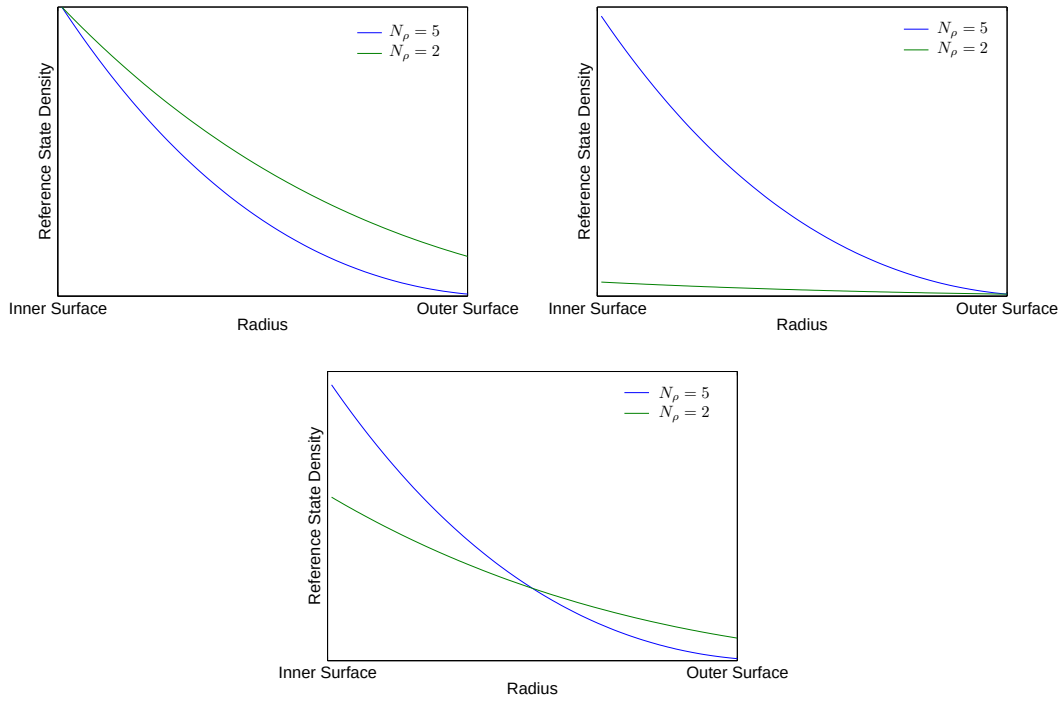

Figure 5.4: *Reference state density structures according to position at which* ρ_0 *is defined.*

Figures 5.6 and 5.7 show the U and u structure, and P and p structure for the external acoustic mode for reference states with density scale factor $N_\rho = 2$ and $N_\rho = 5$ where we have chosen to define ρ_0 at the inner surface. Since the modes for $N_\rho = 2$ and $N_\rho = 5$ have not been calculated as part of the same routine, the normalisation factors will differ and we cannot compare the amplitudes of the structures for the differing reference profiles. Clearly the normalisation will have no impact on the location of minima and maxima or the shape of the mode.

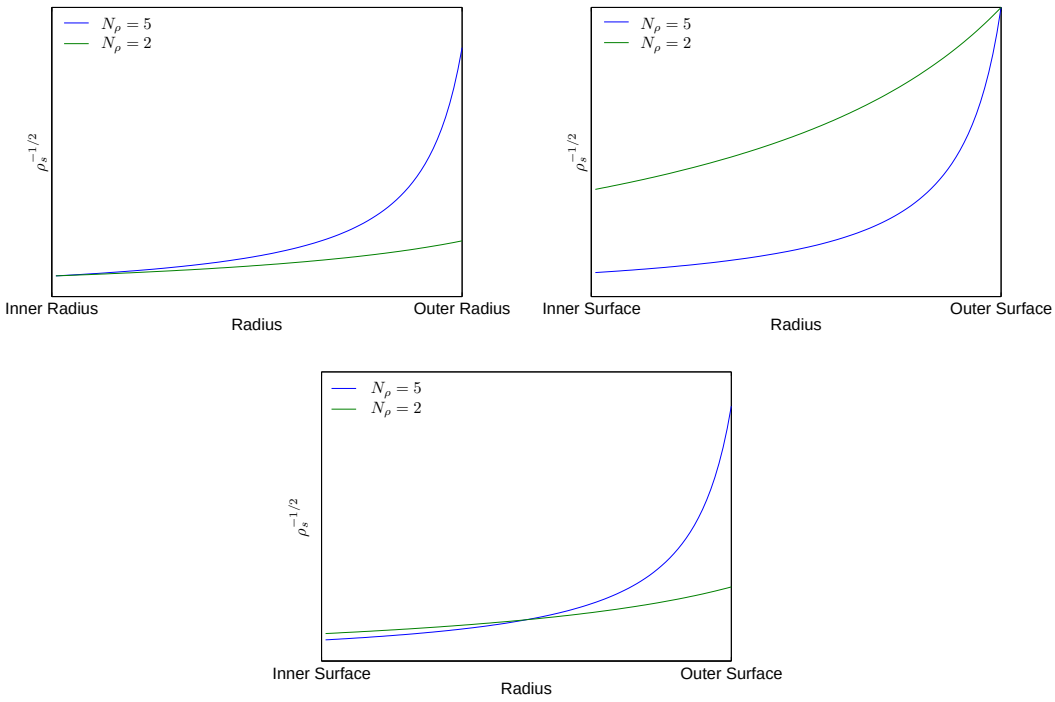

Figure 5.5: *Structure of* $\rho_s^{-1/2}$ *according to position at which* ρ_0 *is defined.*

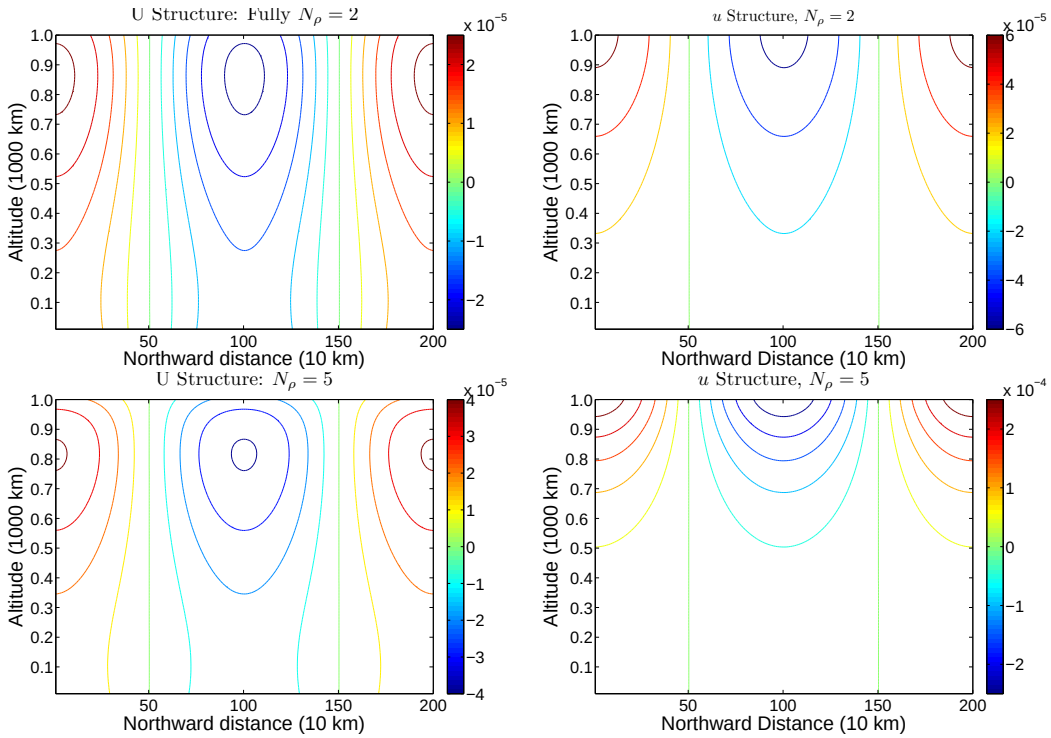

Figure 5.6: *Real U and u structure for the fully compressible external mode on an F-f-plane at $\phi = 45\%$ for density scale factors $N_\rho = 2$ and $N_\rho = 5$. Horizontal wavelength $= 2\times$ layer depth $= 2000km$. Note that the imaginary component is similarly affected by N_ρ.*

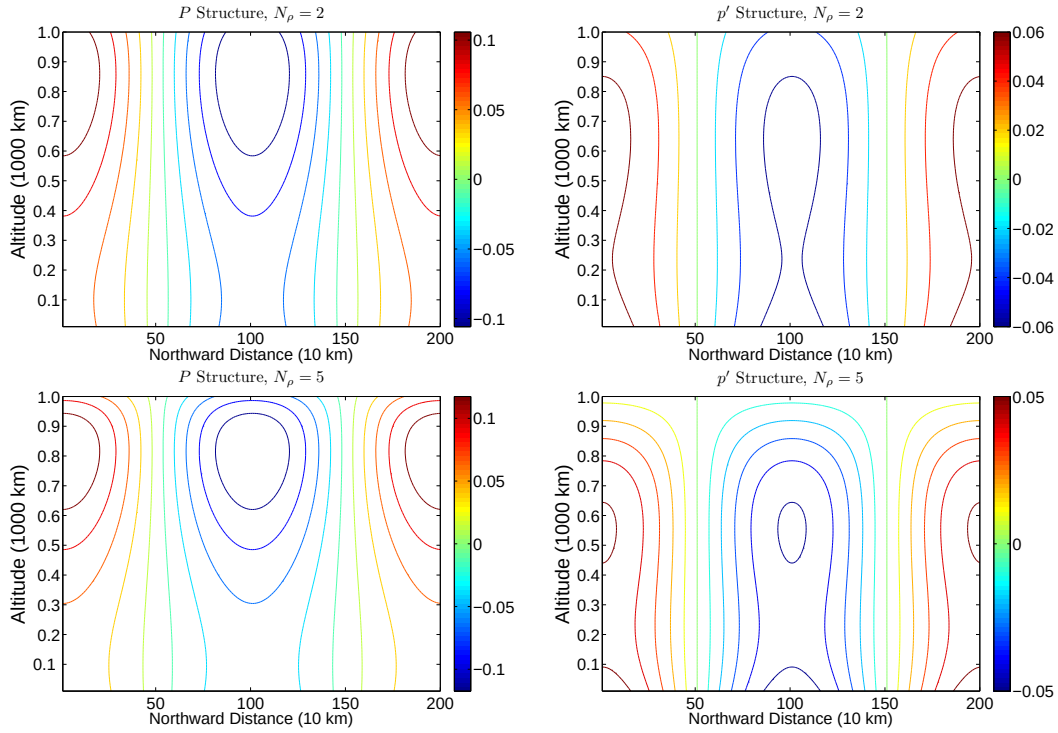

Figure 5.7: *Real P and p structure for the fully compressible external mode for density scale factors $N_\rho = 2$ and $N_\rho = 5$. Horizontal wavelength $= 2\times$ layer depth $= 2000km$. Note that the imaginary component is similarly affected by N_ρ.*

This shows that the location of the maxima and minima, and height dependency of the modes, is affected by the reference state density scaling. If one were to use a constant density reference profile alongside the Boussinesq equation set it would be similar to considering a regime in which $N_\rho \to 0$, which will clearly display more significant differences to the Boussinesq equation set utilised alongside a reference profile which allows density stratification.

5.1.2 Inertio-Gravity Modes

Eigenfrequencies

As expected, the introduction of a polytropic reference state means that we find modes with non-zero imaginary component of σ. These modes are effectively complex conjugate pairs with small positive real component (prograde solutions); the number of these modes found varies with horizontal wavelength. The imaginary component of σ specifies the rate at which the modes grow or decay. The remaining solutions are neutral modes which tend to $\pm f = 2\Omega \sin\phi$ with increasing vertical wave number. The unstable modes are all prograde, which given that the number of modes calculated is finite and defined by the number of grid levels, suggests that the prograde modes are more prone to instability.

Increasing the number of density scale heights in the reference state tends to increase the number of growing/decaying modes, their frequency, and their growth/decay rate. This is as we would expect as at any specified polytropic index an increased density scale factor will result in an increased density gradient. We saw in Chapter 2 that N^2 is directly related to the density gradient; thus, if N^2 is sufficiently negative that the atmosphere is unstable for $N_\rho = 2$, it will be even more negative for $N_\rho = 5$ leading to greater instability and, for a set number of grid levels, the calculation of a greater number of unstable modes.

As we suggested at the beginning of the chapter, the fastest growing modes are found to have the smallest horizontal wavelength, largest vertical wavelength and, for a set number of grid levels, the number of unstable modes calculated is reduced with increasing horizontal wavelength. For a reference state with $N_\rho = 2$ and horizontal wavelength one quarter the depth of the layer approximately 50 complex conjugate pairs are calculated; for horizontal wavelength ten times the layer depth only one complex conjugate pair is calculated. If horizontal wavelength is increased

to become approximately the circumference of Jupiter we find that the only inertial modes calculated have zero growth/decay rate and frequency close to $2\Omega \sin \phi$.

As with the isothermal case we find that none of the approximated sets accurately represent the frequencies of the inertio-gravity modes over all horizontal wavelengths.

As expected the quasi-hydrostatic set misrepresents the frequencies most dramatically for the shortest horizontal wavelenghths, and represents the unstable modes less accurately than the stable ones. The over estimation of the frequency of the deepest unstable mode is over 600% for horizontal wavelength equal to the layer depth and $N_\rho = 2$; the misrepresentation of the growth/decay of the same mode is approximately 170%. By the tenth mode the frequency and growth/decay rate are overestimated by approximately 30% and 15% respectively. For horizontal wavelength equal to twice the layer depth the misrepresentation of the frequency of the deepest unstable mode is reduced to approximately 160%, the growth/decay being 62.7% larger than the true figure. At horizontal wavelength equal to ten times the layer depth only one complex conjugate pair of modes is found; the frequency and growth/decay rates are overestimated by 4.9% and 5.8% respectively. These overestimations are decreased for density scale factor $N_\rho = 5$. For this number of density scale heights and horizontal wavelength equal to the layer depth, the frequency and growth/decay rate of the deepest unstable mode are misrepresented by 326% and 108% respectively. The amount by which the increased density scale factor increases the magnitude of both the frequency and growth/decay rate varies with vertical mode number and horizontal wavelength. For a given horizontal wavelength the deepest modes are the least strongly affected by increased density scale factor, and the modes with longer horizontal wavelength are more strongly affected than those with shorter horizontal wavelengths. For horizontal wavelength equal to the depth of the layer the deepest unstable modes for a full-compressible set have growth/decay rates approximately

50% larger for $N_\rho = 5$ than for $N_\rho = 2$; by the tenth vertical mode the growth/decay rate is approximately 140% larger for $N_\rho = 5$ than $N_\rho = 2$. The increased misrepresentation of the frequencies of the modes with decreased N_ρ is probably due to the fact that the magnitude of N^2 is larger for increased N_ρ; however, we would expect that the overall representation of the modes for increased N_ρ will be worse due to the increased instability.

The neutral modes are also overestimated by the quasi-hydrostatic set though to a considerably lesser o degree; this is in part because the stable modes are shallower, thus for a given horizontal wavelength the ratio of k/k_z will be smaller and the quasi-hydrostatic approximation more applicable. For horizontal wavelength equal to the depth of the layer the frequency of the deepest of these modes is misrepresented by 2.7% for $N_\rho = 2$ and 1.2% for $N_\rho = 5$. For horizontal wavelength equal to ten times the layer depth the frequency of deepest modes is misrepresented by 0.8% for $N_\rho = 2$ and 0.2% for $N_\rho = 5$. In both cases the results point to the conclusion that the quasi-hydrostatic set is inappapropriate for use in modelling convectively unstable inertio-gravity modes.

The Boussinesq set consistently misrepresents the frequencies of the unstable modes. For all other sets the order of the real component of the deepest of these modes, for horizontal wavelength equal to the layer depth, is $10^{-4}s^{-1}$; for the Boussinesq set the frequency is calculated to be approx 2% that of the true value for reference state with $N_\rho = 2$ and approx 3% for $N_\rho = 5$. This misrepresentation is similar for all horizontal wavelengths. Consideration of the dispersion relation for the Boussinesq, isothermal F-f-plane in Chapter 4 provides an indication as to why the frequency of the unstable Boussinesq modes is so small. Since $\Gamma = 0$ in the Boussinesq case, the aforementioned dispersion relation features only terms involving σ^2, whereas for all other equation sets there are terms in σ. If we assume that the unstably stratified polytropic reference state can be approximated by setting $N^2 < 0$ in this equation

we will find that in the Boussinesq case all values for σ will be purely imaginary or purely real. This limitation does not apply in the stably stratified case as in this instance σ is always real.

The growth/decay rates of the deepest unstable Boussinesq modes are overestimated by a lesser degree, though the overestimation is increased with increasing horizontal wavelength and further increased by increased density scale factor. For density scale factor $N_\rho = 2$, and horizontal wavelength equal to twice the layer depth, the overestimation of the growth/decay rate is 3.83%. For density scale factor $N_\rho = 5$, and the same horizontal wavelength, the overestimation of the growth/decay rate is increased to 20.33%. Interestingly the misrepresentation of both frequency and growth/decay rate of the unstable modes decreases and then increases with increasing vertical mode number.

The neutral modes are also misrepresented by the Boussinesq set, though in this case the frequencies are underestimated. For density scale factor $N_\rho = 2$ the maximum underestimation is approximately -3.4% for horizontal wavelength equal to one quarter the depth of the layer. This increases to approximately -19.7% for horizontal wavelength equal to twice the layer depth and decreases again to -2.9% for horizontal wavelength equal to ten times the layer depth. This increase, and then decrease, with increasing horizontal wavelength is similar to that found through the analytic analysis of the isothermal f-plane. The misrepresentation of the neutral modes increases with increasing density scale factor. The underestimation of the frequencies of the neutral modes caused by the Boussinesq approximation drops off rapidly with increasing vertical mode number. By the tenth mode the misrepresentation is less than -0.5% for all of the horizontal wavelengths and density scale factors considered.

Both anelastic sets and the pseudo-incompressible set display similar error characteristics to the Boussinesq set, though the magnitude of the misrepresentations is reduced. For all three equation sets the misrepresentation of the growth/decay

rates of the unstable modes increases with increasing horizontal wavelength, however the misrepresentation of the frequency of these modes decreases. This is also the case with increasing density scale factor. As with the Boussinesq set the misrepresentation of the frequencies and growth/decay rates of the unstable modes decreases with increasing vertical mode number before increasing again. The vertical mode number at which the misrepresentation is minimised varies with equation set, horizontal wavelength and density scale factor. The most dramatic misrepresentation of the frequencies of the neutral modes occurs for modes with the longest vertical wavelength and horizontal wavelength somewhere between 2 and 5 times the depth of the layer. For all horizontal wavelengths the misrepresentation of the frequencies of the neutral modes decreases with increasing vertical mode number and increases with increasing density scale factor. In all cases the largest misrepresentation of σ is found to be for the frequencies of the unstable modes. The relative performance of the anelastic and pseudo-incompressible sets is such that there is significantly less to distinguish between them than there is to distinguish them from the Boussinesq or quasi-hydrostatic sets. Each of the sets performs sufficiently well that their use would be preferable to the Boussinesq or quasi-hydrostatic set in modelling the frequencies of both stable and unstable modes. The choice between use of the pseudo-incompressible or anelastic sets seems to be best determined by which types of mode one wishes to replicate most accurately. We see in table 5.2that the non-energy-conserving anelastic set produces the most accurate replication of growth/decay rates and frequencies of the neutral modes, though the pseudo-incompressible set reproduces the frequencies of the unstable modes most accurately. We believe it is likely that for a more strongly superadiabatic reference profile the pseudo-incompressible set will be more accurate.

Modes with horizontal wavelength equal to twice the depth of the layer are representative of the more extreme misrepresentations of the frequencies for all approximated sets with the exception of the hydrostatic set. The maximum misrepre-

sentations of the various equation sets at this horizontal wavelength are displayed in table 5.2.

	Growth/decay rate of unstable mode		Frequency of unstable mode		Frequency of neutral modes	
Approximated Set	$N_\rho = 2$	$N_\rho = 5$	$N_\rho = 2$	$N_\rho = 5$	$N_\rho = 2$	$N_\rho = 5$
Quasi-Hydro	62.7%	42.9%	160.1%	101.3 %	2.6%	0.97%
Boussinesq	3.8%	20.3%	-97.9%	-97.8%	-8.5%	-19.7%
EC Anelastic	0.16%	0.36%	-4.2%	-4.0%	-0.25%	-0.42%
NEC Anelastic	0.05%%	-0.13%	-2.1%	-2.1%	-0.02%	0.13%
Pseudo-Incomp	-0.07%	-0.61%	0.16%	-0.49%	0.22%	0.70%

Table 5.2: Maximum percentage by which the approximated sets misrepresent the fully compressible inertial modes for horizontal wavelength equal to twice the layer depth.

Eigenfunctions: Neutral modes

The results from the isothermal analysis suggest that, despite the large frequency discrepancies, the vertical mode structures for the quasi-hydrostatic set should be well represented. However, the analysis of the external acoustic mode shows that the results for the polytropic regime can be significantly different to that of the isothermal regime. Figure 5.8 (a) shows the real component of the $\hat{U}$ structure for the fully compressible and quasi-hydrostatic sets for the first neutral mode for reference state $N_\rho = 2$ and horizontal wavelength equal to twice the layer depth. Figure 5.8 (b) shows the real component of the $\hat{U}$ structure for the fully compressible and quasi-hydrostatic sets for the first neutral mode for reference state $N_\rho = 2$ and horizontal wavelength equal to ten times the layer depth. We see that at longer horizontal wavelength the first neutral mode has a lower vertical mode number than the first

neutral mode at shorter horizontal wavelength; this is in agreement with our previous statement that we expect to find more unstable modes for the shortest horizontal wavelengths. The quasi-hydrostatic set replicates the fully compressible solution well in both cases though the errors are more significant for the neutral mode with shorter horizontal wavelength and lower vertical mode number. Once again, this is consistent with expectation as the ratio k/k_z is smaller for the case in which the horizontal wavelength is longer.

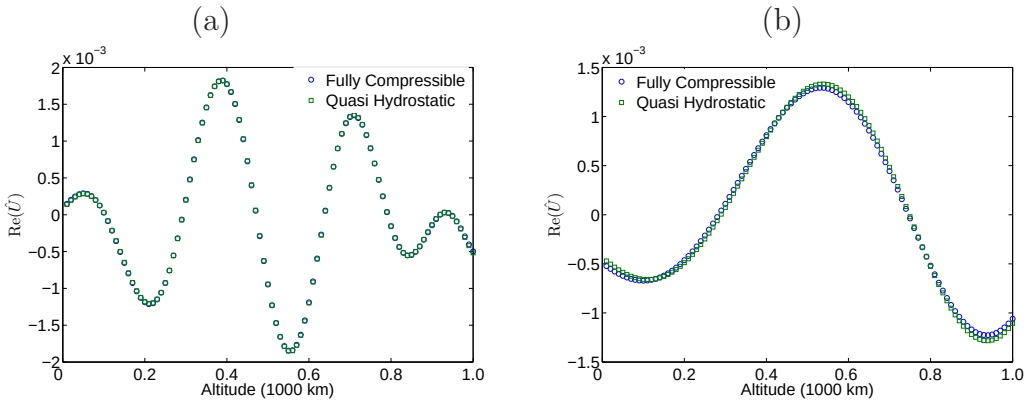

Figure 5.8: *(a) Re($\hat{U}$), $N_\rho = 2$, horizontal wavelength=2×Layer depth. (b) Re($\hat{U}$), $N_\rho = 2$, horizontal wavelength=10×Layer depth.*

Upon initial inspection the Boussinesq set also reproduces the structure of the neutral modes reasonably accurately. Figure 5.9 (a) shows the real components of the Boussinesq and fully compressible U structure for the first neutral mode with horizontal wavelength twice the layer depth and reference state with $N_\rho = 2$. Figures 5.9 (b) and (c) show the real and imaginary components of the $\hat{U}$ and $\hat{P}$ structure for the same mode. Both the real and imaginary components of the $\hat{U}$ structure display good replication of the fully compressible mode structure, with amplitude, height scale and modal zeroes all being reasonably well captured. The $\hat{P}$ structure suffers from larger errors in calculating the maximum amplitude, though the modal zeroes are correctly located.

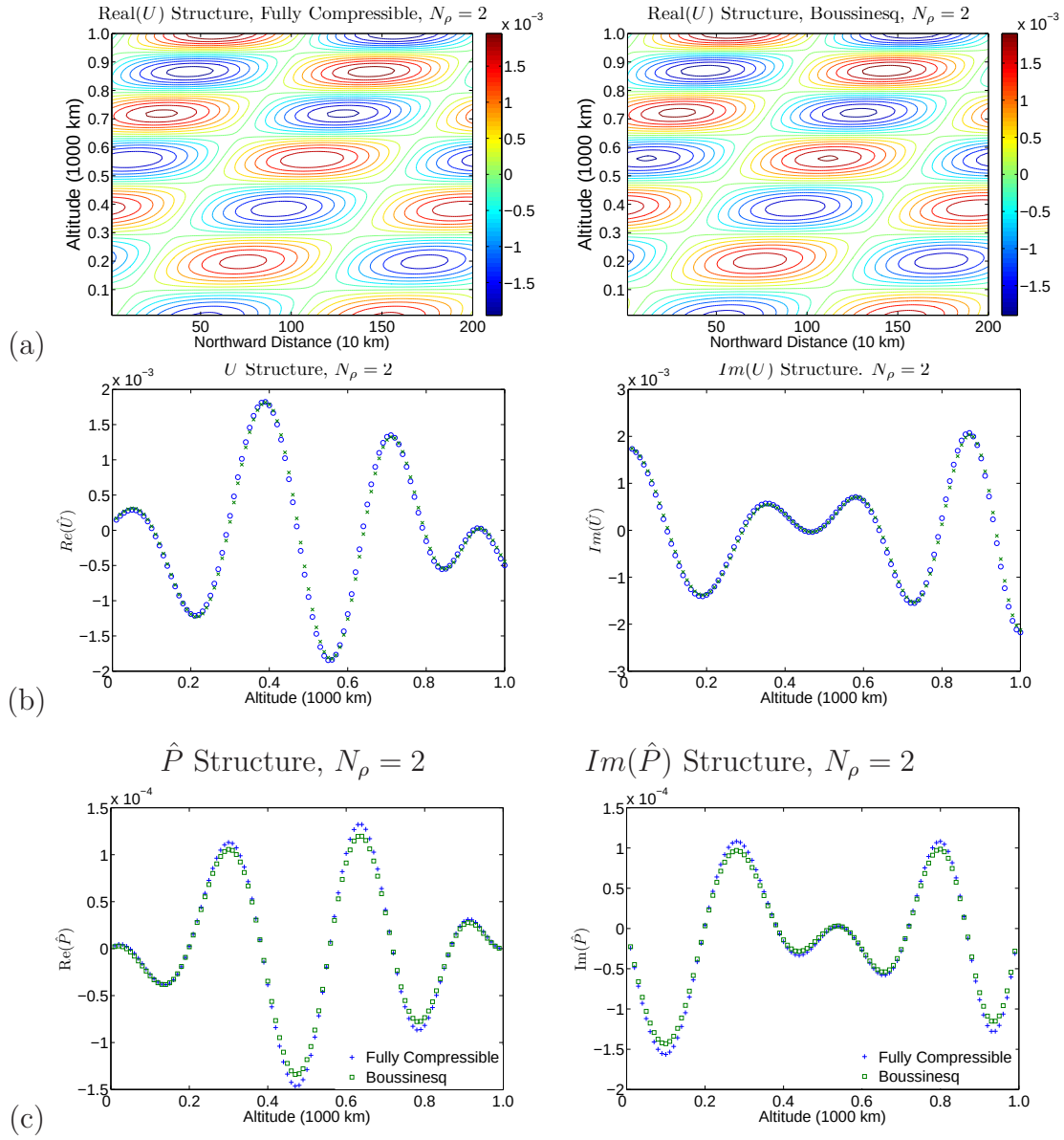

Figure 5.9: *(a) Real components of U structure for Fully Compressible and Boussinesq sets. (b) Real and imaginary components of $\hat{U}$ structure for Fully Compressible and Boussinesq sets. (c) Real and imaginary components of $\hat{P}$ structure for Fully Compressible and Boussinesq sets.*

However, as in the analytic analysis, it is important to remember that Boussinesq equation sets ignore variation of reference state density, thus the unscaled and rescaled versions of the equation sets are identical. Therefore, the accuracy of the

structure of the unscaled variables will be dramatically affected by the application of the appropriate density scaling factor. In the Boussinesq case the unscaled variables will have the same vertical structure as the rescaled variables; whereas the fully compressible case will be dramatically different for equation sets with significant density variation. The application of the density scaling factor shows the considerable differences between the Boussinesq and Fully Compressible sets. It would be reasonable to apply the density scaling factor to the Boussinesq set in the same way that it is applied to the fully compressible set, however it should be noted that if the solutions were calculated using the equations in their unscaled form they would have errors similar to those shown in figure 5.10. If $N_\rho \to 0$ is considered to be the Boussinesq approximation, as is the case in many historical studies of the onset of convection, then the errors are likely to be even more extreme. We will see in chapter 7 that reference state density profile has a strong impact on the structure of convective modes at onset.

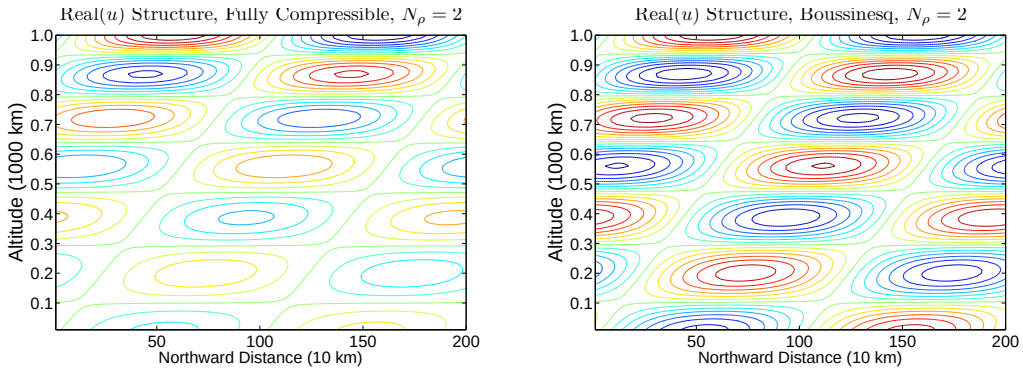

Figure 5.10: *Real components of u structure for Fully Compressible and Boussinesq sets. Calculated assuming ρ_0 is defined at the inner surface, though we have not defined a value for ρ_0.*

The misrepresentation of the structures decreases with increasing vertical mode number. The neutral modes occur at lower vertical mode number for modes with longer horizontal wavelengths, therefore of the neutral modes it is these which

suffer from the greatest errors. Both anelastic sets and the pseudo-incompressible set display reasonable replication of the vertical structures for both long and short horizontal wavelength with $N_\rho = 2$ and $N_\rho = 5$. The modal zeroes are accurately located for each of these sets, though there is some small misrepresentation of the amplitudes. The amount by which the amplitude is misrepresented is not consistent across all variables, therefore this will lead to some energy redistribution. The $\hat{W}$ structure is most significantly overestimated by each of anelastic and pseudo-incompressible sets, most obviously for the case in which $N_\rho = 5$ and for longer horizontal wavelengths. The amount by which the amplitudes are increased is similar for each of the aforementioned equation sets.

Eigenfunctions: Unstable modes

The structures of the deeper, unstable modes display more evident discrepancies. Figure 5.11 displays the structures of U and $\hat{U}$ for the deepest internal mode for the fully compressible and Boussinesq sets. We see that the height scale and modal zeroes of the Boussinesq set are significantly misrepresented. As shown in figure 5.12 the application of the reference state scaling factor, which returns the rescaled variables to their unscaled form, serves to increase the severity of the misrepresentation. The underestimation of the real component of $\hat{U}$ does not apply to all variables; the real component of $\hat{W}$ is overestimated by a similar amount. This points to a redistribution of energy across prognostic variables. The relocation of modal zeroes and maximum amplitudes is not consistent across all variables, and inspections suggest that the perturbation energy at any given amplitude does not necessarily match that of the fully-compressible set; thus energy redistribution is not only across variables, but also across altitude. The misrepresentation of convectively unstable modes by the Boussinesq equation set therefore manifests itself in a variety of ways which indicate that it is unlikely to accurately replicate physical structures resulting from these

modes.

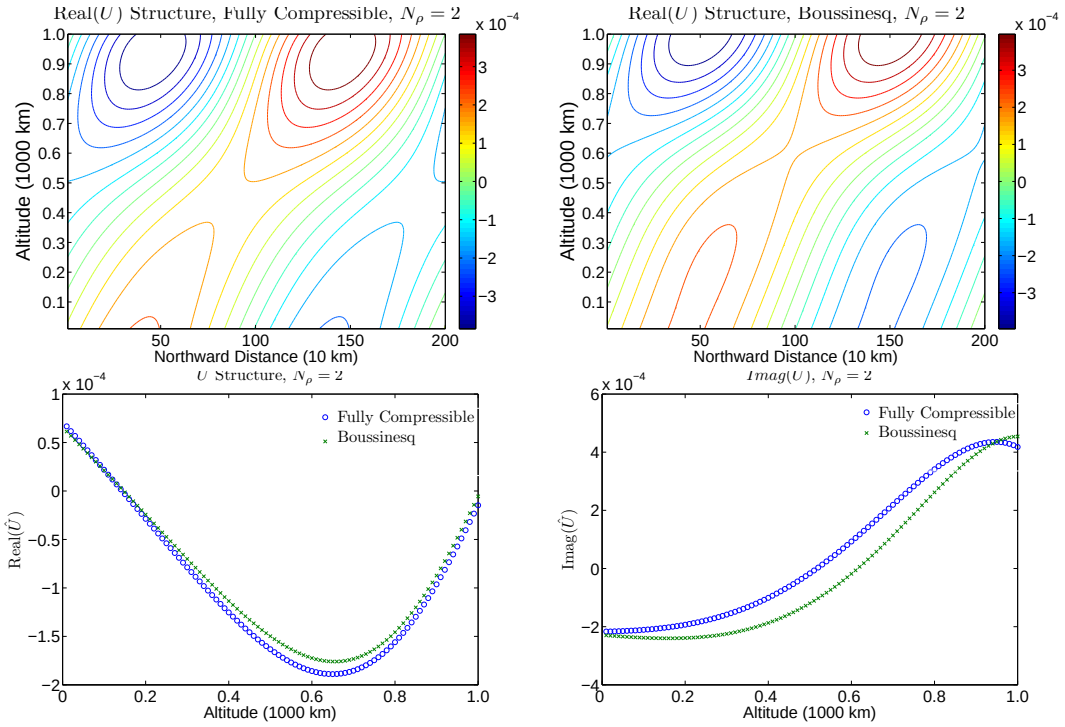

Figure 5.11: *Above: Real components of U structure for Fully Compressible and Boussinesq sets for first internal mode with non-zero growth/decay rate.*

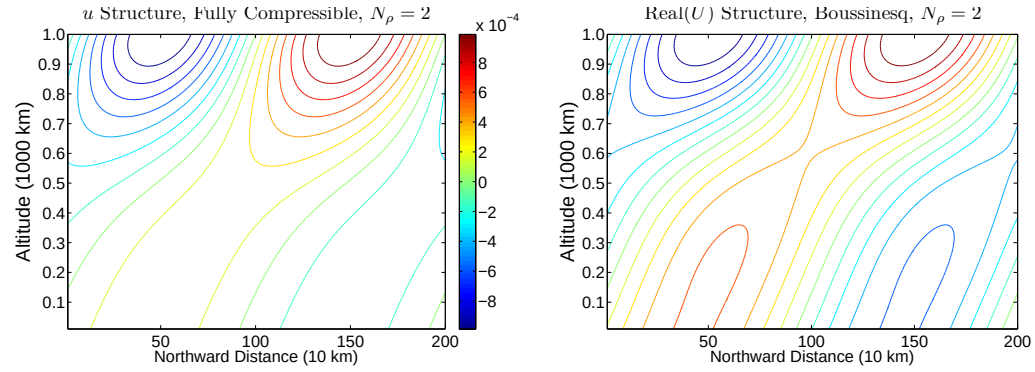

Figure 5.12: *Above: Real components of u structure for Fully Compressible and Boussinesq sets for first internal mode with non-zero growth/decay rate. Note that since the rescaled and unscaled forms of the Boussinesq equation set are identical the Boussinesq U and u structure are also identical.*

The quasi-hydrostatic set is also significantly misrepresented, with relocation of the modal zeroes, a spurious misrepresentation of amplitude and misrepresentation of the height scale. This is displayed graphically in figure 5.13, using U strucure as an example. Once again, we note that not all variables are misrepresented equally. The amplitude of the W structure is significantly reduced relative to other variables, the amount by which the mode is tilted is reduced, the location of the maximum amplitude is further from the outer surface and the modal zeroes are relocated. The misrepresentation of w and p is far more significant than the misrepresentation of the horizontal components of velocity, which in turn leads to significant energy redistribution.

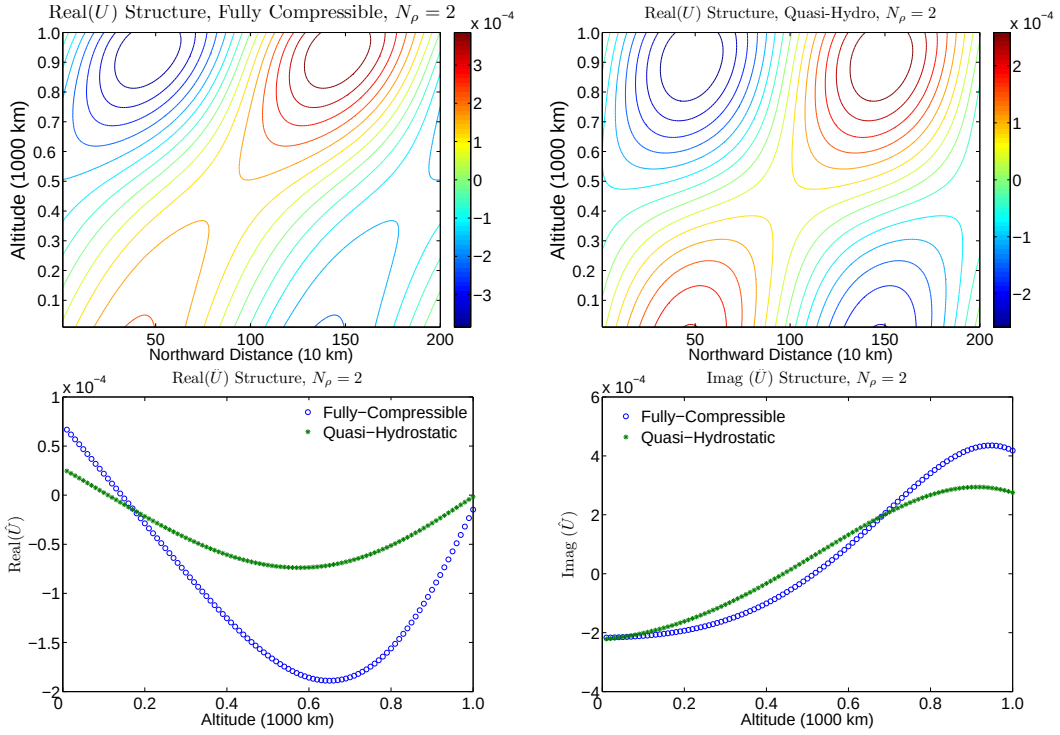

Figure 5.13: *Above: Real components of U structure for Fully Compressible and Quasi-Hydrostatic sets for first internal mode with non-zero Im(σ).*

The other approximated sets misrepresent the vertical structure in a much less dramatic way, with the modal zeroes being correctly located and the changes in

amplitude not being visibly noticeable. The misrepresentation of the vertical structure of the anelastic and pseudo-incompressible sets is sufficiently small that once the horizontal structure function is applied it becomes largely unnoticable. The misrepresentation of these modes is sufficiently small that there will be only a small amount of energy redistribution; any misrepresentation is due only to small misrepresentations of amplitude. The largest horizontal scale tested was $10\times$ the layer depth; it is not possible to test truly large horizontal scales using the F-f-plane as the approximation that F and f are constant becomes inappropriate. Over each of the length scales tested the anelastic and pseudo-incompressible sets represent the modes more accurately than either the Boussinesq or quasi-hydrostatic set. It is possible that for very large horizontal scales the quasi-hydrostatic set may be more appropriate than the anelastic sets.

The misrepresentation of the convectively unstable modes for all approximated equation sets is increased with increased density scale factor. The type of misrepresentations seen remain similar with the anelastic and pseudo-incompressible sets seeing only misrepresenation of amplitude and the Boussinesq and quasi-hydrostatic sets displaying significant discrepancies.

Increasing the number of density scale heights increases the misrepresentation of the amplitudes of the modes for the approximated equation sets; once again the Boussinesq and quasi-hydrostatic sets are sufficiently misrepresented that it seems unlikely they will provide a good model for either the neutral or convectively unstable modes within an unstably stratified polytropic regime. The misrepresentation of the anelastic and pseudo-incompressible sets is much less severe and gives a good overall indication of the structure of the fully-compressible modes, though we note that the consideration of an F-f-plane limits the analysis to smaller horizontal scales and we note that it is possible that the neutral modes with long horizontal scales may be more accurately represented by the quasi-hydrostatic set than by the anelastic sets.

Increasing the number of density scale heights decreases the magnitude of the amplitudes of the horizontal components of velocity relative to the thermodynamic variables for the unstable modes, and concentrates the mode towards the surface. The relative amplitude of the θ' structure increases significantly for larger number of density scale heights. Increasing the number of density scale heights also increases the amount by which the modes are concentrated towards the surfaces; the velocity variables are more significantly pushed towards the outer surface, and pressure perturbation more significantly pushed towards the inner surface. The θ' structure is considerably more concentrated towards the outer surface for $N_\rho = 5$ than for $N_\rho = 2$, with the majority of the mode concentrated in the outer third of the layer compared with the outer two thirds of the layer for $N_\rho = 2$. This indicates that it is not only the introduction of compressibility which affects the location and amplitude of the normal-modes, the level of compressibility introduced is also highly relevant to the vertical structure functions. Increasing the number of density scale heights also causes redistribution of energy amongst the prognostic variables and across altitudes. Figure 5.14 shows u and w structures for the fully-compressible equation set for $N_\rho = 2$ and $N_\rho = 5$, as examples of the effects of increasing the number of density scale heights.

5.1.3 Latitudinal variation

We are not able to directly consider latitudinal variation through use of an F-f-plane however consideration of F-f-planes at different latitudes should provide some indication as to the effects of latitudinal variation.

Our results show that the frequencies of the acoustic modes are only affected a small amount by the latitudinal level at which the F-f-plane is set. This is as we would expect given that for the parameter regime in which we are interested f^2 remains small compared with σ^2 for all acoustic modes at all latitudes.

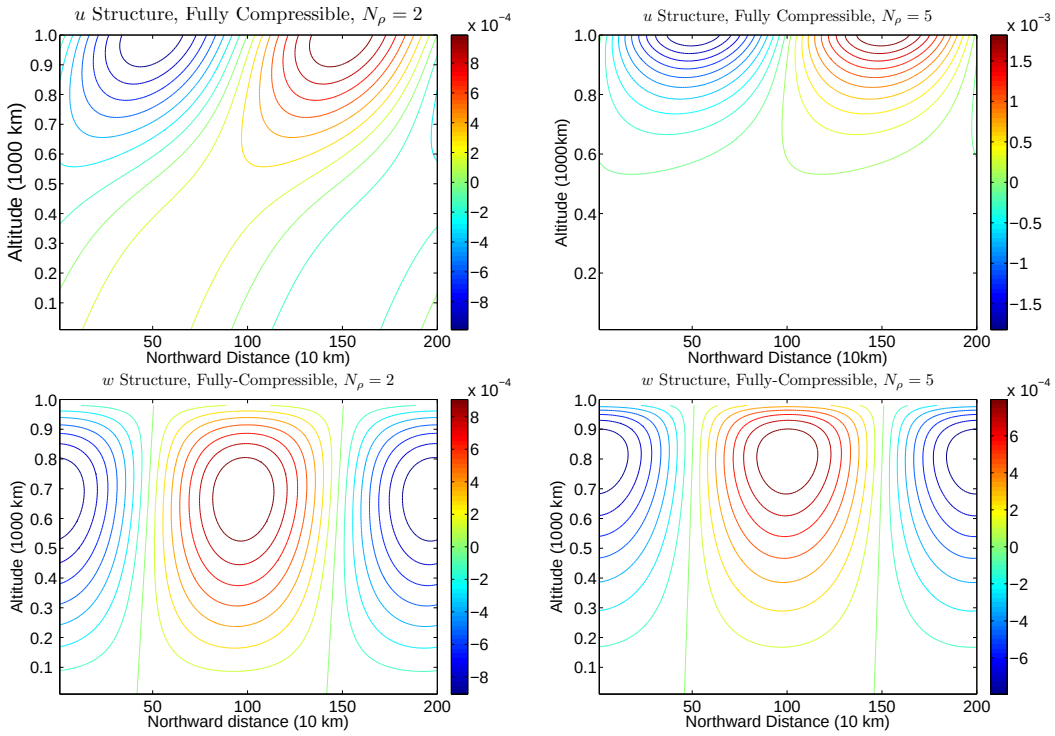

Figure 5.14: *Above: Real components of u and w structure for Fully Compressible set for* $N_\rho = 2$ *and* $N_\rho = 5$

The frequency of the neutral inertio-gravity modes asymptotes to $f = 2\Omega \sin \phi$ with increasing vertical mode number, which is consistent with the dispersion relations calculated for the analytically tractable isothermal f-plane.

We do not undertake a rigorous analysis of the effects of latitude and horizontal wavelength but note that for horizontal wavelengths equal to twice the layer depth and one quarter times the layer depth the maximum growth and decay rates for the unstable modes at each latitude are very close in size and are all found to be the deepest modes at any specified latitude.

For horizontal wavelength equal to twice the layer depth and horizontal wavelength equal to one quarter the layer depth the number of unstable modes increases with decreasing latitude such that the greatest number of unstable modes appears at the equator where, for all numbers of grid levels considered, all non-degenerate

inertio-gravity modes are unstable. The growth/decay rates of modes with vertical mode number greater than one also decrease with increasing latitude; so whilst there is only a 1% difference between the maximum and minimum growth/decay rates for the deepest mode, for the second vertical mode number this increases to approx 12% and the third vertical mode number approx 43%.

For all horizontal wavelengths tested the frequencies of the unstable modes are largest for the modes at the equator, gradually decreasing to zero at the pole; once again this is in agreement with the dispersion relations calculated for the analytically tractable isothermal F-f-plane. $F = 0$ at the pole, thus the analytic dispersion relation will be in σ^2 and all values of σ will be purely real or purely imaginary.

Misrepresentations of the frequencies and growth/decay rates by the various equation sets remains similar at all latitudinal levels considered, such that the misrepresenation seems to be far more dependent on vertical mode number and horizontal wavelength.

The structure functions show that there is significant latitudinally dependent variation across the prognostic variables. The misrepresentation of these structure functions by the approximated equation is also dependent on latitude, though the types of misrepresentation are similar with the Boussinesq and quasi-hydrostatic set displaying the most significant misrepresentations.

5.1.4 Deep polytropic layer

Consideration of a layer of depth 10,000km, with the same density scale factor and polytropic index as that of the shallower layer we have discussed in previous sections, shows that the types of misrepresentation displayed by approximated equation sets modelling the shallower layer are similar to those of the deeper layer. Since we have set N_ρ and n to be constants the main difference between the two models is the ratio

of inner to outer radius, which can result in very different structures and frequencies as has been shown by Evonuk and Glatzmaeir (2006 [28]) and Jones et al. (submitted 2008 [38]). However, the behaviour of the approximated sets relative to the fully-compressible equation set appears to remain similar. For horizontal wavelengths comparable to the layer depth the Boussinesq and quasi-hydrostatic sets continue to significantly misrepresent the eigenfrequencies; the amount by which they are misrepresented is increased by increasing the layer depth. For example, for horizontal wavelength equal to twice the depth of the layer and density scale factor $N_\rho = 2$, the Boussinesq set overestimates the growth/decay rate of the deepest unstable mode by 3.8% for layer depth $1,000km$ and by 6.8% for layer depth $10,000km$. The misrepresentation of the frequency of this mode is such that it is approximately 2% of the true value for both layer depths. The actual growth/decay rate and frequency of modes in the deeper layer are reduced compared to modes with equivalent k/k_z ratio in the shallow layer. The maximum misprepresentation of the frequencies, growth and decay rates by the anelastic and pseudo-incompressible sets is increased compared to the shallow layer, but remains considerably better than that of the Boussinesq and quasi-hydrostatic sets. The most accurate set continues to be the pseudo-incompressible set, followed by the non-energy-conserving anelastic set.

The vertical structures of the most rapidy growing/decaying modes are similar to those of a shallow layer, with the largest instability and highest frequencies being for the deepest modes with shortest horizontal wavelength. The maximum amplitudes of the structures of the prognostic variables relative to each other remains similar, though not identical; and there are differences in the locations of the modal zeroes. The manner in which the approximated sets misrepresent these structures is similar to the shallow layer, with both the Boussinesq and quasi-hydrostatic equation sets significantly distorting the mode structures, and the anelastic and pseudo-incompressible sets representing them much more accurately.

It is worth noting that for a deeper layer maximising the value of k/k_z does not require such physically small horizontal wavelengths; thus we would expect that there will be the potential for modes with larger growth/decay rates.

5.1.5 Stably stratified polytropic regime

Throughout this chapter we have discussed results for an unstably stratified polytropic reference state with polytropic index $n = 2$. Maintaining the values of the other constants and increasing the polytropic index to $n = 4$ produces $N^2 > 0$, thus we would expect all modes within this regime to be stable and have zero-imaginary component of σ. The numerical solutions found are stable as expected, and the misrepresentations found are similar to, though slightly smaller than, those for the unstably stratified regime with the largest misrepresentations found to be for similar ratios of horizontal to vertical wavenumber. The misrepresentation found by the quasi-hydrostatic set is smaller than that of the set in which $n = 2$, this is because whilst N^2 remains relatively small it is now positive. As we would expect from examination of the dispersion calculated for the analytically tractable case in Chapter 4, the frequencies of the deepest of the neutral inertial-gravity modes are significantly larger than their counterparts in an unstable atmosphere, continuing to asymptote to f for the shallowest modes though from higher frequency rather than lower frequency. The misrepresentations are significantly smaller than those seen in an isothermal reference state, as there are considerably fewer density scale heights within the reference state atmosphere.

5.1.6 Lane-Emden reference state

The use of a density scale factor in defining the reference state allows us to consider the effects of increased compressibility across a unstably stratified layer without

having to consider a layer of significant depth compared to the overall radius. This allows for higher resolution computational analysis in order to accurately ascertain the primary differences between the approximated equation sets. It is also the method used by many groups in defining the reference state for modelling of zonal flow, and other convectively driven phenomena, on gas giants. However, we acknowledge that the true reference state structure of the gas giants remains a further point of contention. Therefore, we also computed solutions for a Lane-Emden reference state with polytropic index $n = 2$. For the layer depths considered we found that the misrepresentation of the fully compressible solutions by the approximated equation sets is more severe for the deepest modes with shortest horizontal wavelengths. The magnitude of the growth/decay rates of the unstable modes reduces more rapidly with increasing vertical wavenumber than in the constant mass model. This is as we would expect as the density reduces most dramatically near to the outer surface, thus the unstable modes are more likely to be in the least dense regions close to this surface and the maximum amplitude of the perturbation variables is focused towards the appropriate boundaries more significantly than in the constant mass model. The misrepresentation of the frequencies is only slightly more severe than the constant mass model, however the structure of the unstable modes are far more significantly misrepresented for all equation sets with the amplitude and redistribution of energy amongst the prognostic variables being the most significant problems.

5.1.7 Summary

In this chapter we have considered the various approximated equation sets on an inviscid F-f-plane with an unstably stratified polytropic reference state.

We found that, as expected, all approximated equation sets filter the internal acoustic modes. The external acoustic mode is also filtered by all approximated equation sets with the exception of the quasi-hydrostatic set, which significantly mis-

represents the frequency and structure of the mode. The misrepresentation of the frequency is maximised for the deepest modes with minimum horizontal wavelength, and is increased with increasing density scale factor. The misrepresentation of the structure functions will result in significant energy redistribution amongst the prognostic variables. In contrast with the inviscid, isothermal F-f-plane the w structure is found to be non-zero, indicating that the reference profile has significant effect. This is in agreement with the results of the scale analysis, which suggest that the quasi-hydrostatic set will be poor for a weakly stratified atmosphere.

For an unstably stratified polytropic regime we find that some of the inertial-gravity modes become unstable. For all equation sets the unstable modes propagate in the prograde direction; the neutral modes propagate in both prograde and retrograde directions.

The growth/decay rates of the unstable modes were found to maximal for minimum horizontal wavelength and maximum vertical wavelength. Increasing the density scale factor was found to have significant effect on the frequencies, growth/decay rates and mode structures; the frequencies and growth/decay rates were found to be increased with increased density scale factor and the mode structures were found to be concentrated more significantly towards the outer surface. The results were aligned with our expectations and the indications provided by the dispersion relations for the analytically tractable inviscid, isothermal, approximated equation sets. We expected the quasi-hydrostatic set to misrepresent modes most significantly when the ratio k/k_z is no longer small, as in this case the vertical accelerations can no longer be neglected compared with horizontal accelerations. We also expected these to be the modes with the greatest instability. This was shown to be correct. The quasi-hydrostatic set was shown to be an inappropriate approximation for modelling of convectively unstable modes in this regime, with the frequencies and growth/decay rates displaying massive overestimations and significant errors in the vertical structure including spurious

adjustments to amplitude, relocation of modal zeroes and a redistribution of energy amongst the prognostic variables.

The Boussinesq set was also found to be, in general, inappropriate where density stratification may have a significant effect. In the Boussinesq case the misrepresentation was found to be maximised for horizontal wavelength somewhere between 2 and 5 times the depth of the layer; at these k/k_z ratios we see significant misrepresentation of all modal characteristics. At all horizontal to vertical wavelength ratios the frequencies of the unstable Boussinesq modes were found to be significantly, and systematically, reduced to less than 0.5% of their true value. For horizontal wavelength comparable to the layer depth the growth/decay rates of these modes were also significantly misrepresented, though to a lesser degree. For horizontal wavelengths equal to one quarter the depth of the layer the maximum misrepresentation of the growth/decay rates is reduced to approximately 2% in a reference state with $N_\rho = 2$. Increasing the number of density scale heights increased the misrepresentation of σ by the Boussinesq set. The structure of the unstable modes calculated for the Boussinesq equation set also displays significant discrepancies with relocation of modal zeroes, redistribution of energy amongst the prognostic variables and spurious adjustment of the amount by which the mode is tilted. The misrepresentation of the structures of the rescaled variables is reduced for smaller horizontal wavelengths, however the application of the scale factor which returns the rescaled variables to their unscaled form means that there continues to be significant misrepresentation. We note that the simplicity of the Boussinesq set makes it an attractive approximation for analytical calculations. We will also see in chapter 7 that when considered alongside a uniform density reference state it has significantly reduced computational expense compared with an anelastic set making it a popular choice for initial inspections of the dynamics of large complex regimes. In cases where solutions have been obtained using Boussinesq approximations our results show that the their resemblence to fully compressible

solution could be significantly improved through the application of appropriate reference state density scaling factors. Whilst this factor will cause no improvement to any misrepresentation of the frequency it could provide a more accurate representation of the eigenfunctions as it re-introduces the systematic variation with height due to the reference state density stratification that is otherwise ignored in Boussinesq approximations.

The pseudo-incompressible and anelastic approximations misrepresent the fully-compressible set significantly less severely. As with the Boussinesq set maximum misrepresentation of these sets is found to be for aspect ratios such that horizontal wavelengths are comparable to or slightly larger than vertical wavelength. We note that we are unable to accurately consider very long horizontal wavelengths using an F-f-plane, therefore it is possible that long horizontal wavelength neutral modes may be more accurately represented by the quasi-hydrostatic set than the anelastic sets. The energy-conserving anelastic set is the least accurate of these sets and the pseudo-incompressible set displays impressive accuracy at all vertical and horizontal wavelengths. The anelastic sets enforce a solenoidal $\rho_s \boldsymbol{u}$ field which allows for further analytic analysis than the non-adiabatic pseudo-incompressible set, therefore the anelastic equation sets are more commonly used. Our results show that for a 10,000km deep atmosphere with horizontal wavelength equal to the depth of the layer, the maximum misrepresentation of the frequencies of either anelastic set is less than 5% and the maximum misrepresentation of the growth/decay rates less than 2%. This misrepresentation decreases for decreasing horizontal wavelength. The representation of the eigenstructures is good and suggests that the use of anelastic approximations to investigate the dynamics of unstably stratified regimes in which the magnitude of N^2 is small is well justified. For more accurate modelling of these regimes the use of the pseudo-incompressible seems to be the most appropriate approximation with extremely strong replication of the fully compressible sets. Increasing the number

of density scale heights in the reference state increases the amount by which all the approximated equation sets misrepresent the mode structures.

With the exception of the quasi-hydrostatic set, consideration of a stably stratified polytropic regime displays significantly smaller errors than that of an isothermal reference state. This is due in part to the reduced number of scale heights across the atmosphere, and the small magnitude of N^2 is also the reason for the poor performance of the quasi-hydrostatic set.

The results discussed in this chapter provide us with insight into the types of misrepresentation to expect in a fully 3D spherical model, though we note that we expect to find non-degenerate Rossby modes in the fully spherical case. In the next chapter we will investigate this further.

Chapter 6

Spherical Geometry

In previous chapters we considered the misrepresentations of the normal modes caused by various approximated equation sets on an F-f-plane. We have also seen that the inclusion of the F terms has a significant effect on the structures, frequencies and growth/decay rates of the normal modes in both polytropic and isothermal regimes appropriate to different regions of the Jovian atmosphere; they also have an impact on the level of misrepresentation caused by the approximated equation sets. The geometrical approximation of a tangent plane means that we set $f = 2\Omega \cos\phi = \text{constant}$; the lack of latitudinal variation means that all Rossby modes have degenerate frequency. In this chapter we consider a spherical shell in order to attempt to determine the effects of the approximated equation sets in a more realistic geometry. Unless otherwise stated the results in this chapter have been found for an unstably stratified reference state appropriate to the interior and interior atmosphere of the Jovian regime.

We saw in chapter 4 that the linearised equations governing a fully spherical

regime are such that we can consider separable solutions of the form

$$\left.\begin{array}{lcl} U & & \hat{U}(\phi,r) \\ V & & \hat{V}(\phi,r) \\ W & = & \hat{W}(\phi,r) \\ P & & \hat{P}(\phi,r) \\ \Theta & & \hat{\Theta}(\phi,r) \end{array}\right\} \exp(im\lambda - i\sigma t). \tag{6.1}$$

Application of this form of solution to (3.67)-(3.71) allows us to write the inviscid governing equations in the form

$$\begin{aligned} &-i\sigma\delta_A\frac{\hat{P}}{C_s^2} + \delta_D\frac{N^2}{g}\hat{W} + \delta_C\frac{\hat{W}}{2\rho_s}\frac{\partial\rho_s}{\partial r} + \frac{1}{r\cos\phi}\left[im\hat{U} + \frac{\partial}{\partial\phi}(\hat{V}\cos\phi)\right] \\ &\quad + \frac{1}{r^2}\frac{\partial}{\partial r}(r^2\hat{W}) = 0 \end{aligned} \tag{6.2}$$

$$-i\sigma\hat{U} + F\hat{W} - f\hat{V} + \frac{im}{r\cos\phi}\hat{P} = 0 \tag{6.3}$$

$$-i\sigma\hat{V} + f\hat{U} + \frac{1}{r}\frac{\partial\hat{P}}{\partial\phi} = 0 \tag{6.4}$$

$$-i\sigma\delta_H\hat{W} - F\hat{U} + \frac{\partial\hat{P}}{\partial r} + \delta_E\frac{\hat{P}}{C_s^2}g + \delta_E\frac{\hat{P}}{\rho_s}\frac{\partial\rho_s}{\partial r} - \hat{\Theta}g - \delta_C\frac{\hat{P}}{2\rho_s}\frac{\partial\rho_s}{\partial r} = 0 \tag{6.5}$$

$$-i\sigma\Theta + \frac{N^2}{g}\hat{W} = 0. \tag{6.6}$$

Similarly to the F-f-plane analysis in the previous chapter this allows us to write the equation sets as a matrix eigenvalue problem of the form

$$\boldsymbol{A}\hat{\boldsymbol{s}} = i\sigma\boldsymbol{B}\hat{\boldsymbol{s}} \tag{6.7}$$

where $\hat{\boldsymbol{s}}$ is a state vector containing values describing $\hat{U}$ etc. Since we are considering a spherical shell we are able to vertically discretize the equations in the same way as we did in the tangent plane analysis. We also discretize the equations in ϕ such that values for $\hat{V}$ are stored at the equator but not at the pole, and are staggered relative to all other prognostic variables. The eigenvalue problem can then be solved using the NAG routine described in chapter 5.

To reduce the computational size of the problem we consider only one hemisphere, taking eigenmodes to be either symmetric or antisymmetric about the equator. To find symmetric modes and antisymmetric modes it is necessary to adjust the value of $\hat{P}$ when computing $\partial\hat{P}/\partial\phi$ in the $\hat{V}$ equation on the equator. To find symmetric modes we take $\hat{P}$ at a point immediately south of the equator to be equal to $\hat{P}$ at its mirror-image point north of the equator; to find antisymmetric modes, $\hat{P}$ south of the equator is set equal to -$\hat{P}$ north of the equator. In writing the numerical code it is also important to remember that at the pole the perturbation fields must be non-singular. Therefore, for zonal wave number $m = 0$, $\hat{U}$ and $\hat{V}$ must vanish at the pole but $\hat{W}$, $\hat{P}$ and $\hat{\Theta}$ can be finite and non-zero. For zonal wavenumber $m = 1$, $\hat{W}$, $\hat{P}$ and $\hat{\Theta}$ must vanish at the pole but $\hat{U}$ and $\hat{V}$ can be non-zero where $\hat{U} = \hat{V}$ at that point. For zonal wavenumbers $m > 1$ all perturbation fields must vanish at the pole. To achieve these requirements the tendency equations are modified accordingly. For $m = 0$ the $\hat{P}$ tendency equation is modified such that $\partial(\hat{V}\cos\phi)/\partial\phi$ is calculated correctly and $\hat{U}$ tendency is set equal to zero. For $m = 1$ the $\hat{W}$, $\hat{P}$ and $\hat{\Theta}$ tendencies are set to zero and the $\hat{U}$ tendency estimated by extrapolating the $\hat{V}$ tendency. For $m > 1$ all tendencies are set to zero. We note that due to the grid staggering $\hat{V}$ is not stored at the pole, therefore no change is necessary to the $\hat{V}$ tendency equation.

Using the numerical method described previously calculates σ through calculation of α and β such that $\sigma = \alpha/\beta$. We ignore any 'solutions' in which β is smaller than the machine accuracy. In the fully compressible case this results in all solutions being physically realistic. For the approximated equation sets we find that in the fully spherical case we calculate 'solutions' in which β is greater than machine precision but consideration of σ shows these 'solutions' to be physically unrealistic. In creating switchable equation sets we allow for the possibility to consider cases in which the switches are not set to zero or one, but somewhere in between. Setting the switches to be non-zero helps to eliminate the calculation of spurious results. As δ_A or

δ_H approaches zero the frequency of the acoustic modes approaches infinity. Setting the appropriate switches to be of the order 10^{-8} rather than zero ensures that no spurious solutions are calculated, yet allows calculation of solutions that we believe to be sufficiently close to the solutions for the approximated equation sets that we are able to use them to compare the approximated and fully-compressible equation sets. Comparison with non-spurious results calculated when the appropriate switches are set to zero supports this view. The number of solutions calculated is discrete and dependent on the number of grid points that have been defined, and the number of grid points is constrained by the computational size of the problem. Avoidance of calculation of spurious solutions is important in allowing us to consider as many true solutions as possible. This provides a further reason to consider solutions to the approximated sets that have been calculated through setting the switches to be of the order 10^{-8}.

Since we are not able to find analytic solutions for any of the approximated equation sets it is inevitable that computational errors will be introduced. Computational demands mean that we are restricted to 25 grid levels in the vertical and 35 latitudinal grid levels; this coarse grid means that errors due to averaging could be significant, however experimentation with the number of grid levels and layer depths suggests that the relationship between the approximated and fully-compressible equation sets remain relatively consistent. Whilst this resolution allows for several grid points per density and pressure scale height it is unlikely that it will calculate accurate structures for modes with high meridional, zonal or vertical wavenumber as accurate calculation will rely on several grid points per wavelength.

Therefore we believe that whilst the solutions calculated for each equation set are unlikely to be exact, they will provide an indication towards the levels of misrepresentation experienced by the approximated sets. The type of grid staggering, and numerical method used, will also have an effect on the accuracy of the solutions; it

is not necessarily the case that the best computational method for one approximated equation set will be the same as that of another approximated set. This is another wide ranging topic in itself, and we chose not to dwell on it in this thesis; instead we assume that the majority of the misrepresentation of the fully-compressible set by the various approximated equation sets can be attributed to the approximations made to the governing equations rather than differences due to the optimal computational method for each set. The code was checked with a reference state in which $N^2 > 0$ in order to check that all solutions calculated had zero imaginary component of σ, thus are stable. The code was also used to calculate solutions for a terrestrial atmosphere, and compared with those of Thuburn et al., [59]; this suggests the resolution is adequate for use in determining normal modes with large scales in a stably stratified atmosphere.

6.1 Acoustic Modes

We have seen that analysis of the isothermal, inviscid F-f-plane provides us with dispersion relations that can be approximated to form dispersion relations for the external acoustic modes

$$\delta_A \sigma^2_{acoustic} \approx C_s^2 \left(k_x^2 + k_y^2\right), \tag{6.8}$$

and internal acoustic modes such that

$$\delta_A \delta_H \sigma^2_{acoustic} \approx C_s^2 \left[\delta_H \left(k_x^2 + k_y^2\right) + k_z^2\right]. \tag{6.9}$$

If $\delta_A = 0$ or $\delta_H = 0$ then the acoustic modes are filtered from the solution set. We expect that these will provide an approximate form for the fully-spherical acoustic mode dispersion relations, with k_x, k_y and k_z replaced with vectors appropriate to the co-ordinate system. We therefore expect that, as in the F-f-plane, the acoustic modes will be filtered by all equation sets with the exception of the quasi-hydrostatic

set, which should calculate solutions for the external acoustic modes. Further to this we expect that for non-zero δ_A and δ_H the frequencies of the internal acoustic modes will approach infinity as either switch approaches zero, and the frequency of the external acoustic modes will approach infinity as δ_A approaches zero. C_s^2 and all the appropriate vectors are purely real and greater than zero; therefore, we expect that the acoustic modes will be purely real. As expected, we find this to be the case for all solutions calculated.

We find that the computational results behave similarly to our expectations. The internal acoustic mode frequencies vary according to zonal, meridional and vertical wavenumber with vertical wavenumber having the largest impact. The small layer depth and large circumference of the model mean that this is not surprising. As one would expect, the shallowest modes with shortest horizontal wavelengths have the highest frequencies. Increasing the number of density scale heights across the layer acts to change the profile of the frequencies, though the frequencies of the fastest and slowest modes remain largely unchanged. This is as we would expect as the adjustment to the reference state profile will naturally affect the profile of C_s^2, which has significant impact on the frequencies of the modes.

Despite the vastly increased frequencies, these relationships remain when we consider the acoustic modes calculated when the appropriate switches are set between zero and one. The amount by which frequencies of the acoustic modes are increased by altering the value of the switches depends on the combination and magnitude of the switches; the smaller the switch the greater the increase in frequency such that the frequencies tend to infinity as the switches tend to zero. The switch combination has a significantly lesser effect with all combinations calculating solutions with frequencies of the same order; for switches set close to one the combination appropriate to the Boussinesq approximation most dramatically increases the acoustic mode frequencies, followed by the non-energy conserving anelastic set. The switch com-

binations appropriate to the quasi-hydrostatic and pseudo-incompressible sets least dramatically affect these mode frequencies.

6.1.1 External Modes

Unlike the internal acoustic modes, which are filtered by all approximated sets, the external acoustic modes are not filtered by the quasi-hydrostatic set. The approximated dispersion relation, and isothermal analysis, suggest that the frequencies should be accurately represented by the quasi-hydrostatic set. Similarly to the results of the unstably stratified F-f-plane we find that this is not the case and find that the representation of the external modes is dependent on the ratio of horizontal to vertical wavelength. Modes with longest horizontal wavelength seem to be well represented in terms of both frequency and eigenstructure. The frequencies are misrepresented by less than 1% for all meridional wavenumbers calculated, and zonal wavenumbers $m = 1$ to $m = 30$, with the eigenstructures also being well represented as shown in figure 6.1.

This is in line with the results found for the F-f-plane geometry as the large Jovian radius means that for the layer depth that we are modelling it is necessary to consider high zonal or meridional wavenumbers in order to inspect scenarios in which the horizontal wavelength is comparable to the layer depth. Setting zonal mode number $m = 100$ backs up this argument, with the frequencies of the modes with shortest meridional wavelength being misrepresented by 6.9% and the calculation of several spurious modes. The eigenstructures of the non-spurious modes continue to be reasonably well represented with good replication of the maxima and minima. By $m = 500$ there are sufficient spurious modes calculated that it is not possible to identify the external modes; this is likely to be largely due to poor resolution, but it is also worth noting that we have seen that the quasi-hydrostatic set performs poorly for modes with short horizontal wavelength.

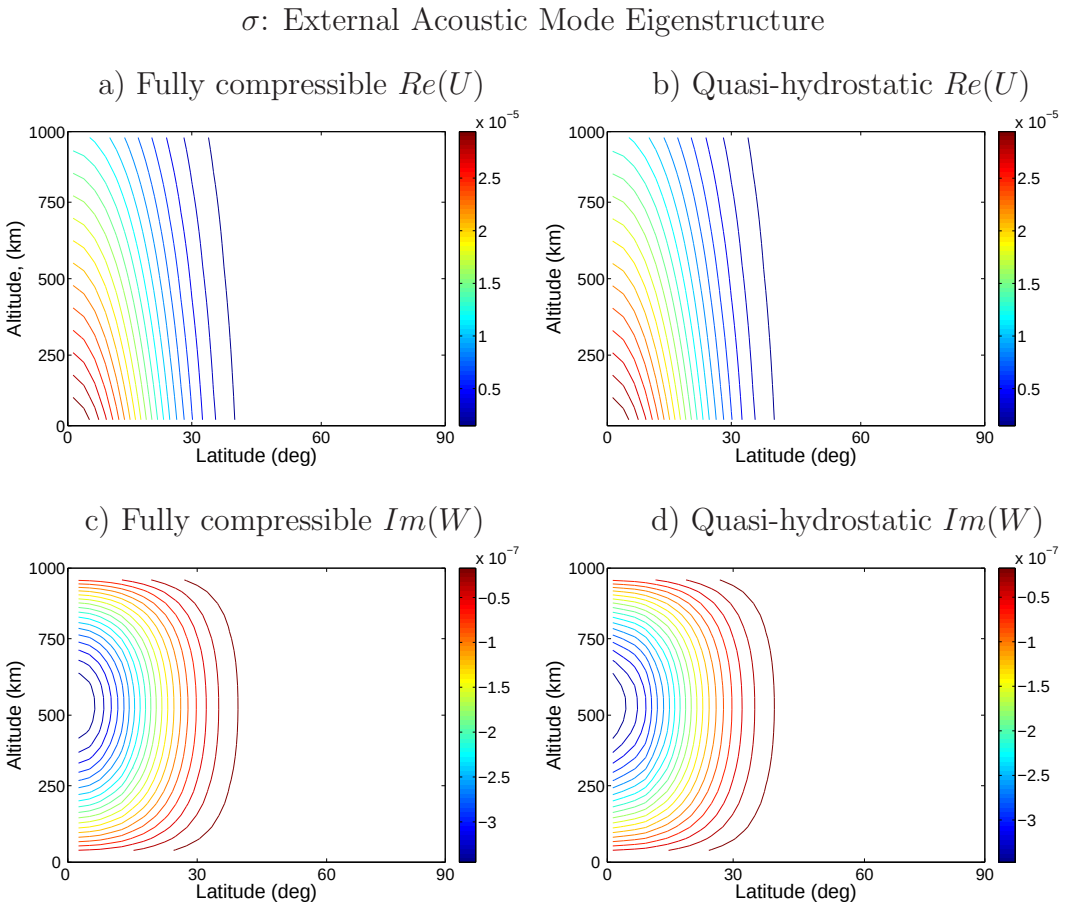

Figure 6.1: *U and W eigenstructures for the prograde external acoustic mode with longest meridional wavelength and zonal wavenumber $m = 10$. Reference state with $N_\rho = 2$, inner surface at $r = 71,430km$, layer depth $1000km$.*

Increasing the number of density scale heights across the layer increases the misrepresentation of both the frequencies and eigenstructures. Therefore, whilst the level of inaccuracy caused by the quasi-hydrostatic set seems to be primarily governed by the aspect ratio, the reference state profile and compressibility of the layer also have discernible effect. The amplitude of the vertical velocity is also affected by these factors with increased superadiabaticity and increased compressibility both increasing its relative contribution to the perturbation energy.

6.2 Inertio-Gravity Modes

In this section we will consider the inertio-gravity modes; naturally these have much lower frequency than the acoustic modes, and consideration of an unstably stratified regime means that there are both unstable and neutral mode solutions. Figure 6.2 shows the order in which the solutions for the inertio-gravity modes are calculated for a reference state with $N_\rho = 2$ and zonal wavenumber $m = 1$. We see that the order in which solutions are calculated is not random and solutions are clearly grouped such that, in general, neutral modes with highest frequencies are calculated first. These neutral modes are interspersed with low frequency unstable modes. The clear order in which the routine calculates modes makes it easier to identify modes for inspection. For higher zonal wavenumber many more of the modes are unstable, thus the first modes calculated often have small frequency and large growth/decay rate.

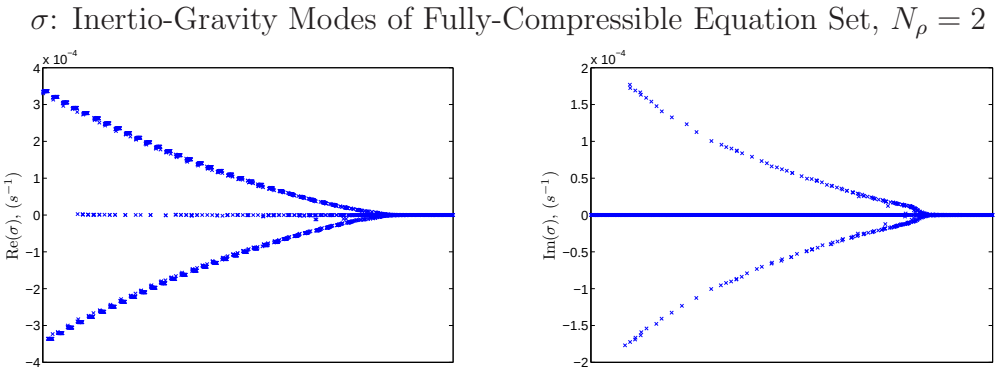

Figure 6.2: *Order in which the normal mode solutions are calculated by the numerical routine for $N_\rho = 2$. Note that the modes with largest growth/decay rates have extremely small frequency relative to the neutral modes with high frequency. Modes are grouped by meridional wavenumber; within each group vertical mode number decreases from left to right along the x-axis.*

Figures 6.3 - 6.5 show the frequency and corresponding growth/decay rates of the inertio-gravity modes for zonal wavenumbers $m = 1$, $m = 10$ and $m = 500$ in

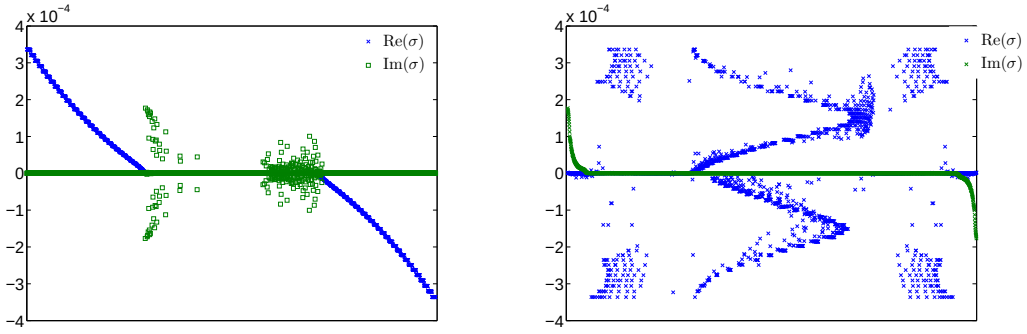

Figure 6.3: *Inertio-gravity mode frequencies and growth/decay rates of the fully compressible set for $N_\rho = 2$. Zonal wavenumber $m = 1$. Left: sorted by frequency, right: sorted by growth/decay rate*

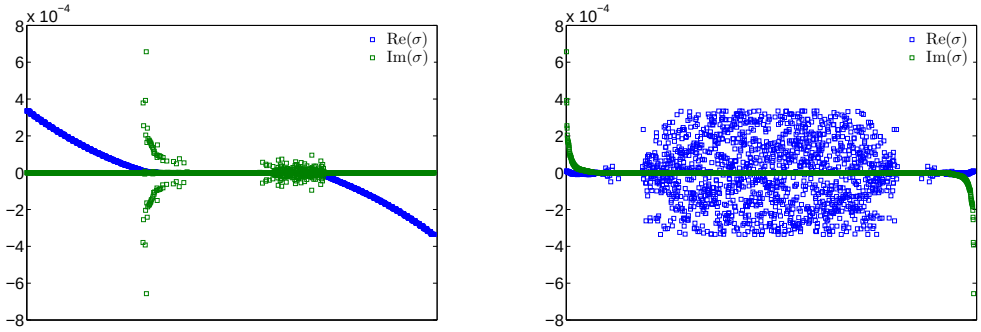

Figure 6.4: *Inertio-gravity mode frequencies and growth/decay rates of the fully compressible set for $N_\rho = 2$. Zonal wavenumber $m = 10$. Left: sorted by frequency, right: sorted by growth/decay rate*

a reference state with $N_\rho = 2$. The leftmost figures sort σ by its real component, the rightmost figures sort σ by its imaginary component. These clearly show that, as in the case of the inviscid F-f-plane, the unstable modes are calculated as almost complex conjugate pairs. The inertio-gravity modes then fall into various categories:

- Unstable modes with small frequency and large growth/decay rate
- Unstable modes with large frequency and small growth/decay rate

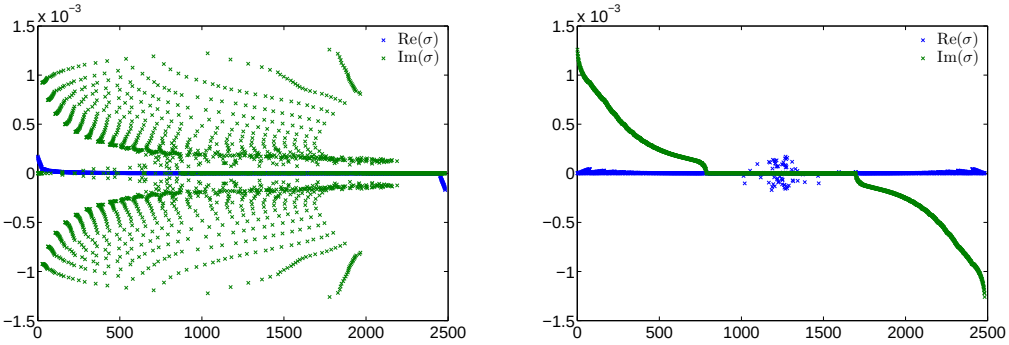

Figure 6.5: *Inertio-gravity mode frequencies and growth/decay rates of the fully compressible set for $N_\rho = 2$. Zonal wavenumber $m = 500$. Left: sorted by frequency, right: sorted by growth/decay rate*

- Stable modes with large frequency
- Stable modes with small frequency

All approximated equation sets display similar patterns to those of the fully-compressible equation set.

In the following sections the accuracy of the representations of modes by the approximated equation sets will be discussed according to the categories in which they appear to lie.

6.2.1 Large frequency and small growth/decay rate

In this section we refer to modes with frequency of the order $10^{-4}s^{-1}$ and growth/decay rate less than $10^{-7}s^{-1}$; and unless otherwise stated, refer to a reference state in which $N_\rho = 2$.

The frequency of these modes is similar to the rate of rotation and the modes are stable or have small growth/decay rate; consideration of the dispersion relation for the isothermal f-plane leads us to believe that these modes are likely to be the shallow

gravity waves. For the polytropic reference state we are considering the approximated dispersion relation for very shallow gravity waves, in which $k/k_z \ll 1$, is given by

$$\sigma^2_{Shallow\,gravity} \approx f^2 + \frac{N^2 k^2}{k_z^2}. \tag{6.10}$$

We assume that this provides an indication as to the frequencies and growth/decay rates of the shallowest gravity waves in an unstably stratified regime and recall that $N^2 < 0$ and $|2\Omega| \gg |N^2|$. Therefore we expect that for a specified zonal and meridional wavenumber the shallowest waves will have the largest frequency; similarly, for a specified vertical wavelength the modes with longest meridional and zonal wavelengths will have the largest frequency. We also expect that as meridional and/or zonal wavenumber increases there will be fewer neutral modes. The lack of switchable terms in the approximated dispersion relation suggests that the modes should be reasonably well represented. Increasing the number of density scale heights across the layer increases the magnitude of $|N^2|$, therefore we expect that for specified zonal, meridional and vertical wavenumbers the frequencies of comparable modes will be reduced compared to those for a set with fewer density scale heights. We expect that the maximum misrepresentations of the shallow gravity waves will be found to be for the deepest of these waves, where our approximated dispersion relation holds least strongly and additional, switchable terms will have impact upon the frequencies.

The computational solutions of the fully-compressible set match our expectations and the approximated equation sets reflect the frequencies of the inertio-gravity waves sufficiently well that it is clear to which groups they belong. For a specified meridional mode number the misrepresentation of the frequencies of all sets is greatest for the deepest modes. The misrepresentation of the frequencies shows only a very small variation with meridional wavenumber, though the number of latitudinal grid levels is sufficiently small that we cannot conclude from this that the meridional wavenumber has no impact on the level of misrepresentation by the approximated sets. The misrepresentation of the frequencies also shows very little variation with zonal

mode-number, with the levels of misrepresentation being small for all zonal mode-numbers less than $m = 100$. For $m = 500$ no neutral modes are calculated which have large frequency, there are also no modes calculated with large frequency and small growth/decay rate. This matches our expectation that as horizontal wavenumber increases, thus k/k_z increases, there will be fewer neutral modes. The maximum misrepresentation of the frequencies by the Boussinesq set is less than 1%, for the quasi-hydrostatic set it is less than 0.5% with both sets underestimating the actual frequency. For the anelastic and pseudo-incompressible sets the misrepresentation is sufficiently small that it cannot be differentiated from machine precision.

Increasing the number of density scale heights across the layer results in similar solutions with the patterns found for the neutral modes of the $N_\rho = 5$ remaining similar to those of the $N_\rho = 2$ regime; however, the actual misrespresentations of the frequencies are slightly increased. For zonal wavenumber $m = 10$ for the pseudo-incompressible and non-energy conserving anelastic sets the misrepresentation remains less than 1%. For the energy-conserving anelastic set it is increased and varies between 0.5% and 3%. The misrepresentations by the Boussinesq and quasi-hydrostatic sets are also increased to between 1% and 5%.

These results are similar to the results of the F-f-plane analysis. When considering the F-f-plane geometry we found that the frequencies of the neutral modes were well represented by the anelastic and pseudo-incompressible sets with the quasi-hydrostatic and Boussinesq sets displaying more obvious distortion. The primary difference between the results of the F-f-plane and spherical geometry is the increased misrepresentation by the energy-conserving anelastic set compared to the non-energy-conserving anelastic and pseudo-incompressible sets.

The growth/decay rates of the modes which have very small growth/decay rate relative to frequency are dependent on meridional, vertical and zonal wavenumber as well as the direction in which the wave propagates and the number of density scale

heights across the layer. For zonal wavenumber $m = 1$ and $N_\rho = 2$ the frequencies and growth/decay rates of several of the fastest inertio-gravity modes are displayed in figure 6.6.

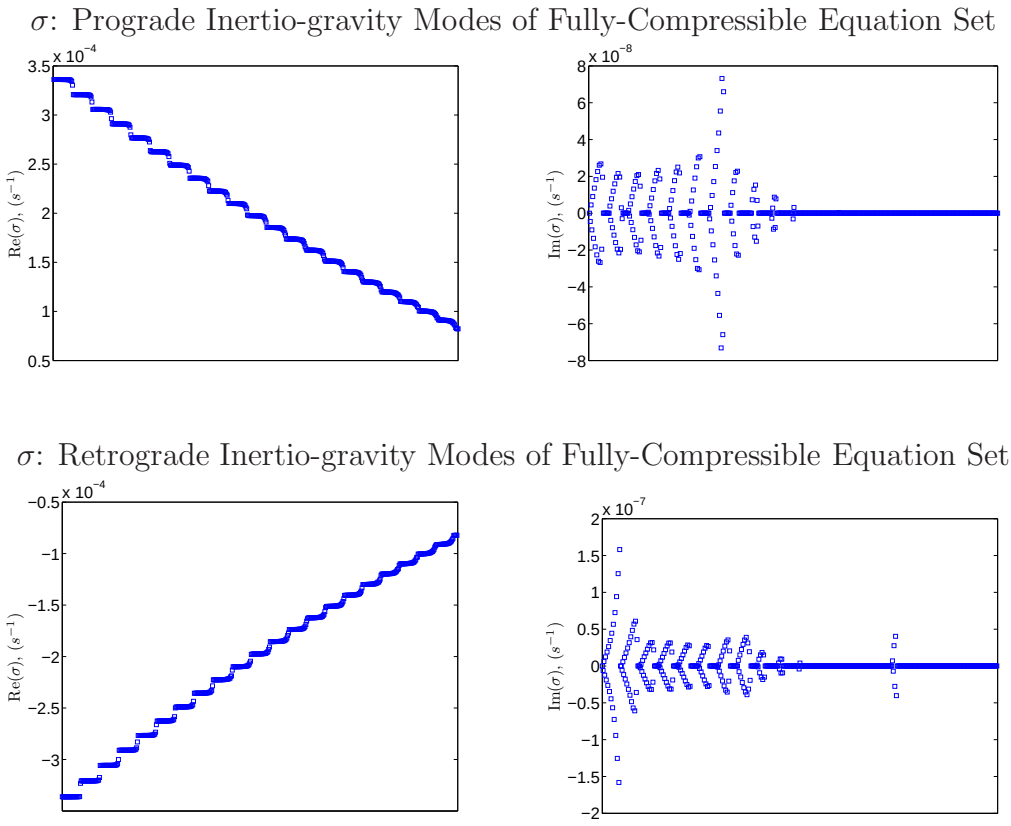

Figure 6.6: *Frequency and growth/decay rate of the $m = 1$ inertio-gravity modes of the fully-compressible equation set. Modes are grouped by meridional wavenumber; within each group vertical wavelength increases from left to right along the x-axis.*

It is interesting to note that the pattern in which growth/decay rates vary with meridional mode number for modes propagating in the prograde direction does not coincide with that of modes propagating in the retrograde direction. The pattern is not static with increased zonal wavenumber; the minimum meridional mode number of modes with non-zero growth/decay rate is increased with increased zonal wavenumber such that by $m = 10$ there are no modes calculated with small growth/decay rate

relative to frequency. The actual pattern also differs with zonal mode number such that there is no obvious way of predicting growth/decay rate according to zonal, meridional or vertical mode number.

The pattern with which the growth/decay rates vary with zonal, meridional and vertical modenumber is accurately reflected by the anelastic, pseudo-incompressible and quasi-hydrostatic sets though there is some misrepresentation of the actual growth/ decay rates. The typical misrepresentation of the growth/decay rate by the anelastic and pseudo-incompressible sets is less than 1%, with the quasi-hydrostatic set displaying errors of approx 5% for zonal wavenumber less than $m = 10$. We recall that there are no modes calculated with large frequency and small growth/decay rate for zonal wavenumber greater than $m = 10$.

Each of these approximated sets display instances in which the misrepresentation is much more significant; either where the frequency and growth/decay rate are not matched correctly or misrepresentation of one or other is large. These instances are not necessarily correlated between equation sets and are usually the deepest of a group of modes with constant meridional and zonal wavenumber.

The pattern of growth/decay rate compared with meridional and zonal wavenumber is largely reflected by the Boussinesq set, such that the frequencies of the unstable modes are of the correct order, however the exact meridional and vertical modenumbers and actual growth/decay rates are not necessarily accurate; the prograde modes for $m = 1$ are shown in figure 6.7 as an example of this.

It is possible that the small growth/decay rates seen for some of the modes with longest zonal wavelength are spurious artefacts of poor computational resolution or the choice of grid used in solving the eigenvalue problem. If this is the case, it is interesting to note that they are replicated by all approximated equation sets with the exception of the Boussinesq case. This would add weight to our argument that

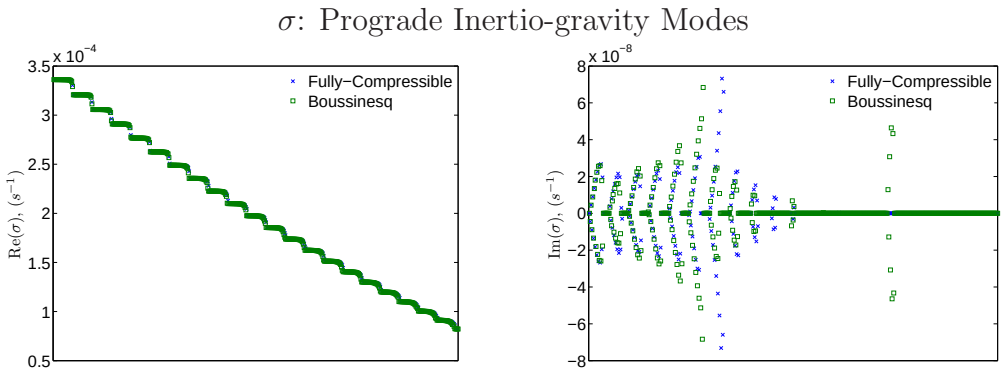

Figure 6.7: *Frequency and growth/decay rate of the* $m = 1$ *prograde inertio-gravity modes of the fully-compressible and Boussinesq equation sets. Modes are grouped by meridional wavenumber; within each group vertical mode number decreases from left to right along the x-axis.* $N_\rho = 2$.

the choice of grid and averaging method should not have as much of an impact on the misrepresentation of σ as the approximations themselves.

Eigenstructures

The replication of the eigenstructures of the neutral modes and the modes with small growth/decay rate relative to frequency is very strong by all approximated equation sets. All sets replicate the overall structure well, accurately replicating the vertical and meridional wavenumber and latitudinal location. There does not seem to be any significant alteration to modal amplitudes, zeroes or tilting and the contribution to the perturbation energy by the various prognostic variables seems to be well represented. Increasing the number of density scale heights across the layer acts to increase any misrepresentation such that the anelastic and pseudo-incompressible sets remain well represented but we now find that in the quasi-hydrostatic case there are spurious adjustments to the amplitudes of the horizontal components of velocity, thus redistribution of energy across the prognostic variables. In the Boussinesq case the

modal amplitudes are well represented but there is some spurious vertical relocation of modal zeroes. We recall that the rescaling of the equation sets to remove some consistent variation due to reference state density means that the eigenstructures reflect the rescaled prognostic variables. In order to return them to their unscaled form it is necessary to apply a reference state density scaling factor which acts to focus the eigenstructures towards the inner and outer surfaces dependent on the scaling factor. In the Boussinesq case the re-scaled and unscaled variables are the same, thus consideration of the structures of unscaled variables would mean that we would see considerably more misrepresentation by the Boussinesq set.

These results are again similar to the F-f-plane analysis, where we found that all sets displayed good representation of the neutral modes of the re-scaled equation sets, with the Boussinesq and quasi-hydrostatic sets displaying the most significant misrepresentations. This is also in line with our expectations from scale analysis where we expect the Boussinesq set to perform less strongly than other sets when the horizontal wavelength is large, and we expect the quasi-hydrostatic set to perform less strongly when $N^2 < 0$ and $|N^2|$ is small.

6.2.2 Large growth/decay rates

The number of faster travelling modes with small or zero growth/decay rate calculated alongside each meridional wavenumber is dependent on zonal wavenumber, number of density scale heights across the layer and equation set. Where fewer of this mode type are calculated we see the calculation of a greater number of modes with large growth/decay rate. These are likely to be the convectively unstable modes, thus their accurate representation is likely to be important in modelling the deep convective zones of the Jovian regime.

Having seen in section 6.2.1 that the shallow gravity waves are stable or have

very small growth/decay rate relative to their frequency, we consider the approximated dispersion relation for the inertio-gravity waves

$$\sigma^2_{Inertio\,Gravity} \approx \frac{(2\boldsymbol{\Omega}.\boldsymbol{k})^2 + N^2 \boldsymbol{k_h}^2}{\boldsymbol{k}^2 + \Gamma^2} \tag{6.11}$$

where $\boldsymbol{k}$ is the three-dimensional wavevector and $\boldsymbol{k_h}$ is the two dimensional horizontal wavevector. Recalling that $|N^2| \ll |2\Omega|$ and $N^2 < 0$ we expect instability when $2\boldsymbol{\Omega}.\boldsymbol{k}$ is minimised, or for modes with extrememly short horizontal wavelength; therefore we expect the maximal growth/decay rates to be found for modes with minimum horizontal wavelength and located at the pole. We also expect that given that the magnitude of N^2 is larger for $N_\rho = 5$ than $N_\rho = 2$, the maximal growth/decay rates will be larger for increased number of density scale heights across the layer.

The solutions that have been calculated match our expectations. The maximal growth/decay rates are increased with increasing zonal wavenumber; whilst computational demands mean a thorough examination of the variation of maximal growth/decay rate with zonal wavenumber is not practical, initial inspections suggest that for $N_\rho = 2$ the relationship is likely to be as shown in figure 6.8. This is consistent with the approximated dispersion relation.

All approximated equation sets approximately replicate the shape of this graph such that it seems likely that the most rapidly growing/decaying modes will be found to have the correct level of horizontal and vertical structure.

For all zonal mode numbers examined the maximum growth/decay rate was also found to be for maximum meridional wavenumber. The meridional wavenumber is limited by the number of latitudinal grid levels; however, the approximated dispersion relation suggests that the maximum growth/decay rate will always be found to have maximal meridional wavenumber. Therefore increasing the number of latitudinal grid levels will not allow us to inspect the horizontal structure more thoroughly as we expect that the maximum growth/decay rate will always have the maximum

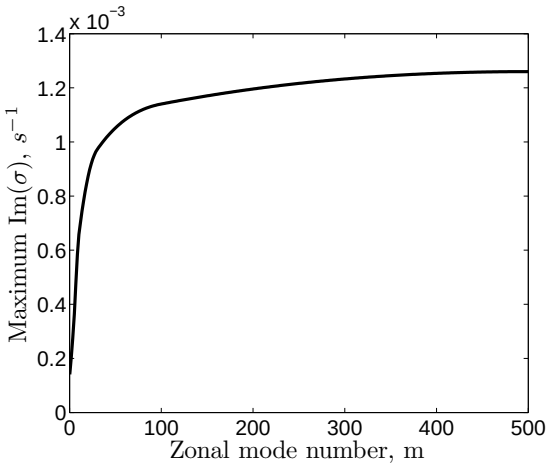

Figure 6.8: *Maximum growth/decay rate versus zonal wavenumber for $N_\rho = 2$; based on a limited number of numerical experiments and consideration of approximated dispersion relation.*

possible meridional wavenumber. We expect that the variation of growth/decay rate with meridional wavenumber will be similar to the way in which growth/decay rate varies with zonal wavenumber.

The approximated dispersion relation is quadratic, therefore suggests that σ will be purely real or purely imaginary. We saw in chapter 5 that this is not the case for the unstably stratified F-f-plane, and consideration of the isothermal F-f-plane dispersion relation shows that there are terms in σ which will allow for small, non-zero, frequency. We expect this to continue to be the case for the fully-spherical solutions. We find that the modes with large growth/decay rate have small frequency which is much smaller in magnitude than the growth/decay rates. For the smallest zonal wavelengths there is no obvious pattern to the frequencies of these modes.

It is also worth noting that the maximal growth/decay rates are usually found for prograde modes whilst there are a greater number of retrograde modes with non-zero growth/decay rate. This can be seen for $N_\rho = 2$ and zonal mode numbers $m = 1$ and $m = 10$ in figures 6.3 and 6.4. For larger zonal wave number the frequencies of

the unstable modes display a more obvious pattern. For zonal wave number $m = 100$ the largest growth/decay rates are found to be for prograde modes, and the frequencies display distinctive patterns. The pattern for zonal wavenumber $m = 500$ is shown in figure 6.9 where we have sorted the modes by growth/decay rate and displayed the 350 most rapidly growing modes. Note that the 350 most rapidly decaying modes display the same frequency pattern. The leftmost figure shows the growth rate and the rightmost figure shows the corresponding frequencies. Inspection of the eigenstructures suggests that in general the modes are grouped by latitudinal location of the mode and vertical mode number; so within a group of modes the mode with highest frequency is located at the equator and has the smallest growth rate, and the mode with smallest frequency has the fastest growth rate and is located at the pole. This is consistent with our expectations deduced through consideration of the approximated dispersion relation. The frequency of the mode located at the pole is smaller than machine precision therefore is likely to be zero.

The group of modes with largest growth rate has the smallest vertical mode number. The modes with frequency of the order $10^{-7}s^{-1}$, which are interspersed amongst the modes previously described, tend to have a very localised, high degree of latitudinal and vertical structure.

Once again the anelastic and pseudo-incompressible equation sets represent the growth/decay rates and frequencies of the most rapidly growing/decaying modes reasonably well whilst the Boussinesq and quasi-hydrostatic sets show considerably more misrepresentation. The pattern of misrepresentation with zonal, meridional and vertical wavenumber is difficult to ascertain as clearly there are many solutions with different permutations of these parameters. It seems that the misrepresentation of the maximum growth/decay rate increases and then decreases with increasing zonal wavenumber; this is similar to the patterns found when considering horizontal wavelength in the F-f-plane case. Graphical inspection of the approximated versions of the

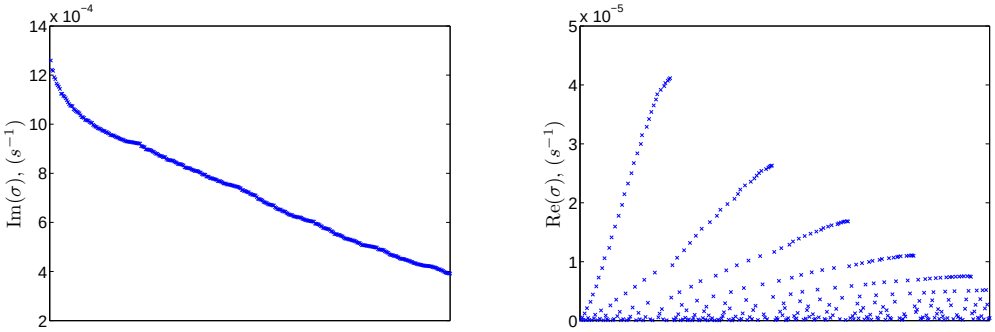

Figure 6.9: *σ for $m = 500$ sorted by imaginary component, 350 most rapidly growing modes. Leftmost figure displays the growth rate; rightmost figure displays the corresponding frequency.*

patterns shown in figure 6.9 suggests that the misrepresentation of frequency is largest for the fastest propagating modes within a group (those located at the equator). However, numerical analysis shows that this is simply due to the small magnitude of the frequencies of the faster travelling modes within a group; the misrepresentation remains relatively constant within a group, increasing and then decreasing slightly as the frequency increases. This suggests a slight increase and then decrease with latitudinal location of the mode. The graphical inspection shows that growth/decay rates are reasonably well represented by all sets with the exception of the quasi-hydrostatic set. The frequencies are well represented by the anelastic and pseudo-incompressible sets; however, the quasi-hydrostatic and Boussinesq sets show significant misrepresentation of the frequencies of many of the most rapidly growing/decaying modes with high zonal wavenumber. Figures 6.10 display this graphically for zonal wavenumber $m = 500$.

Table 6.1 shows the misrepresentation of the growth/decay rates of the most rapidly growing/decaying modes by the approximated equation sets for various zonal wavenumbers. Note that these growth/decay rates are generally of the order $10^{-4}s^{-1}$. Table 6.2 shows the misrepresentation of the frequencies of these modes, where the

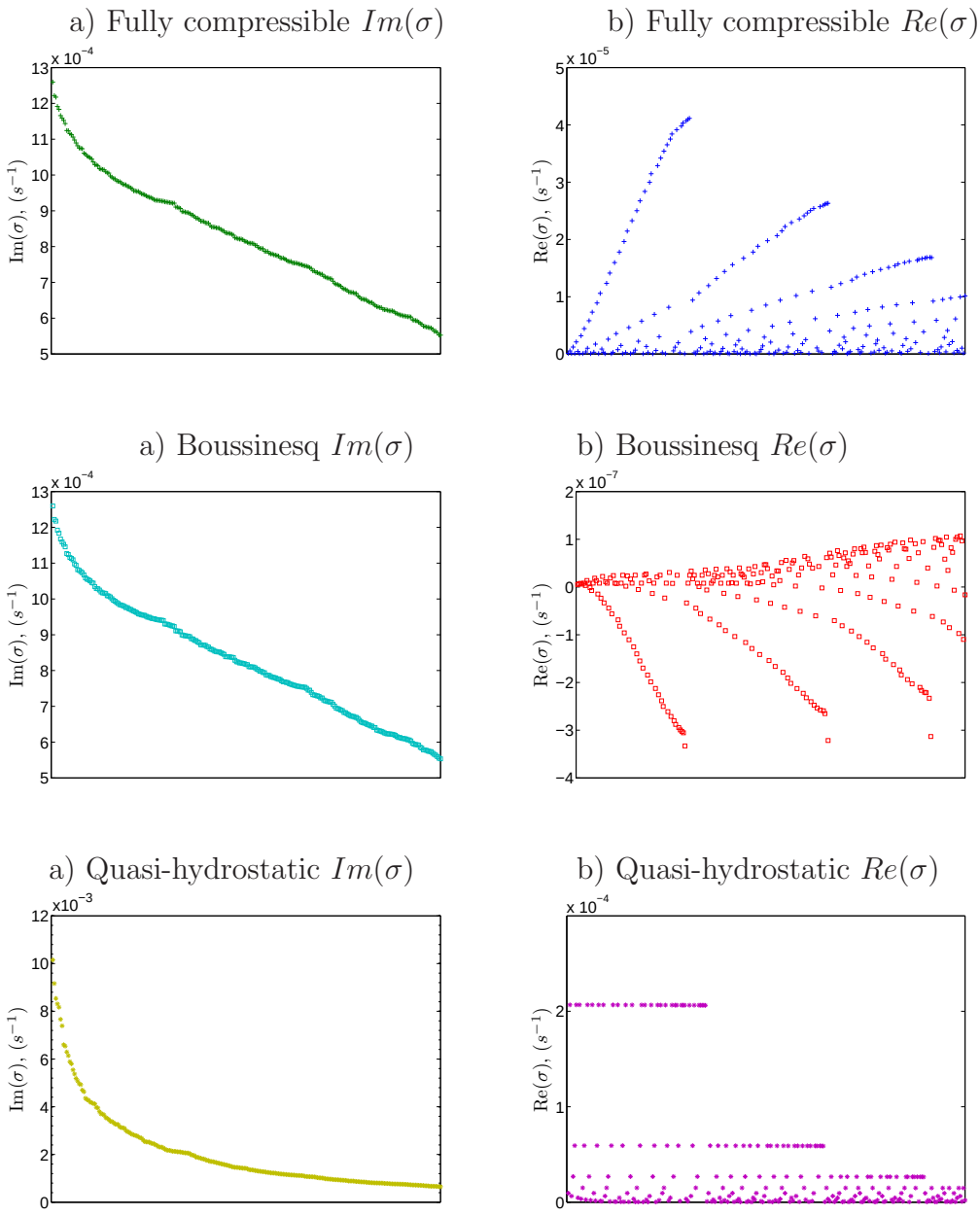

Figure 6.10: σ *for* $m = 500$ *sorted by imaginary component, 250 most rapidly growing modes.*

frequencies are generally of the order $10^{-6}s^{-1}$.

The number of zeros in the vertical and meridional structure of the unstable modes is not obvious from σ alone, but sorting σ by imaginary component and comparing σ for the various equation sets allows us insight into whether the vertical

Zonal Modenumber	m=1	m=2	m=10	m=30	m=100	m=500
Boussinesq	8.9%	10.1%	5.6%	1.3%	0.19%	0.01%
Quasi-Hydrostatic	1.6%	2.1%	35.0%	179.8%	∼700%	∼700%
EC Anelastic	0.11%	0.13%	0.18%	0.07%	0.01%	0.00%
NEC Anelastic	-0.15%	-0.16%	0.01%	0.03%	0.01%	0.00%
Pseudo-Incompressible	-0.41%	-0.45%	-0.16%	-0.01%	0.02%	0.00%

Table 6.1: *Percentage by which approximated equation sets misrepresent the growth/decay rates of the most rapidly growing/decaying modes.*

Zonal Modenumber	m=1	m=2	m=10	m=30	m=100	m=500
Boussinesq	-6.0%	8.3%	-38.2%	-78.7%	-90%	n/a
Quasi-Hydrostatic	4.7%	8.0%	82.8%	624.9%	∼6000%	∼8000%
EC Anelastic	-1.1%	-0.06%	-1.2%	-3.1%	-3.8%	-4.0%
NEC Anelastic	-1.2%	-0.42%	-0.45%	-1.5%	-1.8%	-2.0%
Pseudo-Incompressible	-1.2%	-0.78%	0.31%	0.13%	0.00%	0.00%

Table 6.2: *Percentage by which approximated equation sets misrepresent the frequencies of the most rapidly growing/decaying modes.*

and meridional wavenumber also affect the level of misrepresentation that is caused by the various approximated sets. The analysis shows that misrepresentation is not independent of meridional or vertical wavenumber; the relative misrepresentation by the various equation sets remains similar across the various horizontal and vertical wavenumbers, with the exception of the quasi-hydrostatic set which displays far more dependence on aspect ratio than the other sets.

Similarly to the F-f-plane case it is the frequencies of the unstable modes that are the most significantly misrepresented with the magnitude of the misrepresentations by the anelastic and pseudo-incompressible equation sets being similar to

those found in the F-f-plane geometry. In the Boussinesq and quasi-hydrostatic cases the misrepresentations at high zonal wavenumber are considerably larger than those found in the F-f-plane geometry. In the Boussinesq case the frequencies are often incorrectly represented. In the quasi-hydrostatic case the structures of several of the modes differ sufficiently from the fully compressible case that it is possible that they are spurious solutions. Since no such misrepresentations occurred in the F-f-plane geometry it is likely that these spurious results are artefacts of the poor resolution and computational method. This suggests that the optimal computational method for the quasi-hydrostatic set differs from that of the fully-compressible set, or that it requires considerably higher resolution.

Eigenstructures

Inspection of the eigenstructures shows that the unstable modes take two distinct forms; those with maximum vertical wavelength and varying meridional wavelength, and those with minimum meridional wavelength and varying vertical wavelength. As we expected, for all zonal wavenumbers the maximum growth/decay rate is found to be for the modes with maximum vertical wavelength and minimum meridional wavelength, and are located at the pole. For higher zonal wavenumbers the structure is shifted towards the lower density region near the outer surface. This is accurately reflected by all approximated equation sets. The second most rapidly growing/decaying modes have structure that differs with differing zonal wavenumber. For $N_\rho = 2$ and $m = 1$ the second most rapidly growing/decaying mode also has maximum vertical wavelength and minimum meridional wavelength dependent on the number of latitudinal grid points; however, the mode extends further towards the equatorial region than the most rapidly growing mode. For zonal mode number $m = 10$ the second most rapidly growing/decaying mode has minimum meridional wavelength and vertical wavenumber equal to 2. For zonal mode number $m = 100$ the second most rapidly

growing/decaying mode is located further from the pole but continues to have maximal vertical wavelength and extends further into the layer. The W structures of the most rapidly growing mode and second most rapidly growing mode for zonal mode numbers $m = 1$, $m = 10$ and $m = 100$ are shown in figure 6.11.

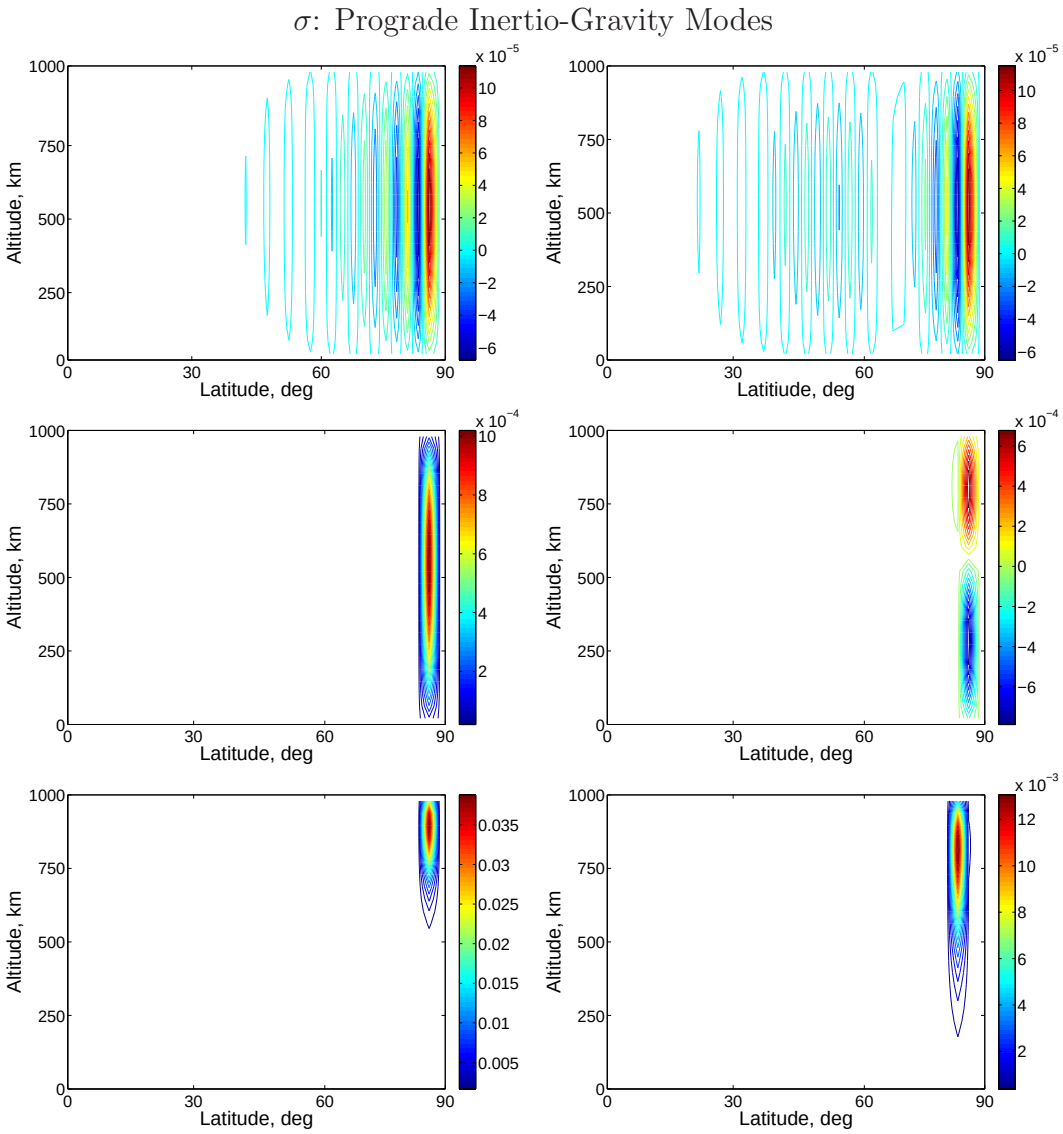

Figure 6.11: *W structure of most rapidly growing mode and second most rapidly growing mode for, from top to bottom, zonal mode numbers* $m = 1$, $m = 10$ *and* $m = 100$. *Leftmost figures show most rapidly growing mode, rightmost figures show second most rapidly growing mode.*

The pattern with which structure is related to the growth/decay rate and frequency is well reflected by all approximated equation sets with the exception of the quasi-hydrostatic set. As one might expect the quasi-hydrostatic set displays good replication of the fully compressible modes at small zonal wavenumber, but at large zonal wavenumber displays significant discrepancies. The W structure for the most rapidly growing modes of the fully-compressible, Boussinesq and quasi-hydrostatic sets for zonal wavenumbers $m = 1$ and $m = 100$ are displayed in figure 6.12. All other equation sets replicate these modes sufficiently well that there are no discernible differences from the fully compressible set. For zonal wavenumber $m = 100$ the quasi-hydrostatic set displays a significant lack of growth with height as well as a reduction in amplitude of all prognostic variables. The relative differences in amplitude between the prognostic variables also suggest a redistribution of energy across the variables, with a tendency for the contribution from pressure to become more dominant. In the Boussinesq case we see that for smaller zonal wavenumbers there are slight errors in the representation of the W structure, though in general it seems well represented. For higher zonal wavenumbers the modes seem more accurately represented, though close inspection reveals that there are slight relocations of modal zeroes. Once again we note that the representation of the structures by the Boussinesq sets would be significantly worsened if we were to apply the rescaling factors which return them to their unscaled form.

6.2.3 Small frequency and small growth/decay rate

The number of neutral solutions decreases with increasing zonal mode number, however there continue to be several solutions which exhibit growth/decay rates significantly smaller than the maximum growth/decay rates and comparable to or smaller than the frequency. In this section we discuss modes with frequency and growth/decay rate of the order $10^{-5}s^{-1}$ or smaller, these are likely to be neutral and slowly grow-

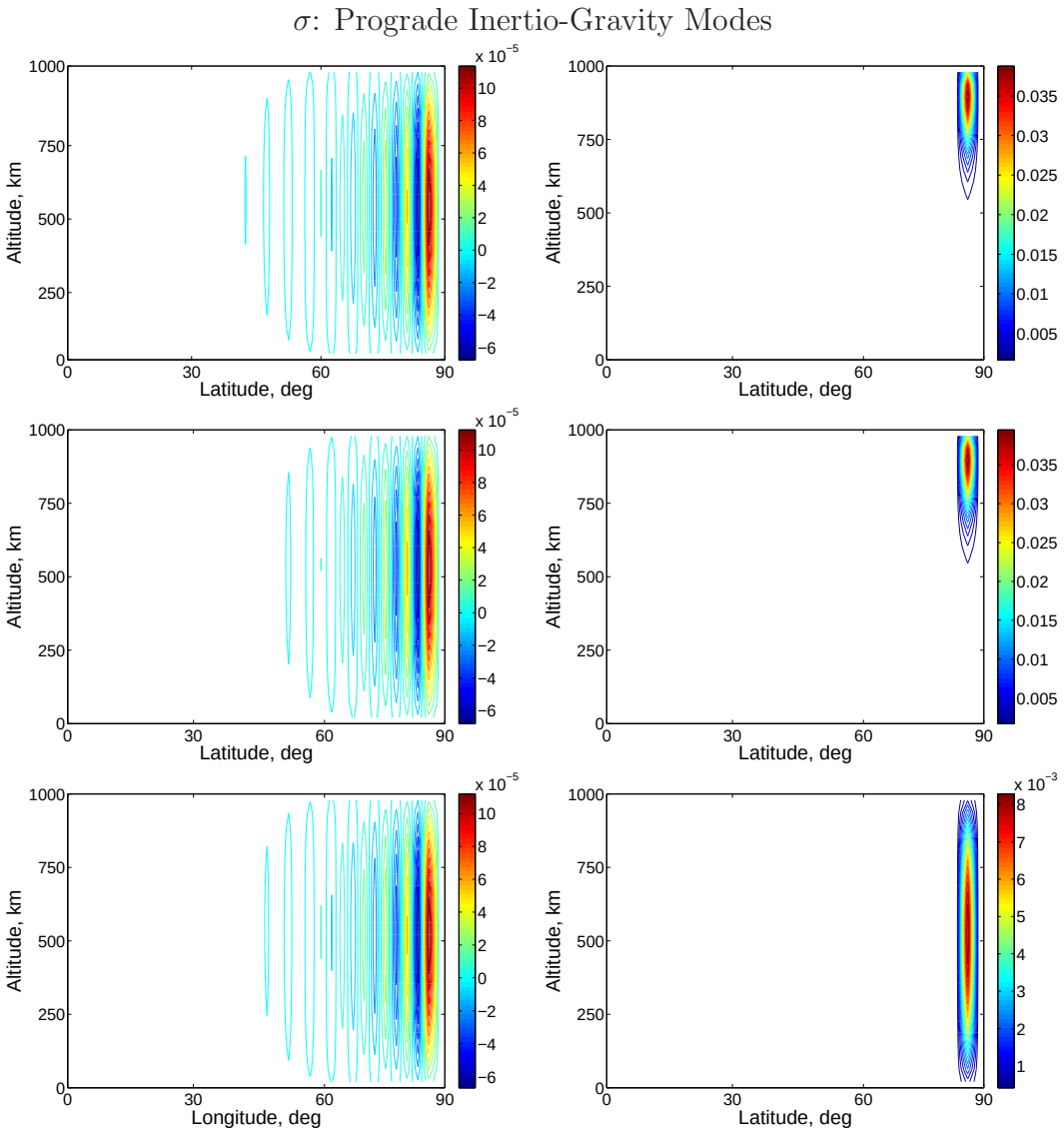

Figure 6.12: $\hat{W}$ *structure of most rapidly growing mode and second most rapidly growing mode for zonal mode numbers* $m = 1$ *and* $m = 100$*. Leftmost figures display* $m = 1$ *modes, rightmost figures display* $m = 100$ *modes; from top to bottom fully compressible, Boussinesq and quasi-hydrostatic sets.*

ing/decaying Rossby modes.

Rossby modes owe their existence to the latitudinal variation of the rotation of the model, thus are degenerate in the F-f-plane analysis. The dependence on latitudinal variation means it is useful to introduce the quantity $\beta = 2\Omega \cos\phi / r_s$

which reflects the gradient of planetary vorticity; in the regime we are considering β is of the order 10^{-12}. The Rossby number describes the relative importance of inertial and coriolis forces and is given by

$$\mathcal{R}_\wr = \frac{U_h}{fL_h}, \tag{6.12}$$

where U_h and L_h represent the characteristic horizontal velocity and lengthscales and $f = 2\Omega \sin\phi$. A large Rossby number indicates that the inertial and centrifugal forces are the dominant forces in a system, whereas a small Rossby number indicates that the Coriolis and pressures forces dominate. In direct contrast with convectively unstable inertio-gravity waves Rossby waves generally have much larger horizontal scales than vertical scales. These modes are then also of huge importance when studying Jovian jets, where $\mathcal{R}_\wr \approx 0.02$ (Vasavada & Showman, 2005 [62]). The eventual accurate modelling of a Jovian regime will likely rely on an equation set which is able to represent both convective inertio-gravity waves and Rossby waves with a strong degree of accuracy.

$$\sigma_{Rossby} \approx -\frac{\beta k_x}{k^2 + 1/\lambda^2}, \tag{6.13}$$

where $k^2 = k_x^2 + k_y^2$ and λ is the deformation radius. We would therefore expect Rossby modes to be neutral, propagate in one direction only and have a wide range of frequencies dependent on the depth of the layer. The propagation of convective columns, latitudinal variation of N^2 and vortex stretching mechanisms can also result in modes analagous to classical Rossby waves. This type of mode requires inclusion of N^2 and $\sigma_{Inertio\,gravity}$ within the dispersion relation and can be approximated as

$$\sigma_{Vortex\ stretching} \approx -\frac{\beta N^2 k_x}{k^2 \sigma^2_{Inertio\,gravity}}. \tag{6.14}$$

We have shown in the previous section that $\sigma_{Inertio\,gravity}$ is not necessarily purely real or purely imaginary, and does not have definite sign. Therefore, the inclusion of this term in the dispersion relation suggests that we may find unstable Rossby modes, which may propagate in either direction.

Through consideration of equation 6.13 one would expect these modes to be stable with the modes with largest frequency having extrememly long horizontal wavelength.

It is difficult to fully assess the accuracy of the representation of the modes with smallest frequency and smallest growth/decay rate as many seem to display sufficiently large misrepresentations that it is impossible to compare individual modes from the various approximated sets using σ alone. All sets display modes which have σ comparable to those of the fully-compressible set, though they also display modes in which σ differs enormously. Consideration of the eigenstructures allows us to confirm whether modes, identified through inspection of σ, are comparable.

As an example we present a mode with zonal wavenumber $m = 10$ which has both frequency and growth/decay rate of the order $10^{-5}s^{-1}$. This mode is one of a pair whose values of σ are almost complex conjugate pairs. In this case the quasi-hydrostatic set represents the growth/decay rate to within 1% of the fully compressible rate; however the frequency is strongly underestimated at only 55% of the fully compressible value. The Boussinesq and non-energy-conserving anelastic sets display more dramatic misrepresentation: the Boussinesq set underestimates the growth/decay rate by almost 11% and underestimates the frequency by 90%; and the non-energy-conserving anelastic set underestimates the growth/decay rate by 13% and underestimates the frequency by 80%. In contrast the other approximated equation sets misrepresent $Im(\sigma)$ more dramatically than the quasi-hydrostatic set, but represent frequency much more accurately: the energy-conserving anelastic set underestimates the frequency by 35%, however the growth/decay rate is underestimated by 29%; and the pseudo-incompressible set displays a 6.5% underestimation of the growth/decay rate and a 17.5% underestimation of the frequency. These errors are reasonably representative of the errors displayed for other unstable modes with $Re(\sigma)$ and $Im(\sigma)$ of similar magnitude though it is possible to find examples for all

sets where the misrepresentations are less obvious, less severe, or much more severe. The errors are also similar at higher zonal wavenumbers. Increasing the number of density scale heights across the layer tends to slightly increase the level of misrepresentation though the pattern across the various approximated sets remains similar. The pseudo-incompressible set seems to represent these modes most accurately and consistently across all zonal wave numbers and density scale heights, and seems to produce the least number of spurious solutions.

The misrepresentation of the frequencies of the neutral Rossby modes with small frequency is generally less severe than for the unstable modes, and the differences between the approximated equation sets are less obvious.

Eigenstructures

It is difficult to ascertain the level of misrepresentation of the eigenstructures of these modes as in order to identify comparable modes it is necessary to ensure that the modes have reasonably similar eigenstructures. There exist cases where the frequency and growth/decay rates of modes for an approximated and fully compressible set are similar, however the eigenstructures are considerably different. In this scenario the small magnitude of the differences between the frequencies and growth/decay rates of modes with differing wavenumbers, and coarse resolution of the vertical and latitudinal grid, mean that it is not possible to identify the modes correctly. It is therefore not possible to conclude whether they represent the same mode and have poor representation of the eigenstructures, or represent different modes and have poor representation of σ such that comparison of σ alone leads one to believe otherwise. Consideration of the types of misrepresentation of modes in which the identification of the mode is more obvious suggest that the latter case is more likely; this naturally leads to the conclusion that the misrepresentation of σ is highly dependent on zonal, vertical and meridional wavenumber thus is not easily predictable across the various

equation sets, particularly when $|\sigma|$ is small. For all cases considered, the modes with small $|\sigma|$ have a high degree of structure.

The eigenstructures of the representative mode, for which σ has been discussed, display similar types of misrepresentation to those discussed for other mode types. As previously mentioned it is only possible to compare modes with similar eigenstructures, therefore the replication of the overall structure of the mode is reasonable for all approximated sets. In all cases there are slight shifts in the positioning of modal zeroes, and small redistributions of energy visible through differences in the relative amplitudes of the prognostic variables. The quasi-hydrostatic set displays the least misrepresentation with only a very slight shift in placement of modal zeroes and small redistribution of energy observed through increased max/min amplitude of $\hat{P}$ and decreased max/min amplitude of other prognostic variables. In the Boussinesq case the representation of the eigenstructures, prior to the re-scaling that returns the variables to their unscaled forms, is reasonable; as is the case for other types of mode, the application of the rescaling factor means that the eigenstructures become significantly misrepresented.

The lack of latitudinal variation on an F-f-plane means that the Rossby modes are degenerate, therefore we have no unstable results for comparision with solutions calculated in a spherical geometry. The fact that many of the modes have growth/decay rate of comparable order to the frequency, and a high degree of structure, leads us to believe that the representation of these modes is more likely to be similar to the unstable inertio-gravity modes than the neutral modes.

6.3 Antisymmetric Modes

With the exception of the obvious change to equatorial symmetry, the antisymmetric solutions display similar frequencies, growth/decay rates and structures to those of the

symmetric solutions. The types of misrepresentation of solutions for the approximated equation sets are similar to those of the symmetric solutions and there appears to be no evidence that symmetry alone should have any influence on the accuracy of the various approximated equation sets. We do note however that many groups have shown that in the Boussinesq case equatorially symmetric modes are preferred at the onset of convection with critical Rayleigh number found to be reduced. Jones et al. (submitted 2008 [38]) have indicated that this continues to be the case for the onset of anelastic convection at various density scale factors. Our analysis of the approximated equation sets relative to the fully compressible set suggests that the representation of normal modes by the anelastic sets is sufficiently accurate that if the anelastic sets prefer symmetric modes at the onset of convection it is likely that this is also the case for the fully-compressible equation set. If this preference continues away from onset then the misrepresentation of the unstable symmetric and antisymmetric modes by the approximated equation sets may differ due to the magnitude of the instability rather than an inherent difference in misrepresentation according to symmetry.

6.4 Deep Polytropic Layer

Poor resolution due to computational limitations means that we are unable to consider a deep layer in the spherical geometry. Consideration of solutions found in the shallower case leads us to believe that the misrepresentations of frequencies, growth/decay rates and structures will be more dramatic in a deeper layer. A limited comparison of misrepresentation of modes for a layer of depth 100km with the misrepresentations found for a layer of depth 1000km supports this view, with the misrepresentations being more evident for the deeper layer. This is particularly true for the quasi-hydrostatic set. In the fully spherical regime the zonal and meridional wavenumbers

have influence on the amount by which the modes are misrepresented; it is important to remember that for a deeper layer and specified zonal and meridional wavenumbers the ratio of horizontal to vertical wavenumber will be different to that of a shallower layer, therefore, it is unlikely that maximum misrepresentations will be found at the same zonal mode numbers as those of the shallower layers.

6.5 Numerical Accuracy

The structures of the modes with largest growth/decay rate are more localised than one would expect, and significantly more localised than those found for a polytropic F-f-plane. There is no obvious physical reason for this degree of localisation, which suggests that the accuracy of their representation is limited by the limited grid resolution. Computational demands mean that we are unable to increase resolution to test whether the eigenvectors, or entire modes, are accurate, artefacts of computational error or poor representations of physical solutions. Consideration of the NAG routine used to calculate the solutions suggests that for situations in which a large number of iterations are required to reduce the matrix A to triangular form a greater reliance can be placed on the accuracy with which the eigenfrequencies are calculated than can be placed on the accuracy of the eigenvectors and, with the exception of the Boussinesq and quasi-hydrostatic sets, the frequencies and growth/decay rates are not disimilar to those found on an F-f-plane. We expect the misrepresentation of the Boussinesq and quasi-hydrostatic modes through consideration of the scale analysis, therefore it seems reasonable to assume that the frequencies of the modes are physically acceptable and the misrepresentations by the approximated sets provide an indication towards the representation that could be expected from a better resolved system. It is also worth noting that the neutral modes, and those calculated as test solutions for stably stratified sets display far less localisation, and are largely as we would expect.

This suggests there may be an inefficiency in the computational method when considering unstable modes within a spherical geometry. The poor resolution also means that such a coordinate system may result in a situation in which there is not enough resolution in the appropriate regions to capture the existence of Taylor columns. In chapter 7 we consider an alternative method, which does not allow for comparison with a fully compressible set but the use of the anelastic approximation means that we expect these modes to be physically realistic at the onset of convection. This method is computationally far less demanding than the inversion of large matrices, therefore we expect errors due to computational resolution to be dramatically reduced.

6.6 Summary

In this chapter we have considered solutions within a spherical shell geometry with unstably stratified reference state. Coarse grid resolution has limited the analysis to a layer of depth $1000km$ which is considerably shallower than many models used in modelling Jovian dynamics. However, comparison of results for spherical shells with layer depths equal to 100km and 1000km, each with the same number of density scale heights across the layer, leads us to believe that the misrepresentations of modes by the approximated equation sets will be more severe for a deeper layer than a shallower one. In this context our results might be used as a 'best-case' scenario, particularly for the quasi-hydrostatic set in which it has clearly been demonstrated that the ratio of horizontal to vertical scales is crucial.

The variation in misrepresentation of modes with meridional wavenumber has also been limited by coarse resolution, though we have considered various zonal wavenumbers up to $m = 500$ and suggest this should also provide some indication as to how misrepresentation varies with meridional wavenumber. We have considered two density profiles, one with 2 density scale heights across the layer, and one with 5

density scale heights across the layer; there are therefore several grid points per density scale height. Computational resolution limits the accuracy with which the modes are calculated, however inspection of the misrepresentations calculated for various grid resolutions suggests that it is sufficient to determine the amount by which the approximated equation sets misrepresent the fully-compressible set.

As in the analytic analysis of an isothermal reference state, and the analysis of a polytropic F-f-plane, we found that all approximated equation sets filter the internal acoustic modes. Setting the switches between zero and one allowed us to see that as the switches approach zero the frequencies of the acoustic modes, calculated by the switch combinations appropriate to the approximated equation sets, approach infinity; however, the way in which frequencies vary with wavenumber remains relatively stable. The quasi-hydrostatic set continues to calculate solutions for the external acoustic modes, and as in the F-f-plane case, the misrepresentation of the modes depends primarily on the ratio of horizontal to vertical scales, as well as being affected by the reference state profile. The misrepresentation is largest when the ratio of horizontal to vertical scales is small and N^2 is increased.

There are four distinct types of internal mode solutions; a) Neutral modes with large frequency, b) Neutral modes with small frequency, c) Unstable modes with large growth/decay rate, d) Unstable modes with small growth/decay rate. The frequencies of the fully-compressible modes largely reflected our expectations through consideration of approximated dispersion relations. The misrepresentations of the frequencies by the approximated equation sets were similar to those found on an unstably stratified F-f-plane.

The representation of the shallow gravity waves was found to be reasonable by all sets, with increased magnitude of N^2 increasing the misrepresentation. The pseudo-incompressible and non-energy-conserving anelastic sets were found to replicate the frequencies of these modes most accurately with both frequency and eigen-

structure well represented. The energy-conserving anelastic set displayed more significant misrepresentation of frequency but also replicated the eigenstructures well. The Boussinesq set strongly replicated the eigenstructures of the modes for reference state with 2 density scale heights across the layer; however, for $N_\rho = 5$ the Boussinesq modes displayed some spurious relocation of vertical modal zeroes. The replication by the Boussinesq set would be significantly weaker if the variables were returned to their unscaled form. The quasi-hydrostatic set displayed good replication of the eigenstructures of the modes for reference state with $N_\rho = 2$; however for $N_\rho = 5$ the amplitudes of the structures of horizontal velocity were found to be significantly reduced which in turn points to redistribution of energy across the prognostic variables. For zonal wavenumbers less than 10 we found modes with large frequency and small, non-zero, growth/decay rate. The misrepresentation of the frequencies and eigenstructures of these modes were found to be similar to those of the neutral modes. The representation of the growth/decay rates were found to vary dramatically with no obvious pattern to the misrepresentation. The anelastic, quasi-hydrostatic and pseudo-incompressible sets were found to replicate the patterns with which the growth/decay rates varied with meridional and vertical wavenumber; however the actual growth/decay rates were occasionally severely misrepresented. The Boussinesq set failed to replicate the pattern with which the growth/decay rates varied. We suggested that these small growth/decay rates could in fact be spurious artefacts of poor resolution, but note that their replication by most sets indicates that the optimal computational methods and grids are likely to be similar for each equation set.

Similarly to the results from analysis of an F-f-plane we found that the misrepresentations of the convectively unstable modes are more severe than the misrepresentations of the neutral modes. In particular the frequencies of the unstable modes are most significantly misrepresented with the Boussinesq and quasi-hydrostatic sets displaying dramatic misrepresentation at high zonal wavenumbers. The representa-

tion of the frequencies of these modes by the anelastic and pseudo-incompressible sets are considerably more accurate, with the relative accuracy of these sets differing with differing mode structure but in general the pseudo-incompressible set displays the most accurate representations. The representation of the growth/decay rates is significantly more accurate by all sets though the quasi-hydrostatic set displays considerable inaccuracies at higher zonal wavenumber, as well as calculating a number of spurious solutions. The eigenstructures are reasonably well represented by all sets with the exception of the quasi-hydrostatic set, which displays extreme misrepresentation including redistribution of energy, adjustment of modal amplitude and differing growth with height to the fully compressible sets. The Boussinesq set displays slight adjustments to the positioning of modal zeroes but the modal amplitudes seem well represented. We note that it is more difficult to ascertain the differences between the sets in a spherical geometry as it is not possible to separate the vertical and latitudinal structure.

Unlike in the case of the F-f-plane the Rossby modes are not degenerate, we find several solutions which have small frequency and comparable growth/decay rate. The representation of these modes is difficult to ascertain as the number of modes and small magnitude of σ means that identification of the modes cannot be through σ alone. Consideration of the eigenstructures shows that there are modes which have similar structures and large discrepancies between the frequencies and growth/decay rates. There are also modes which have relatively similar frequencies and growth/decay rates but vastly differing structures. Finally there are modes which seem to display no similarities to the fully compressible solutions, these modes are most obvious for the quasi-hydrostatic and Boussinesq sets. The levels of misrepresentation of these modes by the approximated sets are more extreme than other modes, particularly by the anelastic and pseudo-incompressible sets. The pseudo-incompressible set represents these modes most accurately and most consistently

across varying zonal wavenumbers.

In general the misrepresentations of the modes in the spherical geometry seem to be similar to those seen on an F-f-plane with the same reference state profile. Whilst the spherical geometry clearly has significant impact on the normal mode solutions it seems to have little effect on the accuracy with which the approximated equation sets replicate the fully-compressible solutions.

Chapter 7

Onset of compressible convection

Within this chapter we consider the linear theory of the onset of compressible convection within a regime appropriate to the interior and interior atmosphere of Jupiter. The analysis within this chapter differs from that of previous chapters in that it does not compare solutions with those of a fully-compressible set. Instead it seeks to identify key differences between the traditional Boussinesq models, which are essentially incompressible, and the use of an anelastic set which allows the introduction of a degree of compressibility. The method of analysis is not well suited to equation sets in which the mass continuity equation has not been significantly simplified, thus it is not possible to consider the fully-compressible equation set.

As we have discussed in previous chapters, the Boussinesq theory of the onset of rapidly rotating incompressible convection for a uniform density reference state is now fairly well understood, but the rapidly rotating compressible case has received much less attention. The compressible problem is however more relevant to the problem of rapidly rotating convection within the Jovian regime where convection occurs over many scale heights of density (Guillot, 1999a,b [33]).

The asymptotic theory of the onset of rapidly rotating convection in a Boussi-

nesq sphere with uniform density reference state was developed by Roberts (1968 [50]) and Busse (1970 [11]). These papers established the local theory of convection. However, although this local theory has many points of contact with experiments and numerical calculations, and forms a useful simple picture of rotating convection, it became clear that the predicted critical Rayleigh numbers were incorrect except at very large Prandtl number. This problem was resolved with the development of the global theory of convection by Jones et al., (2000 [40]) and Dormy et al., (2004 [19]). In this chapter we extend the asymptotic theory to the compressible case.

Much of this work has been undertaken in collaboration with Professor Chris Jones and Dr Kirill Kuzanyan of Leeds University. The asymptotic results discussed here, and results from their numerical eigenvalue code for the full anelastic equations have been recently been accepted for publication in the Journal of Fluid Mechanics (Jones et al., submitted 2008). For the avoidance of confusion with the results in previous chapters and consistency with Jones et al., (submitted 2008 [38]), hereon, we refer to the components of velocity with subscripts denoting their direction, e.g $\boldsymbol{u}(s,\phi,z) = u_s\hat{\boldsymbol{s}} + u_\phi\hat{\boldsymbol{\phi}} + u_z\hat{\boldsymbol{z}}$.

7.1 Governing equations

The geometry of the problem matches that of the spherical regime described in chapter 2, with a spherical shell lying between $r = r_C$ and $r = r_S$ and the effective mass M_0 being entirely within the shell. The gravitational field then falls off as $1/r^2$ within the shell and we assume a hydrostatic polytropic reference state as defined in chapter 2,

$$\frac{dp}{dr} = -\frac{GM\rho}{r^2}, \quad \frac{p}{p_0} = \left(\frac{\rho}{\rho_0}\right)^{1+1/n}. \tag{7.1}$$

where, for consistency with studies undertaken by other groups, we define ρ_0 and p_0 to be the reference values of pressure and density at the midpoint of the layer and again

assume the perfect gas law as our equation of state. For comparison with studies of the onset of convection in an incompressible Boussinesq regime we nondimensionalise using the length unit equal to the layer depth $d = r_S - r_C$; hereon, r refers to the dimensionless radial coordinate and $\eta = r_c/r_S$ the ratio of inner to outer radius. The solution of these equations is then written in the form (Gilman & Glatzmaier, 1981 [31])

$$\rho = \rho_0 \left(\frac{GM_0\rho_0}{rp_0(n+1)d} + c_0 \right)^n = \rho_0 \zeta^n, \quad \zeta = \frac{c_1}{r} + c_0, \quad c_1 = \frac{GM_0\rho_0}{p_0(n+1)d}, \tag{7.2}$$

$$p = p_0\zeta^{n+1}, \quad T = T_0\zeta. \tag{7.3}$$

It is clear that at the midpoint of the layer, where ρ, p and T have their reference values, $\zeta = 1$. Once again assuming the polytrope has N_ρ density scale heights, where $N_\rho = \ln(\rho_C/\rho_S)$, we have

$$\zeta_0 = \frac{\eta + 1}{\eta \exp(N_\rho/n) + 1}, \quad c_0 = \frac{2\zeta_0 - \eta - 1}{1 - \eta}, \quad c_1 = \frac{(1+\eta)(1-\zeta_0)}{(1-\eta)^2}, \tag{7.4}$$

where ζ_0 is the value of ζ at the outer surface. Non-dimensionalisation ensures that the dimensionless polytrope is completely determined once n, η and N_ρ are specified. Note that dimensionless r satisfies

$$r_C = \frac{\eta}{1-\eta} < r < r_S = \frac{1}{1-\eta}. \tag{7.5}$$

For straightforward comparison with the results of groups such as Drew et al., (1995), Gilman & Glatzmaier (1981) and Braginsky & Roberts (1995) it is convenient to utilise the entropy form of the governing equations rather than the potential temperature as used in previous chapters. We saw in chapter 2 that the entropy of a perfect gas can be given by

$$s = C_p \left(\frac{1}{\gamma} \ln p - \ln \rho \right), \tag{7.6}$$

and recall that the anelastic approximation requires that the perturbations to the thermodynamic variables are small compared with their reference state values. We therefore find that the entropy perturbation is given by

$$S' = \frac{C_p}{\gamma}\left(\frac{p'}{p_s} - \gamma\frac{\rho'}{\rho_s}\right). \tag{7.7}$$

We note that in this chapter entropy is represented using a capitalised S in order to avoid confusion with the cyclindrical coordinate system which utilises the direction vector $\hat{\boldsymbol{s}}$.

Consideration of the vertical momentum equation (2.27), alongside the use of (7.7) and the equation of hydrostatic balance which governs the reference state (2.19), allows us to rewrite the pressure and bouyancy terms such that

$$-\frac{1}{\rho_s}\nabla p' + \boldsymbol{g}\frac{\rho'}{\rho_s} = -\nabla\left(\frac{p'}{\rho_s}\right) - \boldsymbol{g}\frac{S'}{C_p} + \frac{p'}{\rho_s}\left(\frac{1}{\gamma p_s}\frac{dp_s}{dr} - \frac{1}{\rho_s}\frac{d\rho_s}{dr}\right)\hat{\boldsymbol{r}}. \tag{7.8}$$

If $\gamma = 1 + 1/n$ the system is adiabatic, using (7.2) and (7.3) the bracketed term on the right hand side is zero. Thus, if it is assumed that the reference state is only marginally superadiabatic and γ is close to this value it is reasonable to assume that the term in the brackets can be neglected. Therefore,

$$-\frac{1}{\rho_s}\nabla p' + \boldsymbol{g}\frac{\rho'}{\rho_s} \approx -\nabla\left(\frac{p'}{\rho_s}\right) - \boldsymbol{g}\frac{S'}{C_p}. \tag{7.9}$$

A fuller discussion of this assumption can be found in section (4.2) of Braginsky & Roberts (1995 [9]). This allows the non-linear anelastic momentum equation to be written

$$\frac{\partial\,\boldsymbol{u}}{\partial t} = \boldsymbol{u}\times\boldsymbol{\omega} - 2\Omega\times\boldsymbol{u} - \nabla\left(\frac{p'}{\rho_s} + \frac{1}{2}\,\boldsymbol{u}^2\right) + \frac{\boldsymbol{F}}{\rho} - \boldsymbol{g}\frac{S'}{C_p}, \tag{7.10}$$

where $\boldsymbol{\omega} = \nabla\times\boldsymbol{u}$ is the vorticity and $\boldsymbol{F}$ is as given in (2.35). The great advantage of this representation, and indeed of the Boussinesq equivalent, is that when the curl and double curl is taken, the only thermodynamic convective variable left is the entropy. Consequently there is no necessity to solve a separate Poisson equation for the pressure perturbation, which would be required to evaluate ρ'. Since it is

often assumed that the efficiency of convection within the Jovian interior and interior atmosphere means that it is close to adiabatic, the simplification of the buoyancy terms through use of the anelastic approximation is likely to be progress compared with the use of a constant density reference state. It is also worth noting that, as mentioned in chapter 2 and proved later in this chapter, there can be no convective motions if the reference atmosphere is an exact polytrope; therefore, the departure from adiabatic must be small but non-zero.

The mass continuity equation has the anelastic form

$$\nabla.(\rho_s \boldsymbol{u}) = 0, \tag{7.11}$$

where a more detailed derivation is given in section 3.2.

We recall that potential temperature is related to entropy through the simple relationship $S = C_p \ln(\theta) + \text{constant}$ and use this to rewrite the nonlinear thermodynamic equation (2.15) in entropy form

$$\rho T \left(\frac{\partial S}{\partial t} + \boldsymbol{u} \,.\nabla S \right) = \nabla.\rho C_p k \nabla T + \Phi. \tag{7.12}$$

The linearised form of this equation was used in the previous studies of linear compressible convection, Gilman & Glatzmaier (1981 [31]) and Drew et al., (1995 [22]). However, in planets and stars it is thought that the turbulent convection will give rise to a diffusion of entropy which will normally be much larger than the molecular conductivity term. It is also the case that, in compressible flow, turbulent elements preserve their entropy, not their temperature, when the conductivity is small. Prandtl's mixing length ideas suggest that turbulent elements will move a certain distance and then release their entropy content into their surroundings. This suggests that the turbulent entropy flux is proportional to the entropy gradient, not the temperature gradient. While in traditionally studied incompressible Boussinesq convection, eddy thermal diffusion can take a similar form to the molecular thermal diffusion but with a much larger diffusivity, in compressible flow this is no longer the case. This was recog-

nised by Gilman & Glatzmaier (1981), who included a diffusive flux proportional to potential temperature rather than actual temperature. There is no universally agreed theory as to how turbulent diffusivity should be modelled, however the suggestion by Drew et al., (1995) that the diffusion of temperature allows convective motions for negative Rayleigh number suggests that modelling of turbulent diffusion is crucial in elminating these modes. The model used here was developed by Braginsky & Roberts (1995) in the context of the Earth's core convection and was used in the stellar convection context by Clune et al., (1999 [15]). The essential assumption is that there is a turbulent velocity $\boldsymbol{u}^t$ which gives rise to a turbulent entropy fluctuation s^t, and that these can be averaged over a short length-scale so that $\overline{\boldsymbol{u}^t} = \overline{s^t} = 0$, but $\overline{\rho\, \boldsymbol{u}^t\, s^t} = \boldsymbol{I}^t$, a non-zero entropy flux. As mentioned in section 2.5 it is widely accepted that the form of diffusive entropy flux can take the form

$$\boldsymbol{I}^t = -\rho\mathcal{K}\nabla S, \tag{7.13}$$

where $\mathcal{K}$ is the eddy diffusivity. The most general form of the turbulent entropy flux is given by

$$I_i^t = -\rho\mathcal{K}_{ij}\frac{\partial S_s}{\partial x_j} \tag{7.14}$$

where $\mathcal{K}_{ij}$ is an anisotropic eddy diffusivity. This argument relies on the effect of turbulence being local, so the correlation length of the turbulence must be much less than any radius of curvature length of the entropy profile S_s. Furthermore, as pointed out by Braginsky & Roberts (1995), it is not clear that the isotropic form $\mathcal{K}_{ij} = \mathcal{K}\delta_{ij}$ is always appropriate in a rotating system, but one might hope that if the unresolved turbulent velocity has sufficiently small length and time scale, it will be unaffected by the rotation. We choose to consider the isotropic form (7.13) as it has been the most popular choice in simulations.

Just as molecular diffusion gives a source term creating entropy, so turbulent diffusion also gives rise to a source term, this is modelled such that it appears in the entropy equation only as a divergence, so there is no source of energy arising from the

turbulence, only a source of entropy, consistent with the first law of thermodynamics. The entropy equation is then

$$\rho T\left(\frac{\partial S}{\partial t}+\boldsymbol{u}.\nabla S\right)=\nabla.\rho T\mathcal{K}\nabla S+\nabla.\rho C_p k\nabla T+\Phi, \tag{7.15}$$

where the factors of T allow the thermodynamic equation to be written in energy conserving form. Consistency with the second law requires that the entropy source term is positive, which requires that $\nabla S.\nabla T\geq 0$. Since the layer we are considering is unstably stratified, this will normally be the case. We choose to take the opposite extreme from that taken in Drew et al., (1995) and ignore the molecular k in comparison with the turbulent $\mathcal{K}$. We can always add an arbitrary constant to entropy so we can take the entropy as zero at $r=r_S$ and equal to the entropy drop across the layer $\Delta S=S(r_C)-S(r_S)$ at $r=r_C$.

In modelling the Jovian regime it is helpful to be able to compare results with laboratory experiments in which similar flow patterns are observed. Similar flow patterns can be replicated utilising different parameter regimes and it is useful to be able to refer to a 'type of flow'. The type of flow is reliant on the coupling between parameters rather than the specific values of the parameters, thus is is sensible to non-dimensionalise the equation sets in order to allow simpler examination of the possible parameter regimes, this also has the advantage of meaning that some of the uncertainty surrounding the values of the specific parameters can be accounted for.

We non-dimensionalise our equations using the length scale d, timescale d^2/ν where ν is the constant kinematic eddy viscosity, mass $\rho_0 d^3$, unit of entropy $\mathcal{P}\Delta S$ where Prandtl number $\mathcal{P}=\nu/\mathcal{K}$, $\mathcal{K}$ being the constant entropy diffusion coefficient, and ΔS being the entropy drop across the layer, so the dimensionless entropy S satisfies the boundary conditions

$$S=0\,\text{at}\,r=r_S,\quad S=\mathcal{P}^{-1}\,\text{at}\,r=r_C. \tag{7.16}$$

The six dimensionless parameters that govern anelastic compressible convection are

$$\mathcal{R}a = \frac{GMd\Delta S}{\nu\mathcal{K}C_p}, \quad \mathcal{P} = \frac{\nu}{\mathcal{K}}, \quad \mathcal{E} = \frac{\nu}{\Omega d^2}$$

$$N_\rho = \ln\left(\frac{\rho(r_C)}{\rho(r_S)}\right), \quad n, \quad \eta = \frac{r_C}{r_S}, \tag{7.17}$$

where $\mathcal{R}a$ is the Rayleigh number and $\mathcal{E}$ the Ekman number.

As in previous chapters, we consider a motionless, time independent reference state about which to linearise our governing equations and assume that perturbation quantities are small. The non-dimensional basic state entropy S_s is determined by the nonlinear entropy equation (7.15) together with the boundary conditions (7.16). Since we are neglecting molecular diffusion we then use (7.2) and (7.3) to give

$$\frac{1}{r^2}\frac{d}{dr}r^2\zeta^{n+1}\frac{dS_s}{dr} = 0. \tag{7.18}$$

The dimensionless solution is then

$$S_s = \frac{\mathcal{P}^{-1}(\zeta_0^{-n} - \zeta^{-n})}{\zeta_0^{-n} - \zeta_C^{-n}}, \tag{7.19}$$

where

$$\zeta_C = c_0 + \frac{c_1}{r_C}, \quad \zeta_0 = c_0 + \frac{c_1}{r_0}. \tag{7.20}$$

It may seem surprising to use the turbulent governing equation to determine the reference state profile as the static reference state can clearly not be turbulent. However, we view the linear theory as the small amplitude limit of the non-linear problem, and even at very low amplitudes turbulent diffusion will dominate molecular diffusion, and so the state described by (7.19) will be approached as the Rayleigh number is reduced towards critical. Ultimately, as the amplitude falls further, convection will be so slow that the turbulent diffusion will fall below even the molecular diffusion and a new reference state determined by (7.15) with molecular diffusion only will be approached. We do not consider such extremely small amplitude convection here, as we are primarily interested in the limit $\mathcal{R}a \to \mathcal{R}a_{crit}$ from above.

Non-dimensionalising and linearising (7.15) then yields

$$\mathcal{P}\frac{\partial S'}{\partial t} = -\mathcal{P}\,\boldsymbol{u}\,.\nabla S_s + \zeta^{-n-1}\nabla.\zeta^{n+1}\nabla S' \tag{7.21}$$

where, unlike in previous chapters the prognostic variables, have been non-dimensionalised. The boundary conditions on S' are taken to be fixed entropy conditions, so as in previous chapters,

$$S' = 0 \quad \text{at} \quad r = r_C, r_S. \tag{7.22}$$

The linearised, dimensionless form of (7.10) is

$$\frac{\partial\,\boldsymbol{u}}{\partial t} = -2\mathcal{E}^{-1}\hat{z}\times\boldsymbol{u} - \nabla\left(\frac{p'}{\rho}\right) + \boldsymbol{F}_\nu + \frac{\mathcal{R}aS'}{r^2}\hat{\boldsymbol{r}}, \tag{7.23}$$

where $\boldsymbol{F}_\nu$ is the non-dimensional form of the viscous force given by $\boldsymbol{F}/(\nu\rho)$ and $\hat{\boldsymbol{z}}$ represents the direction of the axis of rotation.

The non-dimensional version of equation (7.11) and equations (7.21) and (7.23) then form the basis of this chapter, alongside boundary conditions (7.22) and either no-slip or stress-free boundary conditions for the dimensionless velocity $\boldsymbol{u}$.

7.1.1 Boussinesq limit

The equations derived in the previous sections are reliant on the anelastic approximation; similar equation sets for a Boussinesq set have been used in the majority of historic studies of the onset of convection within a rapidly rotating spherical regime, with these models also utilising a uniform density reference state. In previous chapters we considered a Boussinesq set that does not ignore pressure perturbations or prescribe a constant reference density profile; therefore for comparison of forthcoming analysis of the onset of anelastic compressible convection, we now derive the Boussinesq equations that have been used within previous studies using constant reference state density profiles, noting that they represent the limit as $N_\rho \to 0$ for the anelastic equations described earlier in the chapter.

We first consider the nonlinear momentum equation (7.10) and entropy equation (7.15) in the constant reference density limit $N_\rho \to 0$. In this limit (7.4) yields $\zeta_0 \to 1$, $c_0 \to 1$ and $c_1 \to 1$. Using the perfect gas law (2.1) as our equation of state our definition of c_1 in (7.2) then implies

$$\frac{gd\rho_s}{p_s} \to 0 \quad \text{hence} \quad \frac{gd}{C_pT_s} \to 0. \tag{7.24}$$

The term $\nabla(p'/\rho_s)$ in (7.10) has order of magnitude $p'/\rho_s d$ while in the term

$$\frac{\boldsymbol{g}S'}{C_p} = \frac{\boldsymbol{g}}{\gamma}\left(\frac{p'}{p_s} - \frac{\gamma\rho'}{\rho_s}\right) \tag{7.25}$$

the pressure perturbation part has the order of magnitude gp'/p_s and the density perturbation part has the order of magnitude $-g\rho'/\rho_s$. Using (7.24) gp'/p_s is negligible compared with $p'/\rho_s d$, thus the pressure perturbation component of (7.25) tends to zero in the uniform reference density regime. However, in considering free convection, we are assuming that the buoyancy term is of at least the same level of significance as the pressure gradient; therefore the density perturbations must be of significance in the buoyancy term which means that we require $p'/p_s \ll \rho'/\rho_s$. This allows the linearised perfect gas law to be simplified such that

$$\frac{\rho'}{\rho_s} \approx -\frac{T'}{T_s} \quad \text{and} \quad \frac{T'}{T_s} = \alpha T' \tag{7.26}$$

where $\alpha = 1/T_s$ is the coefficient of thermal expansion as described in section 3.1. Thus in the Boussinesq limit the nonlinear momentum equation for a constant density reference state reduces to

$$\frac{\partial\,\boldsymbol{u}}{\partial t} = \boldsymbol{u}\times\omega - 2\Omega\times\boldsymbol{u} - \frac{\nabla p'}{\rho_s} - \nabla(\boldsymbol{u}^2/2) + \frac{\boldsymbol{F}}{\rho_s} - \boldsymbol{g}\alpha T'. \tag{7.27}$$

The entropy equation can also be simplied through this relationship as $S'/C_p \to T'/T_s$ in the limit we have described and Φ can be shown to be negligible relative to the advection of reference state entropy. Therefore (7.15) becomes

$$\frac{\partial T}{\partial t} + \boldsymbol{u}\,.\nabla T = \nabla.\mathcal{K}\nabla T \tag{7.28}$$

where $\mathcal{K}$ now represents the sum of the turbulent and molecular diffusivities. The constant entropy boundary conditions simplify to constant temperature conditions.

7.1.2 Convection at negative $\mathcal{R}a$

We have discussed that Drew et al., (1995) found the surprising result that for compressible convection utilising molecular rather than turbulent diffusivity it was possible to see growing modes for regimes in which the Rayleigh number is negative. They suggested that this was due to the presence of temperature diffusion rather than entropy diffusion in the thermodynamic equation. We now show that using entropy diffusion only negative Rayleigh number always gives stability.

Since we have assumed that no fluid enters or leaves the shell, multiplying (7.23) by $\rho_s \boldsymbol{u}$ and integrating over the whole shell gives

$$\frac{\partial}{\partial t}\int \frac{1}{2}\zeta^n \boldsymbol{u}^2\, dv = \int \zeta^n \boldsymbol{u}\,.\boldsymbol{F_\nu} dv + \mathcal{R}a \int \zeta^n S' \frac{u_r}{r^2} dv, \tag{7.29}$$

where the pressure term is removed using the divergence theorem and anelastic mass continuity equation (7.11). Multiplying the entropy equation (7.21) by $\mathcal{R}a\mathcal{P}^{-1}\rho_s \left(dS_s/dr\right)^{-1} S'/r^2$ and integrating over the whole shell yields

$$\begin{aligned}\frac{\mathcal{R}a\mathcal{P}}{2nc_1}\left(\zeta_0^{-n} - \zeta_C^{-n}\right)\frac{\partial}{\partial t}\int \zeta^{2n+1}(S')^2 dv = \mathcal{R}a \int \zeta^n S' \frac{u_r}{r^2} dv \\ + \frac{\mathcal{R}a(\zeta_0^{-n} - \zeta_C^{-n})}{nc_1}\int \zeta^n S' \nabla.\zeta^{n+1}\nabla S' dv.\end{aligned} \tag{7.30}$$

Subtracting (7.30) from (7.29) we obtain

$$\begin{aligned}\frac{\partial}{\partial t}\int \frac{1}{2}\zeta^n \boldsymbol{u}^2 - \frac{\mathcal{R}a\mathcal{P}}{2nc_1}\left(\zeta_0^{-n} - \zeta_C^{-n}\right)\zeta^{2n+1}(S')^2 dv = \int \zeta^n \boldsymbol{u}\,.\boldsymbol{F}_\nu dv \\ - \frac{\mathcal{R}a(\zeta_0^{-n} - \zeta_C^{-n})}{nc_1}\int \zeta^n S' \nabla.\zeta^{n+1}\nabla S' dv\end{aligned} \tag{7.31}$$

Now if $\mathcal{R}a < 0$, the integral on the left-hand-side of (7.31) is positive, so for growing modes the left-hand-side must also be positive. However, we show below that for negative $\mathcal{R}a$ both integrals on the right-hand-side are non-positive. It is therefore impossible to have growing modes at negative Rayleigh number, thus the terminology 'stably stratified' for $N^2 > 0$ is well founded.

Viscous term

Using our definition of $\boldsymbol{F}$ we have, for the linearised case,

$$\begin{aligned} V = \int \zeta^n \, \boldsymbol{u} \, . \boldsymbol{F_\nu} dv = \int \frac{\partial}{\partial x_j} \{ u_i \rho_s \left(\frac{\partial u_i}{\partial x_j} + \frac{\partial u_j}{\partial x_i} \right) - \frac{2}{3} u_j \rho_s \frac{\partial u_i}{\partial x_i} \} dv \\ - \int \frac{\partial u_i}{\partial x_j} \rho_s \left(\frac{\partial u_i}{\partial x_j} + \frac{\partial u_j}{\partial x_i} \right) dv + \frac{2}{3} \int \rho_s \frac{\partial u_i}{\partial x_i} \frac{\partial u_j}{\partial x_j} dv. \end{aligned} \tag{7.32}$$

The divergence term vanishes if either no-slip or stress-free boundary conditions apply, so

$$\begin{aligned} V &= \frac{1}{2} \int \rho_s \left(\frac{\partial u_i}{\partial x_j} + \frac{\partial u_j}{\partial x_i} \right) \left(\frac{\partial u_i}{\partial x_j} + \frac{\partial u_j}{\partial x_i} \right) dv + \frac{2}{3} \int \rho_s \left(\frac{\partial u_i}{\partial x_i} \right)^2 dv \\ &= -\frac{4}{3} \int \rho_s \left(\frac{\partial u_i}{\partial x_i} \right)^2 dv - \frac{1}{2} \int \rho_s \sum_i \neq j \left(\frac{\partial u_i}{\partial x_j} + \frac{\partial u_j}{\partial x_i} \right)^2 dv \leq 0, \end{aligned} \tag{7.33}$$

establishing that for either no-slip of stress-free boundaries the viscous term is always negative.

Entropy term

We define

$$H = \int \zeta^n S' \nabla . \zeta^{n+1} \nabla S' dv = \int \nabla . \left(\zeta^{2n+1} S' \nabla S' \right) dv - \int \zeta^{n+1} \nabla (\zeta^n S') . \nabla S' dv. \tag{7.34}$$

The divergence term vanishes if either $S' = 0$ on the boundaries, the case studied in this thesis, and also if the normal derivative of S' vanishes on the boundaries. It is not immediately apparent that the second term on the right of (7.34) has definite sign as it is not a square. However, we can write this term so that

$$H = -\int \zeta \left[\nabla (\zeta^n S') \right]^2 dv + \int (\zeta^{1-n} \nabla \zeta^n) . \nabla \frac{1}{2} (\zeta^n S')^2 dv. \tag{7.35}$$

The first term is clearly now negative definite. Using $\zeta = c_0 + c_1/r$ and assuming that $S' = 0$ at the boundaries we are able to rewrite the second term in spherical polar coordinates

$$\int (\zeta^{1-n} \nabla \zeta^n) . \nabla \frac{1}{2} (\zeta^n S')^2 dv = -\frac{n c_1}{2} \int \int \int \frac{\partial}{\partial r} \frac{\partial}{\partial r} (\zeta^n S')^2 \sin\theta dr d\theta d\phi = 0, \tag{7.36}$$

thus H is shown to be negative definite.

We have established that both V and H are non-positive, so there cannot be growing modes if $\mathcal{R}a < 0$. It is also easy to establish that there can be no growing modes for $\mathcal{R}a = 0$ thus we can only have linear growth for $\mathcal{R}a > 0$. Of course, this proof does not rule out the possibility of nonlinear disturbances becoming unstable within a negative Rayleigh number regime.

It is worth noting that the proof fails if we use temperature diffusion rather that entropy diffusion in the entropy equation; in this scenario it is not possible draw definite conclusions about the sign of the integrals in the definition of H. The proof also depends on specific assumptions about the equilibrium model. If for example, there was internal heating rather than a prescribed entropy drop across the layer then the form of dS_s/dr is changed and the method described above may no longer apply. Also, we have required the boundary condition $S' = 0$ on the inner and outer boundaries; it is possible that with other boundary conditions negative Rayleigh number instability can occur even with entropy diffusion.

7.2 Small $\mathcal{E}$ asymptotic theory

The onset of Boussinesq convection in a rapidly rotating uniform density sphere has been solved in the asymptotic limit $\mathcal{E} \to 0$ (Jones et al., 2000 [40]), and in the spherical shell case by Dormy et al., (2004 [19]). Here we extend this Wentzel-Kramers-Brillouin (WKB) theory from the uniform density Boussinesq case to consider anelastic compressible convection.

In cylindrical polar coordinates (s, ϕ, z), with origin at the centre of our spherical system, we can satisfy the anelastic continuity equation (7.11) setting

$$\zeta^n \mathbf{u} = \nabla \times \Psi \hat{\boldsymbol{z}} + \nabla \times \nabla \times \Xi \hat{\boldsymbol{z}}. \tag{7.37}$$

s_C and s_S equate to the radius of the inner sphere and outer sphere resepectively, i.e. $s_C = r_C$ and $s_S = r_S$, and the cylindrical region in which $s < s_C$ is referred to as the tangent cylinder.

In the limit $\mathcal{E} \to 0$, numerical solutions computed by Jones and Kuzanyan (Jones et al., 2008 [38]) suggest that the convection at onset takes the form of tall thin columns in compressible convection as well as in 'incompressible' Boussinesq convection. Following Jones et al., (2000 [40]) we adopt the ansatz that scalings are given by

$$\frac{1}{s}\frac{\partial}{\partial \phi} \sim \frac{\partial}{\partial s} \sim O(\mathcal{E}^{-1/3}), \quad \frac{\partial}{\partial z} \sim O(1), \tag{7.38}$$

when acting on perturbed quantities. This implies that the radial and azimuthal variations are of the same order. Since we are seeking WKB solutions, we assume disturbances are proportional to

$$\exp[i(ks + m\phi - \sigma t)], \tag{7.39}$$

where σ is in general complex. We say that convection occurs at some position s whenever $Im(\sigma) > 0$. So at leading order a consequence of (7.38) is that,

$$\nabla^2,\ \nabla_H^2 \to -\left(k^2 + \frac{m^2}{s^2}\right) = -a^2. \tag{7.40}$$

At the boundaries, $u_r = 0$, so in general u_z and u_s are of the same order, so from (7.37) and (7.38) $\Xi \sim \mathcal{E}^{1/3}\Psi$. It follows that

$$\zeta^n u_s = \frac{\partial^2 \Xi}{\partial z \partial s} + \frac{1}{s}\frac{\partial \Psi}{\partial \phi} \sim \frac{1}{s}\frac{\partial \Psi}{\partial \phi}, \quad \zeta^n u_\phi = \frac{1}{s}\frac{\partial^2 \Xi}{\partial z \partial \phi} - \frac{\partial \Psi}{\partial s} \sim -\frac{\partial \Psi}{\partial s}. \tag{7.41}$$

The appropriate asymptotic scalings for the variables are (Jones et al., 2000 [40])

$$\begin{aligned} &\mathcal{R}a = \mathcal{E}^{-4/3}\mathcal{R}, \quad \sigma = \mathcal{E}^{-2/3}\hat{\sigma}, \quad m = \mathcal{E}^{-1/3}\hat{m}, \quad k = \mathcal{E}^{-1/3}\hat{k}, \\ &a = \mathcal{E}^{-1/3}\hat{a}, \quad S' = S', \quad \Psi = \mathcal{E}^{-1/3}\psi, \quad u_z = \mathcal{E}^{-2/3}\hat{u}_z. \end{aligned} \tag{7.42}$$

We note that following these scalings $\hat{m}$ is no longer restricted to being an integer.

7.2.1 Equations for the z-structure

We insert these expressions into the z-component of the curl of the momentum equation (7.23) and the z-component of the double curl of the momentum equation, retaining only leading order terms. A considerable simplification results because gradients of the density are only $O(1)$ whereas horizontal derivatives of perturbed quantities are larger at $O(\mathcal{E}^{-1/3})$. Together with the entropy equation, we obtain

$$\frac{1}{\zeta^n}\frac{d\psi}{dz} = \frac{1}{2}(\hat{a}^2 - i\hat{\sigma})w - \frac{\mathcal{R}zS'}{2r^3} + \frac{nz\psi}{r\zeta^{n+1}}\frac{d\zeta}{dr}, \tag{7.43}$$

$$\frac{d\hat{u}_z}{dz} = \left(\frac{\hat{a}^2}{2\zeta^n}(\hat{a}^2 - i\hat{\sigma}) - \frac{i\hat{m}n}{r\zeta^{n+1}}\frac{d\zeta}{dr}\right)\psi + \frac{i\hat{m}\mathcal{R}S'}{2r^3} - \frac{nz\hat{u}_z}{\zeta r}\frac{d\zeta}{dr}, \tag{7.44}$$

$$S' = \frac{1}{(i\hat{\sigma}\mathcal{P} - \hat{a}^2)(\zeta_o^{-n} - \zeta_i^{-n})}\frac{d\zeta}{dr}\left(\frac{i\hat{m}n\psi}{r\zeta^{2n+1}} + \frac{nz\hat{u}_z}{\zeta^{n+1}r}\right). \tag{7.45}$$

On eliminating S' we obtain a second order two-point boundary value problem in z with eigenvalue $\hat{\sigma}$. The boundary conditions are

$$i\hat{m}\psi + z\hat{u}_z\zeta^n = 0, \quad \text{on} \quad z = \pm\left(\frac{1}{(1-\eta)^2} - s^2\right)^{1/2}. \tag{7.46}$$

This system is the compressible equivalent of the Roberts-Busse equations (see equation (3.5) of Jones et al., (2000 [40]), and equation (3.11) of Dormy et al (2004 [19]), for the Boussinesq equivalents). It defines the local dispersion relation for $\hat{\sigma}$ in terms of the parameters. There are solutions both symmetric or antisymmetric about the equator, but as in the Boussinesq problem, the first modes to onset always appear to be those symmetric in ψ and antisymmetric in $\hat{u}_z$. The system has to be solved numerically, but of course this is a very simple one-dimensional problem compared to the task of solving the full system numerically, which involves the inversion of very large matrices, this is dicussed further in Jones et al., (submitted 2008, [38]).

7.2.2 Local analysis

The conventional method is to maximise the growth rate $Im\{\sigma\}$ over all real values of s and k. So we seek the marginal modes which are identified by the minimum value of the Rayleigh number $\mathcal{R}$ that gives steady-state solutions, thus

$$Im\{\hat{\sigma}\} = 0. \tag{7.47}$$

This local disturbance does not grow or decay in space or time, thus $Im\{\hat{k}\} = 0$ and $Im\{\hat{m}\} = 0$. If we then consider $\hat{s}$ and $\hat{k}$ fixed and minimise $\mathcal{R}$ over $\hat{m}$ then for an increment $d\hat{m}$ we have

$$Im\{d\hat{\sigma}\} = Im\left\{\frac{\partial\hat{\sigma}}{\partial\hat{m}}\right\}\partial\hat{\Updownarrow} + Im\left\{\frac{\partial\hat{\sigma}}{\partial\mathcal{R}}\right\}\partial\mathcal{R}. \tag{7.48}$$

At the minimum $d\mathcal{R} = 0$ subject to the constraint $Im\{\hat{\sigma}\} = 0$ we have

$$Im\left\{\frac{\partial\hat{\sigma}}{\partial\hat{m}}\right\} = \frac{\partial Im\{\hat{\sigma}\}}{\partial\hat{m}} = 0. \tag{7.49}$$

The remaining local criteria can be derived in the same way and we find that we also require

$$\begin{aligned} \frac{\partial Im\{\hat{\sigma}\}}{\partial\hat{k}} &= 0, \\ \frac{\partial Im\{\hat{\sigma}\}}{\partial\hat{s}} &= 0. \end{aligned} \tag{7.50}$$

The local stability criteria given by (7.47) and (7.50) allow us to find the minimum Rayleigh number $\mathcal{R}_L$, and location as defined by $\hat{m}_L$, $\hat{k}_L$ and s_L at which convection onsets. As in the uniform density Boussinesq case, $\hat{\sigma}$ is a function of $\hat{k}^2$ only so minimising over $\hat{k}$ results in $\hat{k} = 0$. We hold $\mathcal{P}$, N_ρ, n fixed and find the values of $\hat{m}$, $\mathcal{R}$ and s that satisfy these three conditions. Note that we have used subscript L to denote critical parameters using local analysis.

The critical value of s found may lie (i) in $0 < s < \eta/(1-\eta)$ (equivalently $0 < s < s_C$, i.e. within the inner sphere) or (ii) in $\eta/(1-\eta) < s < 1/(1-\eta)$ (equivalently $s_C < s < s_S$, i.e. within the fluid layer), depending on the parameters.

The system is singular at $s = s_S = 1/(1-\eta)$ and critical s cannot exceed that value. As explained in Dormy et al., (2004), these two cases must be treated differently. In case (i) the local maximum of $Im\{\hat{\sigma}\}$ does not lie inside the fluid, instead lying within the inner sphere. In consequence, the minimum critical Rayleigh number is achieved at the tangent cylinder, and convection will onset there first as $\mathcal{R}$ is increased. The leading order value of critical $\mathcal{R}$ is given by setting $s = s_C$, its value at the tangent cylinder, and solving $Im\{\hat{\sigma}\} = 0$ and $\partial Im\{\hat{\sigma}\}/\partial\hat{m} = 0$ for $\mathcal{R}$ and $\hat{m}$. The width of the convective region near onset is $O(E^{2/9})$ and the (non-zero) frequency is given by $Re\{\hat{\sigma}\}$. A more complete derivation of these results can be found in Dormy et al., (2004 [19]).

Local theory has significant shortcomings, as noted by several groups, in that it describes a disturbance that is valid for a short period of time in a localised region but does not necessarily describe the long time evolution of the disturbance. It is also the case that when time dependence is separated out, the local spatial structure cannot necessarily be extended throughout the spatial domain and still meet the boundary conditions. Soward (1977 [57]) first noted this and attributed its inaccuracy to non-zero radial frequency gradient $Re\{\partial\hat{\sigma}/\partial s\}$, which leads to phase mixing. The physical picture this endeavours to cover is one in which the wave beats at slightly different frequencies in neighbouring locations such that the local wave number suffers a secular variation advecting it away from $\hat{k}_L$ in Fourier space to a stable wave number. A similar phenomenon occurs when the group velocity $\partial\hat{\sigma}/\partial\hat{k}$ is non-zero, this is not the case in local theory but it is worth highlighting that non-zero group velocity implies that the wave packets move away from critical s value and are damped by local theory.

The issue surrounding the extension of solution throughout the spatial domain led to the development of global theory, which must be used if case (ii) is relevant.

7.2.3 Global analysis

In this scenario the WKB theory predicts that onset lies in the neighbourhood of some $s = s_M$ inside the fluid layer, so a solution is required for which the amplitude decays to zero as $(s - s_M)/\mathcal{E}^{1/3} \to \pm\infty$. For such solutions to exist, there must be a value of s in the complex plane at which both the real and imaginary parts of $\partial\hat{\sigma}/\partial s = 0$; setting the radial frequency gradient equal to zero prevents Airy type amplitude solutions which cannot be made to decay away at both ends. These two conditions, together with $Im\{\hat{\sigma}\} = 0$ and $\partial Im\{\hat{\sigma}\}/\partial\hat{m} = 0$ give four equations for four unknowns $\mathcal{R}$, $\hat{m}$, and $s = s_r + is_i$. The point at which these conditions are met is a double complex turning point $s_\rfloor$, once this point has been identified it is possible to determine $\mathcal{R}_\rfloor$, $\hat{m}_\rfloor$ and $\hat{\sigma}_\rfloor$, so the dispersion relation $\hat{\sigma}(\hat{k}, s) = \hat{\sigma}_\rfloor$ becomes an equation that determines complex $\hat{k}$ as a function of complex s. At the saddle point $s_\rfloor$ the wave number has a double zero $\hat{k}_\rfloor = 0$; however, as we move away from the saddle point to the real axis $\hat{k}$ splits into two non-zero roots $\pm\hat{k}$. To identify the physically acceptable solution at a point M on the real axis we recall that the s dependence is proportional to

$$\exp\left(\frac{i}{\mathcal{E}^{1/3}}\int \hat{k}(s)ds\right). \tag{7.51}$$

Taylor expansion of $\hat{k}$ about the point on the real axis s_M allows the solution to be locally approximated by

$$\exp\left(i\hat{k}_M\frac{s - s_M}{\mathcal{E}^{1/3}} + \frac{i\hat{k}'_M}{2}\frac{(s - s_M)^2}{\mathcal{E}^{1/3}}\right), \quad \text{where} \quad \hat{k}'_M = \left(\frac{d\hat{k}}{ds}\right)_M. \tag{7.52}$$

In order to find the maximum value of our physically acceptable solution it is then necessary that $Im\{\hat{k}_M\} = 0$ in order that $s - s_M > 0$ and $Im\{\hat{k}'_M\} > 0$ in order that $(s - s_M)^2 > 0$. Providing that these conditions are satisfied the realised solution has radial wavelength $O(\mathcal{E}^{1/3})$, which is the same order as the azimuthal wavelength, and decays away from s_M over a much longer $O(\mathcal{E}^{1/6})$ length scale.

It then follows that using global analysis $s = s_M$ is the point at which the

convection has maximum amplitude. The quantities $\hat{k}_M$ and $Im\{d\hat{k}/ds\}_M$ give the radial wavenumber near the onset of convection and the inverse width of the convecting region respectively.

It is also necessary to determine the points at which anti-Stokes lines associated with the solution cut the real s-axis, these points are defined as s_- and s_+. The anti-Stokes lines are defined by

$$Im\left\{\int_{s_\rfloor}^{s} \hat{k}(s)ds\right\} = 0, \tag{7.53}$$

and the interval (s_-, s_+) defines the interval in which our solution is dominant. As discussed in Jones et al [40], the global asymptotic theory is only valid when the interval (s_-, s_+) lies entirely within the fluid. If this is not the case then the boundary conditions become significant and the asymptotic theory becomes considerably more complicated.

Whilst the Boussinesq and anelastic equation sets and reference states differ from each other, the forementioned mathematical techniques involved in the local and global analysis of the equation sets are the same. The development of local and global theories is discussed in studies such as Jones et al [40] and Dormy et al [19].

7.2.4 Evaluation of asymptotic theory

In order to evaluate the asymptotic theory it is necessary to utilise a suite of five programs. First, for any set of parameters η, N_ρ, n and $\mathcal{P}$ the dispersion relation given by solving equations (7.43)-(7.46) is used to minimise $\mathcal{R}$ over s and $\hat{m}$ (with $\hat{k} = 0$). If the minimising value of s satisfies $s \leq \eta/(1-\eta)$ then we must fix $s = \eta/(1-\eta)$ and use a second program that minimises $\mathcal{R}$ over $\hat{m}$ only, to get the correct value of $\mathcal{R}_\rfloor$. If on the other hand $s > \eta/(1-\eta)$, then the global theory must be applied. We use a third program that solves complex $d\hat{\sigma}/ds = 0$, $Im\{\hat{\sigma}\} = 0$, and $Im\{\partial\hat{\sigma}/\partial\hat{m}\}$ for the four unknowns $\mathcal{R}$, $\hat{m}$, s_r and s_i. Then a fourth program, which inputs the

values of $\mathcal{R}_\rfloor$, $\hat{m}$ and $\hat{\sigma}_\rfloor$ from the global theory program, is used to find $\hat{k}(s)$ from the relation $\hat{\sigma}_\rfloor = \hat{\sigma}(\hat{k}, s)$. This program must find the real value of $s = s_M$ at which $Im\{\hat{k}\} = 0$ and finds the corresponding values of $\hat{k} = \hat{k}_M$ and $Im\{d\hat{k}/ds\}_M$, being careful to select the sign of $\hat{k}_M$ such that $Im\{d\hat{k}/ds\}_M > 0$. The fifth program, which finds s_- and s_+, evaluates the complex path integral

$$Im\left\{\int_{s_\rfloor}^{s} \hat{k}(s)ds\right\}, \tag{7.54}$$

from the double turning point to any real s, again calculating $\hat{k}$ from $\hat{\sigma}_\rfloor = \hat{\sigma}(\hat{k}, s)$. The program must then find the zeroes as s varies to obtain s_- and s_+. Since the dispersion relation always has two roots $\hat{k}$ of opposite sign, care must be taken to ensure that the same root is taken as the complex integral is evaluated.

7.2.5 Numerical Formulation

Jones and Kuzanyan [38] calculate numerical solutions to the governing equations through use of a toroidal-poloidal decomposition. We do not discuss their results in detail in this thesis except in their use to validate the asymptotic results. The use of the anelastic continuity equation allows decompostion of $\boldsymbol{u}$ such that

$$\boldsymbol{u} = \frac{1}{\rho}\nabla \times \nabla \times \hat{\boldsymbol{r}} f \rho_s + \frac{1}{\rho_s}\nabla \times \hat{\boldsymbol{r}} e \rho_s, \tag{7.55}$$

where e and f are the toroidal and poloidal velocity component potentials respectively.

It is then expected that velocity and entropy solutions take the form

$$e = e(r,\theta)\exp(im\phi - \sigma t), \quad f = f(r,\theta)\exp(im\phi - \sigma t), \quad s = s'(r,\theta)\exp(im\phi - \sigma t), \tag{7.56}$$

where m is the azimuthal wave number and positive values of the frequency σ correspond to prograde motion. Within a spherical co-ordinate system (as opposed to the terrestrial system used in previous chapters), using standard div, grad and curl

relationships, this implies that

$$\boldsymbol{u} = \left[\frac{\mathcal{L}^2\{f\}}{r^2}\right]\hat{\boldsymbol{r}} + \frac{1}{r}\left[\frac{1}{\sin\theta}\frac{\partial e}{\partial \phi} + \frac{\partial^2 f}{\partial r \partial \theta} + \frac{\partial f}{\partial \theta}\xi\right]\hat{\boldsymbol{\theta}} + \frac{1}{r}\left[\frac{1}{\sin\theta}\frac{\partial^2 f}{\partial r \partial \phi} - \frac{\partial e}{\partial \theta} + \frac{1}{\sin\theta}\frac{\partial f}{\partial \phi}\xi\right]\hat{\boldsymbol{\phi}}, \tag{7.57}$$

where the operator

$$\mathcal{L}^2 \equiv -\frac{1}{\sin\theta}\frac{\partial}{\partial\theta}\left\{\sin\theta\frac{\partial}{\partial\theta}\right\} - \frac{1}{\sin^2\theta}\frac{\partial^2}{\partial\phi^2}. \tag{7.58}$$

Utilising these relationships within the radial components of the curl and double curl of the dimensionless momentum equation (7.23) and the entropy equation (7.21) allows use of spectral collocation methods to find numerical solutions. The governing equations and numerical method are discussed in greater detail in Jones et al., (submitted 2008 [38]).

7.3 Results from the asymptotic theory

7.3.1 Uniform density Boussinesq case

In the uniform density Boussinesq case it has been shown, through both the asymptotic theory and numerical computations, that in spherical shell models at low $\mathcal{E}$, convection first onsets outside the tangent cylinder surrounding the inner core (see e.g. Jones et al., 2000 [40]; Dormy et al., 2004 [19]). For the case in which there is no internal heating within the fluid, and a prescribed temperature drop across the shell (differential heating), the convection onsets in the neighbourhood of the tangent cyclinder. In the case in which there is uniform internal heating within the fluid layer onset can occur in the interior of the shell. In this thesis we consider only the case of differential heating. It has also been shown that in a rapidly rotating system, the modes with z-vorticity symmetric about the equator is preferred over modes with the opposite symmetry; thus, the z-velocity is antisymmetric and convection always takes

a nonaxisymetric columnar form except at very low Prandtl number where inertial modes may occur first (Zhang, 1994 [66]). In this thesis we do not explore the onset of convection at these very low Prandtl numbers. At very low Ekman number asymptotics show that as $\mathcal{E} \to 0$ the critical Rayleigh number scales as $\mathcal{R} \sim \mathcal{E}^{-4/3}$, critical azimuthal wavenumber as $m \sim \mathcal{E}^{-1/3}$ and the frequency of the most unstable mode scales as $\sigma \sim \mathcal{E}^{-2/3}$. At $\mathcal{E} \approx 10^{-4}$ Al-Shamali et al., (2004 [1]) found that an exponent $\mathcal{E}^{1.16}$ fitted numerical data best when considering Rayleigh number dependence. We have mentioned previously that solving the dispersion relation formed through consideration of the curl and double curl of the momentum equation is considerably less computationally expensive than solving the full equation sets numerically; consequently, it is possible to consider layer depths that are likely to be much more appropriate to the Jovian regime than those considered in previous chapters. In the Boussinesq regime it has been found that the frequency at onset first increases then decreases as radius ratio η is increased. The preferred azimuthal wavenumber at onset and critical Rayleigh number increases with increasing η. If the Prandtl number is decreased, the critical azimuthal wavenumber is significantly reduced and the frequency increased. In order that differential rotation be maintained it is necessary that there be spiralling of the convective rolls, in the uniform density Boussinesq case this spiralling has been found to be prograde.

7.3.2 Compressible results

Dormy et al., (2004 [19]) noted that for the uniform density Boussinesq scenario in the case of differential heating, where a heat flux is applied at the inner boundary, convection always onsets at the tangent cylinder; therefore case i) always applies irrespective of the size of the inner core. The form of gravity adopted here, $g \sim 1/r^2$, favours convection closer to the tangent cylinder than the $g \sim r$ used by Dormy et al., (2004 ?), therefore one might expect that case i) will occur always for the equation

sets used in this study. The asymptotic results show this not to be the case with the onset of convection frequently occurring within the fluid interior, the scenario covered by case ii). The tendency for compressibility to push convection towards the outer boundary was noted in Glatzmaier & Gilman (1981 [31]). The tendency for increased number of density scale heights to focus eigenstructures towards the boundaries is noted in chapter 5. The use of a reference profile which allows density variation clearly has significant effect on the location of the onset of convection, with the degree of density variation also being of importance. The results from previous chapters suggest that these extreme differences in location are more significantly affected by the differing reference profiles than they are by other consequences of the approximated equation sets.

ν		0.5			0.8	
$\mathcal{P}$	0.1	1.0	10.0	0.1	1.0	10.0
N_ρ	2.0	2.0	2.0	1.0	1.0	1.0
$\mathcal{R}_\rfloor$	3.2374	17.6348	24.4301	16.6877	73.4440	98.9767
$\hat{\sigma}_\rfloor$	4.5882	1.3780	0.1260	2.9716	0.9147	0.00853
$\hat{m}_\rfloor$	0.7945	1.5310	1.8190	2.581	4.1368	4.7366
s_r	1.0557	1.3328	1.3670	4.3778	4.2931	4.3310
s_i	-0.2811	-0.1518	-0.0057	-0.7233	-0.2137	0.0466
s_M	1.7438	1.4210	1.3683	4.7044	4.3537	4.3290
$\hat{k}_M$	-0.4974	-0.3247	-0.0150	-0.4623	-0.2141	0.0587
$Im(d\hat{k}/ds)_M$	0.2368	1.3348	2.4801	0.4927	0.8675	1.2003
s_-	0.9610	1.2345	1.3624	3.8290	4.1176	4.2794
s_+	-	1.6260	1.3741	-	4.5723	4.3770

Table 7.1: *Global bifurcation data*

Table 7.1 shows results from a) a wide gap shell with $\eta = 0.5$ and $N_\rho = 2$

and b) a narrow gap shell with $\eta = 0.8$ and $N_\rho = 1$. In both instances results are shown for Prandtl number $\mathcal{P} = 0.1$, 1 and 10. In all these cases, and in contrast to the uniform density Boussinesq case, instability onsets in the interior of the fluid, thus the global asymptotic theory is used in each scenario. In dimensionless units the fluid layer lies in the region $1 < s < 2$ for case a) and $4 < s < 5$ for case b). The turning point in the complex plane is given by $s_r + is_i$ and s_M is the point at which the convection onsets first; we see that in each case s_M is comfortably within the fluid layer.

In both cases the frequency $\hat{\sigma}_\rfloor$ at onset decreases strongly with Prandtl number, and critical azimuthal wavenumber $\hat{m}_\rfloor$ increases. The quantity $Im\{d\hat{k}/ds\}_M$ measures how confined the convection is, it is increased with increased $\mathcal{P}$ indicating that the disturbances are more localised. This is also the case for the uniform density Boussinesq regime, with larger Prandtl number constraining the location of $s_\rfloor$ to be closer to the real axis, which in turn leads to a smaller interval (s_-, s_+) between the points at which the anti-Stokes lines cut the real axis indicating that the solution decays rapidly in both s directions. Global theory is only strictly applicable if this interval lies entirely within the fluid; a failure for this to be the case means that the disturbance is not sufficiently localised that boundary conditions are unimportant. We see that at $\mathcal{P} = 0.1$ the interval does not lie within the fluid for either η; the values of s_- are within the tangent cylinder and there are no values for s_+. In these instances the value of $\hat{k}$ emerging from the dispersion relation becomes singular as $s \to 1/(1-\eta)$. Therefore the asymptotic solutions for low Prandtl number should be treated with caution.

The radial wavenumber at onset is given by $\hat{k}_M$, and since $\hat{m}_\rfloor/s_M$ and $\hat{k}_M$ are of the same order of magnitude the tilt of the convective rolls in the s-ϕ plane is given by $\tan^{-1}(-\hat{k}_M s_M/\hat{m}_\rfloor)$, thus the value of $\hat{k}_M s_M/\hat{m}_\rfloor$ allows us to infer some information about degree to which spiralling occurs. In the uniform density Boussinesq regime $\hat{k}_M$

is always negative, thus spiralling is prograde and has increasing ϕ as s increases. This is generally the case for compressible reference states; however there are instances at high Prandtl number in which $\hat{k}_M$ is positive and spiralling can be retrograde, the $\eta = 0.8$, $\mathcal{P} = 10$ case being an example. As in the uniform density Boussinesq regime the magnitude of $\hat{k}_M s_M/\hat{m}_\rfloor$ is large at small Prandtl number indicating that there is strong spiralling, at high Prandtl number this is reduced and spiralling is weak. As one would expect, the critical Rayleigh number increases considerably with increasing Prandtl number. The azimuthal wavenumber $\hat{m}_\rfloor$ increases strongly with η.

We have seen that in a uniform density Boussinesq fluid convection always onsets at the tangent cylinder whereas for an anelastic fluid in which the reference state has large N_ρ the convection onsets in the interior of the fluid, and have noted that differing locations seem to be strongly affected by the reference state density profile; therefore, for fixed η there must be a critical value of N_ρ below which the convection onsets at the tangent cylinder. We denote this critical value as N_ρ^{LG}, noting that it represents the transition between local and global theory. We have also discussed that global theory does not strictly apply unless the interval (s_-, s_+) lies entirely within the fluid, thus we denote $N_\rho^{AS} > N_\rho^{LG}$ as the point at which s_- lies on the tangent cylinder. For $N_\rho > N_\rho^{AS}$ and $s_+ < 1/(1-\eta)$ the entire interval lies within the fluid and global bifurcation theory gives the correct asymptotic limit as $\mathcal{E} \to 0$. For $N_\rho^{LG} < N_\rho < N_\rho^{AS}$ neither the global or local asymptotic theories apply.

Table 7.2 shows critical values of N_ρ for $\eta = 0.5$ and $\eta = 0.8$ with Prandtl number set as $\mathcal{P} = 0.1$, 1 and 10. N_ρ^{LG} increases with increasing Prandtl number, this is as we would expect given that we have seen that the solutions for higher Prandtl number are more localised. The interval $(N_\rho^{LG}, N_\rho^{AS})$ is smallest for high Prandtl number. The values of N_ρ^{LG} and N_ρ^{AS} are reduced with increasing η.

Figure 7.1 shows the relationship between critical Rayleigh number and N_ρ for $\mathcal{P} = 1$ and $\eta = 0.5$. Below $N_\rho^{LG} = 1.771$ the local asymptotic theory is used, and

ν		0.5			0.8	
$\mathcal{P}$	0.1	1.0	10.0	0.1	1.0	10.0
N_ρ^{LG}	1.7432	1.7706	1.8101	0.8917	0.9064	0.8344
$\mathcal{R}_\rfloor$	1.2618	13.5384	20.7268	5.9826	63.2909	81.6280
$\hat{\sigma}_\rfloor$	5.2824	1.3205	0.1206	3.5073	0.8596	0.0745
$\hat{m}_\rfloor$	0.6123	1.1261	1.3150	1.9957	3.6949	4.0979
N_ρ^{AS}	2.0745	1.8154	1.8092	1.0672	0.9458	0.8546
$\mathcal{R}_\rfloor$	3.5165	14.9529	20.7292	17.9730	69.3181	83.9908
$\hat{\sigma}_\rfloor$	4.6658	1.3255	0.1208	3.1356	0.8786	0.0759
$\hat{m}_\rfloor$	0.8336	1.2155	1.3181	2.6740	3.9455	4.1839
s_r	1.1024	1.0833	1.0103	4.5077	4.19948	4.0327
s_i	-0.2982	-0.1438	-0.0150	-0.6171	-0.2426	0.0295
s_+	-	1.4379	1.0328	-	4.5227	4.0593

Table 7.2: *Local and global bifurcation data. N_ρ^{LG} is the value of N_ρ at which the s-value which gives minimum critical Rayleigh number on loacl theory coincides with the inner sphere. For $N_\rho < N_\rho^{LG}$ convection onsets first at the tangent cylinder. For $N_\rho > N_\rho^{LG}$ convection onsets in the fluid layer, and global theory must be used. N_ρ^{AS} is the value of N_ρ at which the lower anti-Stokes point s_- lies on the tangent cylinder. s_+ is the value of the upper anti-Stokes point at $N_\rho = N_\rho^{AS}$, and $\mathcal{R}_\rfloor$, $\sigma_\rfloor$, s_r and s_i are evaluated using global bifurcation theory at the same point.*

above $N_\rho^{AS} = 1.815$ the global asymptotic theory is used, between the two is a gap in which neither asymptotic theory is applicable. The critical Rayleigh number increases with increasing density variation, as does the preferred azimuthal wavenumber and frequency. The increase in Rayleigh number and azimuthal wavenumber appears to be due to the tendency for the convection to move outwards towards the low density region when the shell contains many density scale heights. In consequence,

the effect of increasing N_ρ is similar to that of increasing η in the uniform density Boussinesq case. The increase in frequency with increasing N_ρ is due to the fact that as fluid elements move from less dense surroundings they contract and their vorticity is reduced as they do so, naturally the opposite is true when fluid elements move from more dense surroundings. This means that there is an additional restoring force acting on the columns compared with the uniform density, incompressible scenario. In the uniform density, incompressible scenario the convection columns take the form of Rossby waves in which the restoring force is due to the vortex stretching associated with the sloping boundary as a column moves towards or away from the axis of rotation. The additional restoring force in the compressible case increases the wave frequency, and the greater the compressibility N_ρ the larger this effect. This can aslo be understood in terms of Taylor-Proudman theorem. In the incompressible case the curl of $2\boldsymbol{\Omega} \times \boldsymbol{u}$ is $-2\boldsymbol{\Omega}.\nabla\boldsymbol{u}$ because $\nabla.\boldsymbol{u} = 0$. In the anelastic compressible situation described above haves $\nabla.(\rho_s\boldsymbol{u}) = 0$; thus there is an additional term in the vorticity equation due to the reference state density profile, this corresponds with the physical mechanism that is described above. In previous chapters we saw that when applied to a realistic reference profile the Boussinesq equation set also has a tendency to significantly underestimate the frequencies of unstable inertial modes whilst overestimating the growth rates.

Figure 7.1 also shows numerical solutions for $\mathcal{E}^{-4}$ and $\mathcal{E}^{-5}$ as calculated by Jones and Kuzanyan utilising toroidal-poloidal decomposition. It appears that the numerical simulations approach the aymptotic solution in the limit $\mathcal{E} \to 0$, doing so most rapidly when convection lies well inside the fluid interior. This is likely to be because when the convection lies at the tangent cylinder the errors are $O(\mathcal{E}^{2/9})$ (Dormy et al., 2004 [19]) whereas in the interior they are $O(\mathcal{E}^{1/3})$. When the convection occurs near the outer shell it is restricted in the z-direction by the geometry, so for the tall thin columns necessary for the asymptotic theory to be a good approximation,

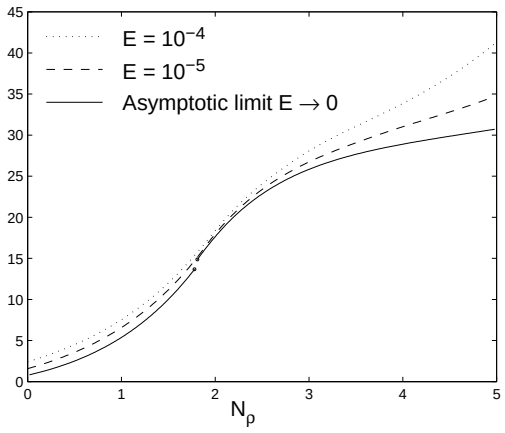

Figure 7.1: *Asymptotic theory compared with full numerical code results.* $\nu = 0.5$, $\mathcal{P} - 1$, $n = 2$. *Solid line* $\mathcal{R}$ *against* N_ρ *from the asymptotic theory. Dashed line,* $\mathcal{R} \times \mathcal{E}^{4/3}$ *against* N_ρ *at* $\mathcal{E} = 10^{-5}$. *Dotted line,* $\mathcal{R} \times \mathcal{E}^{4/3}$ *against* N_ρ *at* $\mathcal{E} = 10^{-4}$. *The small circles denote the asymptotic values at* N_ρ^{LG} *and* N_ρ^{AS}. *For* $N_\rho < N_\rho^{LG}$ *local theory at* $s = s_i$ *is used, for* $N_\rho > N_\rho^{AS}$ *the global theory is used. Reproduced with kind permission of Prof. Chris Jones, University of Leeds.*

naturally the radial extent must be correspondingly less, and this requires even smaller $\mathcal{E}$.

Figure 7.2 shows the numerical solutions for the variation of Ra, σ and m as $\mathcal{E}$ varies for a strongly stratified fluid with $N_\rho = 5$. These are shown alongside the power laws that are expected through asymptotic theory. We see that the asymptotic theory appears to provide a reasonable first estimate, particularly as the lowest values of $\mathcal{E}$ achievable through numerical code are approximately 10^{-5}.

Figure 7.3 shows the numerically calculated eigenfunctions for $N_\rho = 0$, $N_\rho = 2.0$ and $N_\rho = 5.0$, with other parameters set as $\mathcal{E} = 2 \times 10^{-5}$, $\eta = 0.5$, $\mathcal{P} = 1$, $n = 2$. It is interesting that at this low $\mathcal{E}$ the asymptotic behaviour is apparent. In each case the columnar structure, aligned with the axis of rotation, is clear. At large compressibility the convection onsets very close to the outer surface, this cannot

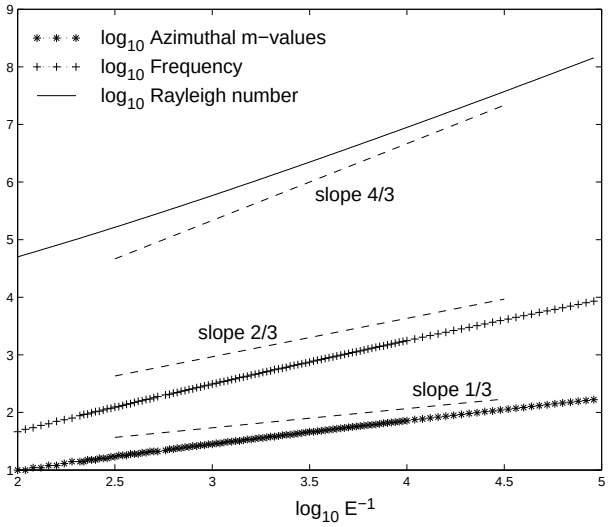

Figure 7.2: $\log_{10}\mathcal{R}_\rfloor$, $\log_{10}\sigma_\rfloor$ *and* $\log_{10} m_\rfloor$ *as a function of* $-\log_{10}\mathcal{E}$. $N_\rho = 5$, $\nu = 0.5$, $\mathcal{P} = 1.0$, $n = 2$. *Reproduced with the kind permission of Prof. C. A. Jones, University of Leeds.*

occur in uniform density Boussinesq convection as the large slope of the boundaries near the equator means the flow becomes strongly ageostrophic and convection avoids this region. Jones et al., [38] suggest that the reason that this phenomena can be observed in the regime is the form of the reference state entropy gradient which, for a given velocity, results in the entropy fluctuation being much larger near the outer boundary. This in turn strongly enhances the buoyancy terms in the curl and double curl of the momentum equation, allowing them to overcome the dissipation. This can only occur near the equator as far from the equator convection columns must extend into the interior, with the thin region of strong driving unable to overcome the larger damping. Once again this points to the make up of the reference state profile being of more significance than other simplifications to the reference state. Indeed, Drew et al.,(1995, [22]) find a similar result for the case in which they use constant thermal diffusivity based on molecular thermal conductivity. In this scenario the temperature gradient is much strong near the outer boundary, resulting in a similar increase in the

driving in this region. Gilman & Glatmaier [31] found that no such effect occurs in the case in which the molecular thermal conductivity is held constant, in this case the reference state temperature gradient is much more uniform. In the strongly stratified scenario the localisation of convection towards the equatorial region suggests that there may be a further asymptotic regime in the limit in which $N_\rho \to \infty$ and $\mathcal{E} \to \infty$. We do not investigate this region in detail, but note that it may be related to the equatorially trapped inertial modes found by Zhang et al., (2007, [68]) in the limit $\mathcal{E} \to 0$ and $\mathcal{P} \to \infty$.

7.4 Summary

Within this chapter we have first shown that if entropy diffusion dominates over thermal diffusion in the thermodynamic equation convective instability cannot occur for negative Rayleigh number, thus positive Brunt-Vaisalla frequency. Since even in weakly turbulent systems it is likely that entropy diffusion is indeed dominant over thermal diffusion it is unlikely that negative Rayleigh convection found by Drew et al., (1995, [22]) is of physical significance.

We have then extended the asymptotic theory of convection to the compressible case. Numerical computation by Jones and Kuzanyan (submitted 2008 [38]) suggests that, despite the fact that Taylor-Proudman theorem does not strictly apply in a stratified atmosphere, in the anelastic case studied the convection onsets as tall thin columns in the limit $\mathcal{E} \to 0$ if the other parameters remain fixed. This in turn adds weight to the asymptotic theory. The asymptotic theory allows rapid exploration of the parameter space and provides an indication towards all the major effects reported through numerical simulations. At Prandtl number about unity or greater the asymptotic results are in excellent agreement with the numerical results of Jones and Kuzanyan (submitted 2008, [38]). At low Prandtl number the aymptotic

theory is not fully established as in scenarios when Prandlt number is low and the convection onsets in the interior of the fluid it is often the case that the anti-Stokes lines do not cut the real-axis such that the interval $(s_-,\ s_+)$ lies entirely within the fluid. In this case the boundary conditions become relevant even in the limit in which $\mathcal{E} \to 0$. Despite the lack of accuracy of critical parameters derived through asymptotic analysis when $\mathcal{P}$ is small the general trends predicted by the asymptotic theory are still found in the numerical case in which $\mathcal{P} = 0.1$.

The asymptotic theory shows that there are significant differences between uniform density Boussinesq convection and compressible anelastic convection; critical Rayleigh number, frequency and azimuthal wavenumber are increased and the convection no longer necessarily onsets at the tangent cylinder. The increased wave frequencies, particularly in strongly compressible cases, is likely to be attributable to the local vortex stretching mechanism proposed by Evonuk & Glatzmaier (2004 [27]). The increase in critical azimuthal wavenumber means that for a specific Ekman number numerical computations for compressible convection require significantly higher azimuthal resolution than in uniform density Boussinesq convection. However, the results from previous chapters suggest that the results for a compressible anelastic set are likely to generate all the essential features of fully compressible convection.

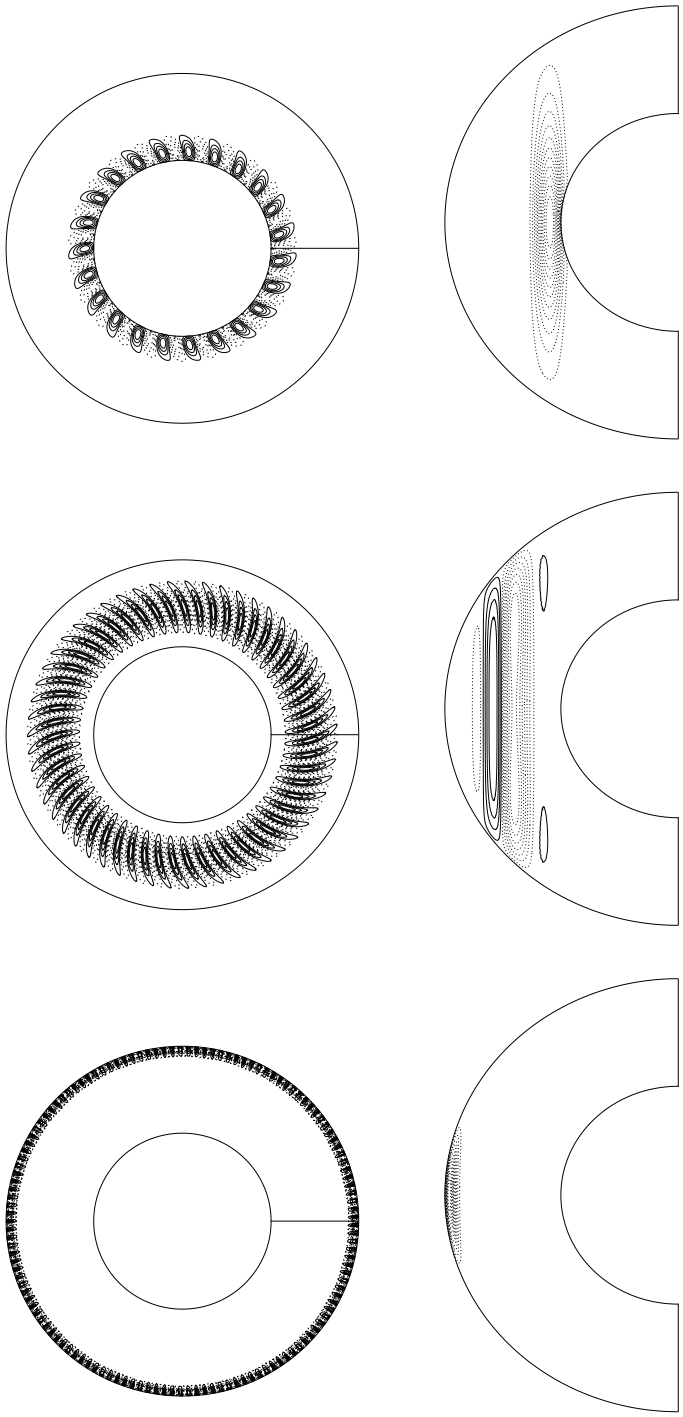

Figure 7.3: *Left panel: equatorial section of entropy fluctuation S'. Horizontal radius marks the ϕ location at which the right hand meridional section is taken. Right panel: meridional section at the longitude marked in the left panel.* $\mathcal{E} = 2 \times 10^{-5}$, $\nu = 0.5$, $\mathcal{P} = 1$, $n = 2$. *a) Boussinesq,* $N_\rho = 0$, $\mathcal{R} = 3.2280 \times 10^6$, $\sigma_\rfloor = 534.36$, $m_\rfloor = 23$. *b)*$N_\rho = 2.0$, $\mathcal{R} = 3.3258 \times 10^7$, $\sigma_\rfloor = 1844.42$, $m_\rfloor = 55$. *c)* $N_\rho = 5.0$, $\mathcal{R} = 6.6570 \times 10^7$, $\sigma_\rfloor = 5614.99$, $m_\rfloor = 133$. *Reproduced with kind permission of Prof C. A. Jones, University of Leeds.*

Chapter 8

Conclusion

Within this thesis we have aimed to consider the accuracy of various approximations used in modelling of planetary atmospheres and interiors. We have not aimed to model the systems accurately, instead to differentiate between the various approximated equation sets compared with the fully-compressible set. We have considered tangent plane and spherical shell geometries under reference systems and parameters which are appropriate to areas of the Jovian regime. In order to remove some of the systematic variation with height due to reference state density variation we re-scaled our perturbation variables, noting that in the Boussinesq regime the perturbation and re-scaled variables are the same.

Initially we considered a stably stratified, isothermal regime appropriate to the isothermal portion of the Jovian atmosphere, following with the analysis of an unstably stratified polytropic regime appropriate to the convective layer below the Jovian 'surface'. As one would expect we found that the normal modes within an isothermal regime were all neutral, whereas in an unstably stratified regime we found that there were both neutral and growing/decaying modes. The dispersion relations formed during analytic analysis of an isothermal F-f-plane suggest that the approximated equation sets will have differing criterion for the onset of instability. When

considering an unstably stratified F-f-plane we found that all approximated sets correctly identified the vertical wavenumbers of the unstable modes. We also found that the inclusion of F terms when considering a tangent plane analysis is generally more significant in the Jovian regime than it is in the terrestrial regime.

We have found that the scale analysis upon which the approximated equation sets are based provides a strong indication as to the regimes under which the linearised approximated equation sets will be valid. We have not considered a non-linear regime, and expect the misrepresentations found for the normal modes of a linear regime to be increased by the introduction of nonlinearities, particularly for the Boussinesq and anelastic equation sets.

The depth of the layer we have considered was limited by computational demands, however inspections suggest that the types of misrepresentation will continue to hold in deeper layers with the magnitude of the mispresentation of most sets continuing to be dominated by the number of density scale heights across the layer whilst also being impacted upon by the ratio of the horizontal to vertical scales.

We will now summarise the misrepresentations of the various types of mode individually.

8.1 Acoustic Modes

The internal acoustic modes are filtered by all approximated equation sets, therefore study of their dynamics requires the use of a fully-compressible equation set. This is predicted by scale analysis, which states that for all approximated sets the modes must have speeds signifcantly less than the Mach number.

The external acoustic modes are filtered by all approximated equation sets with the exception of the quasi-hydrostatic set. In an F-f-plane geometry with

isothermal reference state the external modes of the fully-compressible set are exactly replicated by the quasi-hydrostatic set. For an F-f-plane geometry and unstably stratified regime the quasi-hydrostatic external acoustic mode solutions display significant misrepresentation of the frequencies of external modes with short horizontal wavelength relative to the layer depth. The eigenstructures of the external acoustic mode solutions on an unstably stratified F-f-plane were found to display gross misrepresentation with the vertical structure varying linearly rather than sinusoidally. In a spherical geometry the misrepresentation of the frequencies continues to be dependent on the ratio of horizontal to vertical length scales, though the eigenstructures are generally considerably more accurately represented than those on an F-f-plane. For high zonal wavenumbers we see the calculation of a number of spurious modes which make the identification of the modes which represent the external mode solutions impossible. Increasing the number of density scale heights across the unstably stratified layer serves to increase the level of the misrepresentations. The results indicate that whilst the aspect ratio is normally the most significant factor the reference state profile and geometry of the problem also play a role in the accurate representation of the external mode solutions.

In summary, the fully-compressible model is the only viable model for consideration of all forms of acoustic mode. The quasi-hydrostatic set is suitable for modelling external acoustic modes with very long horizontal wavelength relative to vertical wavelength provided that a spherical shell geometry is used and the reference profile is stably stratified. Modes for unstably stratified and weakly stratified stable regimes, will be poorly represented by the quasi-hydrostatic set. This is predicted by scale analysis.

8.2 Inertio-Gravity Modes

8.2.1 Shallow Gravity Modes

The representation of the frequencies of the shallow gravity modes, in which $K/k_z \ll 1$, is reasonably strong by all equation sets in both isothermal and unstably stratified polytropic regimes. These modes are neutral in both regimes.

For modes with largest horizontal scales and smallest vertical scales the representation of the frequencies by all sets is sufficiently strong that it cannot be differentiated from machine precision. For very long horizontal scale there are modes which are shallow relative to the horizontal scale, but which are the deepest modes with that specific horizontal wavelength. The quasi-hydrostatic set most accurately represents the frequencies of these modes. The shallowest modes for all horizontal wavelengths are more accurately represented than the deepest modes with matching horizontal wavelength, for all equation sets.

The eigenstructures of these modes are also reasonably well represented by all equation sets. On an isothermal F-f-plane the misrepresentation of the eigenstructures is primarily dependent on vertical wavenumber rather than horizontal wavelength, therefore the shallowest modes display little distortion irrespective of the horizontal wavelength. In an unstably stratified regime it is the quasi-hydrostatic and Boussinesq sets which are most obviously misrepresented, with the anelastic and pseudo-incompressible sets having no discernible differences from the fully-compressible solutions. The quasi-hydrostatic set is also reliant on the horizontal wavelength, therefore shallow modes with short horizontal wavelength display some spurious adjustments to the amplitudes of the horizontal components of velocity which in turn leads to energy redistribution. The quasi-hydrostatic approximation breaks down when the stratification is unstable, or weakly stably stratified; however, this has lesser impact

on the very shallow neutral modes, and these are reasonably well represented. The eigenstructures of the rescaled Boussinesq set display small vertical relocation of the modal zeroes for some of the modes when the number of density scale heights across the layer is large. If the Boussinesq results were compared with the results of an unscaled fully-compressible equation set then the misrepresentation of eigenstructures would be significantly worsened.

The misrepresentation of shallow modes by the anelastic and pseudo-incompressible sets is more dramatic in the isothermal regime than in a weakly unstably stratified polytropic regime. This is predicted through scale analysis and likely to be due to the increased magnitude of the reference state density and potential temperature gradients in the isothermal regime. This leads us to believe that if we were to consider a strongly superadiabatic regime the accuracy of these sets would be reduced. This is in line with expectations through consideration of the scale analysis.

Scale analysis also suggests that the Boussinesq and anelastic approximations break down for modes with very large horizontal scales. Inspections suggest that the normal mode analysis is in agreement with this, though the restriction seems to be weaker than that which limits the vertical scales.

8.2.2 Deep Gravity Modes and Deep Convective Modes

All approximated equation sets more severely misrepresent the deep gravity modes than they do the shallow gravity modes, with the misrepresentation being increased as the number of density scale heights across the layer is increased. For truly deep gravity waves, in which $k/k_z \gg 1$, the quasi-hydrostatic set most significantly misrepresents the modes, with dramatic misrepresentation of the frequencies that can exceed several hundred percent. As the horizontal wavelength is increasedwe see the quasi-hydrostatic set increase in accuracy and all other approximated equation sets

decrease in accuracy. This is in line with the expectations of scale analysis.

For an isothermal F-f-plane we find that the quasi-hydrostatic set most significantly misrepresents the truly deep modes; for deepest modes with shorter horizontal wavelengths we find that the Boussinesq set displays the most dramatic misrepresentation followed by the pseudo-incompressible set. The energy-conserving anelastic set most accurately represents the frequencies of these modes. The eigenstructures of these modes are most dramatically misrepresented by the Boussinesq set, which exhibits spurious relocation of modal zeroes, re-distribution of energy amongst the prognostic variables and spurious adjustment to the height dependency. Both anelastic sets relocate the modal zeroes and redistribute energy amongst the prognostic variables, the non-energy-conserving anelastic set also displays spurious adjustment to height dependency. The pseudo-incompressible set accurately represents the eigenstructures.

For an unstably stratified regime the misrepresentations of the frequencies of the deepest modes by the anelastic and pseudo-incompressible sets are not as extreme as for an isothermal set. Once again this leads us to believe that if we were to consider a strongly superadiabatic set we would see these sets produce less accurate representations of the fully-compressible solutions. In an unstably stratified regime the deepest modes are often unstable, and the quasi-hydrostatic and Boussinesq sets display significant misrepresentation of the frequencies and growth/decay rates. At high zonal wavenumber the quasi-hydrostatic set produces a number of modes which are either spurious solutions or gross misrepresentations; this is not unexpected as scale analysis suggests that the approximation will break down not only for modes with large vertical scales but also for weakly, or unstably, stratified regimes. The Boussinesq set displays reasonably strong representation of the growth/decay rates, but underestimates the frequencies significantly. At high zonal wavenumbers the frequencies of the unstable modes do not necessarily even have the same sign and have magnitudes sev-

eral orders smaller than those of the fully-compressible set. The misrepresentation of the growth/decay rates by the anelastic and pseudo-incompressible sets is sufficiently small that it is not possible to distinguish between the sets, interestestingly at high zonal wavenumbers the misrepresentation cannot be distinguished from machine precision. The frequencies of the unstable modes are also reasonably well represented by the anelastic and pseudo-incompressible sets with the non-energy-conserving anelastic and pseudo-incompressible sets being slightly more accurate than the energy-conserving-anelastic sets. The eigenstructures of the convectively unstable modes seem to be well represented by the anelastic and pseudo-incompressible sets with a slight increase in misrepresentation as the number of density scale heights across the layer is increased. The eigenstructures of the most rapidly growing/decaying modes are also reasonably well represented by the Boussinesq and quasi-hydrostatic sets, with the Boussinesq set displaying slight shifts in the location of modal zeroes. The quasi-hydrostatic set produces a number of spurious solutions. Discrepancies between the structures of the modes of the approximated sets are far more clear via the F-f-plane analysis, where the horizontal and vertical structure is separable. In this case the adjustment to amplitudes, vertical tilt and modal zeroes are far more obvious and confirm expectations from scale analysis, that the quasi-hydrostatic and Boussinesq sets are the most inappropriate sets for use in modelling deep convective modes. Re-scaling the vertical coordinate for the Boussinesq set is unlikely to improve the representation of the normal modes as it has no impact upon the physics of the problem. The retropsective application of a reference density scaling factor significantly improves the structural representation, but has no impact on the representation of the frequencies and growth/decay rates thus is likely to remain inappropriate for use in modelling deep convection. The anelastic and pseudo-incompressible sets behave similarly to each other and in the parameter regimes considered there seems to be little benefit in using the more complex pseudo-incompressible equation sets. However, the increase in misrepresentation of the structures of the deep gravity modes

for an isothermal regime leads us to believe that for strongly superadiabatic regimes the pseudo-incompressible set will be the most appropriate. The reduced number of assumptions regarding the size of the perturbations relative to the reference state variables means that we are also of the opinion that this set will perform more accurately when considering a non-linear regime.

These modes are clearly of significant importance when modelling the convective regions of the Jovian interior. We note that the results of many studies that have been undertaken using a Boussinesq equation set are likely to be significantly improved if the factors used to convert the variables of the rescaled fully-compressible equation sets to their unscaled form were to be applied to the Boussinesq results. Increasing numbers of studies are implementing anelastic equation sets, our results suggest that their use will be a significant step forward in understanding the dynamics of the linearised Jovian regime. However, we believe that for more strongly superadiabatic systems, or non-linear equation sets, a pseudo-incompressible set is likely to be more accurate. We also note that many Boussinesq studies have implemented constant reference state density profiles such that pressure is directly proportional to temperature, or through considering $N_\rho \rightarrow 0$ to be the Boussinesq limit. We believe that polytropic regimes in which $N_\rho \neq 0$ can justifiably be used alongside Boussinesq equation sets to provide a far more accurate representation of the fully-compressible system; naturally the sucessful use of such a system would be dependent on the form of analysis undertaken.

8.2.3 Rossby Modes

The lack of latitudinal variation on an F-f-plane means that the Rossby modes are degenerate; all approximated equation sets accurately reflect this. On an isothermal F-f-plane the structures of the internal Rossby modes are defined by the internal mode eigensolutions, and similarly to the internal gravity modes are misrepresented by

the Boussinesq and anelastic sets. The pseudo-incompressible and quasi-hydrostatic sets accurately represent the structures.

In an unstably stratified spherical regime we find stable and unstable Rossby modes, with many of the unstable modes having growth/decay rate of comparable magnitude to the frequency. The level of misrepresentation of the modes with small frequency is sufficiently large that it is impossible to identify modes based on σ alone and inspection of the eigenstructures is necessary to correctly identify like modes. We find that there exist modes in which the modal structures are reasonably well represented, with all sets displaying slight shifts in the location of modal zeroes and small redistributions of energy visible through the adjustments of the amplitudes of the prognostic variables. The quasi-hydrostatic set represents the structure most accurately. However, the frequencies and growth/decay rates of these modes are significantly misrepresented; the quasi-hydrostatic set represents the the growth/decay rate most accurately but underestimates the frequency by over 50%, the Boussinesq and non-energy-conserving anelastic sets display more significant misrepresentation of both frequency and growth/decay rate, the energy-conserving anelastic and pseudo-incompressible sets represent the growth/decay rate less accurately than the quasi-hydrostatic set but represent the frequencies considerably more accurately. The misrepresentation of the neutral Rossby modes is generally less severe than the misrepresentation of unstable modes. Increasing the number of density scale heights across the layer serves to increase the level of misrepresentation. We also find that there are large numbers of modes for which either σ is hugely misrepresented, or the eigenstructure bears no resemblance to the fully-compressible mode with similar σ. The pseudo-incompressible and quasi-hydrostatic sets display the least number of these grossly misrepresented modes, coupled with their accurate representation of the structures for the isothermal F-f-plane and the expectation that these modes will be shallow with long horizontal wavelength we believe that the pseudo-incompressible

and quasi-hydrostatic sets will most accurately represent the neutral modes. We expect that the unstable modes will generally be most accurately represented by the pseudo-incompressible set as the existence of some of the modes will be due to the propagation of convection columns, which are severely misrepresented by the quasi-hydrostatic set.

8.3 Onset of Anelastic Convection

Finally we have considered an alternative form of analysis, extending the traditional uniform-density Boussinesq analysis to an anelastic regime. The extension of the asymptotic theory to a compressible, polytropic regime shows that that the number of reference density scale heights across the layer has significant effect on the location of the onset of convection and the associated critical parameters. Comparison of results with numerical results derived by Jones and Kuzanyan (submitted 2008, [38]) suggests that, despite the fact that Taylor-Proudman theorem does not strictly apply in a stratified atmosphere, Rossby modes and Taylor columns continue to be of importance in considering the onset of convection in a stratified regime.

8.4 Summary

We have found that the most appropriate set for the modelling of the Jovian regime depends primarily on the type of mode one wishes to model, and one can be well-guided by scale analysis in choosing an appropriate set.

As predicted through scale analysis, the stratification is of prime importance in choosing an appropriate approximated equation set. The quasi-hydrostatic equation set is generally inappropriate for unstably stratified regimes, and performs poorly when N^2 is small. The polytropic regimes we considered are, by definition, only

weakly stratified thus N^2 is small; as one would expect, the quasi-hydrostatic set performs more strongly in a stably stratified polytropic regime than one with unstable stratification. When considering a stably stratified regime the quasi-hydrostatic set performs more strongly than all other approximated sets when the horizontal scale is much larger than the vertical scale. Therefore in modelling global circulations, in which the horizontal scale is much larger than the vertical scale, within a stably stratified portion of the Jovian regime, the quasi-hydrostatic set is likely to be the most appropriate approximated equation set. Within an unstably stratified regime it is arguably the weakest set, though it is possible that it remains appropriate for considering neutral modes with extremely large horizontal scales. This result is predicted through scale analysis and supported through analytic and numerical normal mode analysis.

According to scale analysis the Boussinesq and anelastic sets impose greater restrictions on the reference profile than those of the pseudo-incompressible set, thus we expect them to perform more weakly when there is stronger stratification. Normal mode analysis shows this to be the case, though all three sets capture the salient features of the fully-compressible solutions providing that an appropriate reference density scaling factor is applied to the Boussinesq equation set. For unstable modes the Boussinesq set is the weakest set over all possible wavelengths as it systematically reduces the frequency of the most rapidly growing modes to less than 5% of their true value; therefore, for consideration of unstable modes the Boussinesq set is unlikely to be suitable. Whilst the extent of this misrepresentation of the frequency is not predicted by scale analysis, it is arguable that the condition limiting the applicability of the Boussinesq set to situations in which the vertical scale of the motion is much less than the density scale height is broken when considering rapidly growing convectively unstable modes, therefore one would expect significant misrepresentation of the fully-compressible solutions. The neutral modes are significantly better represented,

though misrepresentation is still more dramatic than that of the anelastic set, and reasonable representation is reliant on the application of an appropriate reference state density factor post analysis. The anelastic sets fare considerably better with regard to overall representation; there is no necessity to re-scale the equations, unless it is computationally beneficial to do so, and the frequency misrepresentations are small compared with those of the Boussinesq equation set. This is predicted by scale analysis as the condition relating the scale of vertical motion to the density scale height is less restrictive for the anelastic set. The overall representation of modes in the polytropic regime is reasonably strong, though the representation of modes within the isothermal regime is weaker; once again this is predicted through scale analysis as the number of scale heights across the isothermal regime is larger than the marginally superadiabatic polytropic regime. Scale analysis also suggests that both the anelastic and Boussinesq sets are most appropriate for regimes in which neither the vertical or horizontal scales are large. Analytic and numerical normal mode analysis showed that the vertical scale certainly plays a significant role in determining the accuracy of these approximated equation sets, with the deepest modes at any horizontal wavelength displaying the most significant misrepresentation of the fully compressible solutions. Initial indications suggest that, as expected, the anelastic and Boussinesq approximations also breakdown for large horizontal scales; however, the F-f-plane analysis is limited in examining horizontal scales due to its lack of curvature and constant coriolis terms, and the spherical analysis has significant limitations relating to numerical accuracy. Inspections suggest that within an unstably stratified regime the horizontal scale must be significantly larger than that of a stably stratified regime before the quasi-hydrostatic set is likely to outperform the anelastic set. Once again, this is predicted through scale analysis.

The pseudo-incompressible set also performs similarly to expected. The significant misrepresentation of the frequencies of the normal modes for the isothermal

region of Jupiter is not anticipated by scale analysis, however in every other sense the non-acoustic normal modes exactly replicate those of the fully-compressible set. Therefore, the overall accuracy of the normal mode representation is better than other approximated sets except for very long horizontal scales, in which the quasi-hydrostatic set performs most successfully. Within the marginally superadiabatic regime the pseudo-incompressible set displays extremely strong representation of both neutral and growing modes, though the results are not significantly stronger than those of an anelastic equation set. The normal mode analysis is thus in agreement with the scale analysis and it seems likely that for consideration of deep convection within a linearised, slightly superadiabatic regime the simplicity and tractability of an anelastic set means it is likely to be the preferred approximation. For more strongly stratified, or non-linear, regime, it is likely that the pseudo-incompressible approximation will be beneficial.

Finally, we saw in chapter 7 that the use of a uniform density reference profile reduces computational expense significantly. This simplification is used in traditional models of the onset of convection within a Jovian regime, however the difference between the normal modes at onset for a uniform density reference state and one in which reference density is allowed to vary means that it is likely that the application of a realistic reference profile will have a far more significant effect than the effect of the approximations themselves. For simplicity and tractable analysis, the solenoidal fields enforced by the anelastic and Boussinesq sets mean that these are likely to be the most popular sets for some time to come. Where it is necessary to utilise the Boussinesq approximation we recommend that the structure of the normal mode solutions is re-scaled through use of an appropriate reference density factor, or that this factor is applied to the vertical co-ordinate. This will not improve the accuracy of the frequency representations, but will significantly improve the structural representation making the approximated set more competitive with the anelastic set. We

also note that the Boussinesq approximation we have considered within chapters 3-6 does not neglect pressure perturbations within the gravitational acceleration term in the momentum equation or within the thermodynamic equation, utilising potential temperature instead of temperature; we anticipate that the solutions would be further misrepresented if we were to neglect the pressure terms.

Bibliography

[1] F.M Al-Shamali, M.H Heimpel, and J.M Aurnou, *Varying the spherical shell geometry in rotating thermal convection*, Geophys. Astrophys. Fluid Dynamics **98** (2004).

[2] J Aubert, D Brito, H-C Nataf, P Cardin, and J-P Masson, *A systematic experimental study of rapidly rotating spherical convection in water and liquid gallium*, Phys. Earth Planet. Inter. **128** (2001), 51–74.

[3] D. R Baker and G Schubert, *Deep convective entrainment by downdrafts in jupiters atmosphere*, Icarus **136** (1998), 340–343.

[4] P. R Bannon, *On the anelastic approximation for a compressible atmosphere*, Journal of the Atmospheric Sciences **53** (1996), no. 23, 3618–3628.

[5] G. K Batchelor, *The condition for dynamical similarity of motions of a frictionless perfect-gas atmosphere*, Quart. J. Roy. Meteor. Soc. **79** (1953), 224–235.

[6] G. K Batchelor, *An introduction to fluid dynamics*, Cambridge University Press, 1967.

[7] W.J Borucki, A Bar-Nun, F.L Scarf, A.F Cook, and G.E Hunt, *Lightning activity on jupiter*, Icarus **52** (1982), 492–502.

[8] J Boussinesq, *Theorie analytique de la chaleur*, (1903).

[9] S. I Braginsky and P. H Roberts, *Equations governing convection in earth's core and the geodynamo*, Geophys. Astrophys. Fluid Dynamics **79** (1994), 1–97.

[10] D Brito, J Aurnou, and P Cardin, *Turbulent viscosity measurements relevant to planetary core-mantle dynamics*, Phys. Earth and Planetary Interiors **141** (2004), 3–8.

[11] F.H Busse, *Thermal instabilities in rapidly rotating systems*, J. Fluid Mech. **44** (1970), 441–460.

[12] F.H Busse, *A simple model of convection in the jovian atmosphere*, Icarus **29** (1976), 255–260.

[13] S Chandrasekhar, *Hydrodynamic and hydromagnetic stability*, Oxford University Press, 1961.

[14] U. R Christensen, *Zonal flow driven by strongly supercritical convection in rotating spherical shells*, J. Fluid Mech. **470** (2002), 115.

[15] T. C Clune, Elliotm J. R, M.S Miesch, J Toomre, and G.A Glatzmaier, *Computational aspects of a code to study rotating turbulent convection in spherical shells*, Parallel computing **25** (1999).

[16] G. W Collins, *The fundamentals of stellar astrophysics*, Harvard University Press, 1989.

[17] R Daley, *The normal modes of the spherical non-hydrostatic equations with applications to the filtering of acoustic modes*, Tellus **40A**, 90–106.

[18] T Davies, A Staniforth, N Wood, and J Thuburn, *Validity of anelastic and other equation sets as inferred from normal-mode analysis*, Q. J. R. Meteorol. Soc. **129** (2003), 2761–2775.

[19] E Dormy, A.M Soward, C. A Jones, D Jault, and P Cardin, *The onset of convection in rotating spherical shells*, Journal Fluid Mechanics **501** (2004), 43–70.

[20] T. E Dowling, A. S Fischer, P.J Gierasch, J Harrington, R.P LeBeau, and C.M Santori, *The explicit planetary isentropic-coordinate (epic) atmospheric model*, Icarus **132** (1998), 221–238.

[21] T.E Dowling, M. E Bradley, E Colon, J Kramer, P LeBeau, G. C. H Lee, T.I Mattox, R Morales-Juberias, C. J Palotai, V. K Parimi, and A.P Showman, *The epic atmospheric model with an isentropic/terrain-following hybrid vertical coordinate*, Icarus **182** (2006), 259–273.

[22] S.J Drew, C.A Jones, and K Zhang, *Onset of convection in a rapidly rotating compressible fluid spherical shell*, Geophys. Astrophys. Fluid Dynam. **80** (1995), 241–254.

[23] D Durran and C Bretherton, J. Atmos. Sci. **61** (2004), 1982–1986.

[24] D. R Durran, *Improving the anelastic approximation*, Journal of the Atmospheric Sciences **46** (1989), no. 11, 1453– 1461.

[25] D.R Durran, *A physically motivated approach for filtering acoustic waves from the equations governing compressible stratified flow*, Journal Fluid Mechanics **601** (2008), 365–379.

[26] L Elkins-Tanton, *Jupiter and saturn*, 2006.

[27] M Evonuk and G. A Glatzmaier, *2d studies of various approximations used for modeling convection in giant planets*, Geophys. and Astrophys. Fluid Dynamics **98** (2004), 241–255.

[28] M Evonuk and G. A Glatzmaier, *A 2d study of the effects of the size of a solid core on the equatorial flow in giant planets*, Icarus **181** (2006), 458–464.

[29] M Evonuk and G. A Glatzmaier, *Modelling convection and zonal winds in giant planets*, Proceedings IAU Symposium **239** (2006), 177–187.

[30] U Frisch, *Turbulence*, Cambridge University Press, 1995.

[31] P.A Gilman and G. A Glatzmaier, *Compressible convection in a rotating spherical shell. i. anelastic equations*, The Astrophysical Journal Supplement Series **45** (1981), 335–349.

[32] D. O Gough and N. O Weiss, *The calibration of stellar convection theories*, Ap. J **176** (1976), 589–607.

[33] T Guillot, *A comparison of the interiors of jupiter and saturn*, Planet. Space Sci. **47** (1999a), 1183–1200.

[34] G. A Gulaztzmaier, M. A Evonuk, and T. M Rogers, *Differential rotation in giant planets maintained by density-stratified turbulent convection*, Geophys. Astrophys. Fluid. Dynamics **103** (2009), 31–51.

[35] M Heimpel, J Arnou, and J Wicht, *Simulation of equatorial and high-latitude jets on jupiter in a deep convection model*, Nature **438** (2005), 193.

[36] S.L Hess and H.A Panofsky, *The atmospheres of the other planets*, Compendium of Meteorology, T.F. Malone (ed), American Meteorological Society (1951), 391–400.

[37] A. P Ingersoll, Dowling T.E, P.J Gierasch, G. S Orton, P. L Read, A Sanchez-Lavega, A. P Showman, A. A Simon-Miller, and A. R Vasavada, *Dynamics of jupiters atmosphere*, Cambridge University Press (2004).

[38] C. A Jones, K Kuzanyan, and R. H Mitchell, *Linear theory of compressible convection in rapidly rotating spherical shells, using the anelsatic approximation*, Submitted J. Fluid Mech. **under review** (2008).

[39] C. A Jones, J Rotvig, and A Abdulrahman, *Multiple jets and zonal flow on jupiter*, Geophys. Res. Lett 30 **14** (2003), 1731.

[40] C. A Jones, A Soward, and A. I Mussa, *The onset of convection in a rapidly rotating sphere*, Journal of Fluid Mechanics **405** (2000), 157–179.

[41] C.A Jones, *Convection-driven geodynamo models*, Phil. Trans. R. Soc. London **A 358** (2000), 873–897.

[42] A Kasahara, *The roles of the horizontal component of the earth's angular velocity in nonhydrostatic linear models.*, J. Atmos. Sco. **60** (2003), 1085–1095.

[43] A Kasahara and J. H Qian, *Normal modes of a global nonhydrostatic atmospheric model*, Mon. Weather Rev. **128** (2000), 3357–3375.

[44] H Lamb, *Hydrodynamics, 6th ed.*, Cambridge University Press, 1931.

[45] J.S Lewis, *Physics and chemistry of the solar system*.

[46] F. B Lipps and R.S Hemler, *A scale analysis of deep moist convection and some related numerical calculations*, Journal of the Atmospheric Sciences **39** (1982), 2192–2210.

[47] L Mahrt, *On the shallow motion approximations*, Journal of the Atmospheric Sciences **43** (1986), no. 10, 1036–1044.

[48] Y Ogura and N. A Phillips, *Scale analysis of deep and shallow convection in the atmosphere*, Journal of Atmospheric Sciences **19** (1962), 173 – 179.

[49] P Olson, U Christensen, and G Glatzmaier, *Numerical modeling of the geodynamo: Mechanisms of field generation and equilibration*, J. Geophys. Res. **104** (1999), 10383–10404.

[50] P.H Roberts, *On the thermal instability of a rotating fluid sphere containing heat sources*, Phil. Trans. R. Soc. Lond. **A 263** (1968), 93–117.

[51] J. H Rogers, *The giant planet jupiter*.

[52] C.T Russell and J.G Luhman, *Jupiter: Magnetic field and magnetosphere*, Encyclopedia of Planetary Sciences (1997), 323–373.

[53] D Saumon and Guillot T, *Shock compression of deuterium and the interiors of jupiter and saturn*, The Astrophysical Journal **609** (2004), 1170–1180.

[54] A Seiff, D. B Kirk, T.C.D Knight, L.A Young, F.S. Milos, E Venkatapathy, J.D Mihalov, R.C Blanchard, R Young, and G Schubert, *Thermal structure of jupiter's upper atmosphere derived from the galileo probe*, Science **276** (1997).

[55] A. P Showman, P.J Gierasch, and Y Lian, *Deep zonal winds can result from shallow driving in giant-planet atmosphere*, Icarus **182** (2006), 513–526.

[56] F. H Shu, *The physical universe: an introduction to astronomy*, Cambridge University Press, 1982.

[57] A Soward, *On the finite amplitude thermal instability if a rapidly rotating fluid sphere*, Geophys. Astrophys. Fluid Dynamics **9** (1977).

[58] E.A Spiegel and G Veronis, *On the boussinesq approximation for a compressible fluid*, Astrophysical Journal **131** (1960), 442.

[59] J Thuburn, N Wood, and Staniforth A, *Normal modes of deep atmospheres. i: F-f plane geometry*, Q. J. R. Meteorol. Soc. **128** (2002), 1793–1806.

[60] J Thuburn, N Wood, and Staniforth A, *Normal modes of deep atmospheres. i: Spherical geometry*, Q. J. R. Meteorol. Soc. **128** (2002), 1771–1792.

[61] D. J Tritton, *Physical fluid dynamics*, Oxford University Press, 1989.

[62] A. R Vasavada and P.A Showman, *Jovian atmospheric dynamics: An update after galileo and cassini*, Rep. Prog. Phys. **68** (2005), 1935–1996.

[63] A.A White and R. A Bromley, *Dynamically consistent, quasi-hydrostatic equations for global models with a complete representation of the coriolis force*, QJ Royal Meteorological Soc **121** (1995), 1289–1300.

[64] A.A White, A Staniforth, and N Woods, *Spheroidal coordinate systems for modelling global atmospheres*, QJ Royal Meteorological Soc **134** (2008), 261–270.

[65] R. V Yelle, L. A Young, R. J Vervack, R Young, L Pfister, and B. R Sandel, *Structure of jupiter's upper atmosphere: Predictions for galileo*, J. Geophys. Res **101** (1996), 2149–2162.

[66] K Zhang, *On coupling between the poincare equation and the heat equation.*, Journal of Fluid Mechanics **268** (1994), 211–229.

[67] K Zhang, P Earnshaw, X Liao, and Busse F. H, *On inertial waves in a rotating fluid sphere*, Journal of Fluid Mechanics **437** (2001), 103–119.

[68] K Zhang, P Earnshaw, X Liao, and Busse F. H, *Asymptotic solutions of convection in rapidly rotating non-slip spheres*, Journal of Fluid Mechanics **578** (2007), 371–380.

[69] M Zingale, A.S Almgren, J.B Bell, and C.A Rendleman, *Low mach number modeling of type 1a supernovae. 1. hydrodynamics*, Astrophs. Journal **637** (2006), 922–936.